G1115352 (1981-82)
G5105041 (1980-81)

Final Report

RADIONUCLIDE AND HEAVY METAL DISTRIBUTION IN RECENT SEDIMENTS OF MAJOR STREAMS IN THE GRANTS MINERAL BELT, N.M.

by

Carl J. Popp

New Mexico Institute of Mining and Technology
Department of Chemistry
Socorro, New Mexico 87801

and

John W. Hawley

David W. Love

New Mexico Bureau of Mines and Mineral Resources
Socorro, New Mexico 87801

to

Branch of Mining and Mineral Institutes
Division of Research
Office of Surface Mining
United States Department of the Interior
Washington, D.C. 20204

March, 1983

TABLE OF CONTENTS

LIST OF FIGURES

LIST OF TABLES

SUMMARY

In the absence of historic geochemical baseline data for the Grants Mineral Belt, environmental changes resulting from uranium mine-mill activities can only be determined by indirect methods. A methodology for determining the age of recent sediments in streams draining the region has been established based on combined geomorphic, stratigraphic, and radiometric dating techniques. Because clay-rich sediments retain possible radionuclides and heavy metals derived from mineralization and mined sources, sample sites which contain fine-grained deposits that both predate and postdate mine-mill activity were located in abandoned-channel segments (oxbows) of major streams draining the eastern Grants Mineral Belt. Aerial photographs (and derivative maps) taken between 1935 and 1971 provided the historical and geomorphic documentation of approximate dates of oxbow formation and ages of alluvial fills in the abandoned-channel segments. Pits were dug at these oxbow sites to determine stratigraphy and composition of the deposits. Samples collected from pit walls and auger holes below the pits were subjected to radiometric analysis by gamma ray spectrometry for the artifical radionuclide Cs-137 and the natural radionuclide Pb-210 as well as other U-238 and Th-232 daughters. Because of the dynamic nature of the system, absolute dating with Cs-137 was not possible but samples could be dated as either pre- or post-1950. The 1950 date is important because it marked the beginning of the uranium activity in the region. The Pb-210 dating was not possible because background Pb-210 was very high relative to fallout Pb-210. It may be possible to separate effects of uranium mining and milling activity by comparing U-238 daughter accumulation to daughters in the Th-232 series.

Sediments dated by the correlative Cs-137, stratigraphic, and historic techniques were then analyzed for radionuclides and trace metals which would be associated with uranium ores. The U-238 daughters are generally high in the region and little difference was observed for their values between the control site and the sites in the uranium mining and milling region except for the Paguate Reservoir site. Recent sediments at Paguate clearly show elevated levels of U-238 daughters in sediments unambiguously dated after the mid 1950's. Sediments from the Jackpile uranium mine have been trapped in the reservoir fill.

Trace metals were also analyzed in old and more recent sediments and As, Se, Cd, Hg, and U show elevated values on a regional basis but no correlation with age (i.e. pre- or post-1950). These elevated trace metal values may simply be due to their association with the regionally mineralized material.

I. INTRODUCTION

A. Research Objectives

The major objective of this research proposal has been to determine the extent to which active uranium mining and milling operations in the Grants Mineral Belt of west-central New Mexico may be contributing excess trace metals and radionuclides to Rio Puerco and Rio San Jose sediments. Historical baseline data for the region is not available. The Rio Puerco and Rio San Jose are ephemeral and intermittent streams which drain the active uranium mining area east of the Continental Divide. Episodic major floods deliver large quantities of sediments derived from the region of uranium mineralization and mine-mill activity downstream to the Bernardo-Elephant Butte reach of the Rio Grande. Sediment delivery is very efficient because flood flows are largely transmitted through a regional system of channels confined in arroyo-type valleys. Available historical data on Puerco-San Jose channel behavior permits identification and sampling of stream sediments that both predate and postdate onset of uranium mine-mill operations which began about 1950 (Perkins 1979). In order to determine trace metal and radionuclide contributions from the uranium industry during the past thirty years, the processes of sediment transport and the age of sediments tested must be established. Therefore, subsidiary objectives of this proposal include (1) determination of the modes of sediment movements in the San Jose-Rio Puerco drainage systems and (2) determination of the age of deposits along and adjacent to the modern drainage channels. Comparison of sediments deposited within the past 30 years (1950-1980) with earlier sediments from the same area will establish man-induced contributions to sediments and will provide long-term baseline data on behavior of the affected drainage system.

B. General Approach

Figure 1 shows the study area, including the Rio Puerco-Rio San Jose watershed of the west-central Rio Grande basin and relationships between major streams and uranium mine-mill activity. Procedures used to determine the processes of sediment transport and deposition, the ages of the sediments, and the trace metal-radionuclide content of the sediments include

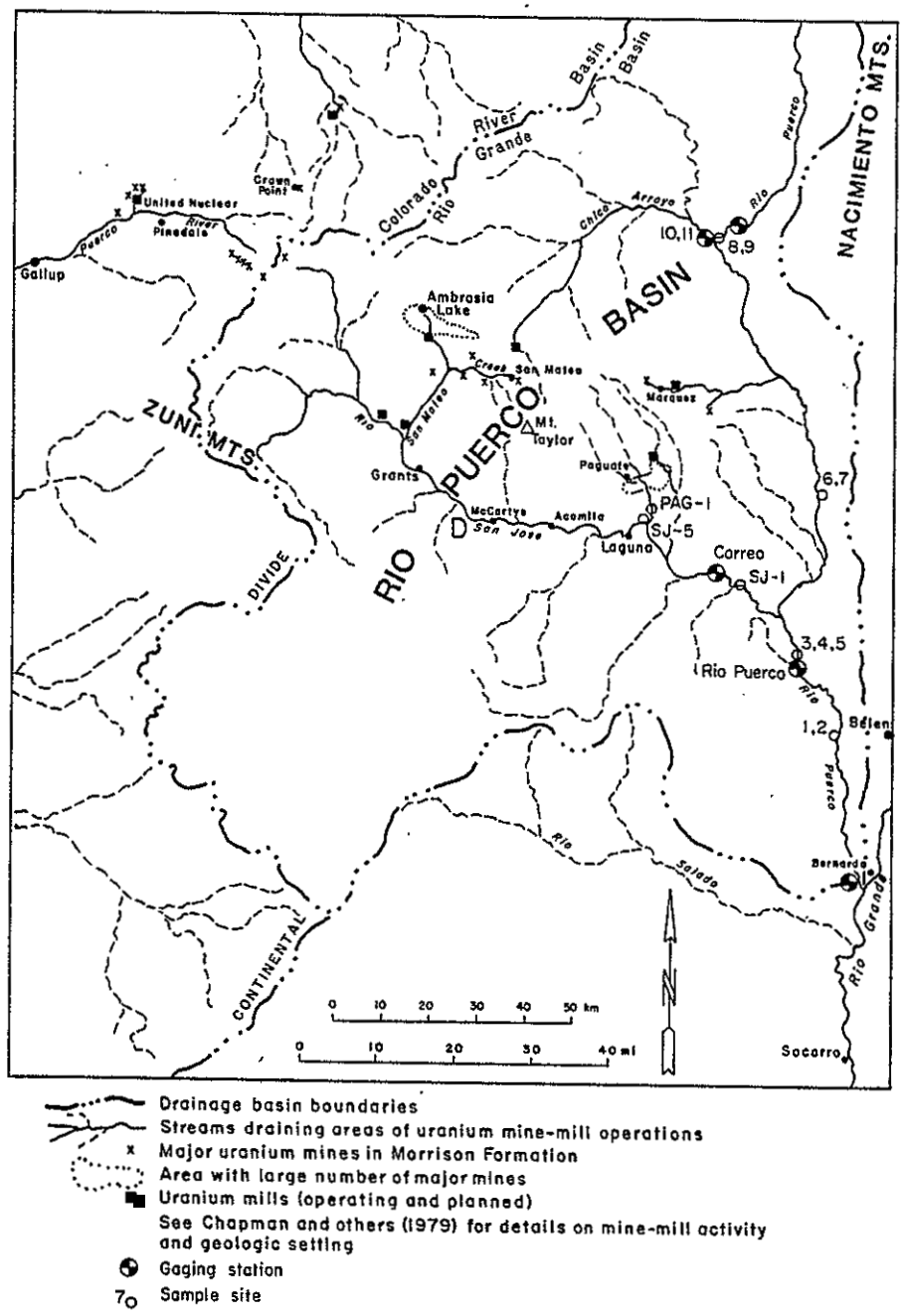

Figure 1. Location of mines and mills of the Grants Mineral Belt, gaging stations, and sample sites in the Rio Puerco drainage basin.

the following categories:

(1) geomorphic evaluation of the fluvial transport and depositional system from the uranium mines and mills in the headwaters through the Rio San Jose-Rio Puerco drainage systems, and evaluation of loci of sediment deposition along the drainages;

(2) historical documentation of loci of deposition to aid in determining the age of sediments;

(3) field sampling and sediment characterization along the drainages;

(4) laboratory characterization of grain size and grain mineralogy of sediment samples;

(5) laboratory determination of trace metals and radionuclide concentrations in sediments; and

(6) laboratory determination of ages of sediments using radioactive Cesium-137 (Cs-137) and Lead-210 (Pb-210).

Categories (2) and (6) should corroborate each other in establishing the age of a particular sediment layer.

C. Overview of Study Area

Since 1948, New Mexico has supplied more than 40% of the nation's uranium production, 99.8% of which came from the Grants Mineral Belt (Rautman 1977). It is estimated that New Mexico has 52% of the United States reserves of U_3O_8 at $ 50 per pound and 16% of the world's reserves excluding China and the U.S.S.R. (Perkins 1979). As of 1978, there were 35 active uranium mines in the Grants Mineral Belt, as well as five mills capable (by 1977) of handling about 21,000 tons of ore per day. Until recently activity in the area was increasing rapidly; nine more mines are under development (Perkins 1979), and a large mill to handle Gulf Mineral Corporation's Mt. Taylor mine is in the planning stage (Rautman 1977). The locations of a number of these facilities are shown in Figure 1. In order to assess the impact of mining operations in the area, it is important to determine both the present and the past condition of the river sediments.

A growing population attracted primarily by the mining activity is located along the Rio San Jose from the Grants area to Laguna (see Figure 1), with the bulk of the habitation in the stream valley; it is important to

ensure the safety of this population as well as the local Indian population. Also, the sediments from the San Jose enter the Rio Grande system through the Rio Puerco and are eventually deposited in Elephant Butte Reservoir. It has been estimated that the Rio Puerco contributes more than 50% of the sediment load to the Rio Grande in central New Mexico while carrying less than 16% of the water (Waite et al. 1972; Popp and Laquer 1980). Excess metals associated with the sediments may be mobilized in the reservoir due to biological activity and the resulting anaerobic conditions occurring on the reservoir bottom. Surface waters in the Rio San Jose show higher amounts of uranium, vanadium, molybdenum, and other trace metals than waters such as the Rio Grande (Brandvold et al. 1981).

It is imperative that regulatory agencies such as the New Mexico Environmental Improvement Division have data of this nature for their assessments and evaluations. The impact of the recent tailings pond spill at the United Nuclear mill near Churchrock, N.M. (July 1979) on the western slope may never be known because baseline data of this type are not available.

D. Radiometric Dating of the Sediments

1. General

Three types of radioactive isotopes are present in the environment: those of primordial, cosmic-ray, and artificial origins. Although those of primordial origin are by far the most widely used in radiometric dating, methods based on all three types of radionuclides are presently employed.

Examples of dating methods based on primordial radionuclides, or on the decay products of these nuclides, include K-Ar, U-Th, and Pb-210 dating. These methods, as well as methods using isotopes of cosmic-ray origin, are based on changes in the isotopic composition of the sample with time. Such changes will begin to occur, as a result of radioactive decay, once the sample is closed to the nuclide(s) in question. The time elapsed since this event can then be determined from the initial and final isotopic compositions.

Isotopes of artificial origin, such as Cs-137, Co-60, and Mn-54 have also been used in radiometric dating. In contrast to the previous methods,

however, most methods of this type are based on the irregular rate of influx of these isotopes, or on their absence in the environment before 1945 (Krishnaswami and Lal 1978).

The use of radionuclides with relatively short half-lives, such as Pb-210 and Cs-137, to date recent sediments such as those in this study and establish anthropogenic inputs of metals is now well-established. This subject has been reviewed by Krishnaswami and Lal (1978).

Robbins and Edgington (1975) have used both Pb-210 and Cs-137 to establish anthropogenic inputs of lead from coal and gasoline use to Lake Michigan sediments. Bennington (1978) has used Pb-210 to determine lead fluxes in Long Island Sound, and Smith and Walton (1980) have used Cs-137, as well as pollen assemblages, to determine the sedimentation rate in a fjord in Quebec. Determination of Pb-210 by direct gamma ray spectrometry, by far the simplest method (and the method used in this study) has been discussed by Gäggeler et al. (1976) and Schery (1980).

A major concern in dating these sediments will be problems of mixing and redeposition which may affect the distribution of the radionuclides. This is due to the dynamic nature of this system as opposed to the normal application to areas such as lakes and estuaries which have a well-behaved depositional pattern.

2. Pb-210 dating

Pb-210 is a naturally occurring isotope with a half-life of approximately 22.3 years (Lederer 1967). Along with Ra-226, Rn-222, Pb-214, and a number of other isotopes, it is an intermediate in the U-238 decay series (see Figure 2).

Because radon is a gas at room temperature, a fraction of the Rn-222 produced by the decay of Ra-226 in the crust diffuses into the atomosphere, where it in turn decays (via a series of very short-lived intermediates) to Pb-210. This isotope is then removed from the atomosphere (over a period of several days) by both wet and dry precipitation (Krishnaswami and Lal 1978). Since Pb-210 is very strongly bound by sediments, virtually all of this influx will be trapped by the surface layer of the soil or sediment.

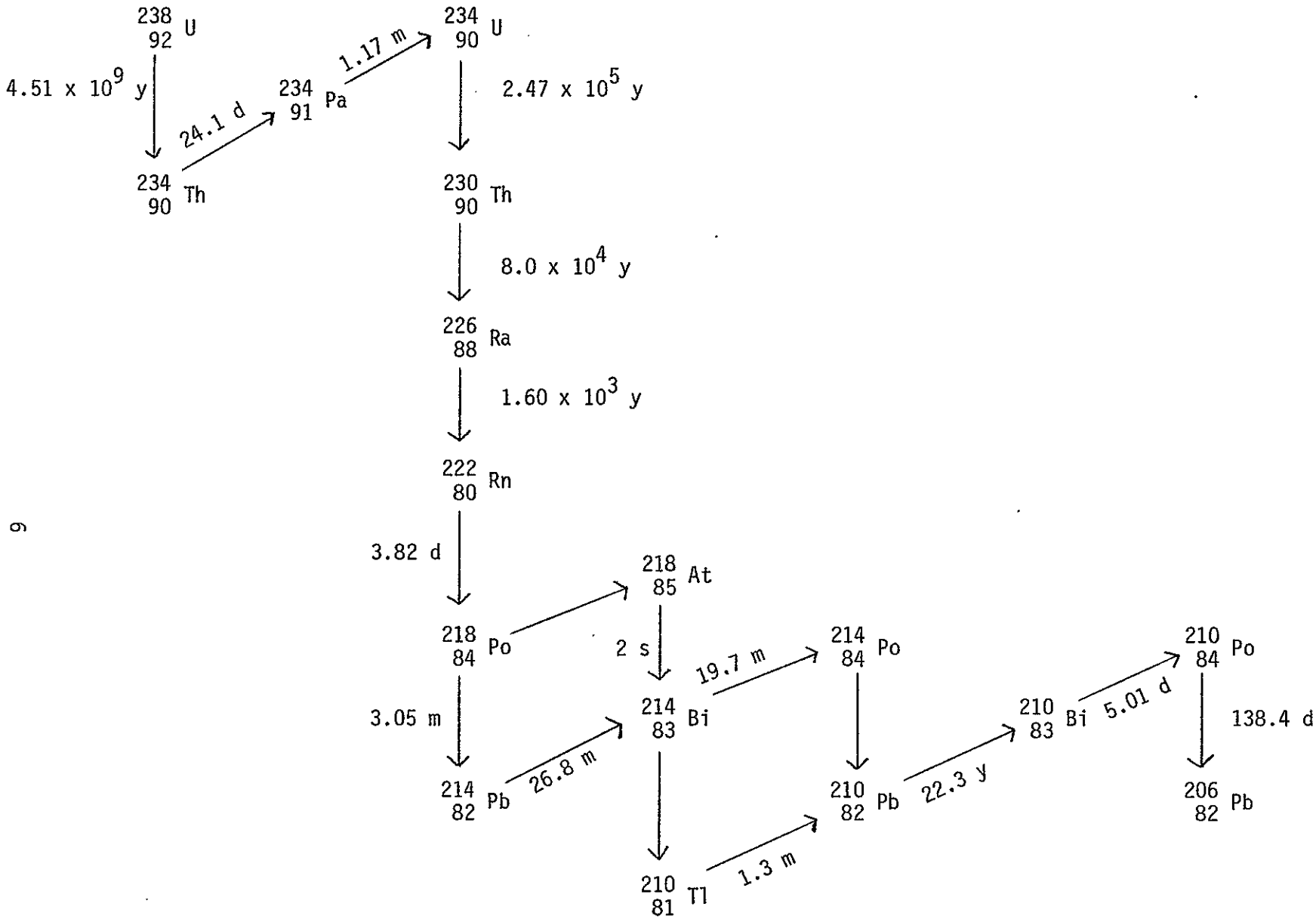

Figure 2. The U-238 Decay Scheme.

In addition, a certain amount of Pb-210 is being constantly produced within the sediment itself by the decay of other nuclides in the U-238 decay series. This Pb-210, termed supported Pb-210, will be in radioactive equilibrium with its precursors so long as the system remains closed with respect to all of the species involved (Jenne and Wahlberg 1968).

The activity of the supported Pb-210 in a sample may thus be determined directly by measuring the activity of Pb-214 or any other isotope in the decay series with which the supported Pb-210 is in radioactive equilibrium. (Alternately, it may be assumed to be equal to the activity of a similar but older sample, in which the unsupported Pb-210 has decayed away). From the activity of the supported Pb-210 and the total Pb-210 activity, the unsupported (atmospheric) Pb-210 can be calculated (Krishnaswami and Lal 1978).

Since the influx of atmospheric Pb-210 to the surface layer will essentially end once this layer is covered by additional sediment, the activity of unsupported Pb-210 in the layer will thereafter decline exponentially with time. The age of the sediment - or, more correctly, the time since its burial - can therefore be calculated using the radioactive decay equation, $A(t) = A(0) \exp(-0.693\ t/t_{\frac{1}{2}})$, where A(0) and A(t) are the activities of the nuclide at time zero and at time t, respectively. In many cases, the value of A(0) can be taken to be equal to the present activity of unsupported Pb-210 at the surface of the sediment (Krishnaswami and Lal 1978).

This method has been used in recent years to date a number of sediment samples (as well as various non-sediment samples) up to 100 years in age. The maximum age is limited by the initial concentration of Pb-210, by the counting statistics, and by the ratio of supported to unsupported Pb-210.

3. Cs-137 dating

Cs-137 is an artificial radioisotope formed by nuclear fission, and has a half-life of approximately 30.0 years (Lederer 1967). It has been introduced into the atmosphere, in irregularly varying amounts, since aboveground nuclear testing began in 1945 (Krishnaswami and Lal 1978; Durham and Jashi 1980).

As is the case with Pb-210, Cs-137 is strongly bound by sediments. It will therefore become trapped by the uppermost layer of the sediment, and as this layer is buried by succeeding ones, a sequence of sediment layers having the same irregular variations in Cs-137 concentration will be built up. This should be true, as pointed out by Ritchie, even in areas where sheet or gully erosion processes predominate (Alberts et al. 1979).

Dating of the sediment is thus possible by determination of the Cs-137 concentration in each interval in the sediment sequence, and by correlation of the resulting pattern of Cs-137 concentrations with the pattern of atmospheric levels since 1945 (Krishnaswami and Lal 1978). The concentration of Cs-137 in the atmosphere peaked sharply (at levels more than an order of magnitude higher than in previous years) in 1958-1959 and 1962-1963, with a further peak in 1971 (Wise 1980).

As a result, it is on these intervals, and on the first appearance of detectable amounts of Cs-137 in the late 1940's or early 1950's that a correlation is generally based.

This method has also been used to date a variety of sediment and non-sediment samples. Unlike Pb-210 dating, however, this method generally requires the analysis of considerable portions of the sedimentary record, and not merely individual samples. Only limited dating may be possible, therefore, in those cases where critical portions of the sedimentary record are not preserved.

E. Factors Affecting Radioisotope Uptake by Sediments

1. Uptake as a function of grain size

It has been shown by a number of authors that Pb-210, (Robbins and Edgington 1975; Goldberg et al. 1978) Cs-137 (Smith and Walton 1981; Edgington and Robbins 1975) and various other radionuclides are significantly enriched in the finest size fractions - a finding which is in agreement with the greater surface area, cation exchange capacity, and hydrous metal oxide and organic contents of these fractions. As a result, the activities of both Pb-210 and Cs-137 may be significantly affected by the silt and clay content of the samples.

Such an effect (which has generally not been significant at sites chosen in previous studies) may be corrected for in a variety of ways. First, the concentration of stable lead or cesium adsorbed by each sample can be determined, and the activities of the Pb-210 or Cs-137 normalized to these values. This approach, however, is based on the assumption that nearly all of the element in question is present as ions adsorbed onto the surface of the particles, and not trapped within the framework of the silicate or metal oxide structures. Such an assumption, although it may be warranted for cesium on account of its large ionic radius, is probably not true for lead, which is scavenged by the hydrous metal oxide phase (Lewis 1977). (In addition, a portion of the lead will be of anthropogenic origin, and will not have been added at a constant rate).

Alternately, several samples of identical age - such as surface samples - can be analyzed for Pb-210 or Cs-137, and an attempt made to determine an empirical correlation between the activity of the isotope and the percentages of the different size fractions. This empirical relationship can then be used to normalize the Pb-210 or Cs-137 activities of the remaining samples.

Finally, samples can be chosen which are all of similar lithology, or which can be mechanically separated to remove certain of the size fractions. Coarser sand fractions, for example, could be removed by passing the sample through a screen or sieve of appropriate size, while silt and clay could be removed manually if it is present as discrete, cohesive layers.

2. Uptake as a function of time

Although the annual flux of Pb-210 to sediments has been shown to remain relatively constant from year to year, (Benninger 1978; Krishnaswami and Lal 1978) the same is not necessarily true over shorter periods of time. The atmospheric concentrations of both Pb-210 (Peirson et al. 1966) and Cs-137 (Burton and Stewart 1960) in fact, have been shown to fluctuate at some sites by nearly an order of magnitude over periods of several days, and also from season to season. Such behavior is indeed not surprising, as weather conditions will clearly affect the transport of nuclides such as Rn-222, Pb-210, and Cs-137 within the atmosphere, as well as the emanation of radon from crust. By scavenging locally available Pb-210 and Cs-137, rainfall

can also be expected to cause temporarily increased (and later decreased) fluxes of both of these isotopes (Krishnaswami and Lal 1978).

As mentioned by Krishnaswami, this effect has not been significant in most previous studies because deposition has been continuous and individual samples have typically represented a year or more of such deposition. In contrast, most samples in the present study appear to represent single brief episodes of sediment deposition, probably lasting a few days to at most a few weeks. It seems inevitable, therefore, that some of these irregular variations will be preserved in the final pattern of Pb-210 and Cs-137 activities of the samples in this study.

Nevertheless, it should be recognized that dry deposition of these isotopes will generally continue even after sediment deposition has ceased. Since dry rather than wet deposition may in fact be the major source of these isotopes in arid areas (Turekian et al. 1977) considerably smaller random variations in activity may therefore result. For the same reason, any variations in Pb-210 and Cs-137 uptake due to the differing lengths of time which the samples spend in contact with the water during deposition (Smith and Walton 1980) will also be partially masked.

F. Other Radionuclides

In addition to Pb-210 and Cs-137 which can be used for radiometric dating, other radionuclides such as Th-234, Ra-226, Pb-214, and Bi-214 (as well as Pb-210) from the U-238 decay series (see Figure 1) may be mobilized in uranium mining and milling activities. The activities of these radionuclides should, in general, parallel the uranium concentrations in sediments. One way of separating general radioactivity from the uranium-related radioactivity is to examine isotopes in the Th-232 decay series. Such an isotope in the Th-232 series is Ac-228 so it is possible to compare relative activities of Ac-228 and the U-238 daughters to attempt to sort out mining and milling contributions.

G. Trace Metals

A number of trace metals such as As, Se, Mo, and V are often found associated with uranium ores and may be mobilized during ore processing. Such metals are often found in high concentrations in mill tailings in

the Grants area (Gallaher and Goad 1981) and depending on transport mechanism, may accompany uranium and its daughters in stream waters and sediments. Previous work by Brandvold et al (1981) and Popp et al. (1981) in the Rio Puerco and Rio San Jose indicated Mo and V values were elevated in filtered water from the Rio Puerco relative to the Rio Grande. Also, suspended sediments in the Rio San Jose carried greater concentrations of As, Cd, Co, Hg, Mo, U, V, and Zn than found in the Rio Puerco and Rio Grande.

H. Geologic Setting

1. Drainage basin characteristics

The Rio Puerco drainage basin is more than 200 km long, encompassing approximately 18,892 km^2. Although most of the drainage basin is less than 2,000 m above sea level, the headwaters lie in the Nacimiento Mountains (up to 3,176 m), the Zuni Mountains (2,821 m), and Mount Taylor (3,345 m) (see Figure 1). Two major subbasins drain the Grants Mineral Belt, Rio San Jose, and Arroyo Chico. Smaller drainages from the Marquez area drain the easternmost part of the mineralized belt. A particularly important tributary to Rio San Jose is Rio Paguate, which is bisected by the extensive open pit and waste piles of the Jackpile-Paguate uranium mine complex (see Figure 3).

The drainage basin straddles the boundaries between the Colorado Plateau, Southern Rocky Mountains and Basin and Range physiographic provinces. The upper portions of the drainage basin are underlain by thick semi-consolidated deposits in the Albuquerque structural basin.

2. Geomorphology of the Rio Puerco and tributaries

The landscape along the Rio Puerco and its tributaries is quite diverse. Pertinent to this study are the general features of the stream valleys. The valleys consist of (1) the sloping valley margins, commonly cut in bedrock or in semiconsolidated basin fill (see geology), (2) the valley floor, underlain by thick alluvial deposits, and (3) the incised axial stream channel (arroyo) and related features.

The valley side slopes are dissected by tributaries which transport sediment from the slopes to the valley floor. Some tributaries deposit sediment in alluvial fans along the margins of the valley floor. Others

Figure 3. Jackpile-Paguate uranium mine complex in center of picture, Rio Paguate drainage and Paguate Reservoir in lower right. Photograph by J.W. Hawley, 1977.

have become integrated with the arroyo system and contribute sediment to the axial stream channel.

The valley floor is relatively flat, consisting of sediment layers built up by flooding from the axial stream when it was not entrenched, and by deposition from the toes of alluvial fans along the valley margins. Valley floors presently are undergoing erosion by lateral and vertical cutting of surface streams (axial arroyos and dendritic tributary arroyos) and subsurface tributaries in pipes (natural cave-like passages through clay-rich sediments).

Rio Puerco and major tributaries have developed distinctive geomorphic features within their confined arroyo walls. Rio Puerco Arroyo ranges from 145 to 245 m wide between walls 8 to 13 m high in studied reaches. Geomorphic features within and adjacent to Rio Puerco Arroyo (see Figure 4) include (A) the inner channel, (B) point bars along the channel, (C) an inner floodplain which may include oxbows, (D) with sand plugs, (E) where the channel has been cut off, (F) erosional and depositional terraces above the inner floodplain, (G) vertical arroyo walls, (H) remnants of valley fill within the arroyo, (I) gently- to steeply-sloping eroded slopes, (J) the mouths and alluvial fans of soil pipes and tributaries, and (K) uneroded valley floor.

According to Love et al. (1983), the pattern of the inner channel of Rio Puerco Arroyo consists of complex meanders, straight reaches, and gentle arcuate reaches. Some meanders are very elongate, but overall sinuosity is about 1.5 (ratio of stream length/straight line distance).

Geomorphological-sedimentological features of the inner channel and inner floodplain commonly include sand bars and ripple-marked surfaces along the floor of the inner channel, slightly finer-grained sand bars along the margins of the inner channel (see Figure 5), natural levees along the outer margins of the inner channel, a relatively flat floodplain, and coppice dunes. Chutes across point bars or parallel to the inner channel produce relief on the inner floodplain. Locally, adjacent to the inner channel, is a subhorizontal zone where sheet flow occurs during large floods (Shepherd 1976). Tamarisks commonly are the dominant vegetation, although willows and cottonwoods are common locally. In broad reaches of the arroyo, tamarisks die out away from the margins of the inner channel and chamisa

Figure 4. Geomorphic features of Rio Puerco Arroyo and adjacent valley floor in reach downstream from site 5. Letters are explained in text. Photograph by K. Novo-Gradac and A. Gutierrez, June, 1982.

Figure 5. Features of the inner channel at site 6. Photograph by D.W. Love, April, 1981.

and four-winged saltbrush dominate.

Sediments accumulate along modern streams in several depositional environments. Sediments are deposited in channel-marginal bars, along the margins of point bars, in low areas along the inner floodplain, and in cut-off channels (oxbows). Oxbows are likely to accumulate the thickest and most fine-grained deposits, so they were sought for study.

Channel meanders can be cut off to form oxbows by two mechanisms. One mechanism occurs as meanders shift laterally downstream, when one meander loop overtakes the meander loop downstream, causing neck cutoff (see Figure 6A). Other meanders are cut off by formation of a secondary channel across the enclosed point bar, forming a chute cutoff (see Figure 6B). Once a meander loop has been cut off, new channel marginal sand bars called "sand plugs" build across the mouths of the abandoned meander loop and the resulting oxbow begins to receive fine-grained overbank sediments when floods overtop the sand plugs or adjacent floodplain. As oxbows fill, they become stable parts of the inner floodplain and receive less sediment as they reach the topographic level of the floodplain. The filling process may take 15 to 30 years in the Rio Puerco.

Topographically above and adjacent to the modern inner floodplain are local erosional and/or depositional terraces at one or more levels. Depositional terraces retain the arcuate form and deposits of abandoned channel and floodplain (see Figure 4H). Other terraces are eroded scarps and benches without depositional features. Eolian sand commonly covers the surface of the terraces.

Tributaries commonly have steeper gradients and have less well developed channel and inner floodplain features than the Rio Puerco.

3. Bedrock geology

The drainage basin is underlain by a variety of rocks and less consolidated deposits (Table 1). Point-counts of 212 township and range line intersections in the drainage basin on the geologic map of New Mexico (Dane and Bachman 1965), were used to estimate the relative proportions of rocks exposed. About 6 percent of the drainage basin has exposures of late Tertiary and Quaternary unconsolidated to semiconsolidated sediments

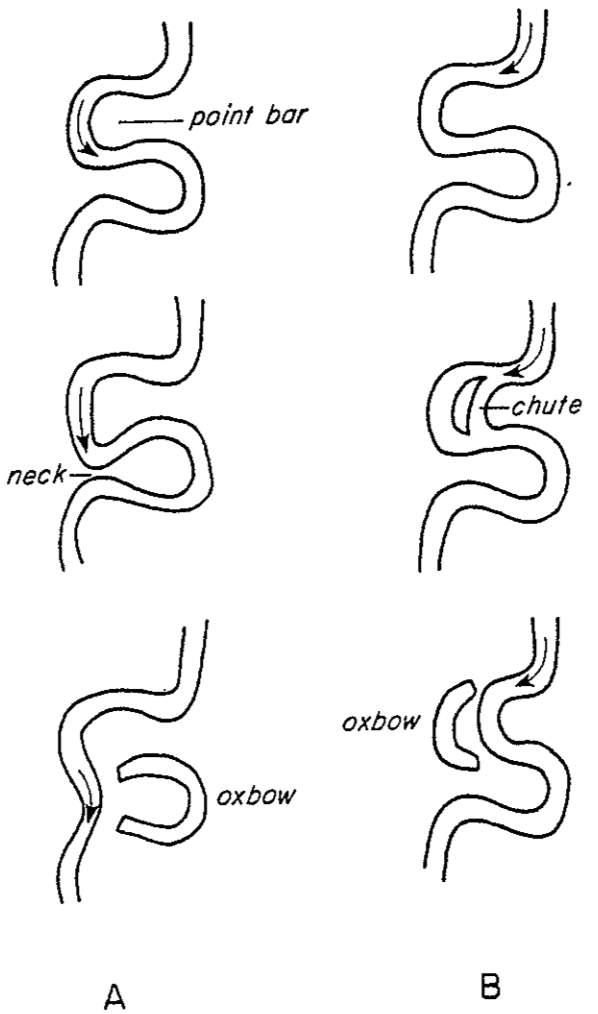

Figure 6. Processes of oxbow formation. A. Neck cutoff by meander migration downstream. B. Chute cutoff by secondary channel development across point bar.

Unit	Percent
Thick Quaternary sediments (8 percent Holocene fill)	9.4
Upper Tertiary and Quaternary basin fill	6.1
Upper Tertiary and Quaternary volcanics	17.0
Lower and Middle Tertiary sediments and volcaniclastics	6.6
Cretaceous sandstones, shale, and mudstones	40.6
Jurassic sandstone, mudstone, limestone, and gypsum	4.7
Triassic mudstone and sandstone	5.7
Upper Paleozoic limestone, mudstone, sandstone	7.5
Precambrian igneous and metamorphic rocks	2.4
Total	100.0

Table 1. Percentages of geologic units exposed in the Rio Puerco drainage basin.

deposited while the Rio Puerco drainage basin was developing. These sediments are derived from sources which continue to contribute sediments to the drainage. Thus, sediments reworked from relatively young basin fill are similar to sediments presently being shed from the headwater areas. Another 8 percent of the drainage basin is underlain by thick Holocene alluvium with characteristics similar to 20th century alluvium. About 17 percent of the drainage basin is underlain by Tertiary and Quaternary volcanic rocks, primarily basalt flows, which contribute little runoff or sediment to present streams. Nearly 18 percent of the drainage basin is underlain by Paleozic to Jurassic sandstone, limestone and shale, including about 3 percent Todilto Limestone and Morrison Formation, the two major uranium host rocks of the Grants Mineral Belt (the amount of mineralized rocks at the surface is estimated to be much smaller than 1 percent of the drainage basin area). More than 6 percent of the rocks are Chinle Formation and Abo Formation, major contributors of red clays to the basin fill and to modern sediments. About 40 percent of the drainage basin is underlain by Cretaceous sandstones and shales. These relatively erodable rocks have as much as 600 m of relief and are major contributors of sediment in modern channels and in valley fills. Precambrian crystalline and

metamorphic rocks account for about 2 percent of exposures in the drainage basin, but clasts of these hard rocks are common in basin fill and younger alluvium.

4. Sources of radionuclides and heavy metals in the drainage basin

As previously mentioned, the major surface occurrence of uranium-bearing rocks is in outcrop areas of the Jurassic, Todilto, and Morrison Formations (<1% of drainage basin). Uranium prospects and mines in the eastern part of the Grants Mineral Belt are discussed by McLemore (1982; Figure 7). Most surface occurrences of uranium mineralization are sites of mines or prospects. Further discussion of uranium occurrences in the Rio Puerco drainage basin is given in Hilpert (1969), Rautman (1980), Perkins (1979), Hatchell and Wentz (1980), and McLemore (in press). Many of the mines and mineral occurrences are underground and have little surface expression other than man-made disturbance. A survey of abandoned mines and prospects (Anderson 1981) revealed that few prospects had extensive surface disturbance with elevated amounts of radioactivity. With several notable exceptions, there appear to be few surface sources for radionuclides and heavy metals from the Grants Mineral Belt.

Uranium is also found in Eocene Baca Formation along the southern margin of the drainage basin (Chamberlin 1981). Uranium mineralization is localized along the eastern margin of the Ladron Mountains (McLemore 1982) and in Cerro Colorado, an exhumed volcanic complex near the Rio Puerco west of Albuquerque (Hilpert 1969).

Other rocks which may produce above-background trace elements or radionuclides within the drainage basin include sedimentary copper deposits along the front of the Nacimiento Mountains (Kaufman et al. 1972), fluorite (-sulfide) deposits in the Zuni Mountains (Goddard 1966) and trace-metal bearing coal and humate deposits of Cretaceous formations (Bachman et al. 1959; New Mexico Bureau of Mines and Mineral Resources unpublished coal data files; Siemers and Wadell 1977).

Another possible source of radionuclides and trace metals has been mine dewatering. Discharges to the Rio Puerco above its confluence with the San Jose are approximately 22.7 m^3/sec and to tributaries of the San Jose about 13.2m^3/sec (Perkins and Goad 1980). The New Mexico Environmental

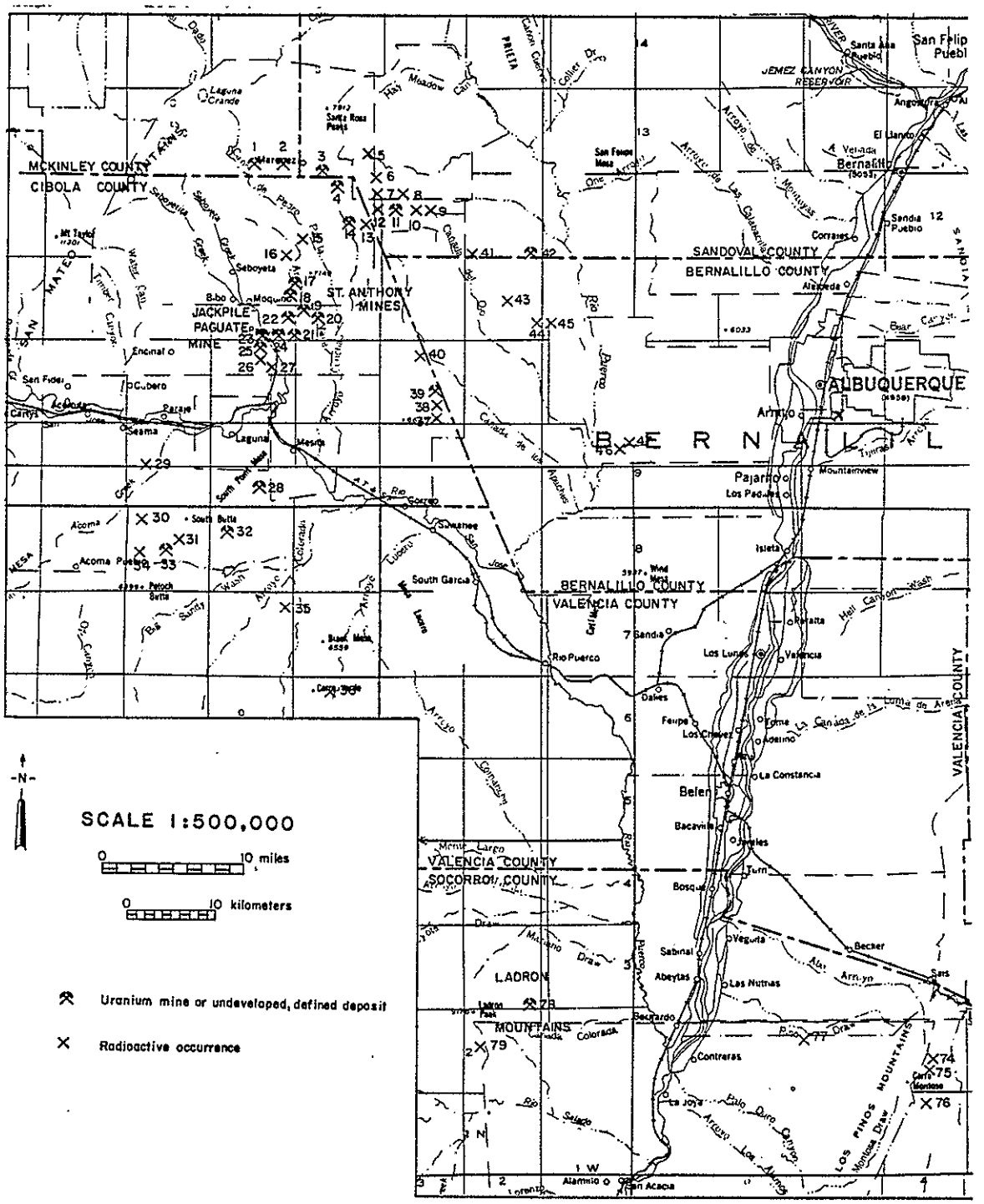

Figure 7. Map showing uranium mines and radioactive occurrences in the Rio Puerco drainage basin, New Mexico (modified from McLemore, 1982). Localities marked by numbers are discussed by McLemore (1982).

Improvement Divison has measured concentrations of trace metals and radionuclides in mine discharges which exceed New Mexico groundwater standards (New Mexico Water Quality Control Commission 1982). The same report also indicates that mill tailings liquids may be contaminating aquifers. Any of this material entering the drainage systems may be moved downstream. Total uranium production to date in New Mexico has been approximately 1.6×10^5 tons with 99% from the Grants Mineral Belt (McLemore, in press). The Jackpile-Paguate mine is one of the largest open pit uranium mines in the world, covering about 10.7 km^2. The Rio Paguate runs through the pit and drains into the Rio San Jose. The sum of activity related to uranium mining in the region could conceivably mobilize radionuclides and trace metals.

5. Possible reworking of sediments within the drainage basin

Recycling (retransporting) previously deposited sediments may account for much of the dilution of sediments derived from primary sources in the drainage basin. Recycling of grains may occur on several scales, including (1) episodic transport and deposition of loose sediment within the modern channel, (2) recycling modern sediment by eroding 20th century bank and floodplain deposits, (3) recycling earlier valley fill by lateral erosion of arroyo walls, (4) recycling earlier valley fill by vertical erosion at the base of the modern channel, and (5) erosion of valley fill by tributaries. There are no data on episodic transport of sediment within the modern channel, but bars are deposited and are reworked by later floods. The distance individual grains are transported probably is related to the size of the grains (whether they are part of the bedload or suspended load) and the stream power of individual floods. Some marshy areas along the modern Rio San Jose above Laguna act as normal sediment traps.

In order to assess the amount of lateral erosion of both 20th century deposits (floodplain) and earlier valley fill, a 10 km stretch of the Rio Puerco between sites 1 and 5 was analyzed by determining the course of the inner channel on 1:4,800 scale maps produced in 1979 by the Army Corps of Engineers. About 77 percent of the length of the inner channel was between banks which appeared to be relatively stable (neither eroding nor receiving sediment). About 9 percent of the length of the channel appeared

to be impinging on 20th century deposits and, in some cases, clearly cutting into the inner floodplain. The inner channel impinged directly onto exposures of older valley fill along 14 percent of the channel.

Vertical cutting into older deposits is difficult to assess because commonly the channel floor is covered with loose sandy sediment or with water. In early fall, 1982, however, a large flood removed loose sediment from some reaches of the Rio Puerco and it was possible to see that the channel locally rests on older valley fill. Nonetheless it is not yet possible to estimate what proportion of the channel length is eroding older valley fill.

Pipes and small incised tributaries contribute reworked valley fill directly onto the inner floodplain and to the inner channel. Larger tributaries recycle sediments from the valley margins as well as valley fill directly into the inner channel.

6. Hydrology of the Rio Puerco and its tributaries

The Rio Puerco is an ephemeral stream throughout much of its length, flowing only in response to precipitation. Water discharge and sediment transport data from five United States Geological Survey gaging stations with long-term records within the Rio Puerco drainage basin were analyzed to determine the size and frequency of floods and the general behavior of the Rio Puerco. The stations included Bernardo (1940-1982), Rio Puerco (1934-1976) Rio Puerco above Chico Arroyo (near Guadalupe 1951-1980), Rio San Jose at Correo (1943-1980), and Chico Arroyo (1943-1980) (see Figure 1). The seasonal distribution of flows at the stations (see Figure 8) reflects the contrasting contributions of spring runoff and summer thundershower runoff in different parts of the drainage basin. At Bernardo, near the mouth of the Rio Puerco, the stream flows an average of only 20 percent of the year. At Rio Puerco, the stream flows 55 percent of the year. Near Guadalupe, the Rio Puerco flows 53 percent of the year, while Arroyo Chico flows 45 percent of the year. Although Rio San Jose is perennial near Grants, at Correo, the stream flows only 40 percent of the year. All stations are marked by great fluctuations in the amount of flow each year (see Figure 9).

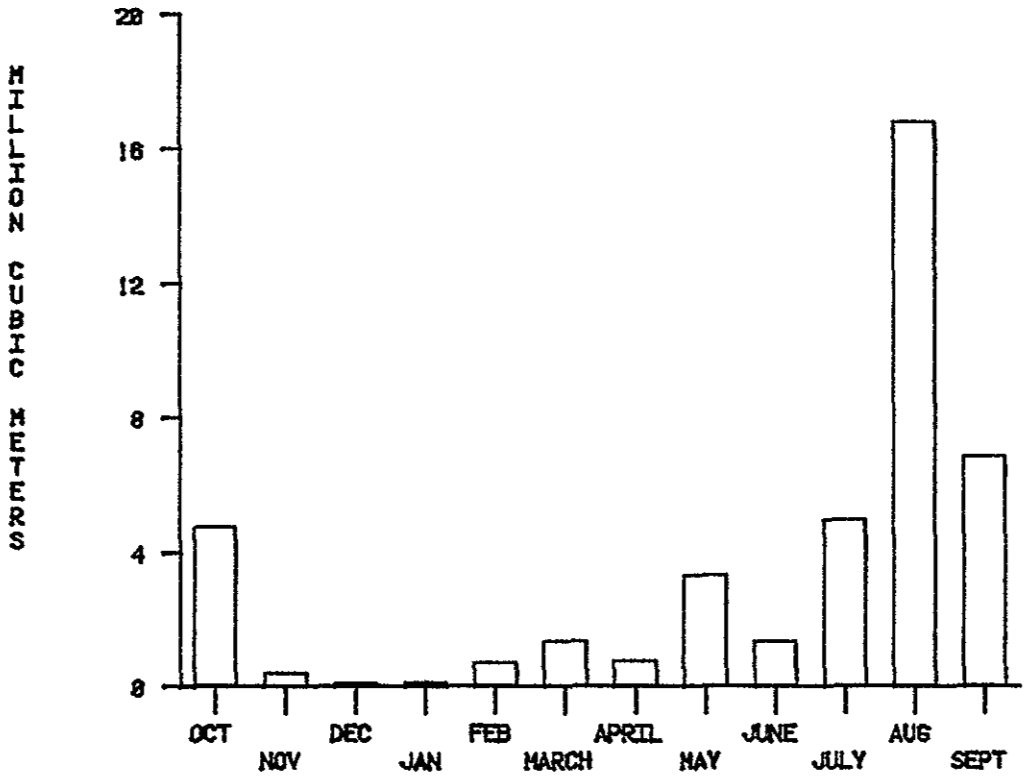

A.

Figure 8. Average monthly flow for water year for five gaging stations in the Rio Puerco drainage basin. A. Rio Puerco at Bernardo, B. Rio Puerco at Rio Puerco, C. Rio Puerco above Arroyo Chico, D. Arroyo Chico, E. Rio San Jose at Correo.

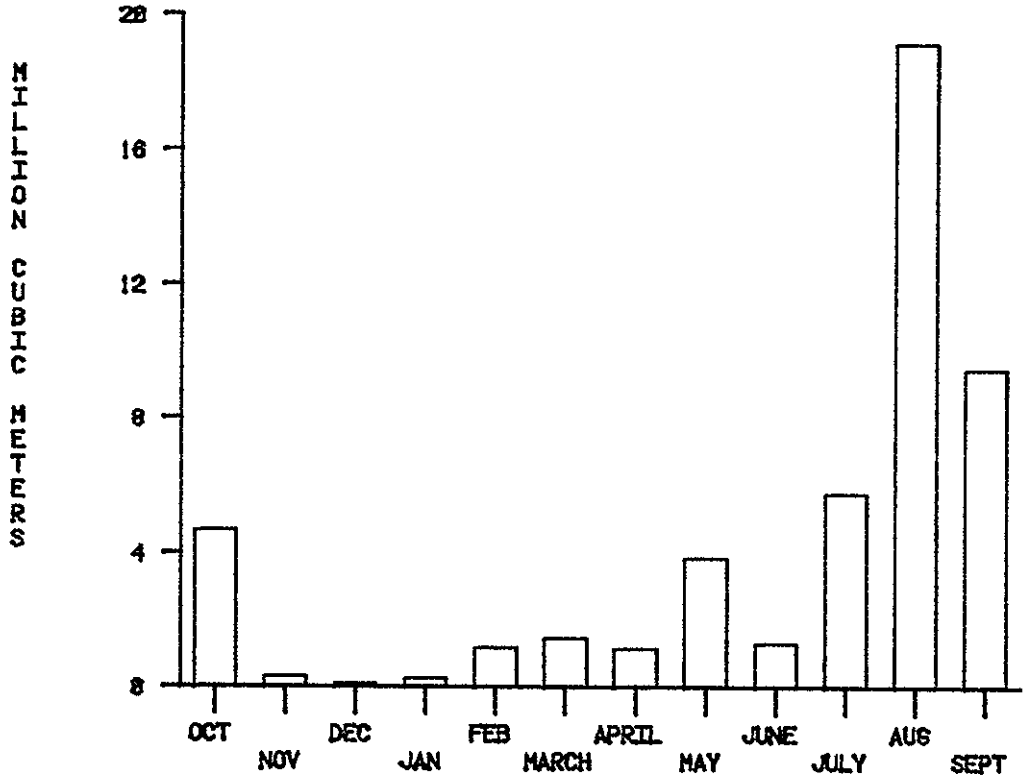
MILLION CUBIC METERS
20
16
12
8
4
0
OCT
NOV
DEC
JAN
FEB
MARCH
APRIL
MAY
JUNE
JULY
AUG
SEPT

B.

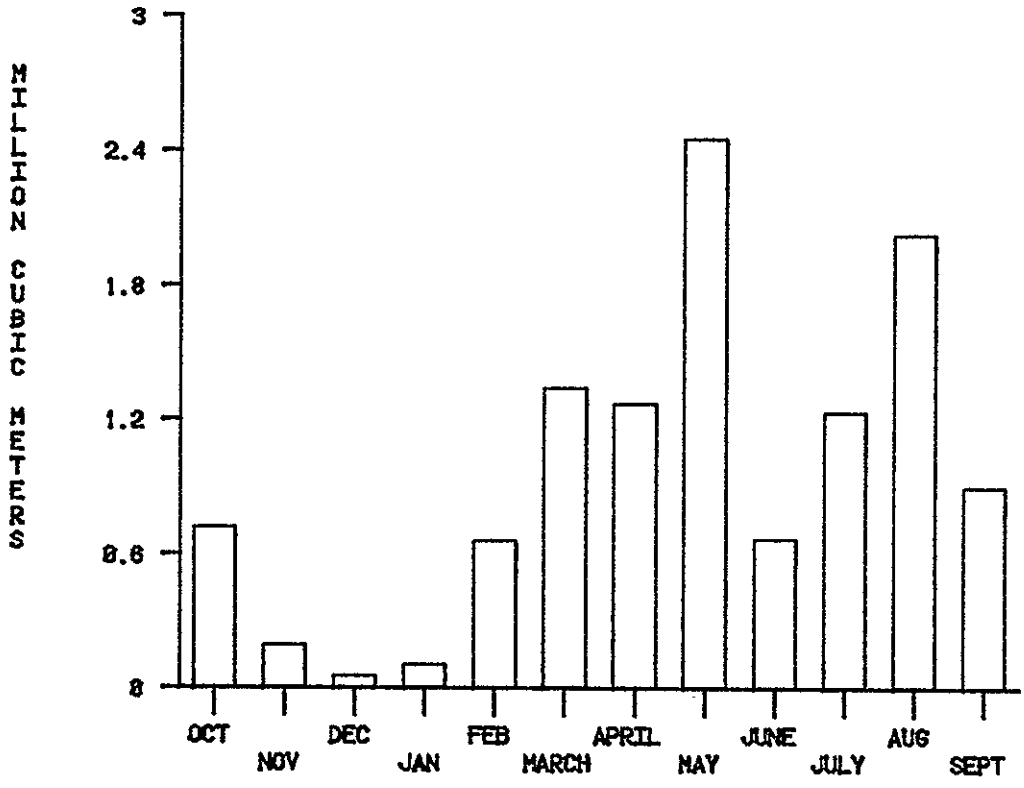
MILLION CUBIC METERS
3
2.4
1.8
1.2
0.6
0
OCT
NOV
DEC
JAN
FEB
MARCH
APRIL
MAY
JUNE
JULY
AUG
SEPT

C.

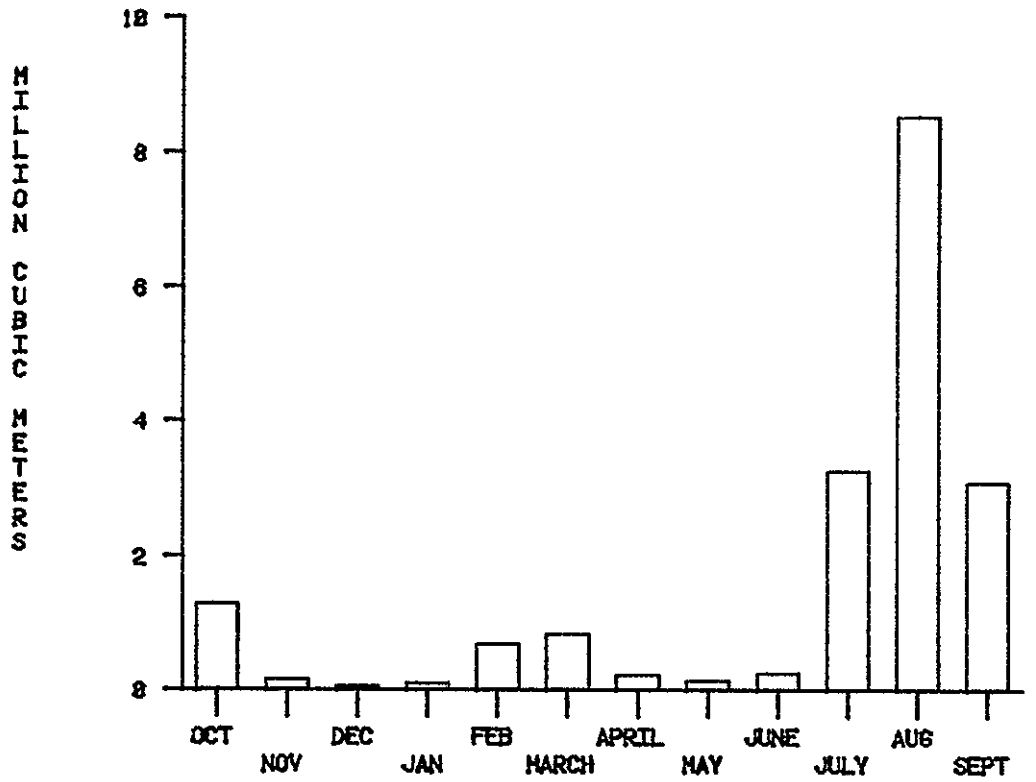
MILLION CUBIC METERS
12
8
6
4
2
0
OCT
NOV
DEC
JAN
FEB
MARCH
APRIL
MAY
JUNE
JULY
AUG
SEPT

D.

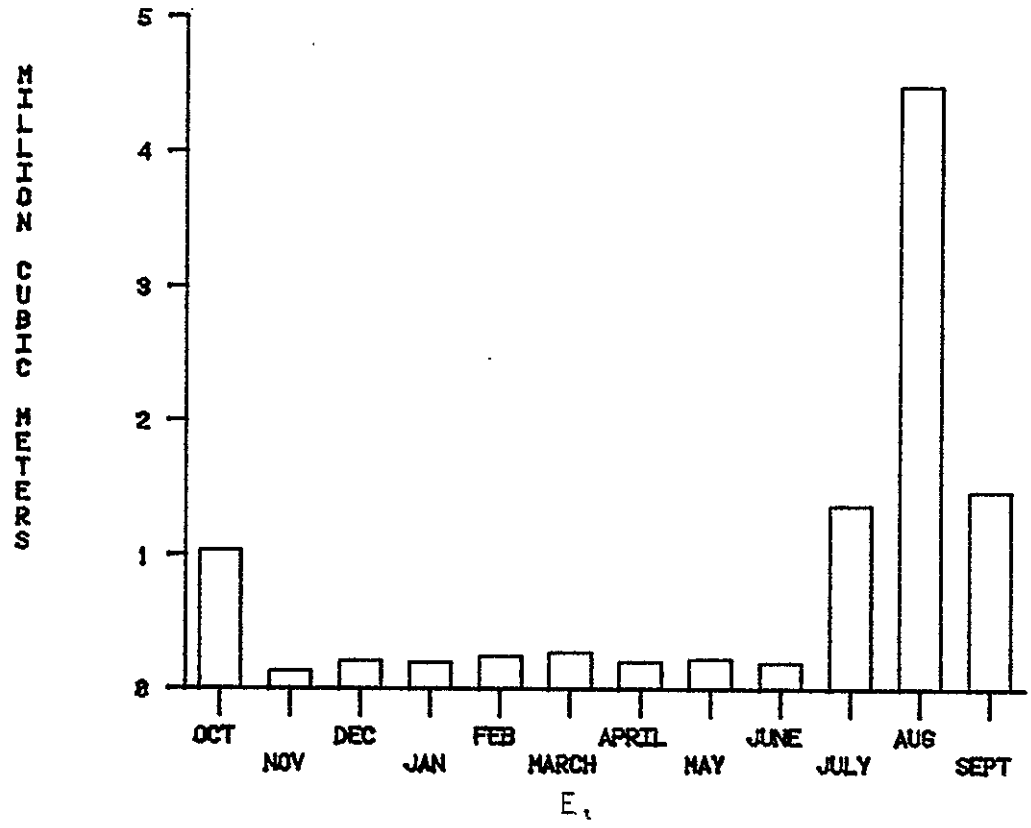
MILLION CUBIC METERS
5
4
3
2
1
0
OCT
NOV
DEC
JAN
FEB
MARCH
APRIL
MAY
JUNE
JULY
AUG
SEPT

E_t

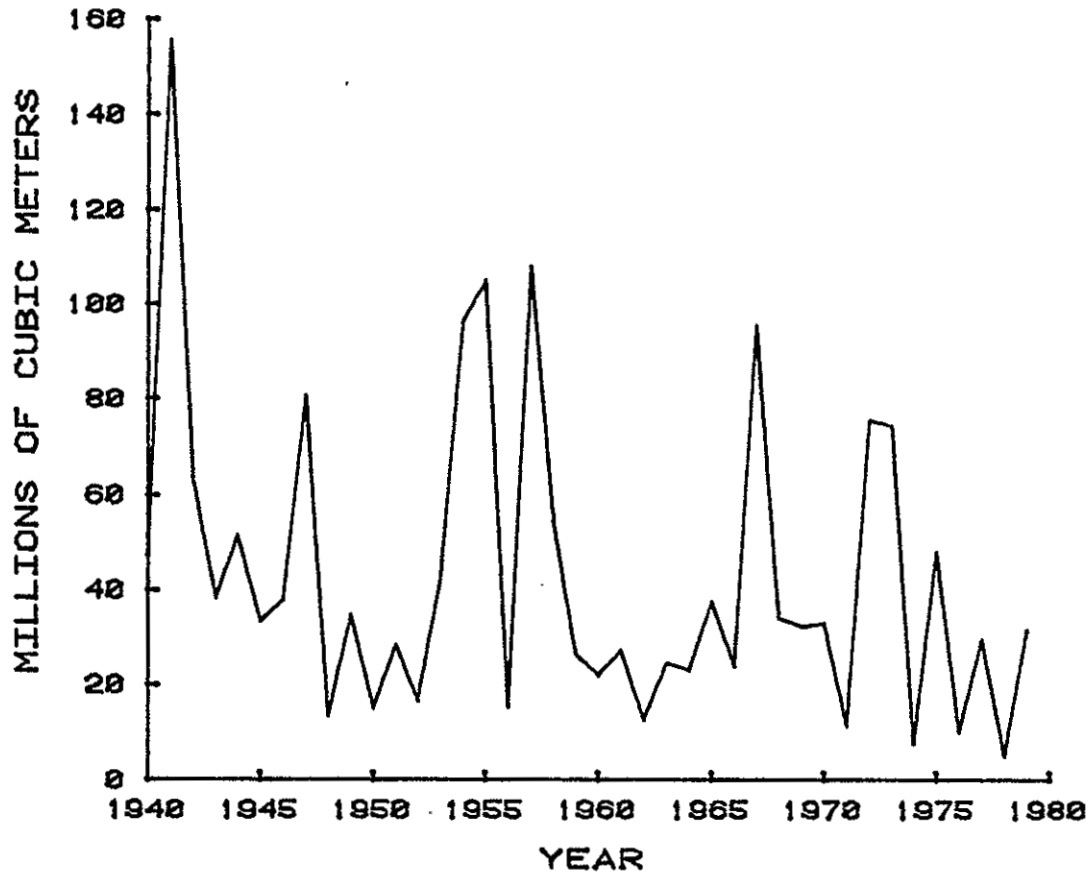

A.

Figure 9. Annual (water year) flow for the period of record for five gaging stations in the Rio Puerco drainage basin. A. Rio Puerco at Bernardo, B. Rio Puerco at Rio Puerco, C. Rio Puerco above Arroyo Chico near Guadalupe, D. Arroyo Chico, E. Rio San Jose at Correo.

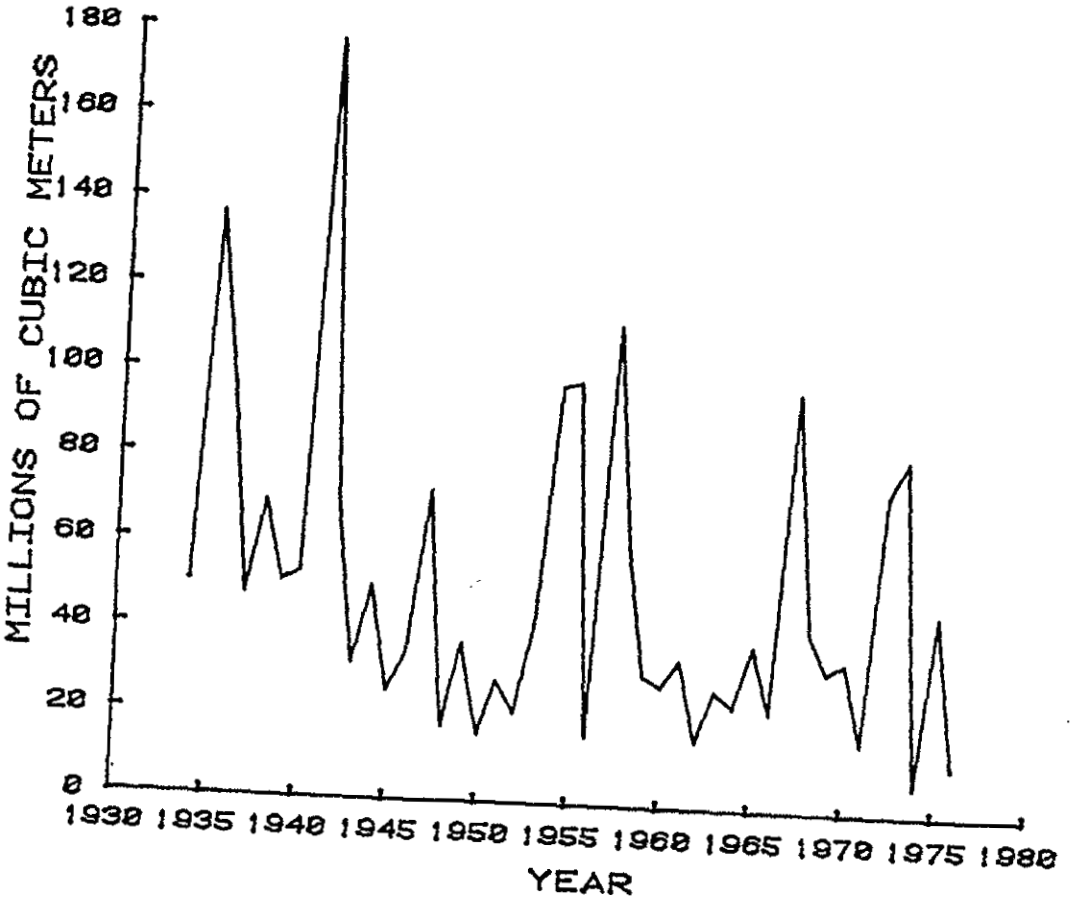
MILLIONS OF CUBIC METERS
180
160
140
120
100
80
60
40
20
0
1930 1935 1940 1945 1950 1955 1960 1965 1970 1975 1980
YEAR

B.

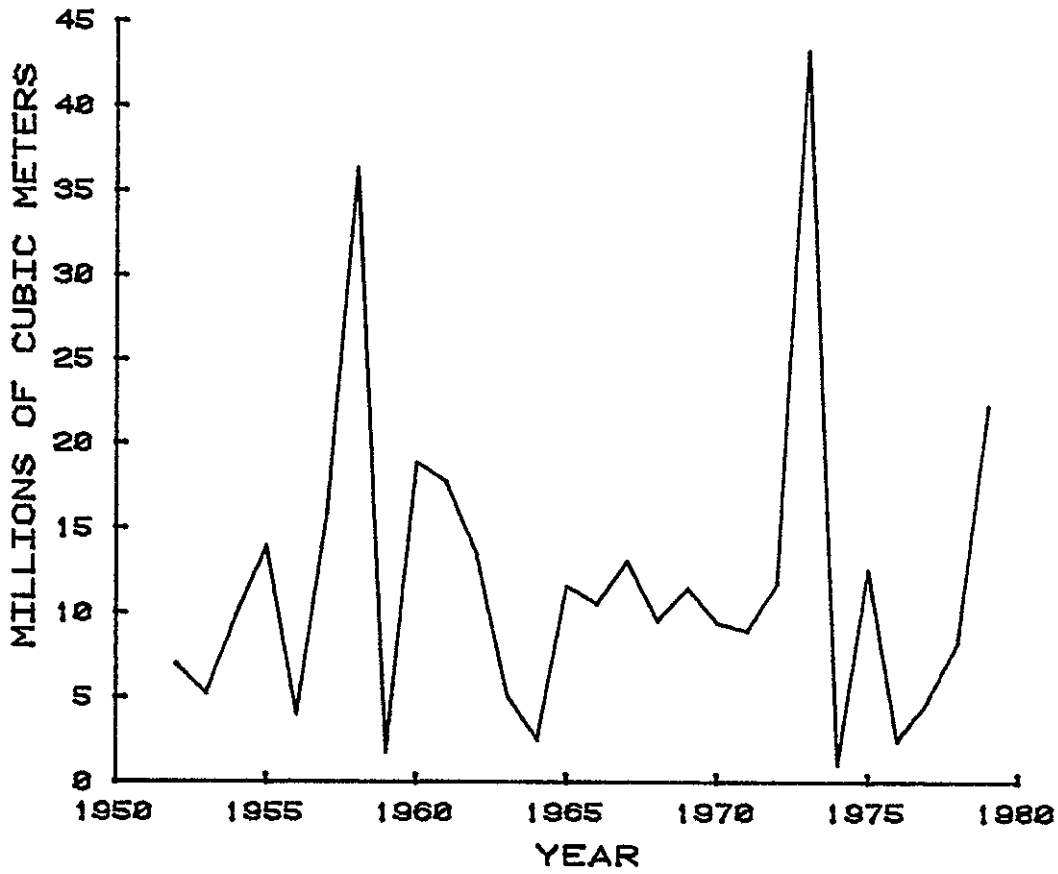
MILLIONS OF CUBIC METERS
45
40
35
30
25
20
15
10
5
0
1950
1955
1960
1965
1970
1975
1980
YEAR

C.

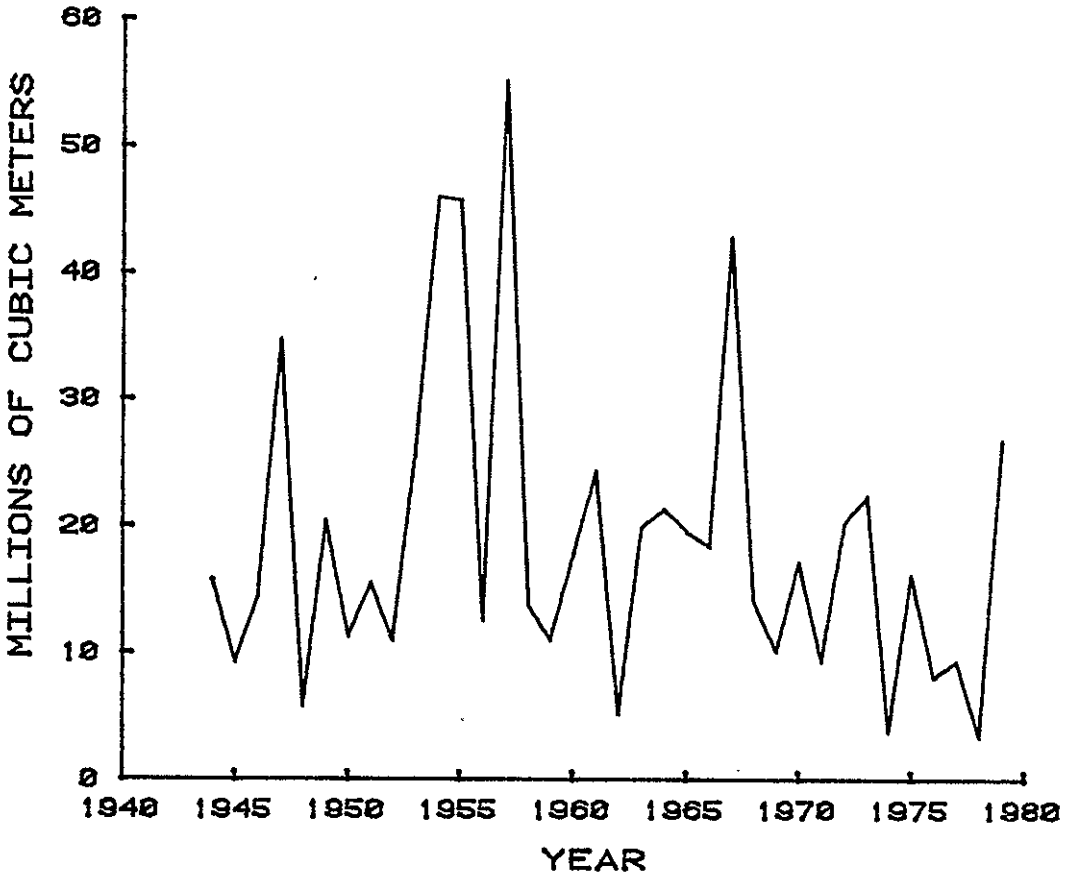
MILLIONS OF CUBIC METERS
60
50
40
30
20
10
0
1940
1945
1950
1955
1960
1965
1970
1975
1980
YEAR

D.

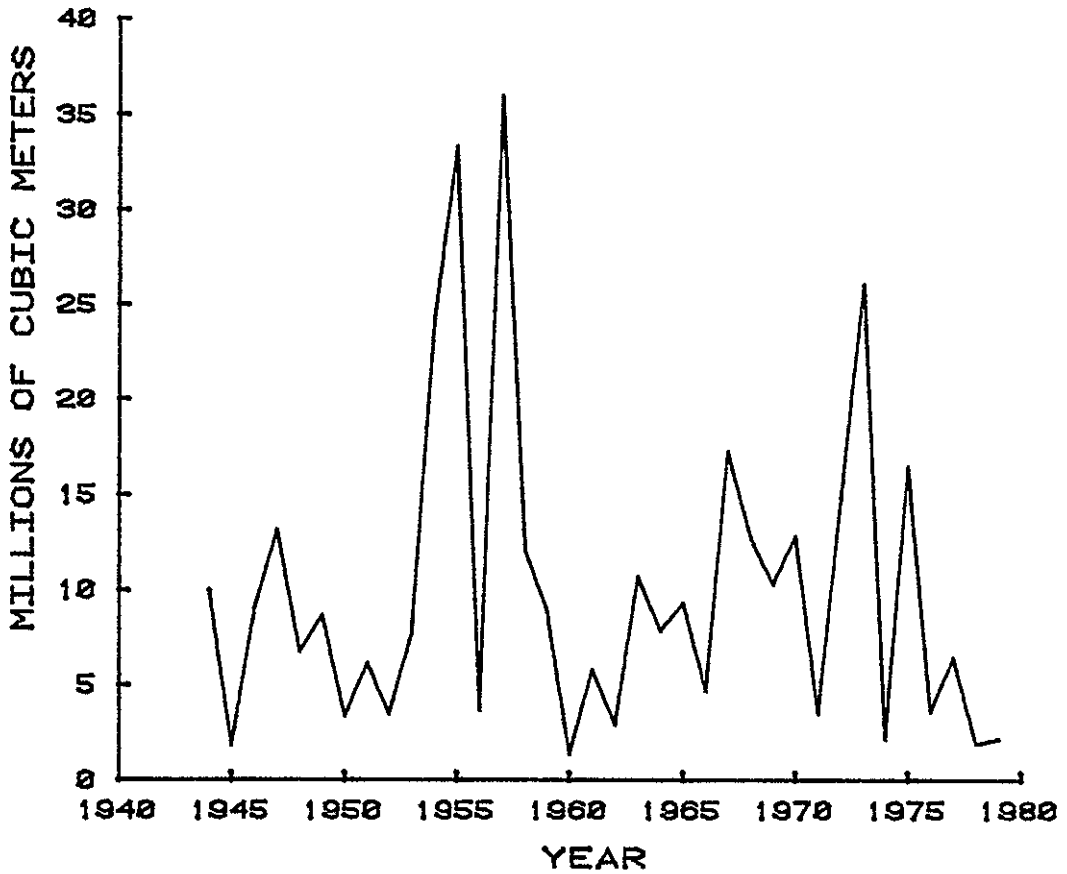
MILLIONS OF CUBIC METERS
40
35
30
25
20
15
10
5
0
1940
1945
1950
1955
1960
1965
1970
1975
1980
YEAR

E.

In general, the amount of flow reflects the amount of precipitation upstream, but precipitation gages within the Rio Puerco drainage basin are so few that individual floods can not be traced from individual precipitation events. Individual flood peaks and large daily flows can be traced downstream from upper gaging stations to lower gaging stations (see Figure 10). Commonly there is a loss of water in a downstream direction, as floods lose water to the channel floor and banks. As in other streams, the duration and size of floods becomes longer and less peaked downstream.

The Rio Puerco is infamous for large discharge and high sediment loads. At the gaging station near Rio Puerco, maximum discharge (September 23, 1929; stage 5.5 m) was estimated to be 1,070 m^3/sec, which destroyed the railroad bridge along with the stream gage. Suspended sediment loads of up to 680,000 ppm have been recorded at Bernardo, and loads up to 400,000 ppm are not uncommon (Nordin 1963).

Two major problems were encountered with the data sets compiled for each of the gaging stations. One problem is that daily average flows are recorded rather than individual flood peaks. Second, floods larger than base flow (defined by the United States Geological Survey to be a flood with a recurrence interval of 1.15 years) were also recorded, but base flow for most stations was redefined every few years, sometimes being increased or decreased by as much as 127 m^3/sec. Therefore similar floods were not treated equally in different years. Although there is some correlation between peak flows and daily average flows, the correlation is not strong enough to predict peak flows from daily average flows. For example, at Rio Puerco above Arroyo Chico, peak flows of 197 m^3/sec (July 29, 1967) and 96 m^3/sec (August 1, 1966) yielded daily average flows of only 14 m^3/sec, and larger daily flows of 30-34 m^3/sec resulted from smaller peak flows of 97 m^3/sec (September 12, 1972) and 128 m^3/sec (August 18, 1961)(J. Boyle, 1983, personal communication). The result of these two problems is that it is difficult to compile complete records of floods at each gaging station with equal precision and therefore impossible to determine the number of floods which may have contributed to sedimentation in the oxbows. Nonetheless, an estimate of the magnitude and frequency of large floods passing each gage are shown in Figure 10. These plots show the relative decrease in numbers of large floods.

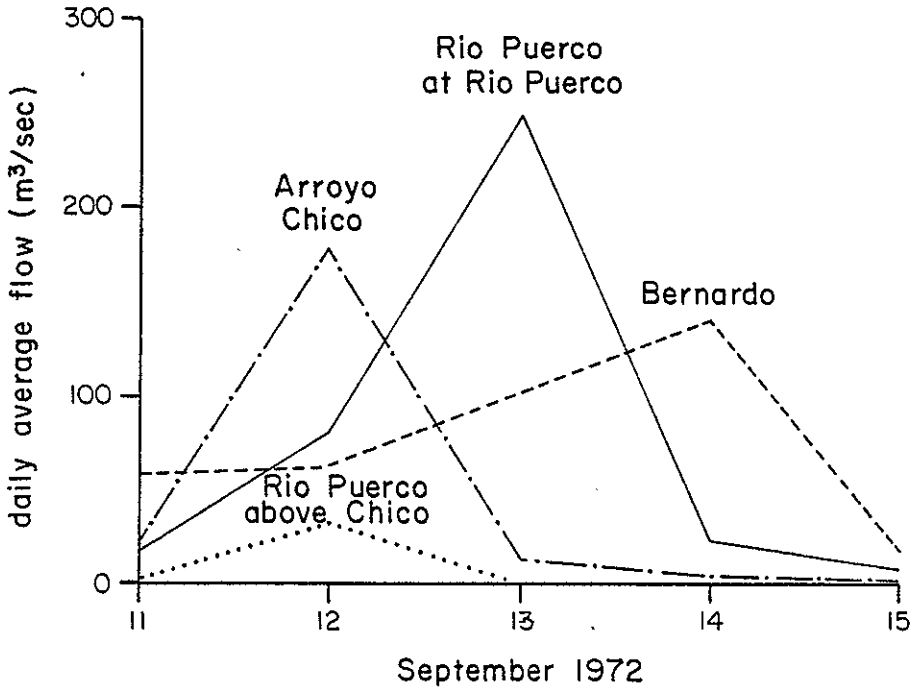

Figure 10. Rise and fall of daily average flows for flood of September 11-14, 1972, from gaging stations along the Rio Puerco and Arroyo Chico.

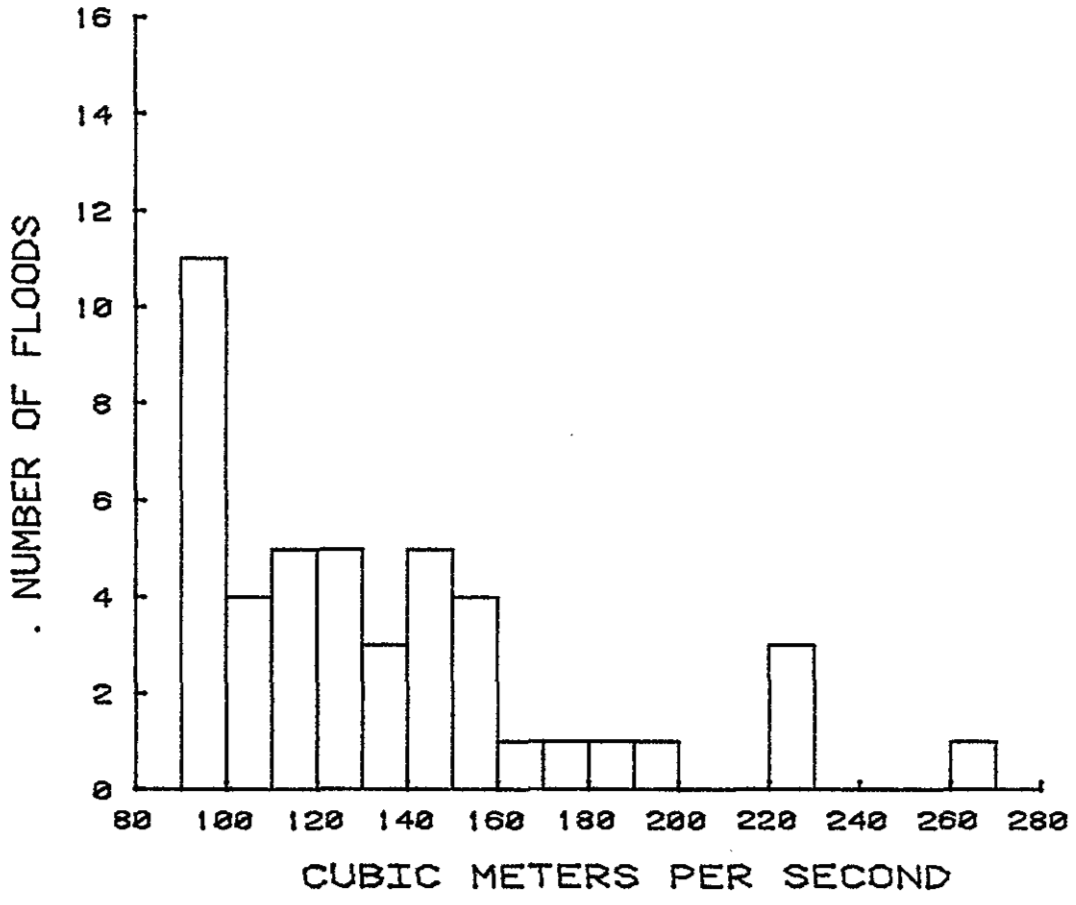

Figure 11. Number of floods larger than base flow at five g gaging stations in the Rio Puerco drainage basin. A. Rio Puerco at Bernardo from 1950 through 1979. Base flow is 91 m^3/sec. B. Rio Puerco at Rio Puerco from 1950 through 1976. Base flow is 170 m^3/sec. C. Rio Puerco above Arroyo Chico from 1950 through 1979. Base flow is 51 m^3/sec. D. Arroyo Chico from 1950 through 1979. Base flow is 82 m^3/sec. E. Rio San Jose at Correo from 1950 through 1979. Base flow is 23 m^3/sec.

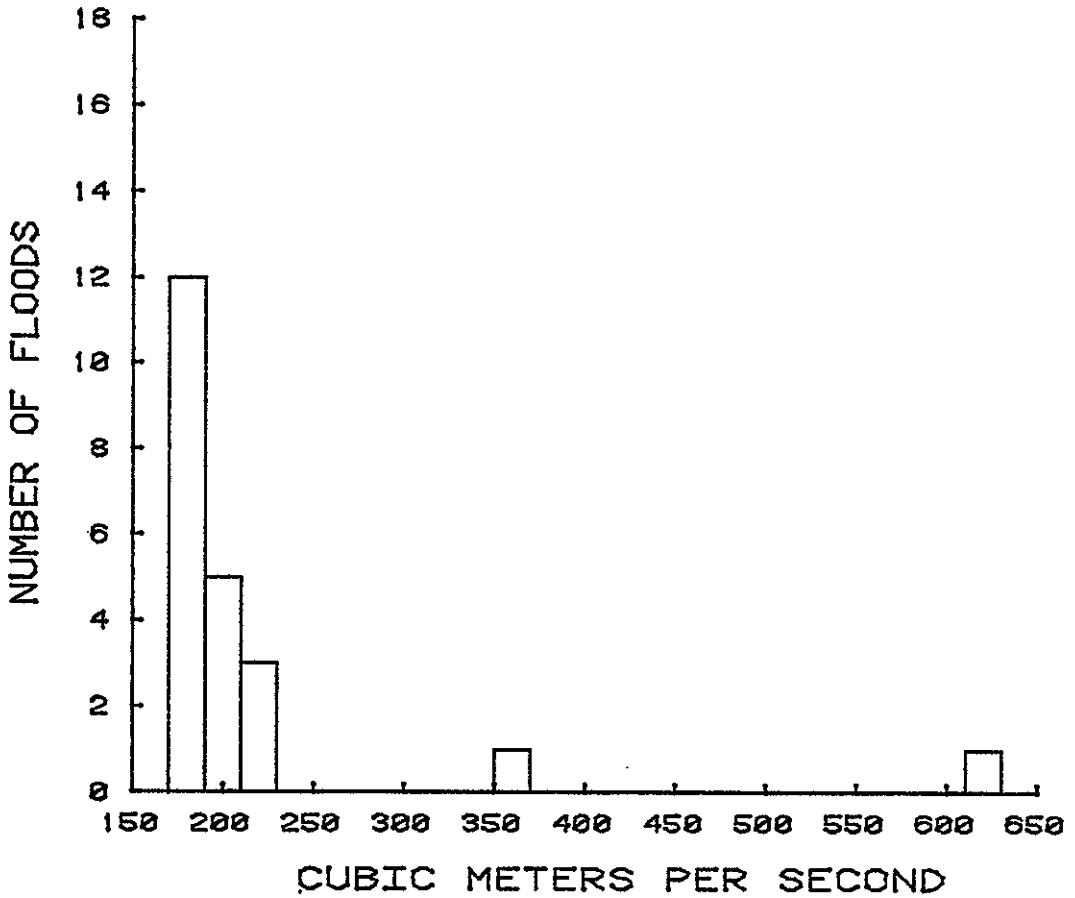
NUMBER OF FLOODS
18
16
14
12
10
8
6
4
2
0
150
200
250
300
350
400
450
500
550
600
650
CUBIC METERS PER SECOND

B.

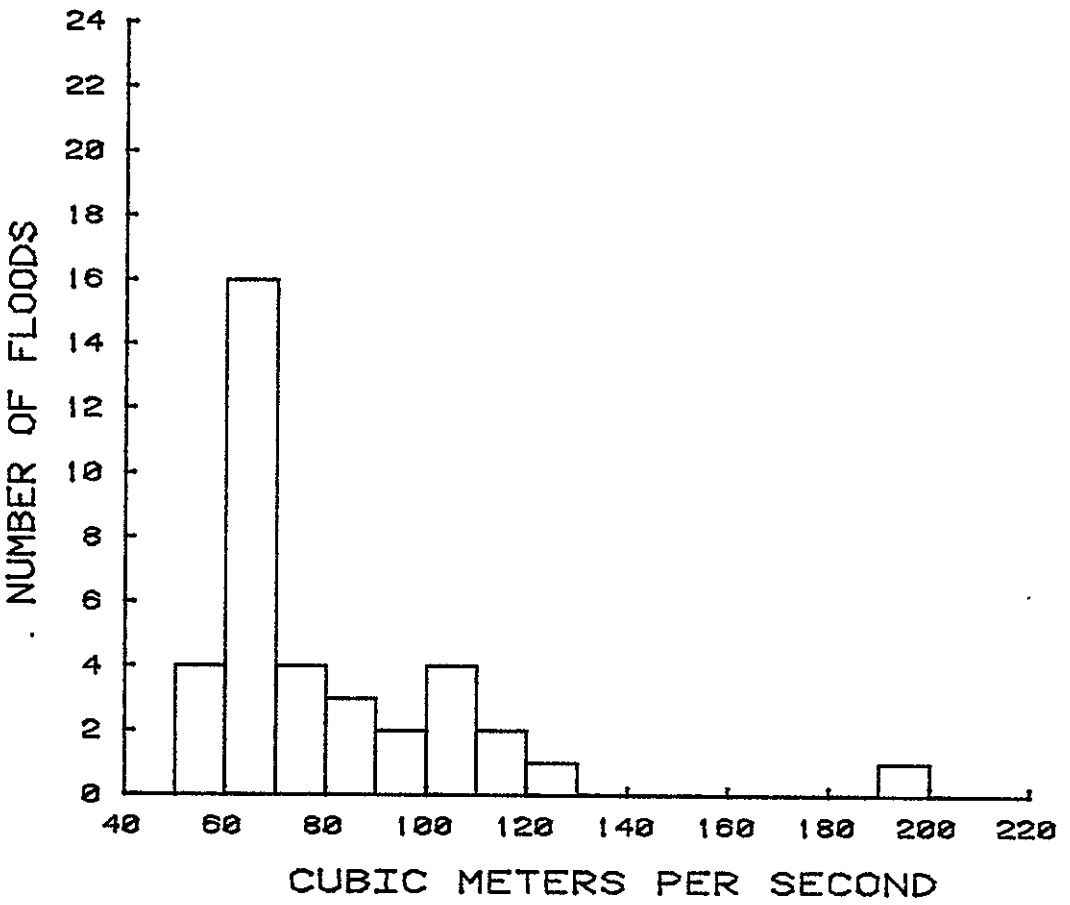
NUMBER OF FLOODS
24
22
20
18
16
14
12
10
8
6
4
2
0
40
60
80
100
120
140
160
180
200
220
CUBIC METERS PER SECOND

C.

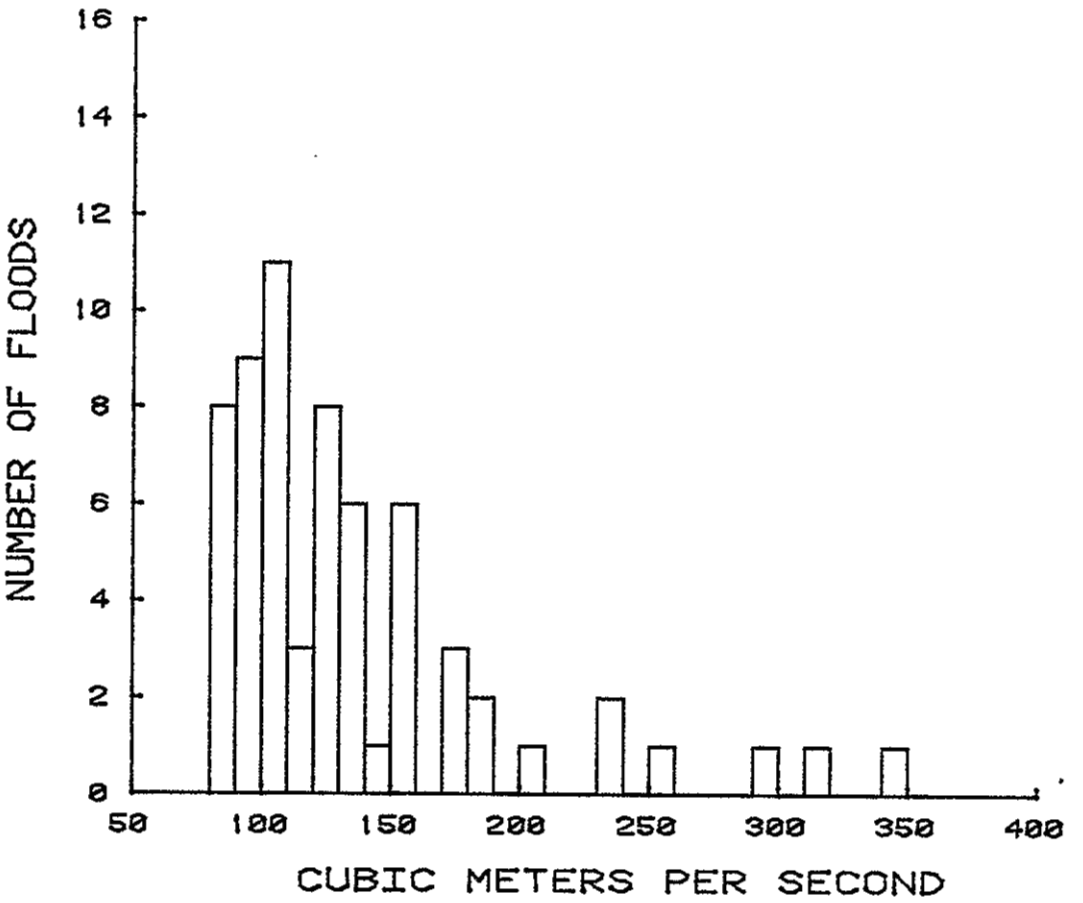
NUMBER OF FLOODS
16
14
12
10
8
6
4
2
0
50
100
150
200
250
300
350
400
CUBIC METERS PER SECOND

D.

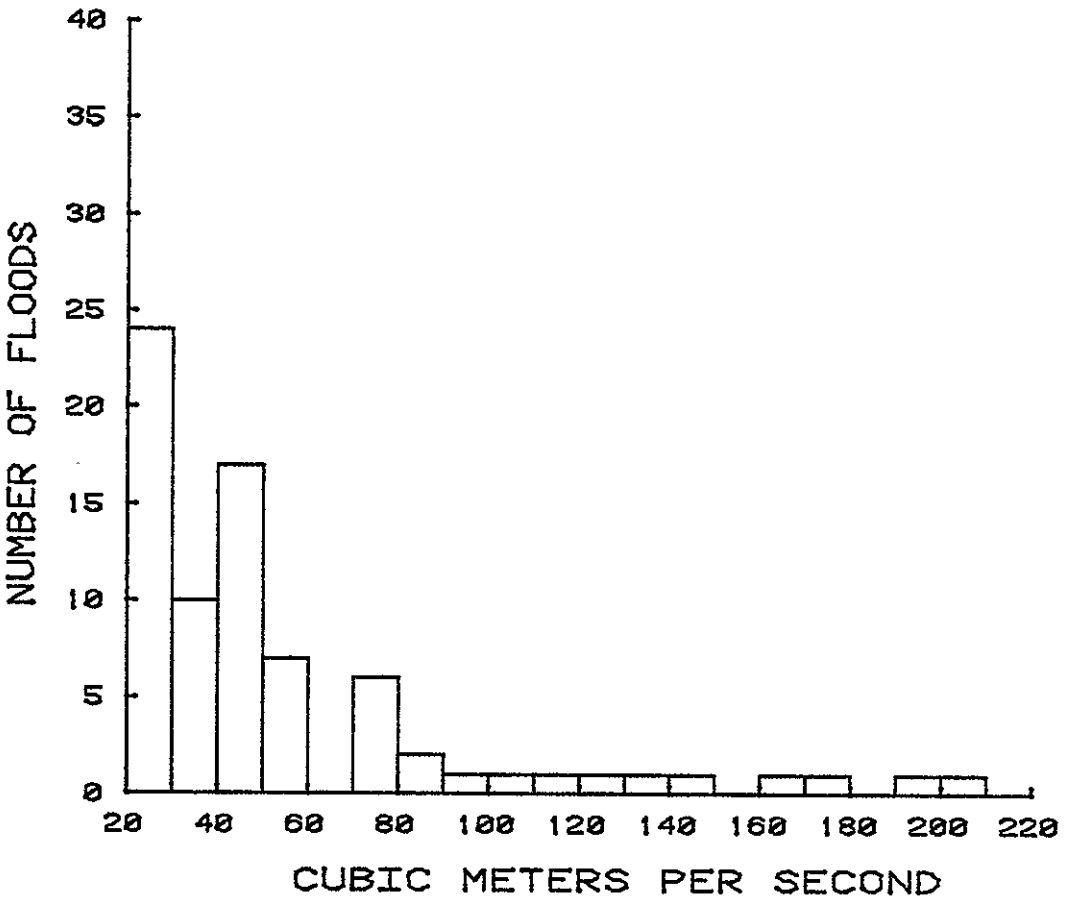
NUMBER OF FLOODS
40
35
30
25
20
15
10
5
0
20
40
60
80
100
120
140
160
180
200
220
CUBIC METERS PER SECOND

E.

II. METHODS AND PROCEDURES

A. Selection of Sample Sites

In order to select sample sites, the general sources and transport directions of sediments were determined by examination of maps and aerial photographs and by field reconnaissance of the drainages. The maps used included 1:250,000 and 1:100,000 scale maps of the region, and 1:24,000 and 1:62,500 scale maps of segments of the drainage basin and 1:500,000 and 1:24,000 geologic maps. Sites were selected on the basis of (1) their location within the drainage basin, (2) the degree of development of abandoned channels which have been active loci of deposition during the past 40-50 years and contiguous active stream channels for comparison, and (3) accessibility. The general areas considered for site location were (A) upper part of Rio Puerco upstream from all uranium mines, (B) central part of Rio Puerco in reaches of possible influence of mines and natural radionuclides, (C) downstream portions of Rio Puerco where radionuclides would have had to have been transported, and (4) along major tributaries directly downstream from mine activity and natural exposures of mineralized rocks (see Figure 1).

Locations of sample sites were chosen on the basis of comparing the position of the inner channels of streams on early maps and aerial photographs with later photographs (see site descriptions for comparisons). In each case, the time of oxbow formation (neck and chute cutoffs) could be bracketed by comparing dated sequences of photographs (e.g. between 1935 and 1954, between 1947 and 1954, or between 1954 and 1972). Locations and depths of samples are given in Table 2.

B. Age of Samples

The age of the cutoffs was partially determined by examination of aerial photography. Historic photographs (Happ, 1948, plate 4) were used at one site to help determine the age of the site. In the field, archeological and historical items were sought in relation to the sample sites. Unfortunately, the only site which yielded an historic artifact (portion of old, light gauge rail for railroad) was unsuitable for sampling due to lack of floods after cutoff. Recently, it was shown that tamarisks can record annual rings and that deposits may be dated by analyzing where and when

tamarisk germination took place (R. Hereford, 1982; 1983, written communication). This technique was used successfully on the sample site which had the least time control (D. Heath, 1983, personal communication; see Site 2, below). Surveyors notes, historical accounts and archeological studies (Betancourt, 1980; Love and others, 1983) were useful in determining long-term behavior of the Rio Puerco, but were not used for selecting sample sites. The 1938 date for construction of Paguate Reservoir was provided by the Laguna Tribal Agency.

C. Surveying Procedures

Topographic profiles across arroyos, detailed stream gradient determinations and detailed profiles across inner channels were done by surveying with a theodolite (commonly a 20" instrument with 7.62 m rod). In two locations, profiles across the inner channel were measured with metric tapes. Elevations were calculated to the nearest centimeter. Distances were measured to the nearest foot and converted to meters.

D. Estimation of Bank-Full Discharge at Ungaged Locations

Williams (1978) investigated numerous methods of estimating bank-full discharge. He found that definition of "bank-full" varied from method to method and that few of the previously proposed techniques came close to predicting measured bank-full discharge in his more extensive data set. Williams found that the best estimators of bank-full discharge (Qb) was the bank-full cross-sectional area of the stream (Ab, in m2) and the slope (S, dimensionless, m/m):

$$Qb=4.0Ab^{1.21}\ S^{0.28}$$

The equation has a standard error of 0.174 log units or an average standard error of 41 percent. It accounts for 96 percent of the sums of squares of log Qb (Williams, 1978). Williams indicated that there appears to be more error for streams with small bank-full discharges (which would include the Rio Puerco). In spite of the large possible error of the estimate, the equation is better than other presently available techniques (including the popular Gaukler-Manning equation, Williams, 1978).

The cross-sectional areas of bank-full discharge and slopes of reaches near the sample sites (estimated using a theodolite) are presented in Table 2

Site Location	Cross-sectional area (m^2)	Slope (m/m)	Bank-full Discharge (m^3/sec)
1	16.8	.00095	17.2
5	38.2	.0013	51.1
6	97.9	.0011	152.3
8	50.8	.0033	93.6
SJ 1	16.3	.0057	27.6

TABLE 2. Estimates of "bank-full" discharge for Rio Puerco at three locations and Rio San Jose at one location.

along with a possible range in bank-full discharge for each locality. Caution should be used in interpreting these numbers, however, because the hydraulic geometry (width, depth, gradient, etc) of the Rio Puerco changes along each reach and changes with each flow. Studies of the Rio Puerco channel (Young, 1982) determined that more than 90 percent of the channel along the lower Rio Puerco has shifted laterally since 1954. The shape of the channel has changed as well, being relatively wide with low banks and unvegetated point bars in the 1930's to being relatively narrow with high banks in the 1980's. The change in channel shape affects the magnitude and frequency of overbank floods and the efficiency of transport of sediments.

E. Examination of Sediments and Sampling Procedures in the Field

Sampling at sites consisted of taking 2-kg samples of typical surface deposits near a designated sample site and by digging and augering below the surface. Commonly the pits dug to expose stratigraphy and sedimentary structures were 1.5 m deep, 2 m long and 0.75 m wide, with steps cut in the south wall to let in sunlight and to facilitate entry for description and sampling. Approximately 2-kg sediment samples were taken in vertical succession from each unit of interest exposed in the walls of the pits. Once the floor of the pit had been cleaned, two auger holes were sunk approximately 40 cm apart, using a 7.62 cm-diameter auger which took 15 cm incremental samples. Possibly contaminated material at the very top of each sample was discarded, as was any contamination visible on the sides of the sample. Samples from the same depth in both holes were combined in order to insure at least 2 kg of sample for lab work. Depths of each hole were checked during sampling to insure that the same intervals were being sampled in both holes. Augers disrupt the sample in part, but chunks of sediment remain intact to aid description of each sample interval. The Munsell color (chroma and hue), grain size and texture of each sample were described in the field along with sedimentary structures and other notable features (such as organic remains and evaporite crystals within the matrix). The sample number and description were recorded in one or more notebooks, and the sample was placed in a plastic sample bag and sealed.

F. Sample Handling in the Laboratory

In the laboratory, 450 mL of material were removed from each sample, using a riffle splitter with 1¼ cm openings. Any pebbles coarser than 1¼ cm were also removed at this point, as were any clay balls (armored mud balls), twigs, and similar objects.

A series of additional, smaller samples were further characterized by a variety of techniques. These included wet-sieving through 80- and 230-mesh U.S. Standard stainless steel sieves (mesh openings 175 and 63 microns, respectively), examination of the size fractions under a 400X optical microscope, determination of the percentage of clay-size material in the finest size fraction, X-ray diffraction analysis of clay-size fractions and selected sand-size material, and chemical analysis. It was found that copper contamination was signficant if brass sieves were used so it was necessary to use stainless steel sieves.

G. Determination of Pb-210, Cs-137, and other Radionuclide Activities

The previously obtained 450 mL splits were mixed to ensure homogeneity and transferred to plastic Marinelli beakers. These were sealed with tape and, if Pb-210 analysis were desired, allowed to stand for a minimum of two weeks to allow for Rn-222, and hence Pb-214, ingrowth. Procedures for Pb-210 followed those of Schery (1980).

Activities of the radioisotopes Pb-210, P-214, and Cs-137 used for dating were obtained by gamma spectrometry, using an N-type, high purity germanium detector. These gamma spectra were obtained using one of three lead-shielded Ortec Gamma-X spectrometers linked to a 4096-channel pulse-height analyzer. Minimum counting times for Cs-137 and Pb-210 were 4,000 and 16,000 seconds, respectively, and the energy range of the spectra in both cases was approximately 0-1500 KeV. For low levels, counting times of about 40,000 seconds were found to be sufficient. Activities of the radionuclides Th-234, Ra-226, Th-230, Pb-214, and Bi-214 from the U-238 decay series and Ac-228 and Pb-212 from the Th-232 decay series were also determined.

The efficiency of each detector at a number of different energies was determined by counting several sediment samples impregnated with known quantities of nine radionuclides (Reference Standard QCY, 44, Amersham Corp., Amersham, England). As the efficiencies were found to be largely unaffected by the mean grain size of the sediment matrix of the standards, values obtained

from a mixture of equal quantities of medium sand and silty clay were used. Efficiencies at other energies were found by interpolation, using programs provided for this purpose by Nuclear Data Corporation (ND 6600, 1980).

The areas of the Pb-210 peak at 46.5 Kev were calculated using a peak area extraction program also provided by Nuclear Data (1980). The areas of selected peaks were checked visually to verify the accuracy of the program, and to verify that these peaks had been adequately resolved from neighboring peaks in the spectrum.

Activities of each isotope (in pCi/g) were calculated from the peak areas, sample weights, and branching ratios, using previously determined efficiencies at these energies. The branching ratios for measured Pb-210, Pb-214, and Cs-137 decays were taken to be 4.05%, 37.2%, and 84.6% respectively (Erdmann and Soyka, 1979). Where necessary, corrections were made for the presence of peaks at the same locations in background spectra.

H. Trace Metal Analysis

Selected 230- fractions and clay fractions were digested by the following hydrofluoric acid-aqua regia-perchloric acid digestion prior to determination of metals (Johnson and Maxwell, 1981). The hydrofluoric, nitric, and hydrochloric acids used were redistilled in Teflon (Mattinson, 1972) from Baker Reagent Grade acids.

For every 1.00 gram of sample added to a Teflon beaker, a few milliliters of distilled water were added. Six mL of hydrofluoric acid and 6 mL of aqua regia were added to the resulting slurry and the solution evaporated to near dryness in a hood. A mixture of 6 mL of hydrofluoric acid and 2 mL of perchloric acid was added and subsequently evaporated to dense white fumes near dryness. The solution was brought up to desired volume with 10% nitric acid.

In general 2.00 g of 230- fraction samples and 0.25 g of clay samples were digested and brought up with 10% nitric acid to a total final volume of 100 mL for analysis. To test the analytical procedures, SY-2, SY-3, (Canadian Certified Ref. Mat'l.), SL-1 (Canadian Atomic Energy Commission), and NBS 1645 river sediment were used as standard materials and digested according to the procedure described above.

Mercury (Hg) was determined by cold vapor atomic absorption on a Coleman MAS-50 spectrophotometer according to EPA procedures (1979). The

trace metals As, Cd, Cr, Cu, Mo, Ni, Pb, Se, and V were determined on a Perkin Elmer 403 atomic absorption spectrophotometer (A.A.) As and Se were determined by hydride generation with a Perkin-Elmer Mercury Hydride System (MHS-10) using electrodeless discharge lamps. Cr and Cu were determined by direct aspiration techniques as described by EPA standard methods 218.1 and 220.1, respectively (1979). Mo, Ni, Pb, and V were determined by furnace techniques on either a Perkin-Elmer HGA 2000 or HGA 400 graphite furnace as described by EPA standard methods 246.2, 249.2, 239.2, and 286.2 respectively (1979). Generally, charring temperatures 50 to 100 degrees lower than those recommended as general operating parameters by the manufacturer were employed for Pb. Uranium was analyzed spectrophotometrically with dibenzoylmethane after separation by solvent extraction with tri-n-octylphosphine oxide adapted from the procedure described by Houston and White (1958). Generally a 5 mL aliquot of the acid digested material was sufficient due to the high U levels in the sediments.

Sensitivities for the various metals are shown in Table 2

Metal	Sensitivity - ppg (µg/L)
As	2.0
Cd	0.3
Cr	1.0
Cu	0.5
Hg	1.0
Mo	1.0
Ni	1.0
Se	2.0
U	5000
V	2.0

Table 3. Analytical Sensitivities for Metals

I. Neutron Activation Analysis Procedure for Ba, Cr, Cs, and Fe

Samples were disaggregated by grinding and approximately 0.500 grams were placed in plastic vials. The weight, to the nearest milligram, of each of these samples was recorded. After the vials were sealed, they were irradiated at the Sandia National Laboratory reactory facility.

Data was collected on a series of samples from the Rio Puerco in the form of seven day and thirty day counts. These samples varied in order to represent the various size fractions within a sample, the sample sites themselves, and the various types of beds sampled at each site. Clays were chosen as the most representative portion for irradiation since by surface area phenomena they should concentrate the most trace metals.

The samples were then counted approximately seven days after irradiation for 4000 seconds and again thirty days after irradiation for 5000 seconds on a Nuclear Data ND6600 system using MIDAS 7 or MIDAS 8 operating systems. The detector was a Canberra model 7229 (with a cryostat model 7500) operated at 2000 volts. The data are summarized in Appendix G.

The counts obtained were compared to standard materials SL-1, and NBS 1645 which were irradiated with each set of samples by standard routines available from Nuclear Data Corporation. Barium was determined from the decay of Ba-131 which has a half-life of 12 days. The peaks used for this determination are a thirty day peak at 124 KeV, a seven day peak at 216 KeV, and a seven day peak 496.2 KeV. These three peaks are averaged to obtain the final value and associated analytical error.

Chromium was determined from decays of Cr-51 which has a half-life of 27.8 days. The concentration was determined from the peak at 320.1 KeV in the thirty day count.

Cesium was determined from the decay of Cs-134 which has a half-life of 2.05 years. The concentration is determined from the peak at 797.0 KeV in the thirty day counts.

Iron was determined from the decay of Fe-59 which has a half-life of 45.6 days. The concentration is determined from the peaks at 192.2, 1099.3, and 1291 KeV in the thirty day counts.

J. Determination of Relative Proportions of Silt and Clay

A representative portion of the crushed <63 micron fractions of the sample was obtained using a riffle splittler with 1.25 cm openings. This material was weighed to the nearest 0.01 g and dispersed in approximately 100 mL of water. A 1.0 mL volume of 50 g/L sodium hexametaphosphate solution was added to promote disaggregation of the sediment and prevent flocculation. The sample was placed on a magnetic stirrer and allowed to stir for approximately 18 hours. An alternative procedure involved stirring for about

3 hours in distilled water followed by sonification with a Bronson Sonifier for 8 minutes at a setting of 6.5.

Additional water was then added to the sample, such that the final depth of liquid was equal to the distance which a particle of 2 micron effective spherical diameter would settle in six hours according to Stokes' Law (assuming a particle density of 2.6 g/cm^3 and a viscosity equal to that of pure water at the ambient air temperature). The sample was stirred rapidly for one minute to ensure complete homogeneity, and allowed to settle for the six hour period.

The majority of the liquid (the clay suspension) was then removed by siphoning and pipetting, in such a manner that the material which had settled to the bottom of the beaker was not disturbed. The latter material was then transferred to a weighed, stoppered glass tube, and water added until the level of liquid equalled the distance a 2 micron particle would settle in 16½ hours. The sample was mixed by repeatedly inverting the tube, and allowed to settle for the required time. This was repeated two more times. The majority of the liquid was again pipetted off, and the settling tube dried at 80°C and reweighed. The weight of the silt in the tube was calculated by difference, and converted to a weight percentage.

K. X-Ray Diffraction Analysis of the Clay Size Fraction

A small quantity of clay-size material was obtained for X-ray analysis by the ultrasonic procedure treatment previously described. Four oriented mounts of this fraction were then prepared by placing 15-20 drops of clay suspension on glass slides and allowing the mounts to air-dry. One mount was subsequently heated to 350°C for 1 hour and placed in a dessicator containing phosphorus pentachloride. A second mount was heated to 550°C for 1½ hours and allowed to cool in air, and a third mount was placed in an ethylene glycol-saturated dessicator and heated to 60°C for 1.5-2 hours. A partially unoriented ("smear") mount was also prepared by placing a thick past of <2 micron material on a glass slide and spreading it uniformly over the exposed surface.

Diffractograms were made of each mount, extending from 3° to 33° 2θ for the oriented mounts, and from 3° to 65° 2θ for the smear mounts. A Norelco Philips Model 5001 X-Ray diffractor was used, with CuKa radiation (40KV/20mA), 1° - 4° - 1° slits, 3% standard deviation, and a recording speed of 2° 2θ/minute.

Peak intensities above background were measured, and normalized using the intensity of the quartz peak at 26.65° 2θ.

The ratio of discrete montmorillonite to discrete illite was estimated from the (normalized) heights of the montmorillonite and illite (001) peaks at approximately 5.8 and 8.8° 2θ in the glycolated slides, assuming a characteristic intensity ratio of 4:1(Dr. George Austin, NM Bureau of Mines, Personal Communication). The ratio of montmorillonite to illite in mixed layers was arbitrarily assumed to be the same as that of the discrete minerals, and the proportion of mixed layering estimated from the increase in height of the peak at 8.8° 2θ in the 350° slide over that resulting from the shifting of the montmorillonite (001) peak to this position.

The ratio of chlorite to kaolinite was estimated from the (normalized) heights of the kaolinite (002) and chlorite (004) peaks at approximately 25° 2θ, assuming an intensity ratio of 2:1 (Dr. G. Austin). The height of the chlorite (004) peak in this calculation was that measured in the 550° slide, and the height of the kaolinite (002) peak was obtained by subtracting this height from the height of the combined peaks in the air-dried slide.

The ratio of illite to kaolinite was estimated from the (normalized) heights of the illite (001) peak in the glycolated slide and the kaolinite (001) peak, assuming an intensity ratio of 1:1 (Dr. G. Austin). Again, the height of the kaolinite peak was calculated from the height of the chlorite (002) peak at 12.5 - 13° 2θ in the 550° slide and the height of the combined peak at this position in the air-dried slide. This ratio was then used in conjunction with the previous ratios to calculate the fraction of each clay mineral (expressed in tenths).s

The calculations can be summarized in the following equations:

$$M' = \frac{M}{4} + \frac{M/4}{(M/4) + I} X (S_1 - I - (M/4))$$

$$I' = I + \frac{I}{(M/4) + I} X (S_1 - I - (M/4))$$

$$K' = S_2 - C_2 \text{ , and}$$

$$C' = 2K' X \frac{C_4}{S_3 - C_4} \text{ , where}$$

M, I and S_1 are the normalized intensities of the montmorillonite and illite (001) peaks in the glycolated slide, and the combined peaks in the 550^{o} slide.

It should be noted that the values obtained by this method are subject to considerable inaccuracies, and are therefore only semiquantitative (as are virtually all estimates of this type).

Relative amounts of the non-clay minerals present in the clay-size fraction were estimated from smear slides. The peaks used were those of quartz at 26.65^{o}, calcite at 29.4^{o}, and clay at 19.8^{o} 20. The intensity ratios of these peaks were assumed to be 20 : 10 : 2.5 : 1 (Schultz, 1964).

III. RESULTS AND DISCUSSION

A. Geologic Description of Sample Locations

1. Rio Puerco

a. Sites 1, 1A, 2, 2A

The study sites near Popalitito Windmill (Table 4, sites 1, 1A, 2A; Fig. 1) were chosen for their position in the lower part of the drainage basin and because the oxbow is particularly well developed (Fig. 12). Figure 13 shows positions of the inner channel in 1954 and in 1979. The channel cutoff occurred sometime after 1954. There are no known photographs of the site between 1954 and 1972. During reconnaissance and pit excavation, no historic artifacts were found to indicate a possible time for channel abandonment. However, in a related study of the cutoff, Heath (1983, written commun.) determined that tamarisks growing in the sand plug about 2 m above the present channel at the downstream end of the oxbow germinated in 1960. Therefore the sand plug was in place in 1960. Heath estimates that the oxbow formed in 1957. The oxbow at Popalitito continues to be inundated. Two floods in 1982 (August 28; September 19) flooded the site. Water from the second flood was still 24 cm deep in February, 1983.

Figure 14 is a cross-arroyo profile of the sample sites, showing the relative elevation of the present inner channel, the inner floodplain, the oxbow and the 10 m walls of the arroyo. Profiles of the present inner channel (Fig. 15) suggest that flooding of the oxbow presently occurs at discharges of greater than about 17 m^3/s (depending on channel geometry and formula used). Even though channel geometry has changed in the past 25 years, the size distribution of floods at Bernardo (Fig. 10A) and Rio Puerco (Fig. 10B) suggest that more than 22 floods have reached the oxbow since 1957.

Sediment within the oxbow is dominated by overbank clay from the Rio Puerco (Fig. 16 and 17). Although natural pipes and short dendritic tributaries debouch from the arroyo walls into the area of the oxbow, alluvial fans from these tributaries are minor and do not affect sample site 2-2A.

Detailed descriptions of the trench walls and auger samples are given in Appendix A. Briefly, in oxbow site 2-2A, laminated silts and clays occur from the surface to a depth of 2.41 m (Figs. 17 and 18), resting on sand and coarse sandy gravel of the 1954 channel. Sand interpreted to be part of the

SITE	QUADRANGLE	UTMG COORDINATES		DEPTH (m)
1A	Belen NW	3837000 N,	326220 E	4.27
2A	Belen NW	3837000 N,	325825 E	5.05
3A	Rio Puerco	3852950 N,	317940 E	6.71
5	Rio Puerco	3833060 N,	317760 E	3.94
6	La Mesita Negra	3884940 N,	322680 E	5.18
7	La Mesita Negra	3884880 N,	322800 E	8.62
7A	La Mesita Negra	3884880 N,	322800 E	1.72
8	Guadalupe	3940820 N,	302700 E	0
9	Guadalupe	3940700 N,	302600 E	2.54
10	Guadalupe	3940900 N,	301520 E	0
11	Guadalupe	3940900 N,	301420 E	0
SJ-1	South Garcia	3868700 N,	304950 E	1.50
SJ-5	Mesita	3882760 N,	286940 E	2.0
PAG-1	Mesita	3883430 N,	288145 E	2.20

TABLE 4. Site Numbers, Topographic Quadrangle Location, UTMG Coordinates and Depth of Sampling.

Figure 12. Oxbow and arroyo walls at site 2. Photograph by C.J. Popp, 1979.

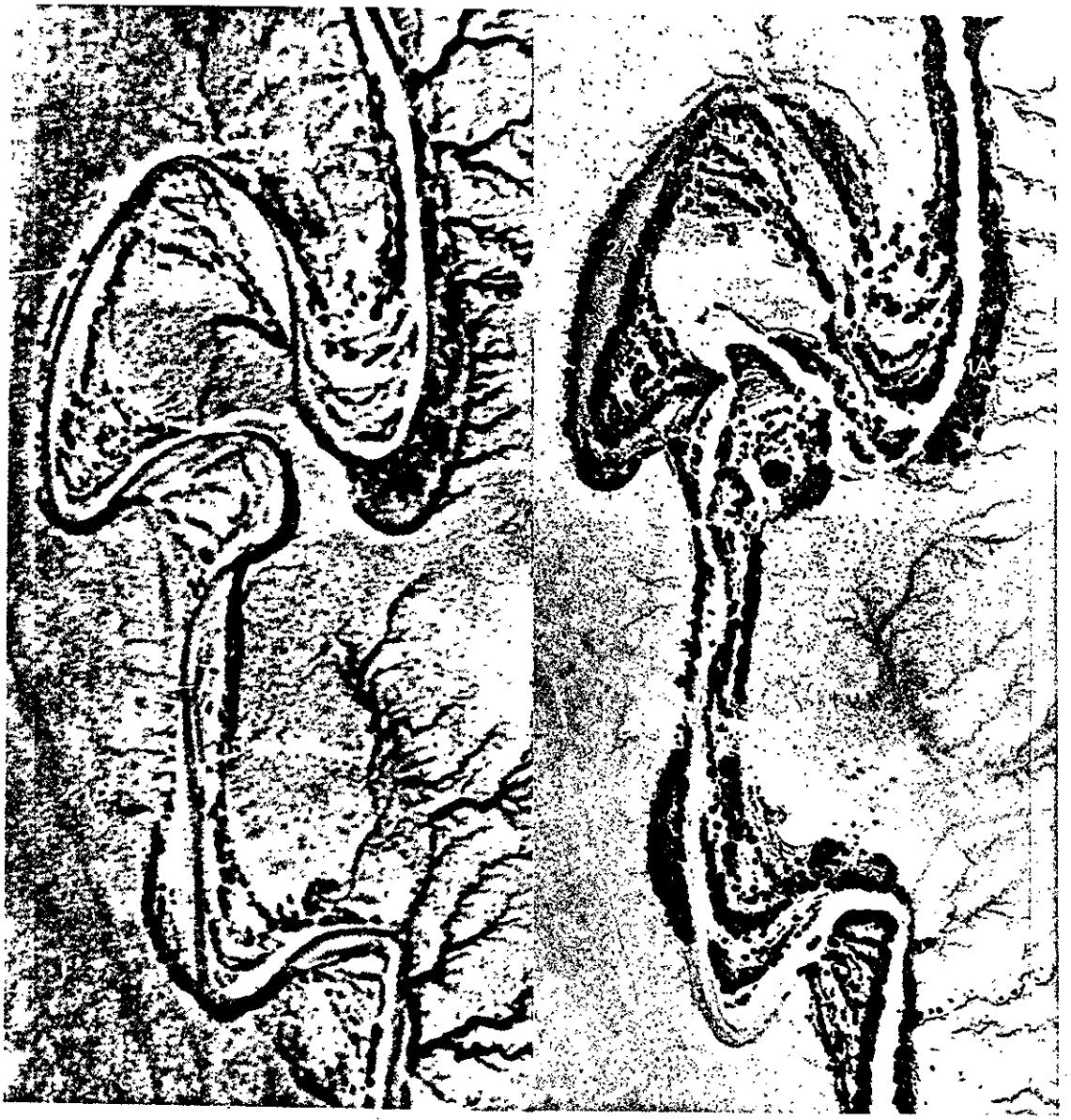

A. B.

Figure 13. Aerial photographs of the area including sites 1 and 2 taken in 1954 (A) and 1979 (B).

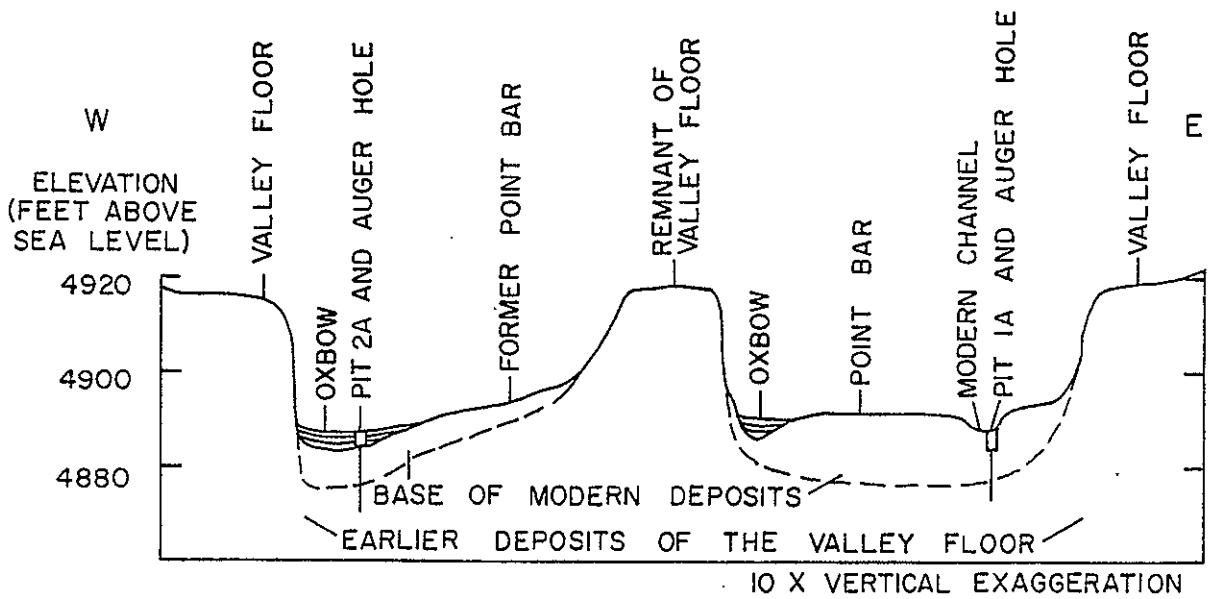

Figure 14. Cross section of Rio Puerco Arroyo at sample sites 1A and 2A.

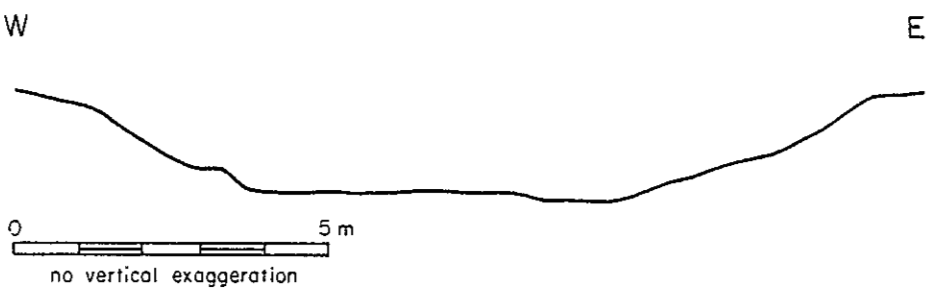

Figure 15. Profile across inner channel of Rio Puerco near site 1A (from data of D. Heath, 1983).

Figure 16. Sample site 2A in oxbow fill. Photograph by J.W. Hawley, February, 1981.

Figure 17. Pit exposing laminated silt and clay in oxbow at site 2A. Photograph by D.W. Love, February, 1981.

Figure 18. Laminated and structureless silt and clay in upper 1.1 m of oxbow deposits at site 2A. Tape measure is 1.25 cm wide. Photograph by D.W. Love, February, 1981.

1954 channel continues to a depth of 5.05 m (base of hole). Large clasts at the base of the hole which prevented further augering suggest that the base of the 1954 channel was nearly reached.

In sites 1 and 1A, along the present inner channel, deposits to a depth of 2.07 m consist of fine sand, silt and clay in small cross-laminated beds which appear to be modern channel-marginal bars deposited under low-discharge conditions. Below 2.07 m, there are two coarse-grained channel sequences, one to a depth of 2.92 m and one below 3.09 m to at least 4.27 m at the bottom of the auger hole. The upper coarse-grained sequence is part of the modern (post-1950) channel. The lower coarse-grained sequence may be either modern or a buried channel in the valley fill.

b. Sites 3, 3A, 4 and 5

Study sites 3-3A, 4 and 5 were chosen because of their accessible location downstream from the confluence of the Rio San Jose and Rio Puerco and because the oxbow appeared to be receiving sediments both before and after 1950. Figure 19 shows the position of the channel in 1936 and 1954. The present inner channel has shifted about 60 m east of its position in 1954 (Fig. 20; Wells and others, 1982). Figure (19) suggests that the oxbow continued to receive sediments after 1954.

The cross profile of Rio Puerco Arroyo in this reach (Fig. 20) shows extensive development of the floodplain between the inner channel and the oxbow. The inner channel (Fig. 21) is relatively narrow compared to the channel at localities upstream and downstream. Alluvial fans from natural pipes debouching along the arroyo walls (Figs. 20 , 22 A) have buried the oxbow at site 3-3A.

The relatively small width and depth of the inner channel at this locality (Fig. 21) and low slope of the reach imply that the threshold bank-full discharge under present conditions is about 51 m^3/sec. Records at the Rio Puerco gaging station 2 km downstream suggest that at least 22 overbank flood events have occurred at this locality since 1950. However, because the oxbow is presently buried by sediments derived from the valley fill section to the east (Fig. 22 A and B), and the present gradient is toward the present inner channel, floods may not have reached sample site 3-3A often in recent years.

Figure 19. Aerial photographs of the reach including Sites 3, 4 and 5 taken in 1935 (A) and 1954 (B).

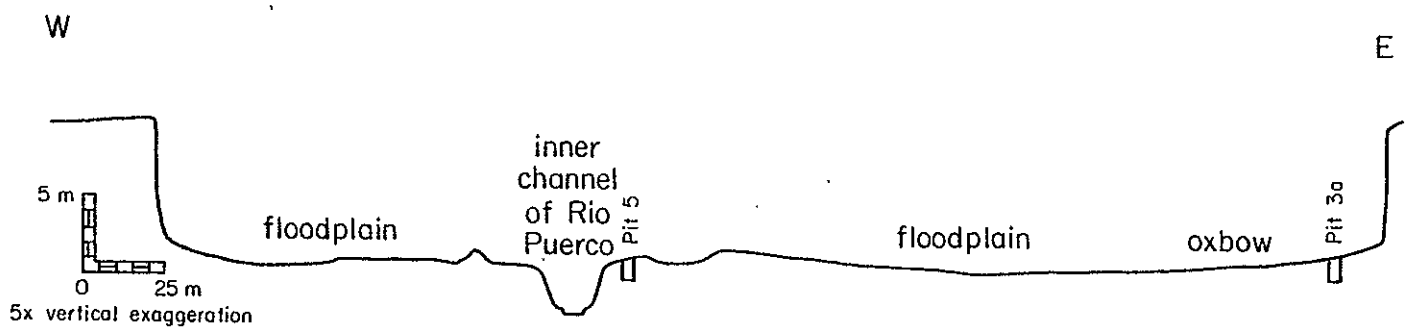

Figure 20. Cross profile of Rio Puerco Arroyo at sites 3A and 5.

Figure 21. Profile across inner channel of Rio Puerco near site 5.

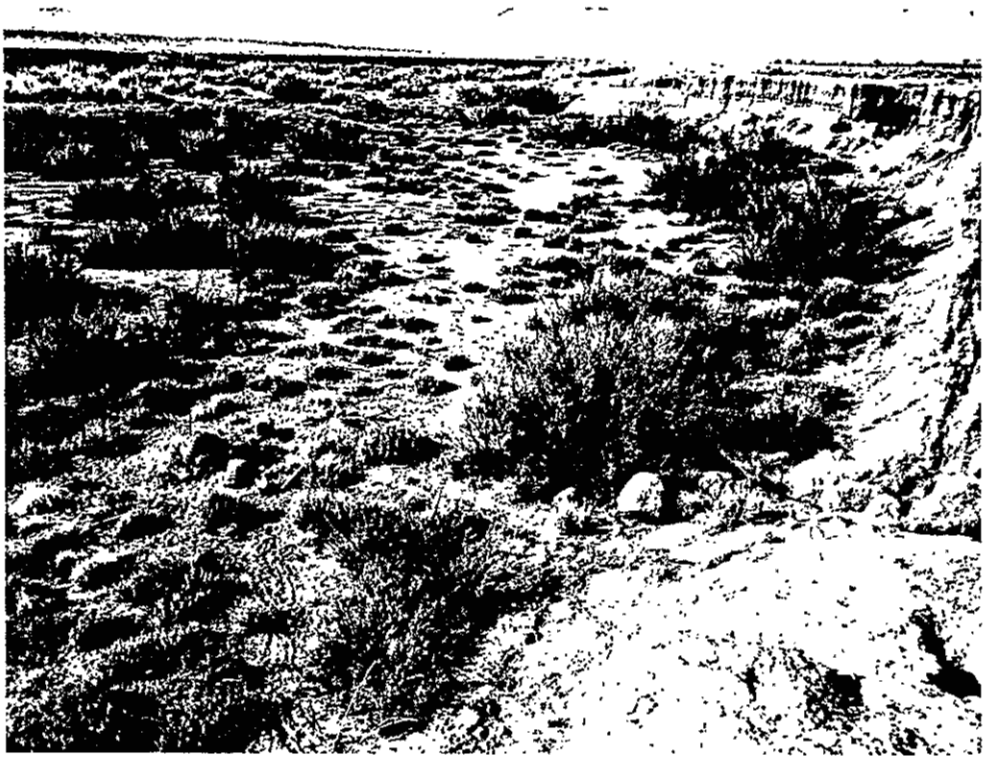

Figure 22A. Sample site 3A in oxbow and edge of tributary fan. Photograph by D.W. Love, February, 1981.

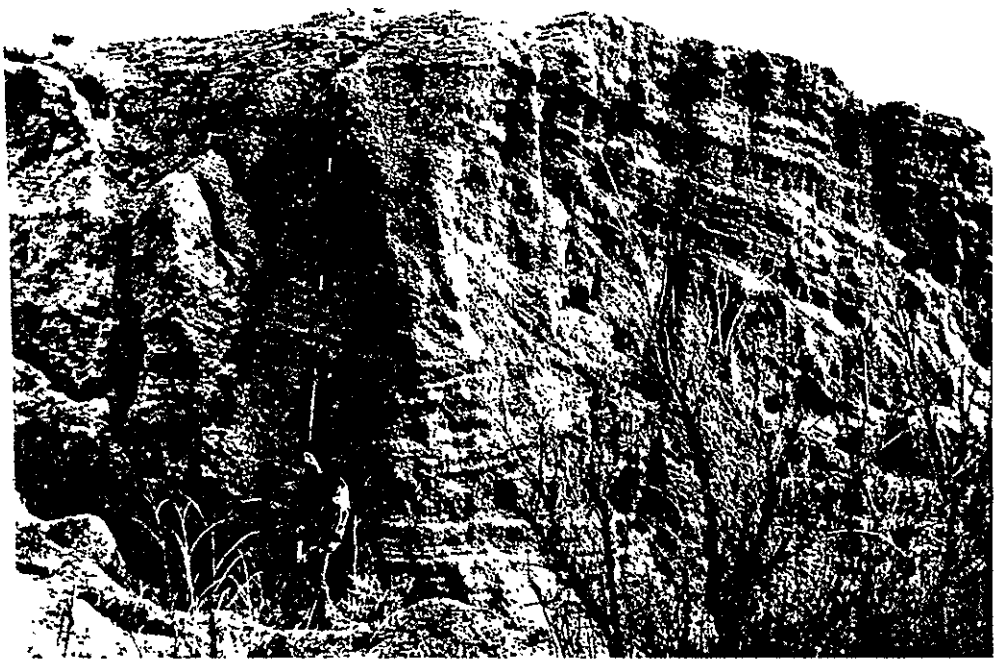

Figure 22B. Details of section of valley fill exposed in arroyo wall adjacent to site 3A. Auger is 5.2 m long. Photograph by D.W. Love, February, 1981.

The sources of the deposits are indicated by the sedimentary structures and grain sizes seen in the pits and auger holes. In pit 3A (Fig. 23 and Appendix A), sedimentary structures in the upper part of the pit (to 1.04 m) dip westward and include cross-laminated sand and clay with clay platelets. The lower part of the pit and auger hole below include horizontal clay layers up to 8 cm thick interlaminated with very fine sand and silt. Between 1.67 and 2.54 m, find sand and clay of the former channel margins predominate, overlying coarser channel sand and pebbly sand. Although it is difficult to choose a lower boundary for the 20th century deposits because the modern sands overlie a channel sand within the older valley fill, there is a break in grain size and amount of moisture at 4.17 m, which may indicate the base of modern deposits. This elevation is nearly the same as the base of the present inner channel to the west (Fig. 20). The lower channel deposits continue to a depth of at least 6.71 m.

Site 4 was an initial auger hole in the 1980 channel and was not studied further.

The location for pit 5 was chosen along the margins of the present channel because the sediments beneath the inner channel were water-saturated and impossible to excavate. Saturated sand was reached at a depth of 3.94 m in the auger hole beneath the pit at essentially the same level as the channel floor. Sediments sampled in the pit and auger hole (Appendix A) are predominantly cross-laminated fine sand (including climbing ripples) separated by westward-dipping clay drapes. Near the base of the auger hole, 0.45 m of coarse sand with mud balls occur, suggesting that the level of the former (20th century) channel had been reached. The grain size, sedimentary structures and clay drapes all indicate that the sediments above the coarse-grained layers were deposited by floods along the margin of the inner channel.

c. Sites 6, 7 and 7A

The oxbow at sample sites 6, 7 and 7A was selected for its position in the drainage basin upstream from the Rio San Jose and downstream from Arroyo Chico and other tributaries of the Grants Uranium region and its age. The oxbow was abandoned between 1935 and 1954 (Fig. 24) and was capable of receiving overbank sediments during the period of uranium mining. As both aerial photographs show, the inner channel is relatively wide (see also Figs. 5, 25 and 26). The tamarisk-dominated levees along the east bank of the channel

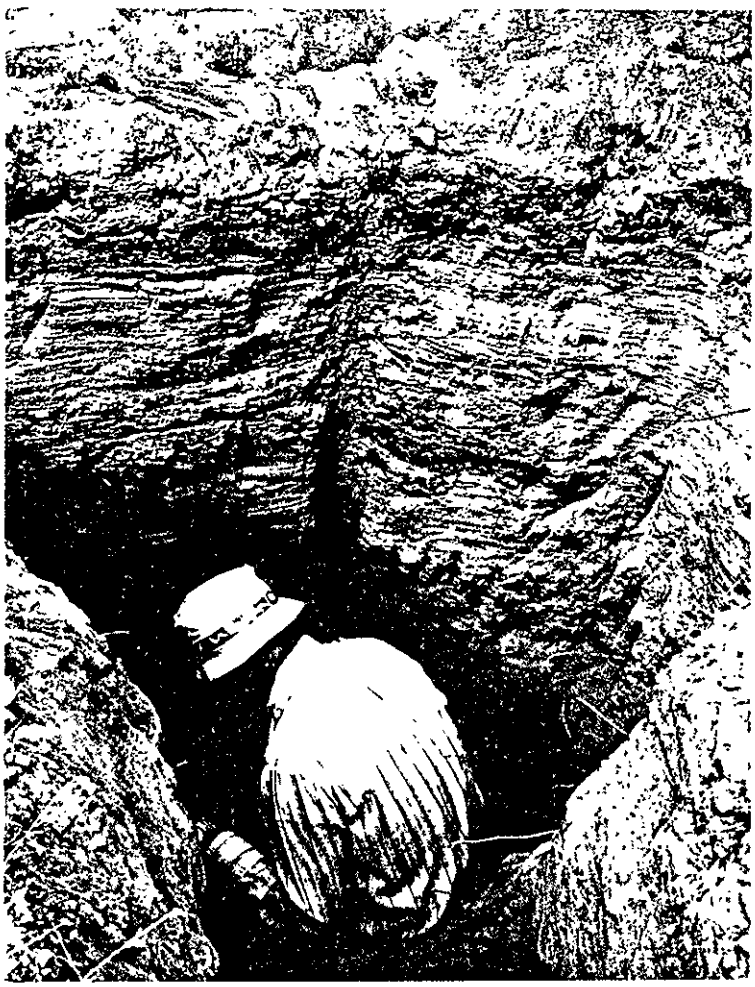

Figure 23. Cross-laminated fine sand in upper part of pit 3A. Photograph by D.W. Love, February, 1981.

A. B.

Figure 24. Oxbow at sites 6 and 7 in 1935 (A) and 1954 (B).

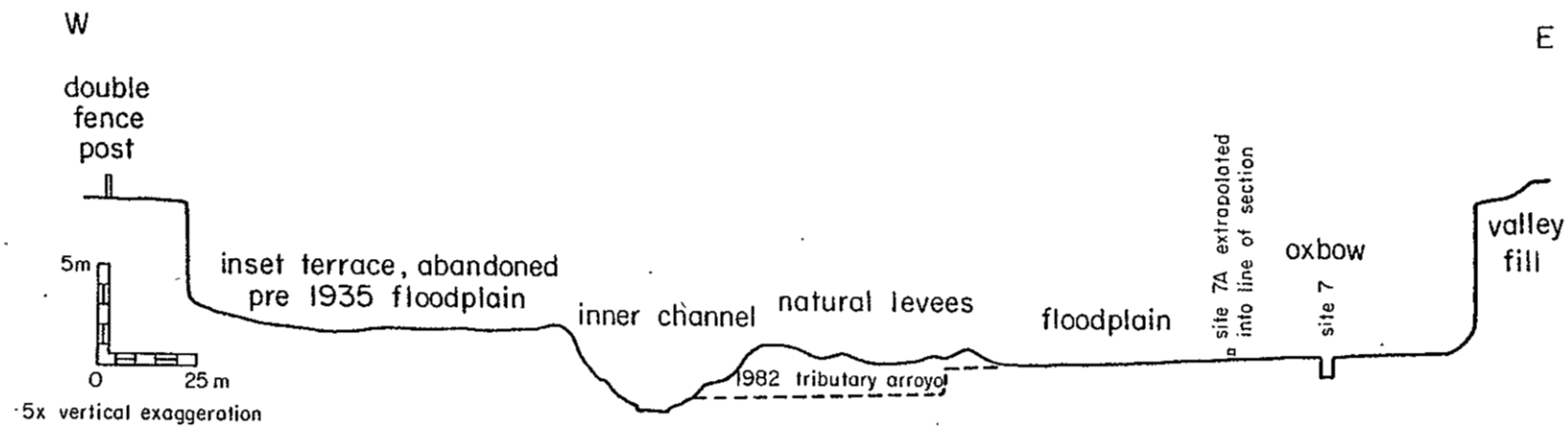

Figure 25. Profile across Rio Puerco Arroyo at sites 6 and 7.

Figure 26. Profile across the inner channel of the Rio Puerco near site 6.

are relatively high, while the floodplain east of the levees is low. Alluvial fans from active soil pipes and from a recently breached water-control structure on the valley floor to the east presently dominate deposition on the floodplain. West of the inner channel is an older, higher floodplain which is abandoned as an inset terrace. Locally-derived sediments from tributaries and natural pipes west of the arroyo continue to aggrade this terrace.

Because the inner channel at this location is wide (Fig. 26), discharge must exceed about 150 m^3/s in order to reach the floodplain. The distribution of floods at Rio Puerco (Fig.10 B) downstream and Arroyo Chico (Fig.10 E) and Rio Puerco above Arroyo Chico (Fig.10 C) suggest at least 18 floods may have exceeded the minimum for flooding.

Sample site 6 was placed on a channel-marginal bar at an intermediate level 9 m west of the east bank of the channel (Fig. 5 above) because the floor of the inner channel was water-saturated and was composed of coarse sand. Sedimentary structures within the bar included discontinuously laminated and cross-laminated sand, fining upward couplets of fine sand, silt and clay, and coarser, low-angle cross-laminated channel sand (Fig. 27). Below about 3 m, the two auger holes encountered different stratigraphy although they were only 40 cm apart. One hole penetrated predominantly coarse sand with some pebbles and mud balls. The water table was encountered at 4.2 m. The other auger hole penetrated predominantly sandy clay deposits (mudballs in part?) below 4 m and continued to be relatively dry to a depth of 5.18 m. The differences in the two holes may reflect extremely localized deposition of mudballs or perhaps a clay deposit crosscut by a later channel sand.

The upper 50.8 cm of site 7 in the oxbow to the east (Fig. 28; Appendix A) consists of cross-laminated fine sand, silt and gray clay platelets deposited in thin (5-10 cm) layers as part of an alluvial fan complex derived from the valley floor to the east. Below these clay-rich layers, the deposits consist of layers of cross-laminated fine sand, coarsening downward to pebbly sand at a depth of 3.31 m. The gravelly sand at this depth may indicate the base of 20th century deposits. Clay and rusty sand layers below the gravelly sand to a depth 8.6 m probably are older valley fill.

Because the upper 50.8 cm of clayey deposits at site 7 had unexpected geochemistry (see below), the entire oxbow area was searched for thicker sections of clay-rich fill. Site 7A was selected 36 m northwest of site 7

Figure 27. Sedimentary structures of a channel-marginal bar at site 6. Photograph by D.W. Love, April, 1981.

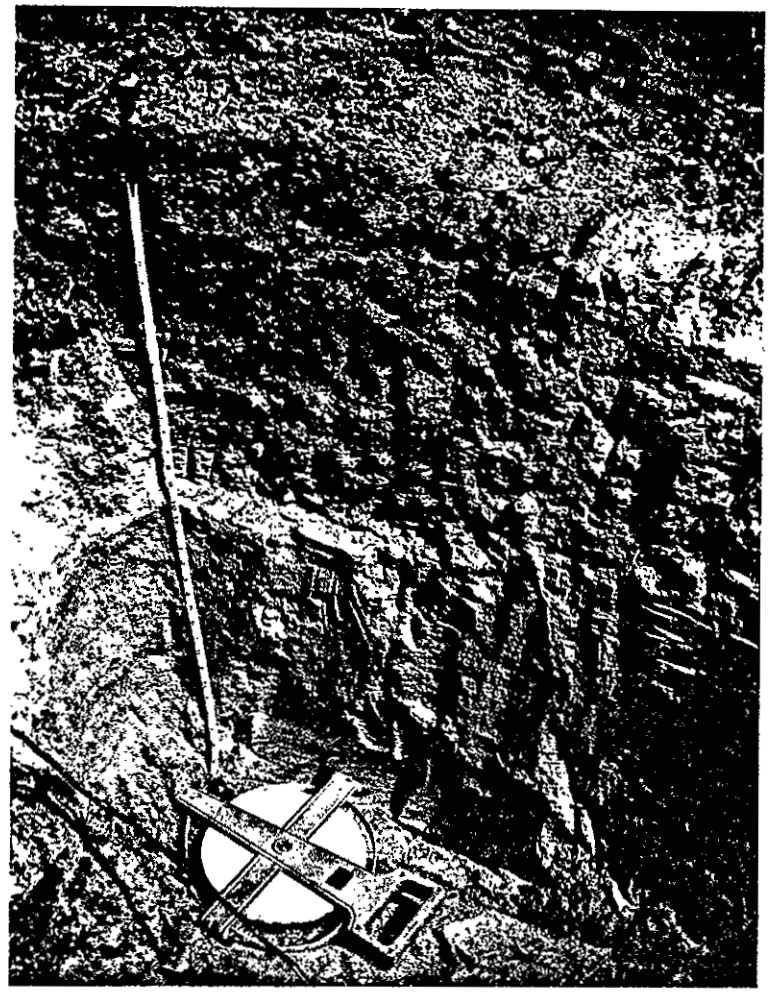

Figure 28. Stratigraphy of pit at site 7. Note change of deposits at 50 cm. Photograph by D.W. Love, May, 1981.

in order to sample more than 70 cm of similar clay (Appendix A). Fine sand was encountered from 1.28 to 1.72 m, suggesting that channel-marginal bars had been reached below the clays. Geochemical properties of the clay layers in site 7A, however, were somewhat different from clay layers in site 7 (see discussion of geochemistry), but no other thick clay deposits were found in the oxbow, so further checks on natural variations in chemistry of a single oxbow fill sequence could not be made.

During the 1982 summer rainy season, an artificial levee and the valley floor east of site 7 were eroded badly by a flash flood. The arroyo wall north of site 7 underwent rapid gullying and the alluvial fan at the surface of sites 7 and 7A received 15-25 cm of new locally derived sediment. The flood cut a new tributary arroyo channel in the vicinity of site 6 (Fig. 25), exposing the stratigraphy of the natural levees and floodplain.

From these new exposures as well as from several shallow auger holes and the auger holes at 7 and 7A, it is apparent that sedimentation in this abandoned meander was predominantly sandy, with little clay derived from overbank flooding near the sample sites. Even the channel margins (both past and present) are dominated by sand.

d. Sites 8 and 9

The location of sites 8 and 9 was selected because it is upstream from all major uranium mining, and because meander cutoff occurred between 1936 and 1954 (Fig. 29; c.f. Happ, 1948, Plate 4). The cross-profile of the locality (Fig. 30) shows the relative elevations of the oxbow and present inner channel. Extrapolated onto the line of the profile are the pit at site 9 and a remnant of older valley fill. Flood access to site 9 may be provided by lower banks along the inner channel downstream from the cross-profile. Upstream from the cross-profile, the banks at the head of the oxbow are at least as high as those of the cross-profile, and no overbank flooding appears to have occurred recently.

The two cross sections of the channel near site 8 (Fig. 31) were used to estimate bank-full discharge at about 93 m^3/sec. This amount of flow has been exceeded at the gaging station 2.4 km upstream between 8 and 10 times (Fig. 10 C). However, configuration of the inner channel has changed considerably during the past 30 years. It is not clear whether large discharges of equal magnitude have flooded similar areas in the past.

Figure 29. Confluence of Rio Puerco and Arroyo Chico in 1935 (A) and 1954 (B).

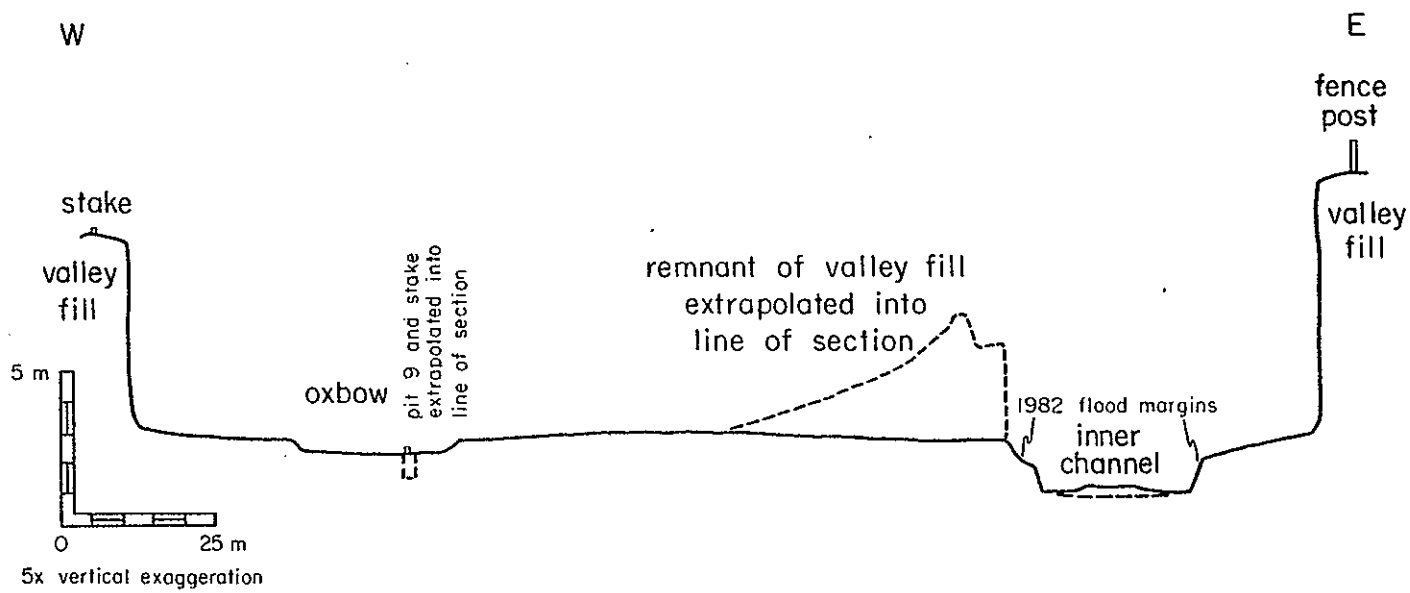

Figure 30. Cross profile of Rio Puerco Arroyo in the vicinity of site 9.

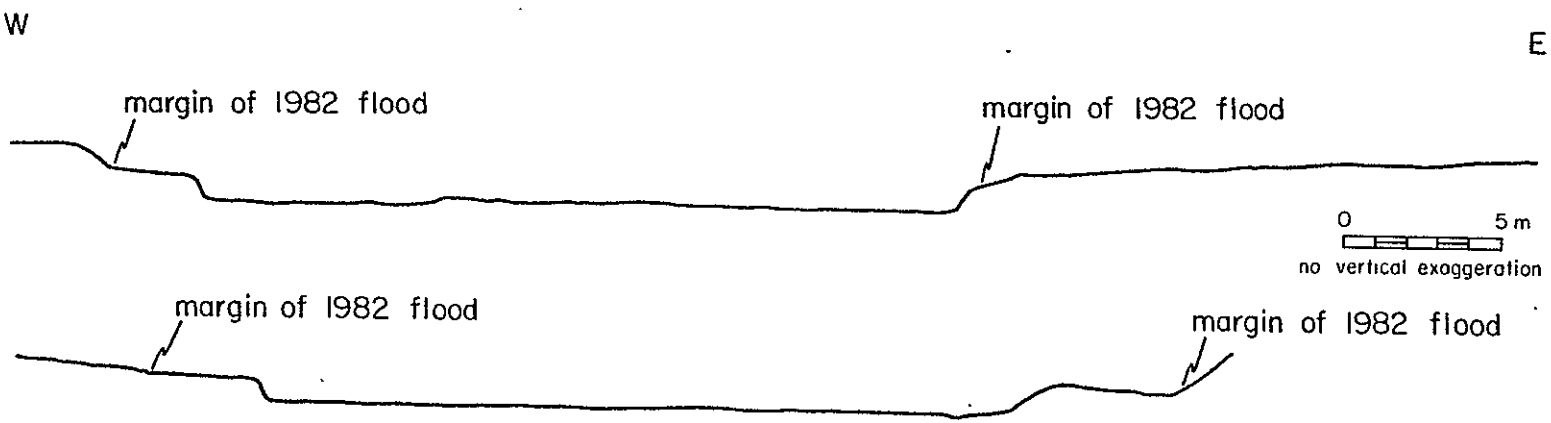

Figure 31. Profiles across the inner channel of the Rio Puerco near site 9.

The surficial deposits within the oxbow are predominantly sandy. It remains to be determined whether floods did not deposit silt and clay or whether floods did not reach most of the oxbow. It may be that the inner channel has incised to the point where floods do not reach the oxbow. Alternatively, the gradient of the oxbow may be large enough that floodwaters drain rapidly back to the inner channel without depositing much silt and clay.

A major natural pipe debouches into the oxbow 45 m upstream from site 9. The gradient of the fan and the fine grain size of the sediments suggest that the clay-rich surficial sediments at site 9 are reworked from the valley fill west of the river.

The uppermost 36 cm of deposits of site 9 (Fig. 32; Appendix A) includes beds of dry sandy clay which may have been reworked from upstream in the oxbow. Below these beds to a depth of 81 cm is a sequence of couplets 2-to-3 cm thick composed of sandy clay grading upward to clay. These couplets reflect repeated depositional events probably derived from upstream in the oxbow. Below 91 cm are sandy to gravelly sand layers of the abandoned channel. The base of the hole at 2.54 m reached pebbly sandy clay and cohesive sandy loam which may be the base of the 20th century sandy channel.

Only surface samples were taken along the channel at site 8 because the channel consisted of water-saturated coarse sand.

e. Sites 10 and 11

Arroyo Chico was examined a few hundred meters upstream from the confluence with Rio Puerco (Figs. 1, 33) where there was an abandoned channel. Although an inner channel and floodplain had developed, and former channels had been cut off, the entire system was dominated by sand, so that no thick clay layers were encountered in augered test holes in the abandoned channel. Therefore, only surficial samples were taken near the line of the profile in Figure 33 along with samples of muddy water (discharge from mine-dewatering).

2. Rio San Jose

a. Site SJ-1

Site SJ-1 was chosen because of its location between Correo and the confluence with Rio Puerco (Figs. 1 and 34). Small subsidiary channels

A.

Figure 32. Sample pit in oxbow at site 9. Scale is in increments of 0.1 m. A. Oxbow and pit. Photograph by J.W. Hawley, November, 1981. B. Detailed stratigraphy in wall of pit. Photograph by D. Heath, November, 1981.

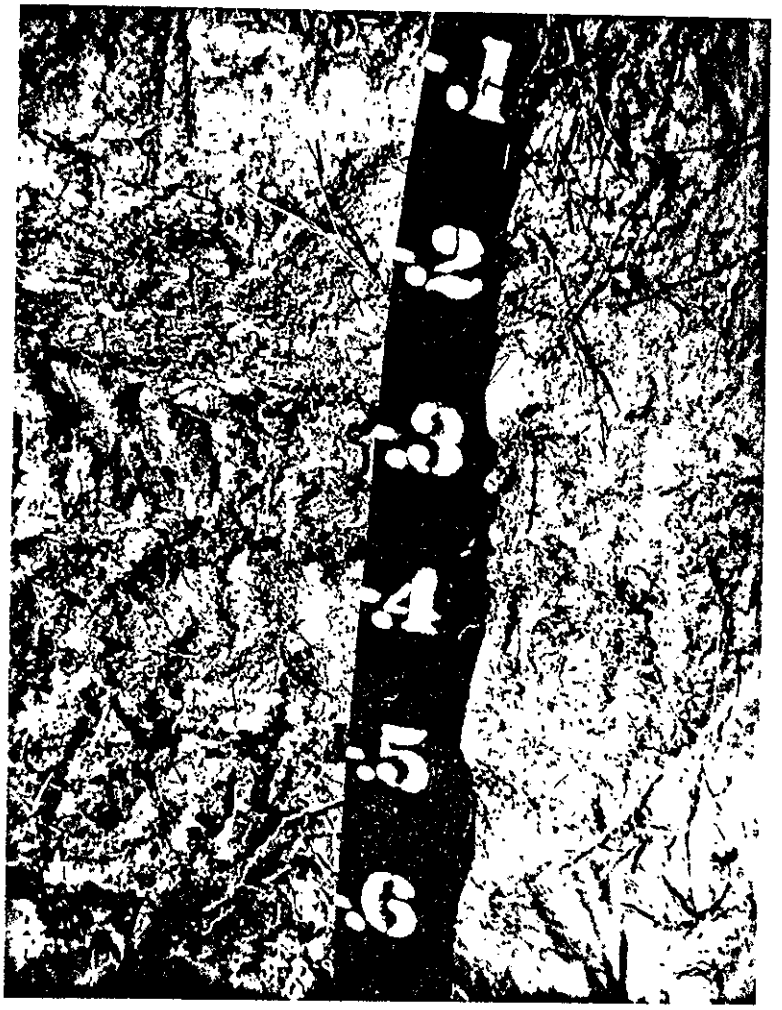

B.

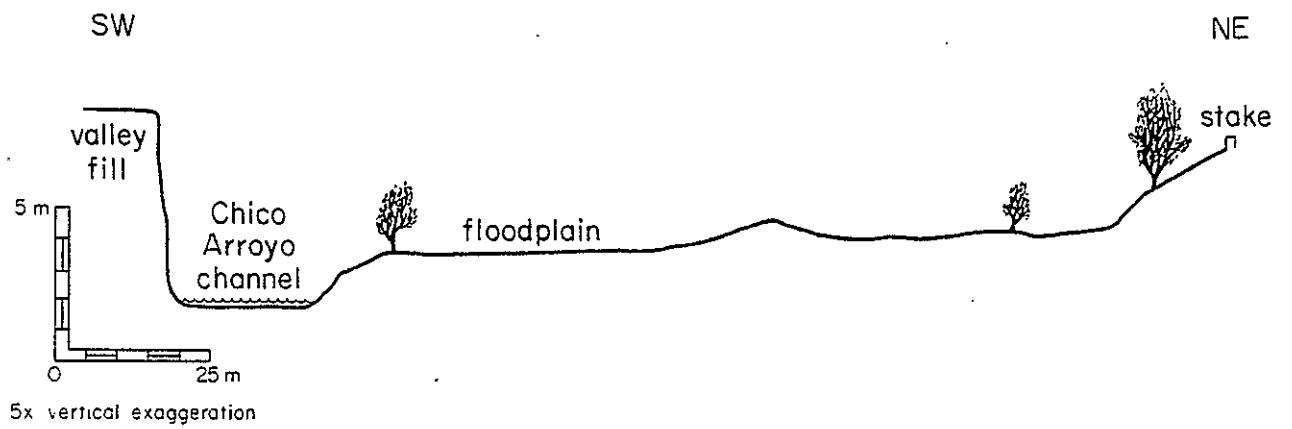

Figure 33. Cross profile of Arroyo Chico near sample sites 10 and 11.

A. B.

Figure 34. Aerial photographs showing the area around site SJ-1 in 1935 (A) and 1954 (B).

appeared to parallel the main inner channel as seen in the 1954 aerial photographs (Fig. 34 B). The channels were located on the ground and tested for clay layers. One with several clay layers was sampled although the age of the fill could not be determined in the field.

The present inner channel, 10 to 15 m to the north of the sample site, has a small cross section (Fig. 35). Bank-full discharge appears to be about 27 m^3/sec.

Stratigraphy in pit SJ-1 includes two major fining-upward sequences from gravel to clay, but individual units within each sequence suggest that deposition occurred as fill of an auxiliary channel. The gravel may have been deposited when large floods spilled from the main channel and were routed down the subsidiary channels. With smaller floods, the subsidiary channels received finer-grained deposits such as cross-laminated sand, silt and clay layers. Thick clay layers may represent settling of clay in backwater areas. Thus within the major cycles are lesser fining-upward deposits 10 to 12 cm thick. Another facet of the layers at this site are the variety of colors of sands and clays (Appendix A). Red sands and clays generally are derived from the Triassic-Paleozoic terrane which predominates in southern tributaries of the Rio San Jose. Gray and brown sands and clays are derived from Cretaceous strata to the north.

b. Site SJ-5

Site SJ-5 is located near the upstream inlet of a large oxbow of the Rio San Jose immediately upstream from the mouth of Rio Paguate (Fig. 1). The oxbow was formed when Rio San Jose was rerouted along an artificial chute cutoff (related to railroad bridges?) sometime between 1954 (Fig. 36) and 1971 (Mesita 7½ minute quadrangle). The date of cutoff remains to be established. Between 1971 and 1980, 14 floods have been greater than base flow at Correo. Many of these floods should have reached the oxbow. Field reconnaissance of the oxbow revealed that parts of the oxbow are isolated from flooding by eolian sand dunes and receive only eolian sand and reworked clay eroded from valley fill exposed in low arroyo walls. Although the Rio San Jose presently appears to have perennial flow of muddy water in the nearby new channel and the sand plug blocking the oxbow is relatively low, there is more sand than clay in the thin oxbow deposits.

Figure 35. Profile across inner channel of Rio San Jose near site SJ-1.

A. B.

Figure 36. Aerial photographs of the area including sample sites SJ-5 and PAG-1 in 1935 (A) and 1954 (B).

The stratigraphy of site SJ-5 (Fig. 37) includes thin (1-2 cm) clay layers interbedded with unlaminated-to cross-laminated sand (Appendix A). The lowest (70-85 cm below the surface) cross-laminated sand includes pebbles and clay balls up to cobble size indicative of the base of the channel. The coarse-grained deposits rest on a reddish brown (7½ Yr 3/2) mottled clay with crystals of an unidentified evaporite mineral (probably sodium sulfate). This clay layer and the sequence of thin sand and clay below is a widespread deposit which was noted in other auger holes in the oxbow and in exposures along the present stream channel. This deposit appears to be part of the older valley fill.

c. Site PAG-1

Site PAG-1 is located on the delta of Rio Paguate where it encroaches into Paguate Reservoir (Fig. 36). Paguate Reservoir, built in 1938, is filling with sediments derived from the Rio Paguate drainage basin. The drainage basin includes over 10 km2 of uranium mine workings which began to accumulate in 1950. The sample site was located above a topographically low part of the Rio Paguate channel upstream from the dam, based on the 1935 aerial photographs (Fig. 36).

Because the surface sediments were nearly water-saturated, no pit was dug. Stratigraphy in the auger hole included an upper series of layers of dark grayish brown (10 YR 4/2) clay and silty clay 90 cm thick (Appendix A). From 90 to 220 cm are interbedded clays, sandy clays and thin sand beds. The water table was reached midway through a clayey sand layer at a depth of 110 cm. It was impossible to sample below 220 cm because the walls of the auger hole kept collapsing. The upper clay layers are interpreted to be overbank flood deposits between distributary channels on the delta. The interbedded sand and clay below are interpreted to be adjacent to a distributary. Perhaps some of the clay layers are lake deposits within the reservoir.

B. Sample Characterization - Physical and Mineralogical Aspects

Optical and XRD analyses were performed on eighteen selected samples from four sites and results are shown in Appendix B. As expected, samples of similar mean grain size were also shown to be relatively similar in mineralogy. Sites 1 and 4 were channel sites and sites 2 and 3 were oxbow sites.

Figure 37. Stratigraphy exposed in pit SJ-5. Photograph by D.W. Love, August, 1982.

The most abundant non-clay mineral in all size fractions was found to be quartz. Feldspar (apparently largely albite, with minor microcline) and calcite were also present in smaller quantities in all size fractions. Evaporites and magnetite were not detectable by XRD, but were noted in field samples from later sites. The presence of trace quantities of other minerals, including mica and dolomite, was also suggested, although optical and XRD evidence was not conclusive.

The most abundant clay mineral in all eighteen samples was found to be kaolinite. Significant quantities of montmorillonite, illite, and chlorite were sometimes found but varied considerably between samples. Mixed layering of the montmorillonite and illite was also noted.

No systematic variations in mineralogy of individual size fractions with either site or depth were noted, except for a possible increase in the proportion of chlorite in the clay-size fraction with depth. Furthermore, no systematic variations were apparent in the proportion of fine-grained material in samples of a given mean grain size, or in the relative proportions of silt and clay in this material.

C. Dating the Sediments Using Pb-210, Pb-214, and Cs-137

Both Pb-210 and Pb-214 peaks were clearly resolved by gamma spectrometry, with full peak widths at half the maximum peak height above background (FWHM) of approximately 1.1 and 1.3 KeV, respectively. Peak shapes were consistently Gaussian, and centroid energies were in good agreement with one another and with published values (NCRP 1978), again indicating that no significant interferences were present.

Cs-137 peaks were occasionally less clearly resolved, on account of the greater full width at half maximum (approximately 1.7 KeV) and the presence of a neighboring peak at 665 KeV. The iterative nature of the peak area calculation, however, does appear to accurately separate the peaks in most cases. In the remaining cases (marked by small Cs-137 activities and atypical centroid energies of FWHM values), visual estimation of the peak areas was occasionally necessary.

No other interferences were indicated for any of the isotopes in tables of known peaks from major fission products and isotopes in the U-238, U-235, and Th-232 decay series.

Because of the random nature of the individual radioactive decays, the measured activities were subject to statistical uncertainties which were inversely proportional to the square root of the number of decays measured. It was therefore possible, for example, to halve the uncertainty in a particular measurement by increasing the counting time by a factor of four. The typical counting times of 1½ - 24 hours for Cs-137, and 4 - 48 hours for Pb-210, Pb-214, and Cs-137, thus reflect an attempt to balance the relative errors of the activity measurements against the counting required. (For example, the longer counting times within each range often correspond to those samples which, on account of their grain size or depth, could be expected to have relatively low Pb-210 or Cs-137 activities). Counting times of about 12 hours were finally adopted. This time allowed counting statistics to generate relative errors of usually less than 10%, even for the low level isotopes.

In addition to statistical errors, the measured activities may also be subject to systematic errors in the peak areas and efficiencies used, due to such factors as differences in self-absorption between sand and clay samples. The resulting relative errors are expected to be on the order of 10 percent, and will vary depending on both the nuclide and the detector. Although such systematic errors should not significantly affect any Cs-137 dating, they would seriously affect the accuracy of Pb-210 dating of any sample in which supported Pb-210 levels are high, or in which unsupported Pb-210 levels are low due to age. This difficulty may be partially overcome by dealing with the ratio of Pb-210 to Pb-214, rather than the difference between the two values. In accordance with the radiometric decay equation, this ratio will decay exponentially with time to a value of unity in any closed system.

Finally, the measured Pb-214 activities will be subject to a further systematic error due to differences in the rate of radon emanation with depth. Continual escape of gaseous Rn-222 from a sample can, over time, substantially lower the amount of supported Pb-210 present. After sealing of a sample, however, Rn-222 (and hence Pb-214) would re-equilibrate at a higher level. The calculated Pb-210/Pb-214 ratio, which like the calculated unsupported Pb-210 activity is based on assumed secular equilibrium between the measured Pb-214 and supported Pb-210, would therefore be too low in those samples nearest the surface. To estimate the magnitude of this error, a

previously counted sand sample was unsealed and allowed to stand for two weeks, then recounted. The decrease in the measured Pb-214 activity was found to be 0.21±0.04 pCi/g, or 27%. The resulting increase in the measured Pb-210/Pb-214 ratio, if statistical variations in the Pb-210 activities were neglected, would be 0.40. The typical increase for finer-grained sample would presumably be less.

D. Pb-210, Pb-214, and Cs-137 Activities

The activity of Pb-210 in the 213 samples was found to range from 0.55 to 15.6 pCi/g, with a mean of 1.35. Pb-214 activities ranged from 0.51 to 13.6 pCi/g, with a mean of 1.18. Typical uncertainties for the two nuclides were on the order of 0.1 and 0.025 pCi/g, respectively; the larger uncertainty for Pb-210 as a result of the low probability of γ emission.

The ratio of Pb-210 to Pb-214 activities in the samples generally fell in the range of 0.7 - 0.2, with a typical uncertainty of 0.1 - 0.2. Again, the uncertainties are due primarily to the relatively high uncertainty in the Pb-210 activities.

The highest Pb-214 ratio found in any of the samples, including the additional surface samples collected at other nearby sites, was 2.3. Thus, in sharp contrast to previously studied areas, the level of supported Pb-210 on the lower Rio Puerco is greater than the atmospheric (unsupported) Pb-210 flux. This is presumably the result of natural and mining-related erosion of uranium-rich material (such as Morrison Formation outcrops and mine-mill tailings) in the upper portions of the drainage basin. Such erosion would result in the transport of elevated amounts of U-238 and its decay products in both soluble and particulate form.

The measured Cs-137 activities of the samples ranged from <0.002 pCi/g to 0.73 pCi/g, with most upper core samples falling in the 0.1-0.3 pCi/g range. Uncertainties were typically on the order of 0.01 - 0.03 pCi/g with 0.03 pCi/g background levels.

The radionuclide activities of the individual samples are summarized in Appendix C.

E. Correlation of Pb-210, Pb-214, and Cs-137 Activities with Grain Size

The Pb-210/Pb-214 activity ratios of the surface clay and clayey silt samples are plotted in Figure 38. (For the purposes of the plots, the mean

Figure 38. Pb-210/Pb-214 Activity Ratios in Surface Clay Samples

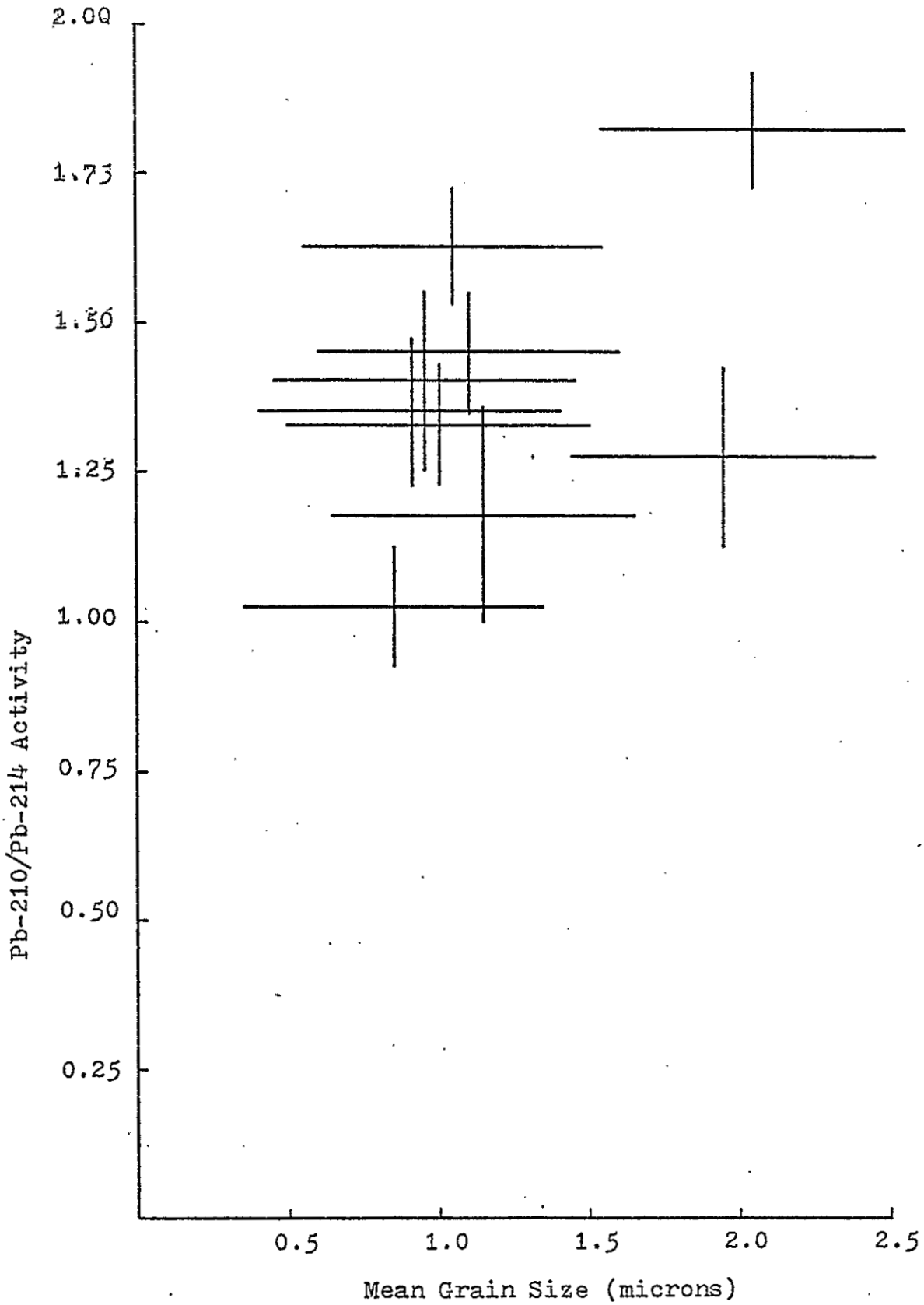

grain sizes of the clay samples were arbitrarily taken to be approximately 1μ, those of silty clays approximately 2μ and those of silts approximately 30μ). The activity ratios of the silt and sand samples are plotted in Figure 39.

As expected, the ratio is highest in the clay and silt samples (as are the Pb-210 and Pb-214 activities themselves). Despite the large uncertainties in the individual ratios, however, it also appears that the ratio varies significantly even among samples of similar mean grain size.

The Cs-137 activities of the same samples, plotted in Figures 40 and 41, also show increases in finer-grained samples and large variations among similar samples (as illustrated by the seven clay samples, which range in activity from 0.078 to 0.248 pCi/g).

These variations may be partially explained by fluctuations in the rates of Pb-210 and Cs-137 deposition over the course of the year during which these surface samples were collected, and by random variations in the mineralogy of the clay-size fractions, as indicated in Appendix B. Nevertheless, the variations appear to be only partially random, as indicated by significantly higher Cs-137 activities in those clay samples from the upper (oxbow) portion of site 2A, relative to clay samples from similar depths at other sites.

As shown in Appendix B, neither the percentage of clay minerals, nor their relative proportions, are markedly different in the upper portion of site 2. The relative proportion of silt- and clay-size material also show no gross differences.

Nevertheless, the higher site 2 activities, as well as the generally higher activities of surface samples from the other oxbow sites 3A and 7, San Jose 1, 4, and 5, and Paguate Reservoir fill indicate that some factor or factors in the depositional environment of these silts and clays plays a significant role in Cs-137 deposition.

In determining an empirical relationship between Cs-137 activity and mean grain size, oxbow and active-channel surface samples were therefore considered separately. The points were fitted to a curve in which the activity decreased exponentially with increasing grain size, and this curve was then used to derive a set of approximate normalization factors (Table 5) used in correcting the activities of samples from depth for the effects of grain size variations.

Figure 39. Pb-210/Pb-214 Activity Ratios in Surface Sand and Silt Samples

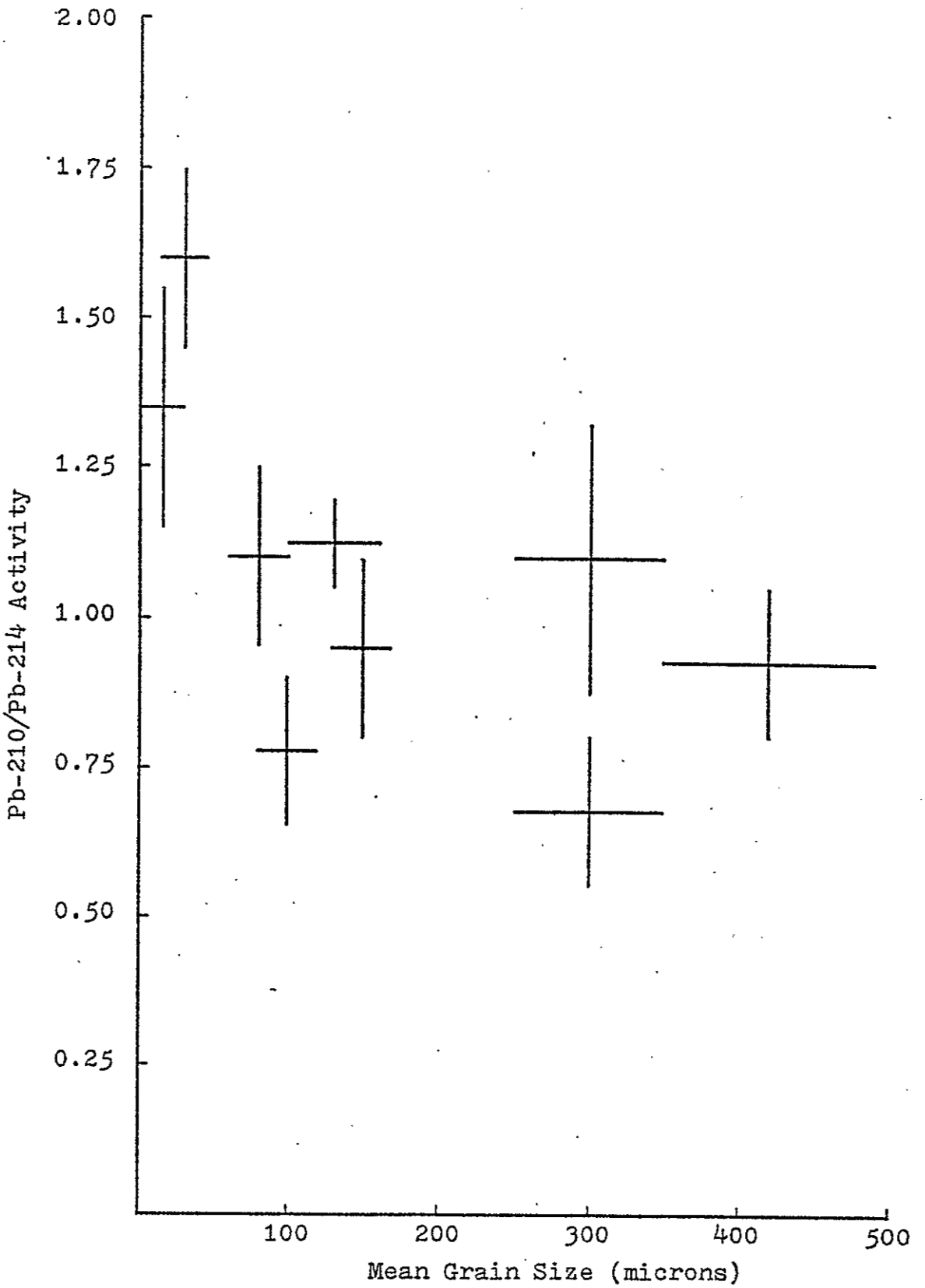

Figure 40. Cs-137 Activity in Surface Clay Samples

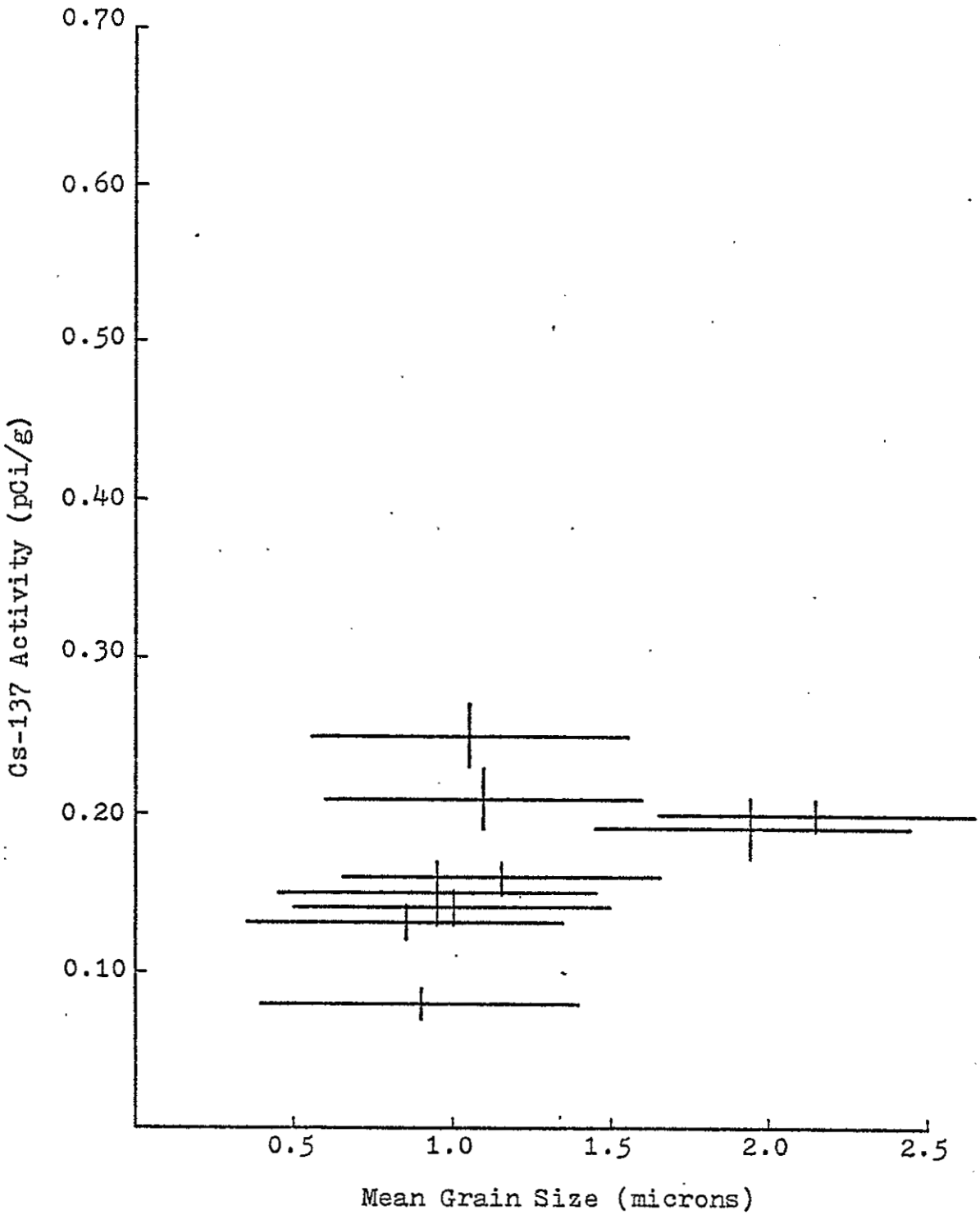

Figure 41. Cs-137 Activity in Surface Sand and Silt Samples

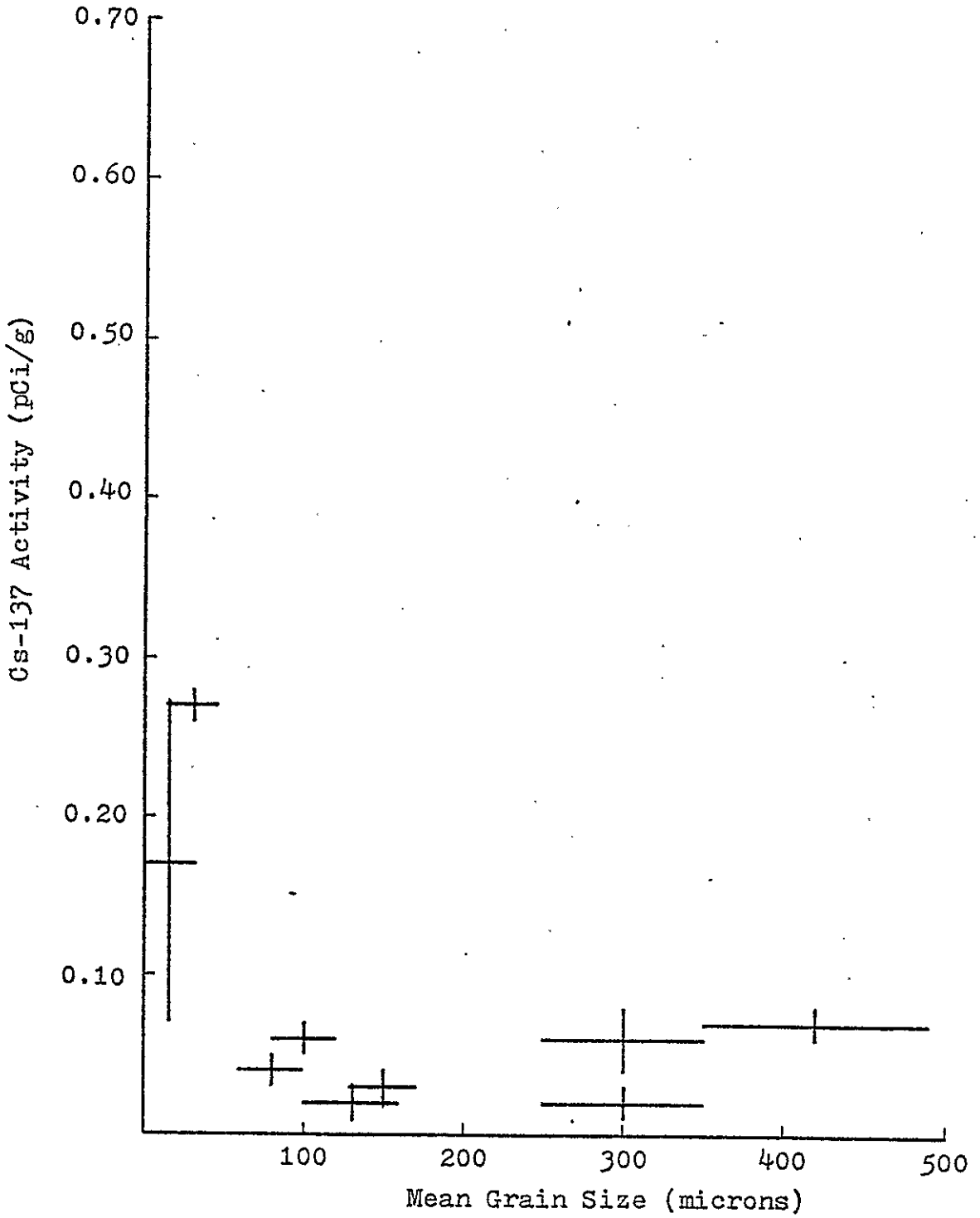

Mean Grain Size (μ)	Cs-137 Activity of Sample / Cs-137 Activity of Clay
1	1.00
2	0.99
30	0.86
61	0.73
88	0.63
125	0.52
177	0.39
250	0.27
350	0.16
500	0.07
1500	0.01

Table 5. Normalization factors used in Cs-137 dating.

F. Correlation of Pb-210, Pb-214, and Cs-137 Activities with Depth

Interpretation of the activity profiles of the small sites is complicated by the existence of systematic as well as random variations in grain size with depth; even in the sandiest channel deposits, for example, the surface layer may consist of silt or clay. Nevertheless, it does appear that the Pb-210 activities - and hence the Pb-210/Pb-214 ratios - are higher in surface samples, reflecting the effects of atmospheric Pb-210 deposition. In contrast, the non-atmospherically-derived Pb-214 typically reaches its maximum at some point below the surface.

The Pb-210/Pb-214 ratio does not, as expected, decrease to unity with depth. Rather, it immediately drops from a value of 1 - 2 to a value of approximately 0.8 - 0.9, and generally remains between 0.8 and 1.0 throughout the remainder of the core. This clearly indicates that the majority of the samples had not remained closed with respect to the immediate precursors of Pb-210 (presumably Rn-222 in particular) during the time between their deposition and the sampling. The magnitude of the discrepancy appears to be approximately 0.1 to 0.5 pCi/g, in good agreement with the value of 0.4 pCi/g obtained (as previously described) by measuring the effect of radon emanation on a typical sand sample. The radon loss from individual samples will presumably vary with both grain size and proximity to the surface, being highest in shallow sand samples.

Profiles of normalized Cs-137 activities of samples from sites 1-7 (Appendix D) also show a consistent pattern, with a broad subsurface maximum followed by a transition, at a depth of a few meters, to samples with little or no detectable activity. Although smaller variations are superimposed on this general pattern, these show little or no correlation between cores, and may be due to the same random variations in Cs-137 activity seen in the surface samples. Alternately, in the case of relatively coarse-grained samples, they may represent artifacts of the normalization process.

In those samples below the transition in which Cs-137 was reported, measured activities are typically less than 2 standard deviations above background after background corrections are made. These occurrences may therefore represent either contamination of the samples with small quantities of Cs-137 during sampling or handling, or statistical fluctuations in the background. In the latter case, the correspondence of the reported centroid energies with that of Cs-137 can be largely accounted for by the inclusion of the background

Cs-137 counts in the energy calculation.

G. Pb-210 Dating

Pb-210 dating of the samples was not possible for several reasons, the most important of which involves the error introduced by radon emanation. Although it is possible to correct for the effects of radon emanation (Christensen 1982; Imboden and Stiller 1982) the actual emanation rates at the sites studied are expected to depend in a complex fashion on the individual sediment sequence.

Additional factors preventing dating of the sediments include the variability of the initial unsupported Pb-210 activity among relatively similar surface samples, and the high levels of supported Pb-210. The latter will tend to magnify the effect of systematic errors in the efficiency calculations, in addition to increasing the uncertainty due to counting errors.

H. Cs-137 Dating

Relatively narrow and well-defined maxima in the Cs-137 profiles, on which most previous dating has been based, were not seen in any of the oxbow sample sites (Figures 42-44). This may be due either to non-deposition or subsequent erosion of the sediments corresponding to times of peak Cs-137 fallout, or later redistribution of the sediments. Such redistribution, if it produces sufficient upward tailing of the individual maxima, could result in the observed pattern of a single very broad maximum. The most stable or regular depositional environment was at the Paguate site where sediments were deposited behind the Paguate Reservoir dam (Figure 44). At this site several maxima were indicated but a more detailed core segment would be necessary to corroborate these data.

In the absence of datable maxima in the profiles, the scope of the Cs-137 dating is limited to determining whether or not significant levels of Cs-137 are present, and therefore whether or not the samples in question postdate 1950.

1. Site 1A - Rio Puerco

The sediment sequence at site 1A, an active channel site, consists primarily of alternating fine sands and clays (0-208 cm), underlain by coarser sands (208-249 cm), gravel (249-259 cm), and further sands. The gravel layer is

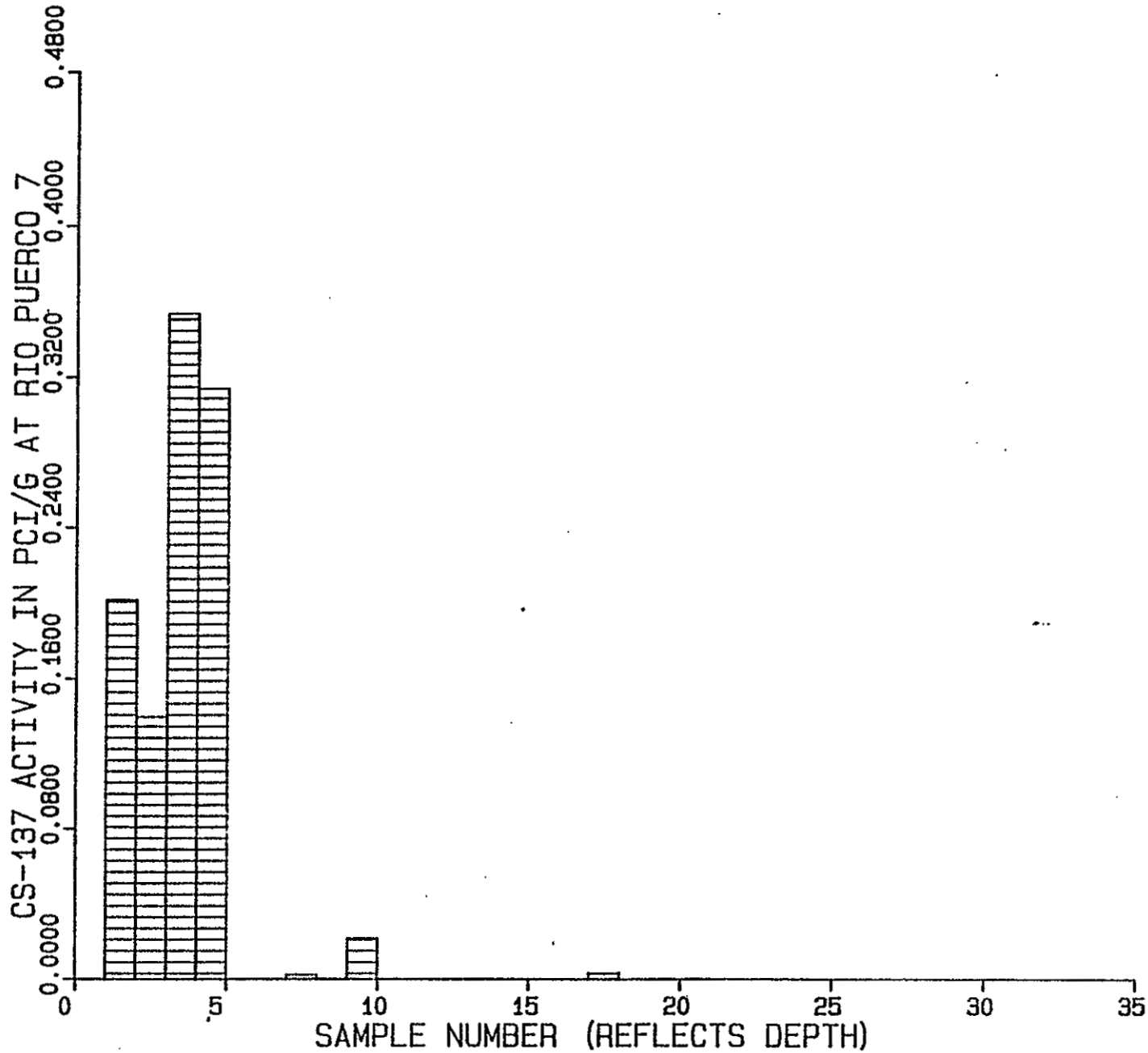

Figure 42. Cs-137 activity as a function of depth. Site 7 oxbow.
All samples greater than number 9 were zero or less than the detection limit.

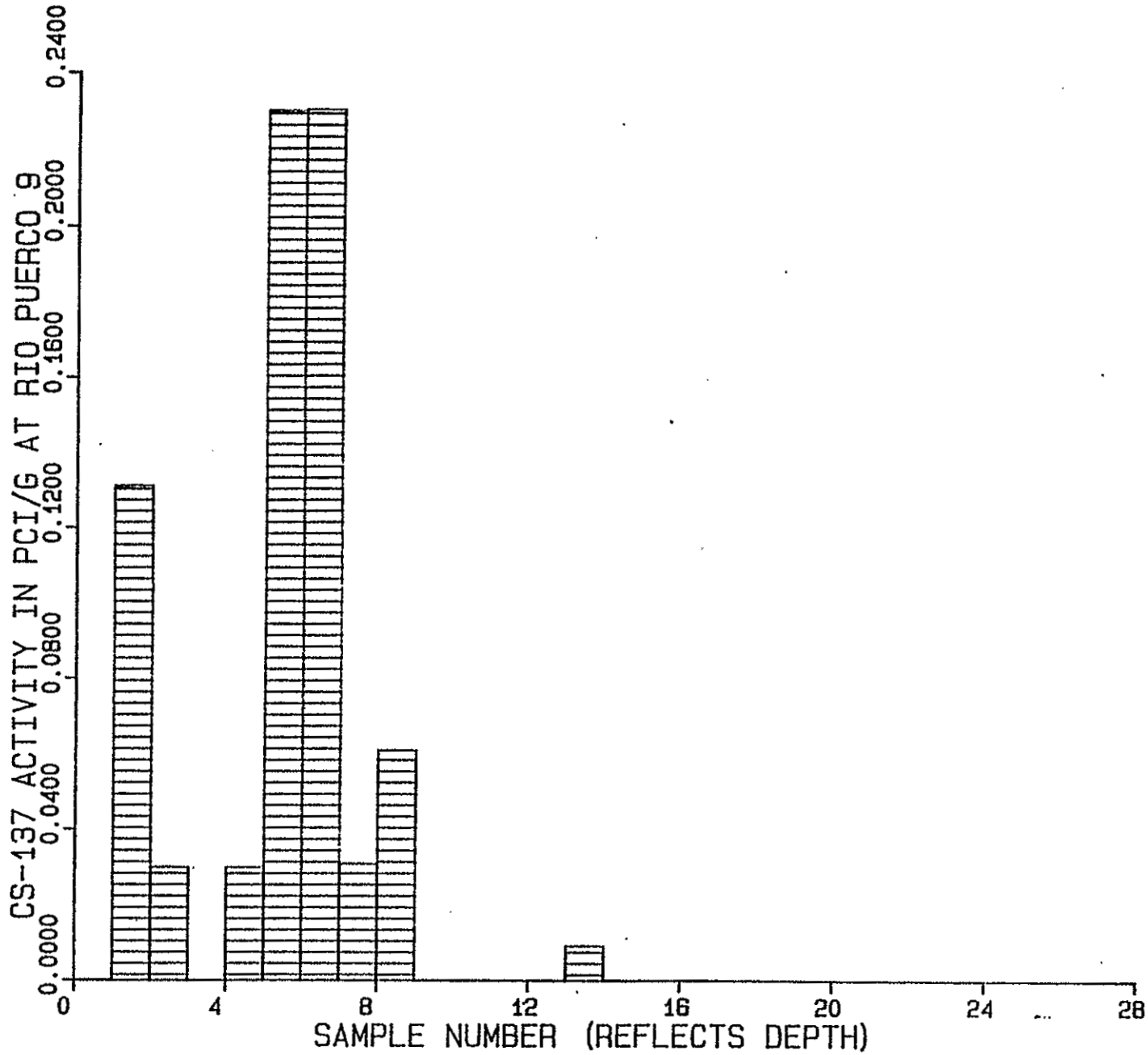

Figure 43. Cs-137 activity as a function of depth. Site 9 oxbow.
Samples greater than number 8 were zero or less than the detection limit.

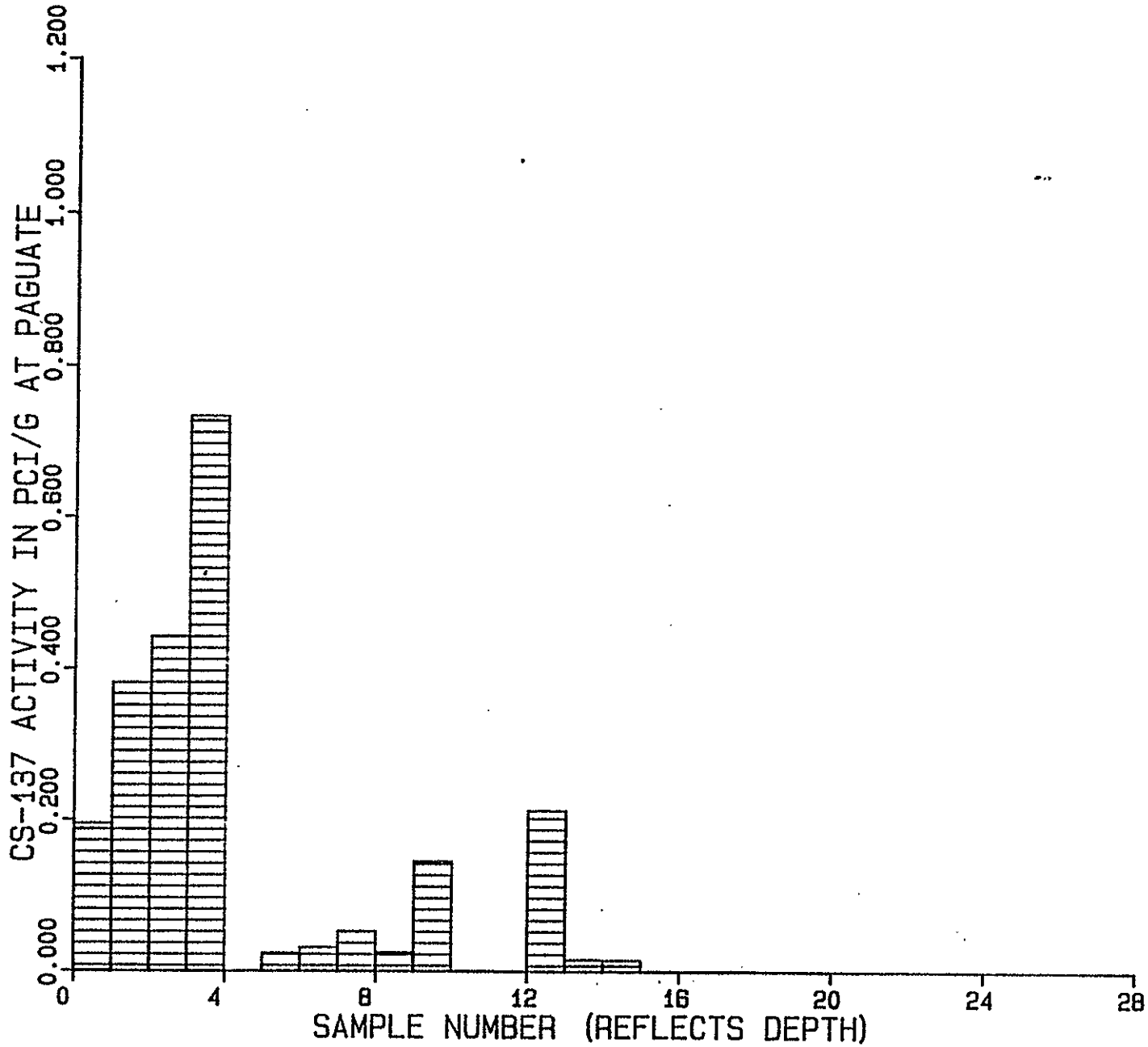

Figure 44. Cs-137 activity as a function of depth. Paguate Reservoir.

presumed to correspond to the base of the channel sequence, and thus to a date of circa 1950.

With a few exceptions, the Cs-137 activities of the samples in the upper 208 cm were sufficient to indicate post-1950 ages, in accordance with the stratigraphic date (Appendix C). Below 208 cm, the activities fell to zero. As the mean grain size of these samples was relatively large, however, this does not necessarily indicate pre-1950 ages for the sediments in question. Cs-137 dating of this portion of the core was therefore not possible.

2. Site 2A - Rio Puerco

The sediment sequence at site 2A, an abandoned-channel (oxbow) site, consists of clays (0-152 cm), underlain by further clays interbedded with increasing amounts of fine sand and silt (152-267 cm), and sands coarsening to gravel (279-523 cm). The upper clays are presumed to represent the later stages of oxbow deposition, and the underlying clays and the fine sands the earlier stages. The position of the base of the oxbow sequence can not be precisely determined, but should fall between 152 and 267 cm.

With only one exception, the Cs-137 activities of the samples in the upper 185 cm were high to extremely high, again clearly indicating post-1950 ages. From 185 to 262 cm, activities were lower but still significant. Thus, assuming the Cs-137 evidence is correct, the base of the oxbow deposit should fall much closer to 267 than to 152 cm. Activities were zero or near zero below 262 cm, although the evidence was again inconclusive on account of the coarse grain size of the sediments (Appendix C).

3. Site 3A - Rio Puerco

The sediment sequence at site 3A, an abandoned channel (oxbow) site, consists of a mixture of fine sands and clay clasts (apparently from the nearby bluff face) and oxbow clays (0-163 cm), underlain by fine sands (163-213 cm). The base of the oxbow deposits is presumed to lie between 163 and 254 cm.

The Cs-137 activities of the samples in the upper 68 cm are, with two exceptions, sufficiently high to clearly indicate their post-1950 ages. Very low levels of Cs-137 were also detected in most of the samples from 168 to 254 cm. Because of the longer counting times and lowered levels of background Cs-137, however, the activities of many of these samples were still

statistically significant. The Cs-137 dating, therefore, again indicates that the 1950 horizon lies close to the lower limit set by the stratigraphic evidence. Cs-137 dating of the samples below 254 cm was again not possible because of the coarse grain size of these sediments (Appendix C).

4. Site 5 - Rio Puerco

The sediment sequence at site 5, an active channel site, consists of generally fine sand with minor clay and silt (0-290 cm), underlain by sands coarsening to gravel (290-353 cm), and further sands. Once again, the gravel presumably represents the base of the post-1950 channel.

The Cs-137 activities of these samples are low, even in comparison with the channel sediments from site 1A. The activities of several of the samples in the upper 198-213 cm are sufficient, however, to indicate post-1950 ages for this portion of the core. Below 213 cm, the Cs-137 evidence is once again inclusive on account of the coarse grain size of the samples (Appendix C).

5. Site 6 - Rio Puerco

The sediments sequence at site 6, an active channel site, consists of generally fine to medium sand, with rare clays and pebbles (0-295 cm), underlain by gravel (295-345 cm) and further sands and clays. The principal gravel layer, rather than either of the slightly pebbly horizons, is presumed to represent the base of the recent channel.

The Cs-137 activities of only 2 of the samples (at 0-3 and 46-64 cm) were found to be statistically significant, and therefore indicative of post-1950 ages. The level of Cs-137 present in the post-1950 samples thus appears to be extremely low at this site, presumably due primarily to the coarser grain sizes of most of the channel sands. In spite of this fact, however, one additional Cs-137 date was obtained. The sample in question, a clay sample from a depth at 457-475 cm, was found to have less than 0.004 pCi/g of Cs-137, clearly indicating its pre-1950 age (Appendix C).

6. Sites 7 and 7A - Rio Puerco

The sediment sequence at site 7, an abandoned channel (oxbow) site, consists of silt and clay (0-51 cm), underlain by fine sand (51-213 cm), and sand grading into gravel (213-437 cm). The base of the oxbow deposits is

presumed to lie at a depth of slightly greater than 51 cm.

The high Cs-137 activities of the samples in the upper 41 cm once again clearly indicate their post-1950 ages. The Cs-137 activity of the clay sample at 41-51 cm, however, is less than 0.010 pCi/g, suggesting that the 1950 horizon has been reached. This is once again in good agreement with the depth indicated by the stratigraphic evidence (Figure 42).

7. Site 9 - Rio Puerco

The sediment sequence at site 9, an abandoned channel (oxbow) site upstream from all active uranium mining and milling activity consists of silt and clay (0-99 cm) underlain by coarse sand and gravel (99-183 cm) grading to sandy clay-loam (183-254 cm). The base of the oxbow deposit is presumed to be at a depth of about 100 m.

The high Cs-137 values in the upper 110 cm again clearly indicate a post-1950 age. All samples lower in the core have Cs-137 activities <0.01 pCi/g including several clay samples which is in good agreement with depth indicated by the stratigraphic evidence (Figure 43).

8. Site 1 - San Jose

The sediment sequence at site on the Rio San Jose consists of interbedded sands and silt clays to a depth of 120 cm followed by a bluish-gray clay presumed to be quite old and at the base of the oxbow deposit.

The Cs-137 values decrease to background in the bottom two samples, again in agreement with the stratigraphic evidence (Appendix C). This oxbow site was probably part of the active channel a number of times due to the narrow, confined nature of the stream bed.

9. Paguate Reservoir

This site is located in the fill deposits of the Paguate Reservoir which is only 6 km downstream from the Jackpile open pit uranium mine (see sample sites, Section III A.c. The entire core was quite uniform being primarily silty clay interbedded with fine sand to 220 cm. The core did not penetrate to below the reservoir deposits. Cs-137 was <.02 pCi/g below 120 cm which clearly indicates pre-1950 age for the bottom 5 samples (Figure 44). Because the grain size was uniform in this case, there is no ambiguity to this conclusion.

I. Radionuclide Distribution

1. General

Naturally occurring radionuclides which are commonly present in uranium deposits as daughters of U-238 decay (see Figure 2) and which may be transported away from mining and milling activities are Pb-210, Pb-214, Ra-226, and Th-234. These radionuclides are not soluble under oxidizing conditions, as opposed to uranium itself, and therefore may be transported within the sediment load of streams. If finer-grained material is responsible for the transport of the radionuclides, they may be expected to accumulate in the oxbow deposits (or further downstream in reservoirs). Individual sample radionuclide values are summarized in Appendix C.

2. Pb-210

Data for Pb-210 are shown plotted as a function of depth at oxbow and Paguate Reservoir sample sites on Figures 45-51 . A general decrease in Pb-210 activity from recent to older samples from Sites 2 (Figure 45), 7 (Figure 47), San Jose 1 (Figure 50), and Paguate (Figure 51) is evident. The most striking differences are at Paguate and Rio San Jose-1 which are the closest sites to the Grants Mineral Belt. The highest values found were at Paguate at 16 pCi/g which is about 10x the average level of Pb-210 in the oldest sediments tested. No trends are apparent at Site 9-Rio Puerco (Figure 49). This site is above the confluence of the Chico Arroyo which is the furthest upstream from contribution of active uranium mining. Samples from Site 9 should then be indicative of regional effects and none are apparent. The values for recent sediments (from Cs-137 concentrations and aerial photography) are about the same as for the valley-fill and deep-core sediment samples which may be thousands of years old. Pb-214, which is in secular equilibrium with Pb-210, shows similar trends and data are summarized in Appendix E.

A somewhat puzzling set of data for Site 7A is shown in Figure 48. In order to test the results from Site 7, which showed a decreasing trend in radioactivity with age, a second field trip to the site was made to sample another portion of the oxbow. As previously described, located upstream from the Rio San Jose and a minimal amount of mining activity (with the exception of exploration and some dewatering) was present. It was unexpected that radionuclides

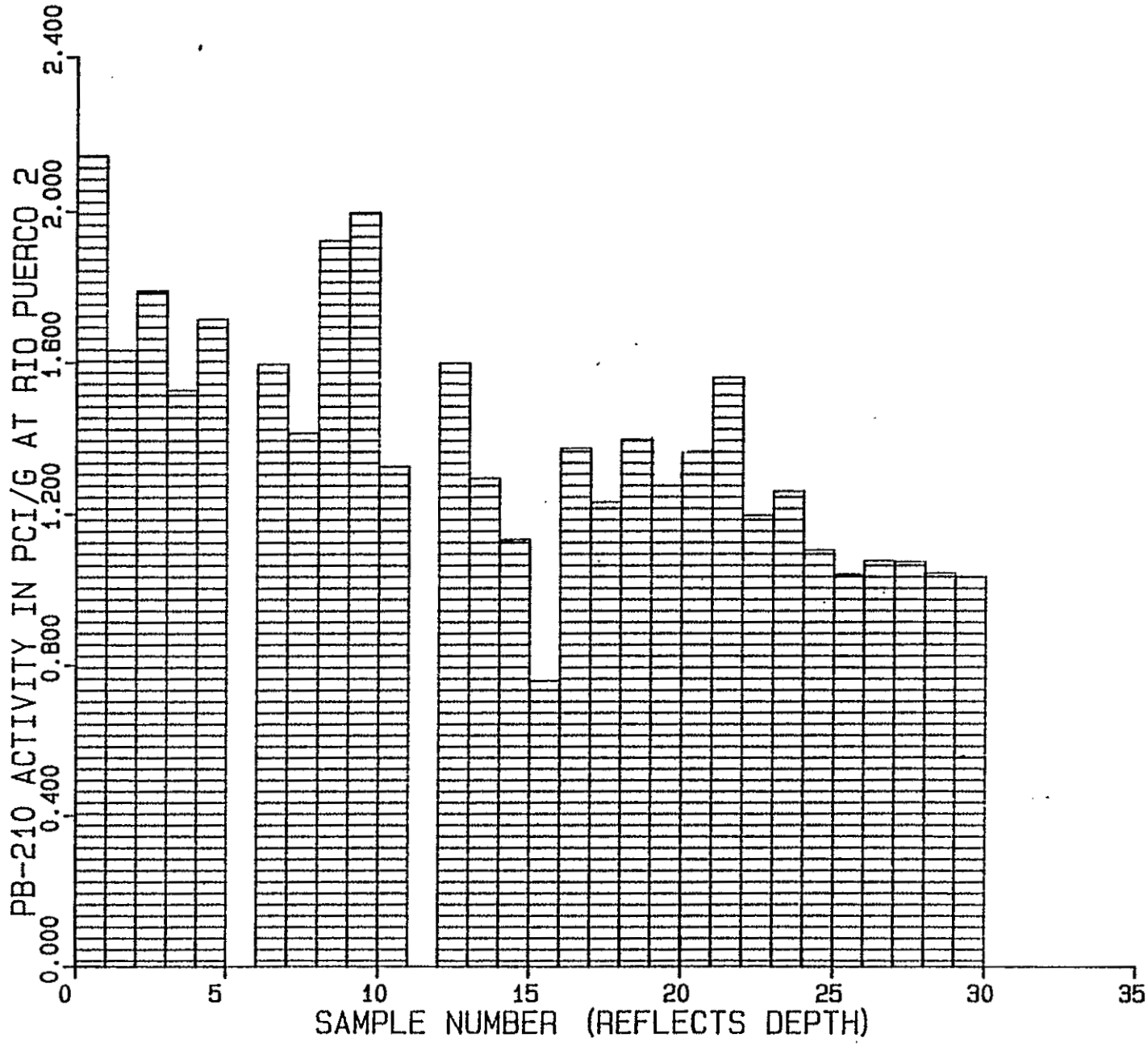

Figure 45. Pb-210 activity as a function of depth. Site 2 Rio Puerco.

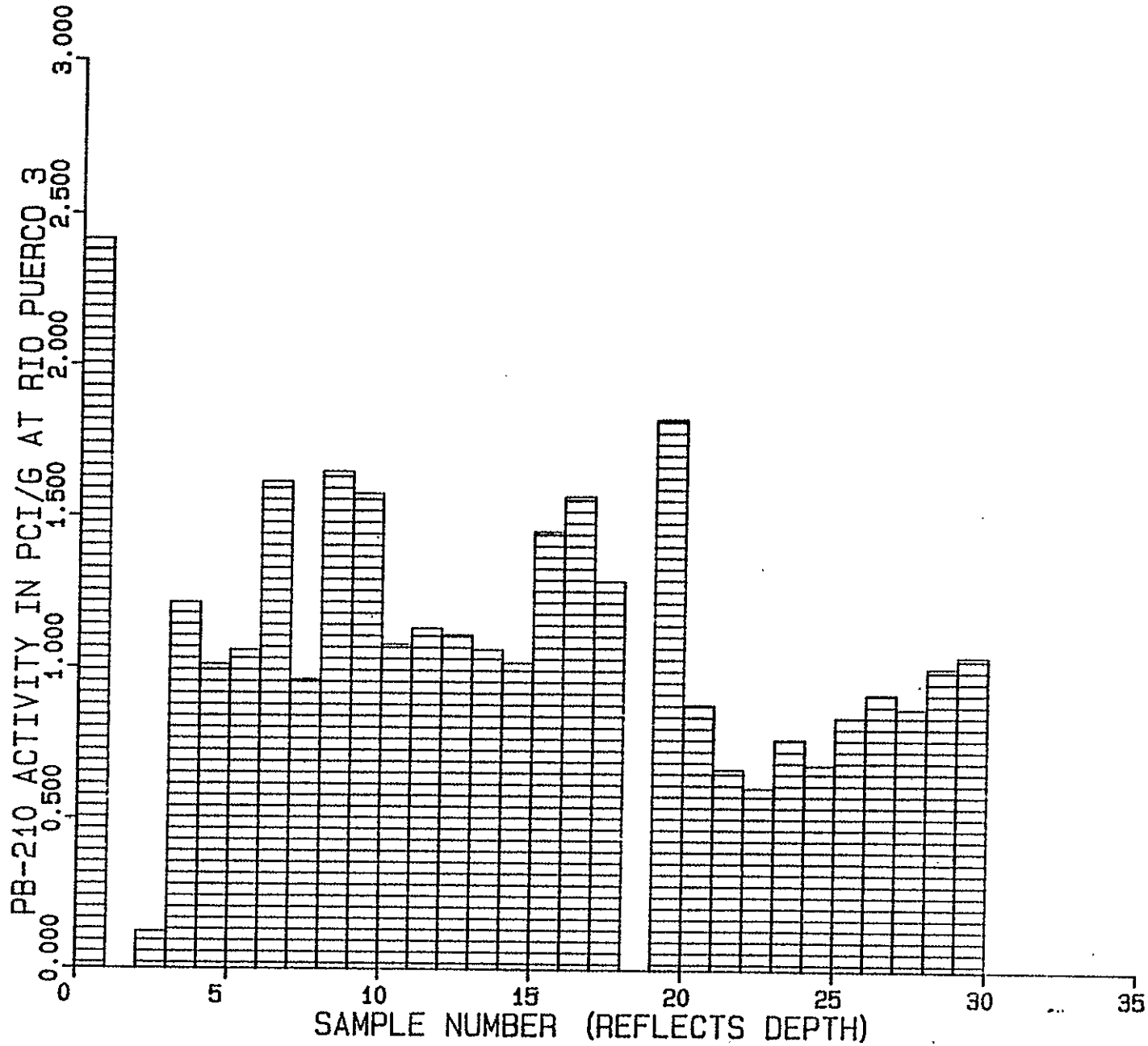

Figure 46. Pb-210 activity as a function of depth. Site 3 Pio Puerco.

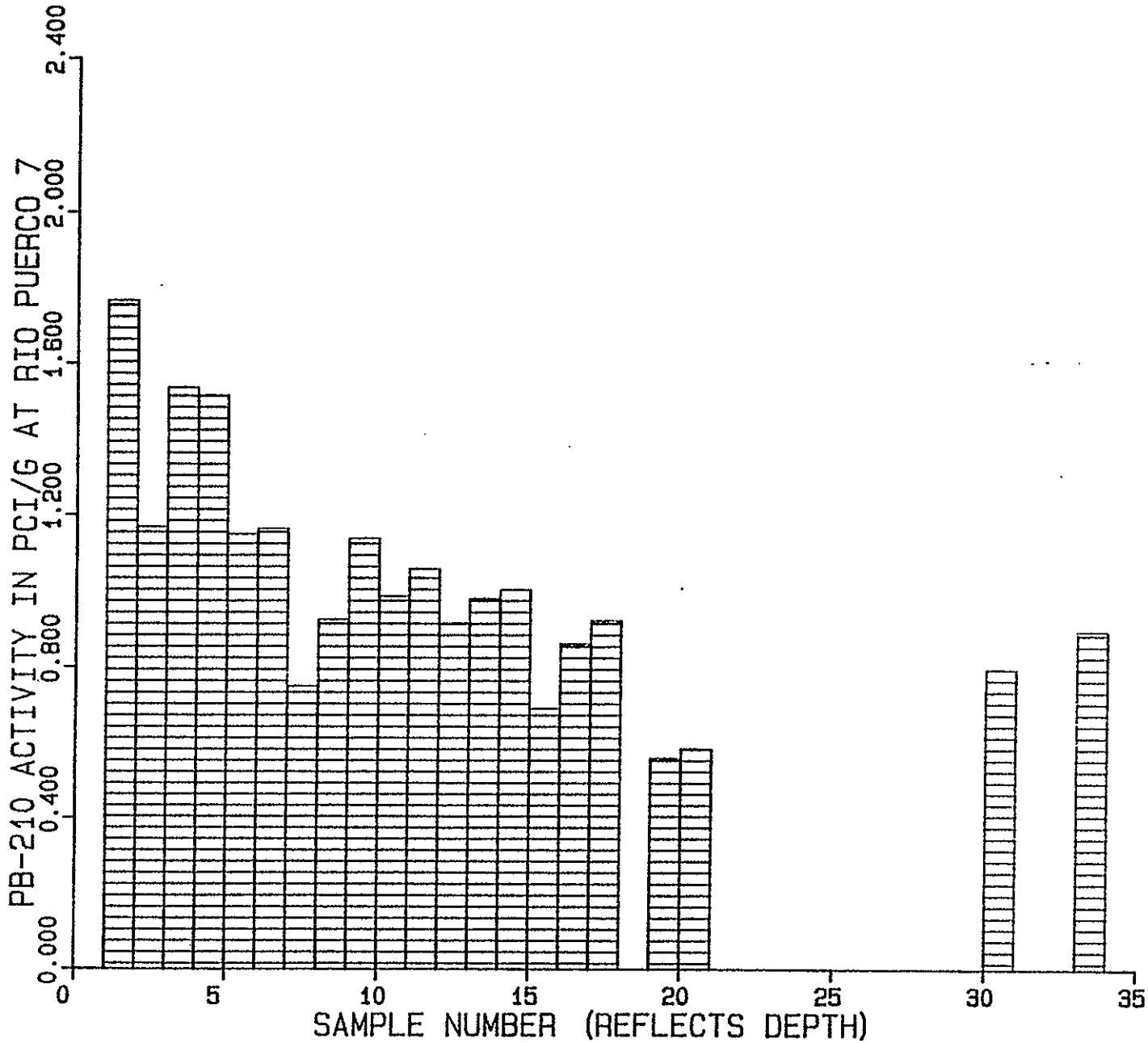

Figure 47. Pb-210 activity as a function of depth. Site 7 Rio Puerco.

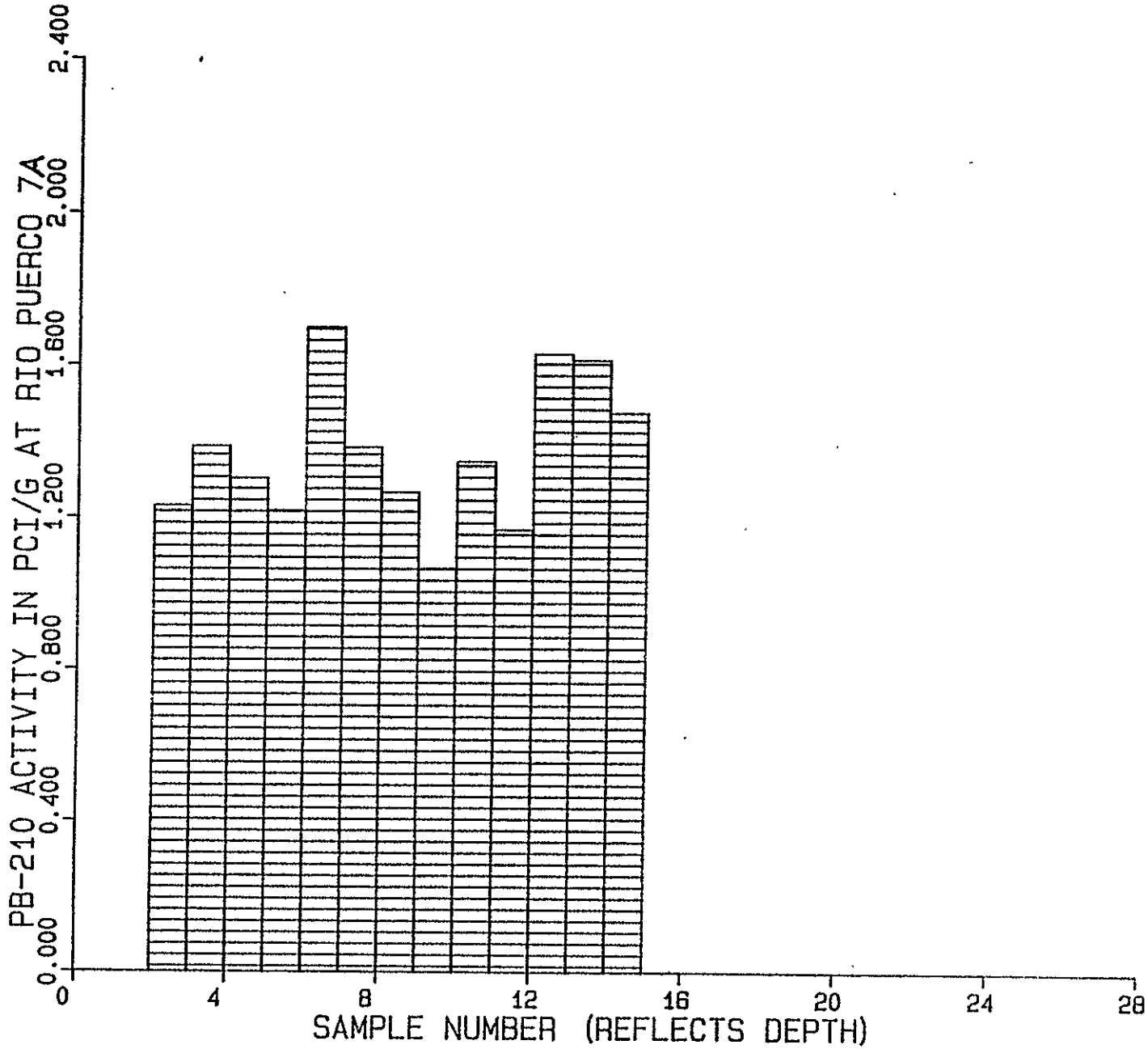

Figure 48. Pb-210 activity as a function of depth. Site 7A Rio Puerco.

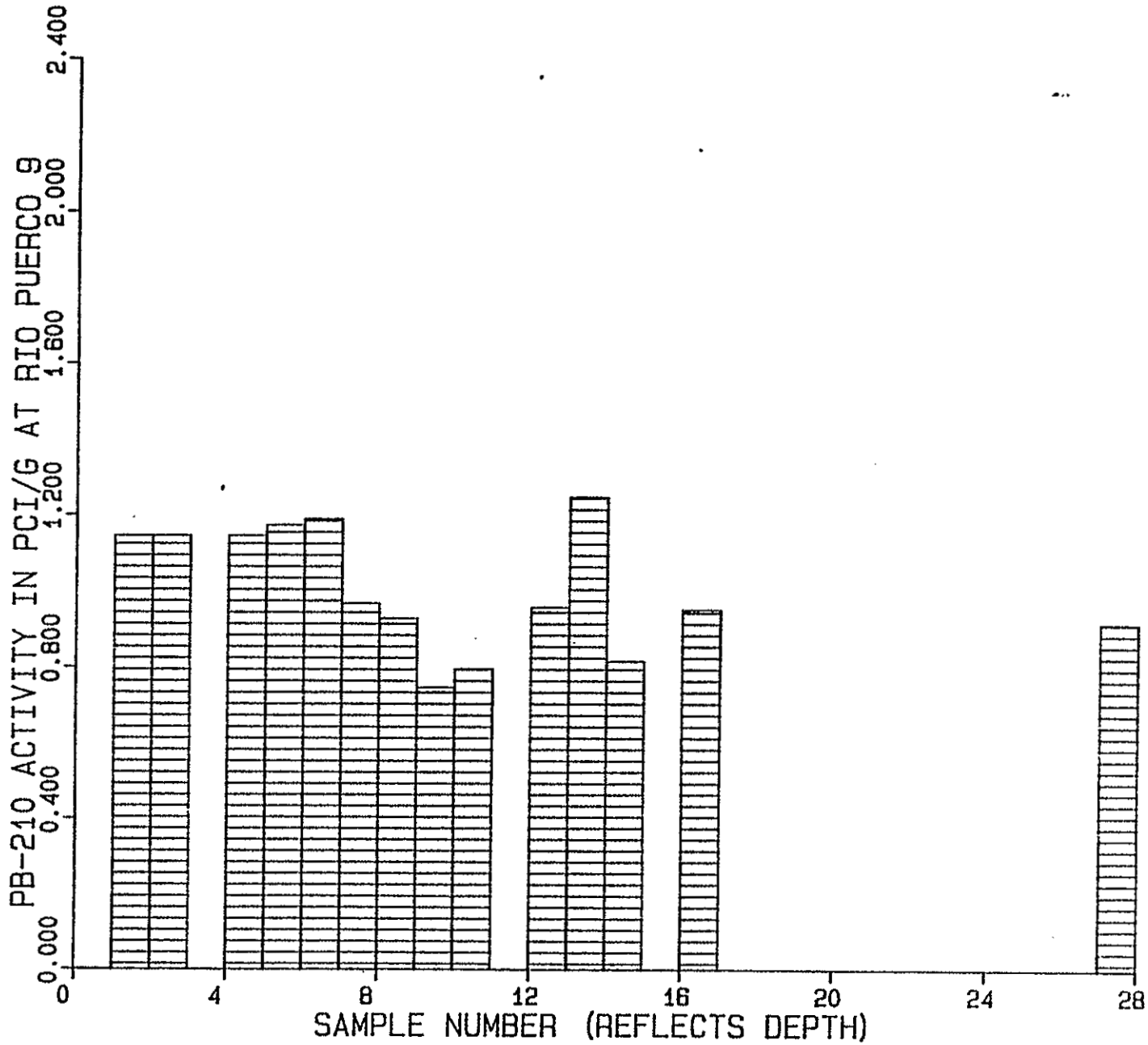

Figure 49. Pb-210 activity as a function of depth. Site 9 Rio Puerco.

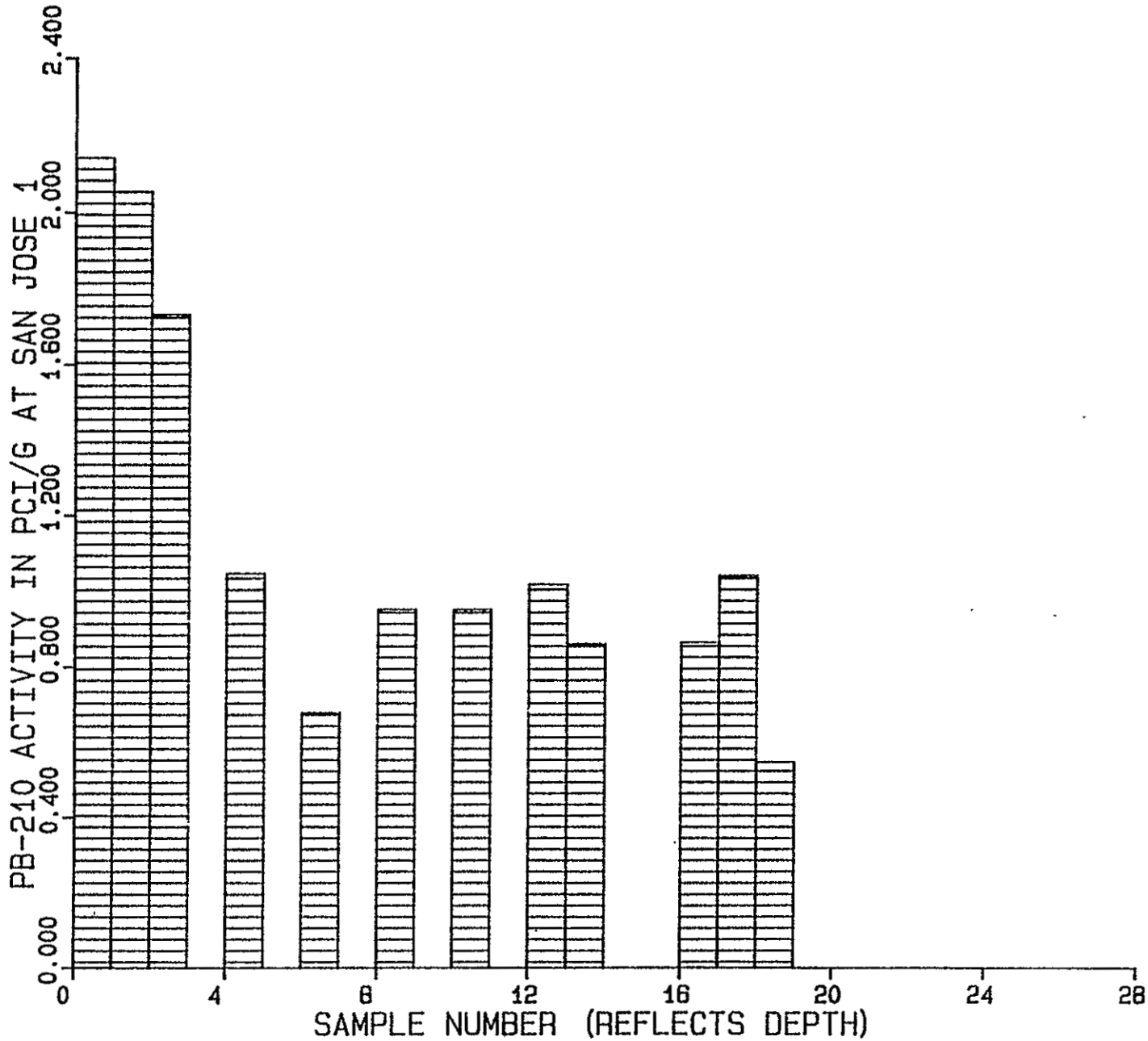

Figure 50. Pb-210 activity as a function of depth. Site 1 Rio San Jose.

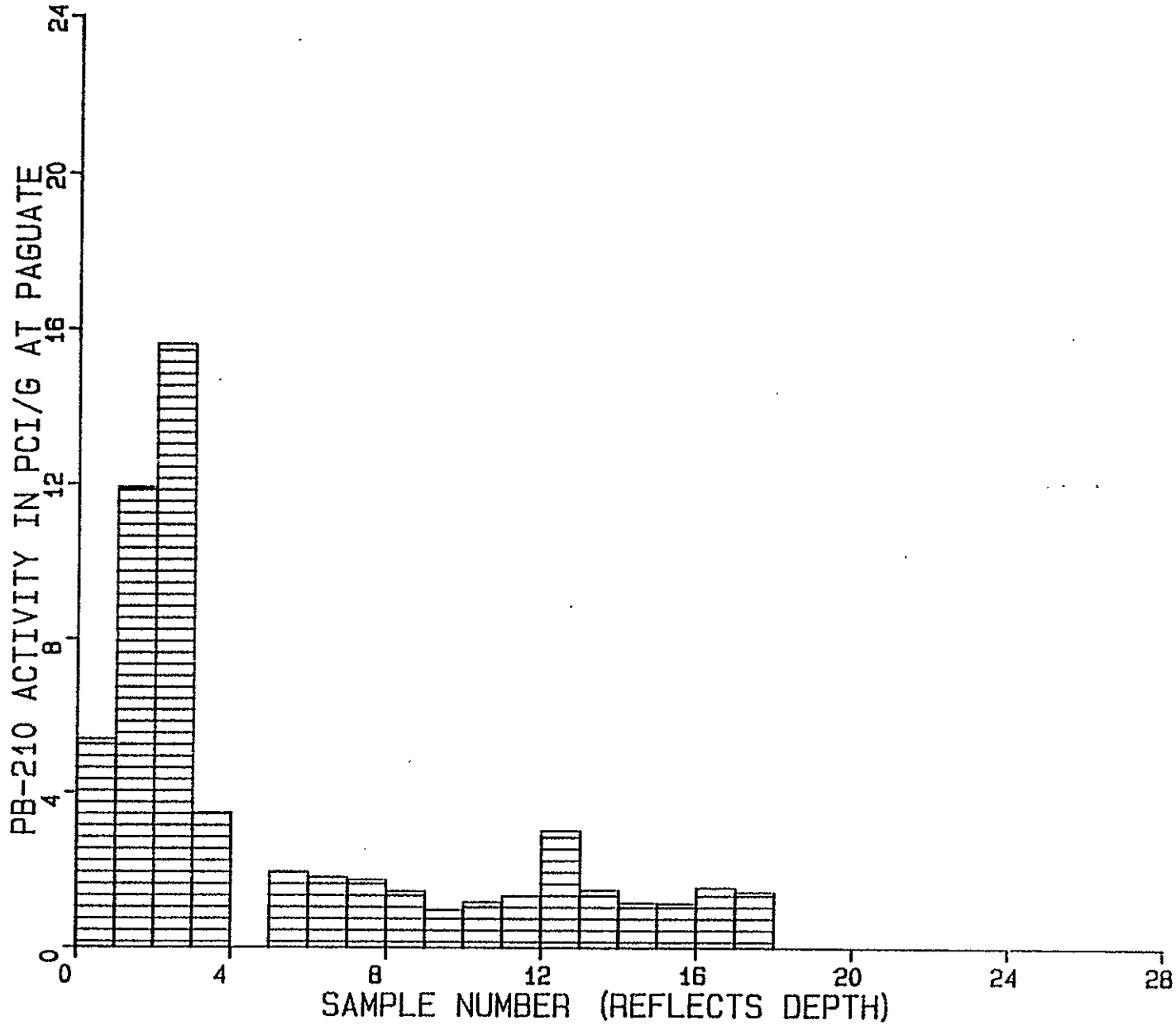

Figure 51. Pb-210 activity as a function of depth. Paguate Reservoir.

such as Pb-210 would show increased levels and, in fact, as opposed to Site 7, the 7A levels were relatively constant. Site 7A may show dilution of the silt-clay samples by older valley fill clays from the side walls and tributaries and what was found for the auger core at 7 may simply be a function of grain size (more silt-clay, more adsorption of radionuclides).

3. Ra-226, Th-234

These radionuclides, as expected, show exactly the same trends as those observed for Pb-210. This is expected because they are all members of the U-238 decay series, are insoluble and are strongly sorbed by sediments. The data for these two isotopes are summarized as histograms in Appendix E. The highest value found for any radionuclide of 26.85 pCi/g was found for Ra-226 in Paguate Reservoir sample #2 which was found at a depth of 15-30 cm.

4. Ac-228

Actinium-228 is a relatively long-lived isotope in the Th-232 natural decay series. The natural thorium concentations found in uranium deposits may not be elevated like the Th-234 levels because Th-234 is a daughter of U-238. If this is the case,the Ac-228 levels would not show the drastic increases shown by U-238 daughters in the mining region. The Ac-228 values at Paguate (Figure 52) does not show any trends with depth which is in stark contrast to the U-238 daughters. However, the Ac-228 trends at Sites 2 and 7 (Rio Puerco - Figures 53,54) and Site 1-Rio San Jose (Figure 55) mimic those shown by the U-238 daughters and suggest that the trends indicated at these sites are simply a function of grain size as was previously discussed for Cs-137 dating(Section III E). This relationship warrants further investigation.

J. Trace Metal Distribution

The 230-(<63μ) fraction of sediments from the core samples were analyzed for a number of trace metals including As, Cd, Cr, Cu, Hg, Mo, Pb, Se, V, and U. A number of these trace metals have been found to have concentrations in stream sediments in the region which are much higher than crustal abundance (Brandvold et al. 1981,1981) and the Grants Mineral Belt is suspected as a source. Also, the composition of uranium mill tailings often shows high levels of these same trace metals (Dreesen et al. 1982) and if the tailings material

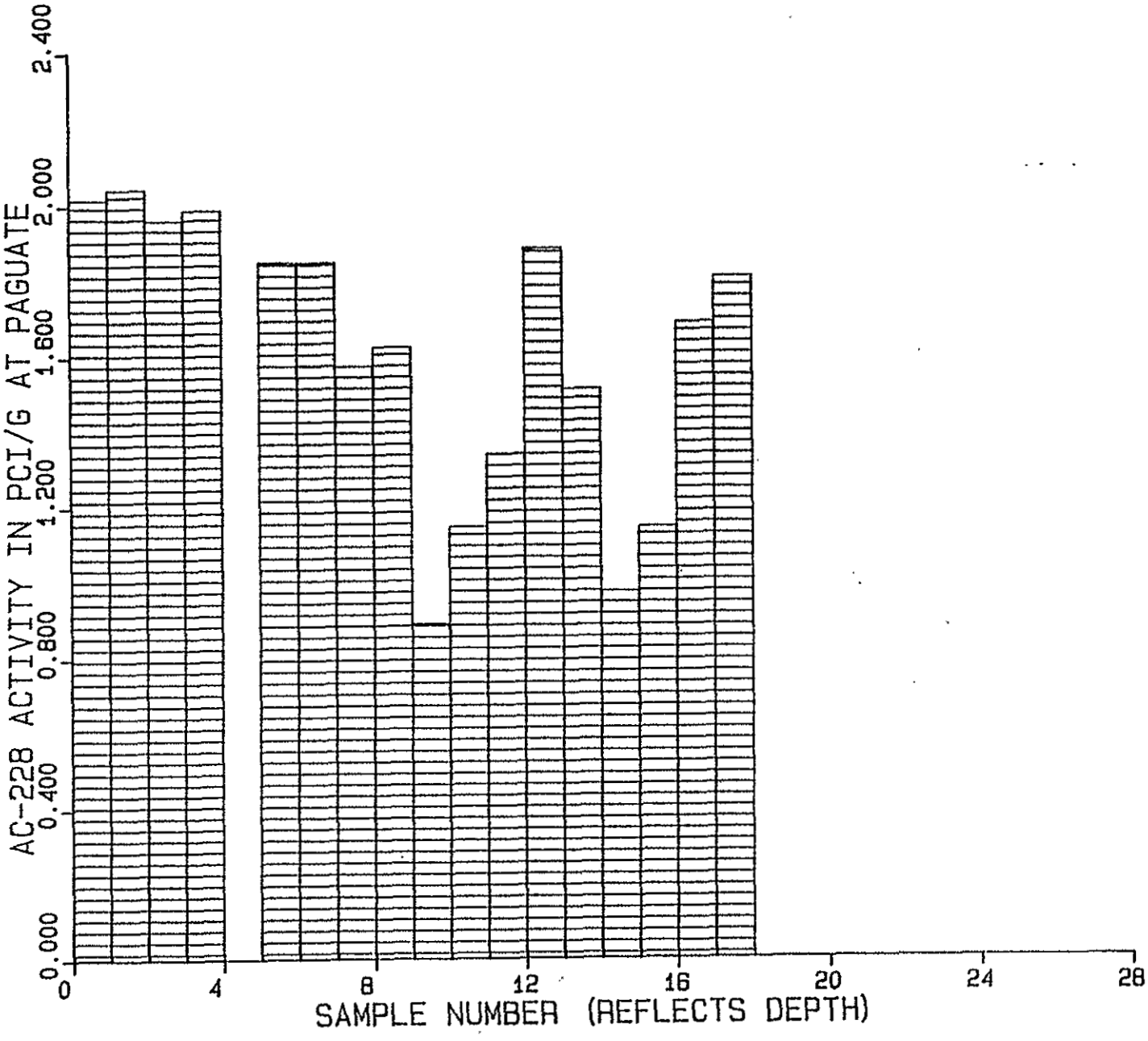

Figure 52. Ac-228 activity as a function of depth. Paguate Reservoir.

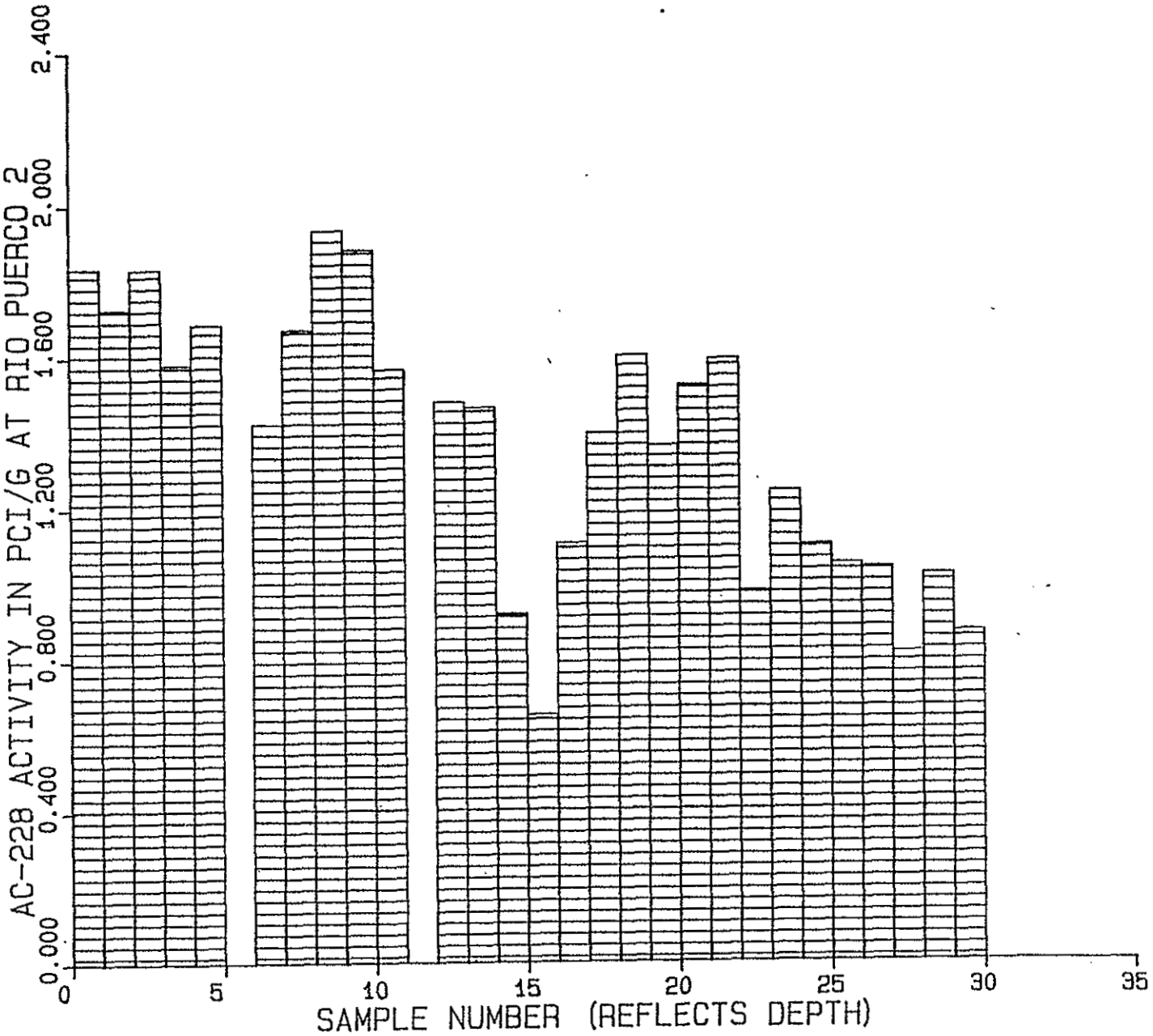

Figure 53. Ac-228 activity as a function of depth. Site 2 Rio Puerco.

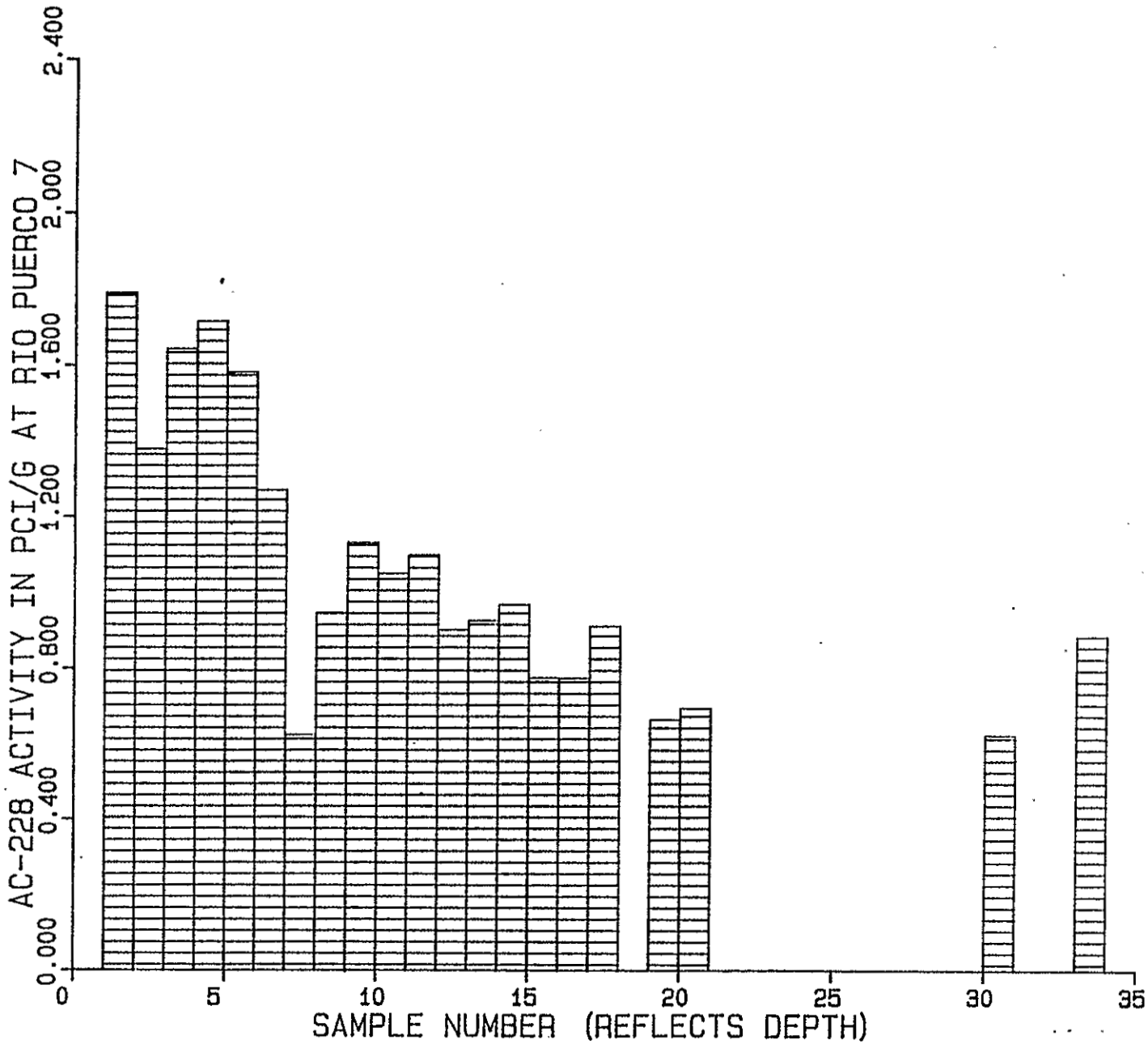

Figure 54. Ac-228 activity as a function of depth. Site 7 Rio Puerco.

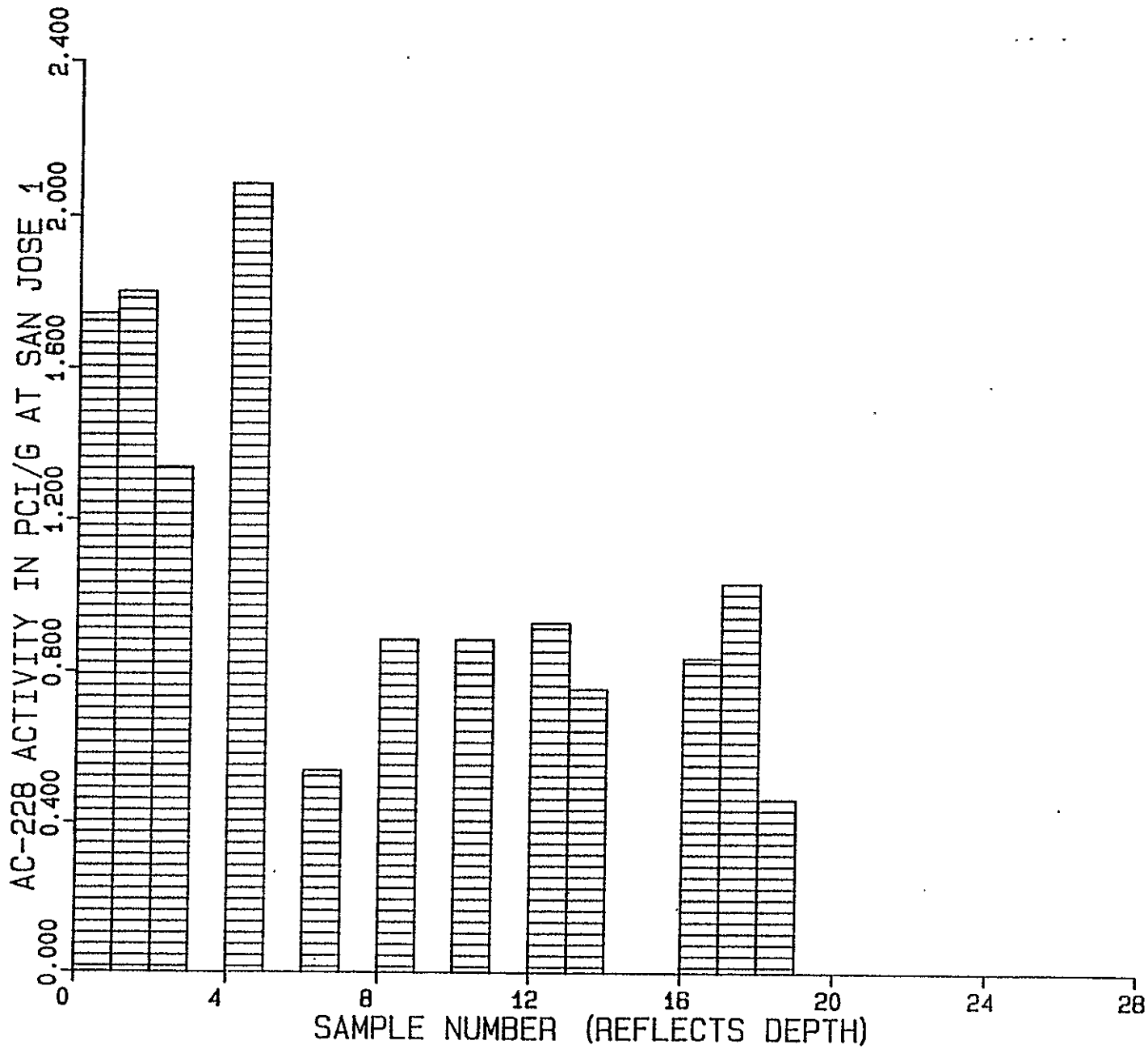

Figure 55. Ac-228 activity as a function of depth. Site 1 Rio San Jose.

is transported by surface waters, the metals may be enriched downstream. In order to compare similar sediments, the 230- sieved fractions were digested and analyzed.

1. Trace metals in post- and pre-1950 oxbow sediments

Data for trace metals in core samples from oxbow sites in the streams and in the Paguate Reservior fill are shown in Table 6. The elements As, Se, Cd, Hg, and U are considerably elevated above crustal abundances (Krauskopf 1979). Mercury values are an order of magnitude higher and uranium two orders of magnitude higher and mercury is considerably higher in the Rio San Jose sediments. As, Se, and U are associated in many of the ore deposits in the region. These same five elements have previously been reported to be elevated in regional sediments (Popp and Laquer 1980; Brandvold et al. 1980). There does not appear to be any significant trend with depth at any of the sites. This is quite different than the radionuclide results. Apparently the solubilities of As, Se, Cd, Hg, and U under oxidizing conditions are sufficiently high that they are eventually transported downstream while the radioactive species measured (Th-234, Ra-226, Pb-210, and Pb-214) are less likely to be transported. Because most of the Pb is not radioactive, the overall Pb values need not be present in elevated concentrations even though the radioactive Pb is high.

2. Trace metals in surface sediments - 230- fractions

Surface sediments collected in the oxbow sites and in Paguate Reservoir would reflect very recent depositional events and the trace metal analyses are shown in Table 7 . These sediments show the same trends in concentration as do the core sediments (Section J. 1.) in that As, Se, Hg, Cd, and U are elevated above crustal abundance with Hg again highest in the Rio San Jose sediments. The Paguate Reservoir site has higher U and V values in its surface sediments as well as elevated Pb-210, Ra-226, and Th-234 which are U-238 daughters. These radioactive species plus U and V are probably elevated due to the proximity of the Jackpile mine. The Rio San Jose does not seem to have a significant effect on the Rio Puerco sediments except perhaps for mercury as judged by values in the Rio Puerco surface sediments above and below its confluence with the San Jose.

		Rio Puerco					Rio San Jose	Paguate	
		2	3	7	7A	9	SJ1	PAG	Crustal Abundance
As	U	12.4	10.4	12.0	6.3	16.8	11.8	6.7	1.8
	L	8.8	15.0	11.1	-	12.9	8.3	7.2	-
Se	U	0.40	0.40	0.41	0.13	0.26	0.20	1.3	0.05
	L	0.29	0.58	0.33	0.19	0.19	0.13	0.5	-
Cd	U	0.22	0.30	0.28	0.37	0.32	0.33	0.62	0.15
	L	0.46	0.39	0.24	0.48	0.37	0.37	0.83	-
Cr	U	57	55	53	53	44	51	38	100
	L	57	49	48	29	37	45	32	-
Cu	U	31	79	36	29	63	19	18	50
	L	61	68	49	20	27	17	18	-
Hg	U	0.16	0.24	0.22	0.51	0.22	0.98	0.13	0.02
	L	0.15	0.22	0.18	-	-	2.30	0.56	-
Pb	U	22	32	19	-	42	-	25	13
	L	30	41	31	47	27	-	30	-
Mo	U	1.4	3.4	1.5	2.7	1.8	2.4	1.4	1.5
	L	5.3	2.8	3.1	1.6	1.8	2.3	2.2	-
V	U	115	124	115	108	99	94	110	123
	L	106	97	104	93	134	82	91	-
U	U	352	243	560	284	370	425	368	2.7
	L	373	343	398	-	375	300	380	-

Table 6. Trace metal concentrations in auger core 230-(<63μ) sediments. Values in ppm dry weight. U stands for upper sections determined to be deposited post-1950 and L stands for lower sections determined to be pre-1950.

	Rio Puerco Above San Jose	Rio Puerco Below San Jose	Rio San Jose	Paguate
As	14	8.5	22	4.6
Se	0.29	0.20	0.15	2.0
Cd	0.32	0.35	0.92	0.31
Cr	48	37	34	43
Cu	73	39	19	20
Hg	0.17	0.67	0.93	0.06
Pb	40	13	9.7	16
Mo	1.3	2.2	1.4	2.4
V	110	61	95	180
U	420	340	310	550
Cs-137	0.138	0.167	0.184	0.195
Pb-210	1.27	1.16	1.92	5.39
Ra-226	1.93	2.57	2.41	11.5
Th-234	0.906	1.23	1.06	4.45
Ac-228	1.19	1.55	1.48	2.02

Table 7. Trace metal concentrations in 230-(<63μ) fraction in surface sediments at oxbow sites. Values in ppm dry weight.

3. Trace metals in active channel sediment core samples - 230- fraction

The trace metal data shown in Table 8 for the 230- in active channel sediment core samples show about the same trends as all the other sediments. Again, Hg, Cd, and As show slight elevations in the Rio San Jose sediments. However, because the 230- fraction is so much larger in the oxbow sediments than in active channel sediments, the total metals stored in the oxbow sediments will also be much greater.

	Rio Puerco Below San Jose	Rio Puerco Above San Jose	Rio San Jose
As	10.2	10.6	35.1
Se	.30	.45	.14
Cd	.49	.37	1.32
Cr	52	44	33
Cu	53	55	23
Hg	.42	.49	1.23
Pb	22	21	35
Mo	2.6	2.4	.95
V	91	92	88
U	353	361	380

Table 8. Trace metal concentrations in 230-(<63μ) fraction in sediments from active channel sites. Values in ppm dry weight.

IV. SUMMARY, CONCLUSIONS, AND SUGGESTIONS FOR FURTHER WORK

A methodology for establishing the age of recent sediments in streams draining a major uranium mining and milling region has been established based on combined geomorphic, stratigraphic, and radiometric dating techniques. In the absence of historic geochemical baseline data for the region, environmental changes resulting from uranium mine-mill activities can only be determined by indirect methods.

The primary goal of geological studies was to determine the age of recent sediments in order to evaluate possible contributions of radionuclides and heavy metals to alluvial deposits of the lower Rio Puerco-San Jose drainage system. These studies focused on (1) processes of sediment transport and deposition along the Rio Puerco and Rio San Jose downstream from the lower Arroyo Chico and Rio Paguate areas, and (2) identification of stream deposits that immediately predate and postdate the onset of uranium mine-mill activity in the early 1950's. Because clay-sized sediment is primarily responsible for sorption of radionuclides and heavy metals, datable sites of clay-rich sediments were sought along the drainage system downstream from the major mine-mill areas of the eastern Grants Uranium Belt. Abandoned channel loops (oxbows) were chosen for study because they are easy to locate on aerial photographs taken since 1935, can be assigned an age for development, and commonly have thick clay-rich fill. Adjacent reaches of the present stream channel were studied for comparison.

Pits were dug at oxbow sites to determine stratigraphy and composition of deposits. Samples collected from pit walls and auger holes below the pits were subjected to radiometric analysis by gamma ray spectrometry for the artificial radionuclide Cs-137 and the natural radionuclide Pb-210 as well as other U-238 and Th-232 daughters. Because of the dynamic nature of the system, absolute dating with Cs-137 was not possible but samples could be dated as either pre- or post-early 1950's. The Pb-210 dating was not possible because background Pb-210 was very high relative to fallout Pb-210.

Sediments dated by the correlative Cs-137, stratigraphic, and historic techniques were then analyzed for radionuclides and trace metals which would be associated with uranium ores. The U-238 daughters are generally high in the region and little difference was observed for their values between the control site and the sites in the uranium mining and milling region except for the Paguate Reservoir site. Recent sediments at Paguate clearly show elevated

levels of U-238 daughters in sediments unambiguously dated after the mid 1950's. Sediments from the Jackpile uranium mine have been trapped in the reservoir fill.

Trace metals were also analyzed in old and more recent sediments and As, Se, Cd, Hg, and U show elevated values on a regional basis but no correlation with age (i.e. pre- or post-1950). These elevated trace metal values may simply be due to their association with the regionally mineralized material.

From study of aerial photographs, there appears to be much larger changes in configuration of the inner channel and inner floodplain between 1954 and the present (29 years) than between 1935 and 1954 (19 years). These changes may be related to hydrologic changes in the drainage basin and to changes in vegetation on the inner floodplain. Many oxbows, particularly those abandoned prior to 1954, have not developed extensive clay-rich deposits. Instead, the fill is predominantly sand along with poorly-sorted sediments from small tributaries eroding adjacent valley fill. Along the Rio San Jose and the lower Rio Puerco, sediments from different source areas may be distinguished in a general way by color.

Although deposits have been placed in a general time framework, correlations between individual fining-upward deposits and individual recorded floods remain to be completed. Changes in the geometry of the inner channel and complexities in the records for gaging stations along the Rio Puerco make it difficult to determine the number of floods which inundate each sample area. By tracing floods downstream from distinctive headwater areas, it may yet be possible to correlate some sand-plug or inner-floodplain deposits based on further work with tamarisk germination ages and depth of burial of former surfaces.

The following recommendations are made:

1) The approach developed in this study can be used to evaluate mine-mill effects in fluvial environments downstream from the activity. The procedures should be generally applicable to western mining regions.
2) Sediments deposited in environments closer to mine-mill operations should be studied, especially in areas which appear to be 'sinks' such as Paguate Reservoir and the McCarty's marshes along the Rio San Jose.
3) A study of this nature in the Rio Puerco of the West near Gallup may help answer questions regarding the effects from the United Nuclear tailings pond spill in 1979.
4) It may be possible to separate effects of uranium mining and milling activity from natural background by comparing U-238 daughter accumulation to daughters in the Th-232 series.

REFERENCES CITED

Alberts, J.J., L. J. Tilly, and T. J. Vigerstad (1979). Seasonal cycling of Cs-137 in a reservoir. Science 203, pp. 649-651.

Anderson, O. J. (1981). Abandoned or inactive uranium mines in New Mexico. New Mexico Bureau of Mines and Mineral Resources Open-file Report 148, 778 p.

Bachman, G. O., J. D. Vine, C. B. Read, and G. W. Moore (1959). Uranium-bearing coal and carbonaceous shale in the La Ventana Mesa area, Sandoval County, New Mexico. U.S. Geological Survey Bulletin 1055-J, pp. 295-307.

Benninger, L. K. (1978). Pb-210 balance in Long Island Sound. Geochimica et Cosmochimica Acta 42, pp. 1165-1174.

Brandvold, L. A., D. K. Brandvold, and C. J. Popp (1981). Effect of uranium mining and milling on surface water in New Mexico, in Environmental and Economic Considerations in Energy Utilization. Ann Arbor Science, pp. 467-476.

Burton, W. M., and N. G. Steward (1960). Use of long-lived natural radioactivity as an atmospheric tracer. Nature 186, pp. 584-589.

Chamberlin, R. M. (1981). Uranium potential of the Datil Mountains- Pie Town area, Catron County, New Mexico. New Mexico Bureau of Mines and Mineral Resources Open-file Report 138, 58 p.

Christensen, E. R. (1982). A model for radionuclides in sediments influenced by mixing and compaction. Journal of Geophysical Research 87, pp. 566-572.

Dane, C. H., and G. O. Bachman (1965). Geologic map of New Mexico. U.S. Geological Survey, scale 1:500,000.

Dreesen, D. R. and J. M. Williams (1982). Mobility and bioavailability of uranium in mill tailings contaminants. Environmental science and Technology 16, pp. 702-708.

Durham, R. W., and S. R. Joshi (1980). The Pb-210 and Cs-137 profiles in sediment cores from Lakes Matagami and Quevillon, Northwest Quebec, Canada. Canadian Journal of Earth Science 147, pp. 1746-1750.

Edgington, D. N., and J. A. Robbins (1975). The behavior of plutonium and other long-lived radionuclides in Lake Michigan: II. Patterns of deposition in the sediments. Argonne National Laboratory, Argonne, Illinois 18 p.

Environmental Protection Agency (1979). Methods for chemical analyses of water and wastes. U.S. Environmental Protection Agency, Cincinnati, Ohio

Erdmann, G., and W. Soyka (1979). The Gamma rays of the radionuclides. Verlag Chemie, New York, New York, 862 p.

Gaggeler, H., A. R. VonGunten, and V. Nyffeler (1976). Determination of Pb-210 in lake sediments and in air samples by direct gamma-ray measurement. Earth and Planetary Science Letters 3, p. 119.

Gallaher, B. M. and M. S. Goad (1981). Water-quality aspects of uranium mining and milling in New Mexico. New Mexico Geological Society Special Publication 10, pp. 85-91.

Goddard, E. N. (1966). Geologic map and sections of the Zuni Mountains fluorspar district, Valencia County, New Mexico. U. S. Geological Survey Misc. Geol. Inv. Map I-454.

Goldberg, E. D., V. Hodge, M. Koide, J. J. Griffin, E. Gamble, O. P. Bricker, G. Matisoff, G. R. Holdren, Jr., and R. Braun (1978). A pollution history of Chesapeake Bay. Geochimica et Cosmochimica Acta 42, pp. 1413-1425.

Happ, S. C. (194). Sedimentation in the middle Rio Grande Valley, New Mexico. Geological Society of America Bulletin 59, pp. 1191-1215.

Hatchell, B., and C. Wentz (1981). Uranium resources and technology; a review of the New Mexico uranium industry 1980. New Mexico Energy and Minerals Department, 226 p.

Hereford, R., (1982). Alluvial stratigraphy and discharge of the Little Colorado River, Arizona, since 1927 (abs.). Geological Society of America with Programs 14, no. 4, p. 172.

Hilpert, L. S. (1969). Uranium resources of northwestern New Mexico. U.S. Geological Survey Professional Paper 603, 166 p.

Horton, C. A. and J. C. White (1958). Separation of uranium by solvent extraction with tri-n-octylphosphine oxide. Analytical Chemistry 11, pp. 1779-1984.

Imboden, D. M. and M. Stiller (1982). The influence of radon diffusion on the Pb-210 distribution in sediments. Journal of Geophysical Research 87, pp. 557-565.

Jenne, E. A., and J. S. Wahlberg. (1968). Role of certain stream-sediment components in radioion sorption. U.S. Geological Survey Professional Paper 433-F, pp. F1-F16.

Johnson, W. M., and J. A. Maxwell (1981). Rock and mineral analysis, 2nd edition. John Wiley and Sons, New York, 489 p.

Kaufman, W. H., O. L. Schumacher and L. A. Woodward (1972). Stratiform copper mineralization in the Nacimiento region, New Mexico. New Mexico Bureau of Mines and Mineral Resources Target Exploration Report 1, 9 p.

Krauskopf, K. B. (1979). Introduction to Geochemistry, 2nd edition. McGraw-Hill, New York. p. 544-545.

Krishnaswami, S., and D. Lal (1978). Radionuclide limnochronology in Lerman, A., ed., Lakes-Chemistry, Geology, Physics. Springer-Verlag, New York, p. 153-177.

Lederer, C. M., J. M. Hollander, and I. Perlman (1967). Table of isotopes, 6th edition. John Wiley and Sons, New York.

Lewis, D. M., (1977). The use of Pb-210 as a heavy metal tracer in the Susquehanna River system. Geochimica et Cosmochimica Acta 41, pp. 1557-1564.

Love, D. W., J. W. Hawley, and J. D. Young (1983). Preliminary report on the geomorphic history of the lower Rio Puerco in relation to archeological sites and cultural resources of the lower Hidden Mountain Dam Site, in Eidenbach, P., editor, Inventory survey of the lower Hidden Mountain floodpool, lower Rio Puerco drainage, central New Mexico. Human Systems Research, Tularosa, New Mexico, pp. 21-65.

Mattinson, J. M. (1972). Preparation of hydrofluoric, hydrochloric and nitric acids at ultralow lead levels. Analytical Chemistry 44, pp. 1715-1716.

McLemore, V. T. (1982). Uranium in the Albuquerque area, New Mexico. New Mexico Geological Society Guidebook, 33rd Field Conference, p. 305-311.

-----, (1983). The uranium industry in New Mexico: History, production, and present status. New Mexico Geology 5, no. 3

New Mexico Water Quality Control Commission (1982). Water quality and water pollution control in New Mexico, 1982. New Mexico water Quality Control Commission, Santa Fe, New Mexico., 113 p.

Nordin, C. F. (1963). A preliminary study of sediment transport parameters, Rio Puerco near Bernardo, New Mexico. U.S. Geological Survey Professional Paper 462-C, p. C1-C21.

National Council on Radiation Protection and Measurements (1978). A handbook of radioactivity measurement procedures. National Council on Radiation Protection and Measurements Report 58, Washington, D. C., 504 p.

Nuclear Data Corporation (1980). ND6600 operational instruction documentation. Nuclear Data Corporation, Schaumberg, Illinois.

Peirson, D. H., R. S. Cambray, and G. S. Spicer (1966). Lead-210 and Polonium-210 in the atmosphere. Tellus 28, pp. 427-433.

Perkins, B. L. (1979). An overview of the New Mexico uranium industry: New Mexico Energy and Minerals Department, 147 p.

Perkins, B. L., and M. S. Goad, editors (1980). Water quality data for discharge from uranium mines and mills in New Mexico. New Mexico Health and Environment Department, Santa Fe, pp. 20-27.

Popp, C. J., and Laquer F. (1980). Trace metal transport and partitioning in suspended sediments of the Rio Grande and tributaries in central New Mexico. Chemosphere 9, p. 89-98.

Popp, C. J., L. A. Brandvold and D. K. Brandvold (1981). Transport mechansims in sediment-rich streams: Heavy metal and nutrient load of the Rio San Jose-Rio Puerco systems. New Mexico Water Resources Research Institute Report No. WRRI 1423642, Las Cruces, New Mexico.

Rautman, C. A. (1977). The uranium industry in New Mexico. New Mexico Bureau of Mines and Mineral Resources Open-File Report 74, 24 p.

-----, compiler (1980). Geology and technology of the Grants uranium region 1979. New Mexico Bureau of Mines and Mineral Resources Memoir 38, 400 p.

Ritchie, J. C., J. R. McHenry, and A.C. Gill (1973). Dating of recent reservoir sediments. Limnology and Oceanography 18, pp. 254-263.

Robbins, J. A., and D. N. Edgington (1975). Determination of recent sedimentation rates in Lake Michigan using Pb-210 and Cs-137. Geochimica et Cosmochimica Acta 39, pp. 285-304.

Schery, S. D. (1980). Determination of Lead-210 in environmental samples by gamma spectrometry with high purity Germanium detectors. Analytical Chemistry 52, pp. 1957-1958.

Schultz, L. G. (1964) Quantitative interpretation of mineralogical composition from X-ray and chemical data for the Pierre Shale. U.S. Geological Survey Professional Paper 391-C, pp. C1-C31.

Shepherd, R. G. (1976). Sedimentary processes and structures of ephemeral-stream point bars, Rio Puerco near Albuquerque, New Mexico (abs). Geological Society of America Abstracts with Programs 8, no. 6, p. 1103.

Siemers, C. T., and J. S. Wadell (1977). Humate deposits of the Menefee Formation (Upper Cretaceous), Northwestern New Mexico. New Mexico Geological Society Guidebook, 28th Field Conference, Supplemental Articles, p. 1-21.

Smith, J. N., and A. Walton (1980). Sediment accumulation rates and geochronologies measured in the Saguenay Fjord using the Pb-210 dating method. Geochimica et Cosmochimica Acta 44, pp. 225-240.

Turekian, K. K., Y. Noazaki, and C. K. Benniger (1977). Geochemistry of atmospheric Radon and Radon products. Annual Review of Earth and Planetary Science 5, pp. 227-255.

Waite, D. A. et al. (1972). Rio Puerco Special Project evaluation report 1242.3. U.S. Department of Interior, Bureau of Land Management, Santa Fe, New Mexico, 35 p.

Wise, S. M. (1980). Caesium-137 and Lead-210: A review of the techniques and some applications in geomorphology, in R. A. Cullingford, D. A. Davidson, and J. Lewin, editors, Timescales in Geomorphology. John Wiley and Sons, London, pp. 109-127.

Young, J. D. (1982). Late Cenozoic geology of the lower Rio Puerco Valencia and Socorro counties, New Mexico (M.S. thesis). New Mexico Institute of Mining and Technology, Socorro, 126 p.

Wells, S. G., T. F. Bullard, C. D. Condit, M. Jercinovic, R. P. Lozinsky, and D. E. Rose (1982). Geomorphic processes on the alluvial valley floor of the Rio Puerco: New Mexico Geological Society Guidebook, 33rd Field Conference, p. 45-47.

Williams, G. P. (1978). Bank-full discharge of rivers. Water Resources Research 14, p. 1141-1154.

VI. ACKNOWLEDGEMENTS

We are grateful to the Huning Land Trust, Westland Corporation, Benjamin Benavidez, and the Laguna Indian Tribe for permission to sample on their land. Virginia McLemore was very helpful in providing background data and production figures for the Grants Uranium Belt. Several of the ideas and procedures discussed in this report, especially relating to radioisotope dating, were initially pursued by Michael Dehn, who incorporated some of the site data in his Master's thesis (in preparation). Kevin Novo-Gradac carried out much of the analysis of radionuclides and heavy metals as part of his Master's thesis (in preparation). John Young (1982) investigated long-term behavior of the lower Rio Puerco as part of his Master's thesis, and aided in digging pits and describing samples along the Rio Puerco. Jim Boyle, Dough Heath, Steve Rosen, Jack Purson, and Phil Coleman helped in surveying sample sites, in digging pits, and compiling hydrologic and sedimentological data on the Rio Puerco drainage system. We are particularly grateful to Lois Devlin and Margo Moore who typed the manuscript and aided with the compilation of the report and to Teresa Mueller who drafted several of the figures.

Appendix B. Descriptions of Sample Pits and Auger Holes

Site 1A

Depth (cm)	Sample No.	Description
0	1A-1	surface sediments from center of channel; silt and clay (57%) with very fine to medium sand (43%; 62-500 u). Color 10 YR 7/3 dry, 10 YR 5/3 wet
0-5	1A-2	silt and clay (98%) with minor very fine to medium sand (2%; 62-350 u). Color 10 YR 6/3 dry, 10 YR 4/3 wet
5-25	1A-3	silt and clay (70%) with very fine to fine sand (24%; 62-177 u). Color 10 YR 6/3 dry, 10 YR 4/3 wet
25-51	1A-4	very fine to fine sand (73%; 62-250 u) with silt and clay (24%). Color 10 YR 6/3 dry, 10 YR 4/3 wet
51-81	1A-5	very fine to coarse sand (61%; 62-1,000 u) with silt and clay in thin laminae. Color 10 YR 7/3 dry, 10 YR 5/3 wet
81-94	1A-6	very fine to medium sand (50%; 62-350 u) with equal silt and clay. Color 10 YR 6/3 dry, 10 YR 4/3 wet.
94-122	1A-7	silt and clay (53%) with fine to medium sand. Color 10 YR 6/3 dry, 10 YR 4/3 wet
122-135	1A-8	very fine to medium sand (58%; 62-350 u). silt and clay. Color 10 YR 6/3 dry, 10 YR 4/3 wet
135-152	1A-9	base of pit; very fine to medium sand (52%; 62-350 u)
152-163	1A-10	almost water-saturated clayey sand; ~15% brown and red clay, (177-250 u) sand
163-173	1A-11	very wet loose fine sand (58%; 62-350 u) with brown clay at base. Colors predominantly 10 YR 6/3 dry, 10 YR 4/3 wet; some clay has reddish tinge
173-183	1A-12	clay at top, fine sand (83%; 177-250 u) getting coarser below. Color 10 YR 7/3 dry, 10 YR 5/3 wet
183-196	1A-13	very fine sand (65%; 62-710 u) at top, (10 YR 4/3) clayey wet sand at base.
196-208	1A-14	clayey sand (62-1,410 u), particularly clayey at base. Sand (47%), silt and clay (53%). Colors 10 YR 7/3 dry, 10 YR 5/3 wet

208-218 1A-15 medium sand (85%; 62-2,000 u), 3mm max size with silt and clay

218-229 no sample medium sand, not as water saturated as above

229-239 no sample same medium (350-500 u) sand with flat pebble 16mm diameter

239-249 1A-16 pebbly (350-500 u) sand; rose quartz grain, pebbles up to 8 mm in diameter

249-259 1A-16 pebbly (up to 35 mm) sand (500-710 u)

259-264 no sample same pebbly sand

264-274 no sample fine (250-300 u) sand

274-284 1A-17 medium coarse (500-700 u) sand, up to 7 mm pebbles

284-292 no sample medium (500 u) sand

292-297 no sample (350-500 u) sand with clayey matrix, redder clay (7.5 YR 4/2) and pebbles with up to 11 mm

297-312 1A-18 reddish (7.5 YR 4/4) clayey sand (125-177 u); sand (75 %), silt and clay (25%)

312 no sample (177-250 u) sand

312-317 no sample coarse (710-1,000) sand, no pebbles

317-330 no sample coarse (710-1,000 u) sand; reddish sand clasts up to 4 mm

330-340 no sample coarse (1,000 u) pebbly sand

340-348 no sample reddish (7.5 YR 5/4) (510-700 u) sand

348-356 1A-19 coarse (500-710 u) (10 YR 4/3) sand

356-371 no sample fine (250-350 u) sand

371-378 no sample fine (7.5 YR 4/2) sand and red clay (2.5 YR 3/6) in sand, red sand at base

378-389 no sample brown clay in fine (250-350 u) sand

389-401 no sample (250-350 u) sand

401-427 1A-20 loose fine to medium sand (93%; 350-500 u)

427 no sample gray (10 YR 5/2) clay base with rusty mottles (5 YR 4/6) 8 mm pebble in clay

Site 2A

Depth (cm)	Sample No.	Description
0-2.5	2A-surface	clay with color 10 YR 6/3 dry, 10 YR 4/3 wet
2.5-15	2A-1	clay and silt with color 10 YR 6/3 dry, 10 YR 4/3 wet
15-30	2A-2	clay and silt with color 10 YR 7/2 dry, 10 YR 5/2 wet
30-41	2A-3	laminated silt and clay with color 10 YR 6/3 dry, 10 YR 4/3 wet, grain size from < 2 u to 61 u
41-61	2A-4	clay and silt with color 10 YR 6/3 dry, 10 YR 4/3 wet
61-81	2A-5	clay and silt with color 10 YR 6/3 dry, 10 YR 4/3 wet
81-91	2A-6	clay and silt with color 10 YR 6/3 dry, 10 YR 4/3 wet
91-112	2A-7	clay and silt with color 10 YR 6/3 dry, 10 YR 4/3 wet
112-132	2A-8	clay and silt with color 10 YR 6/3 dry, 10 YR 4/3 wet
132-152	2A-9	base of pit at 152; clay and silt with color 10 YR 6/3 dry, 10 YR 4/3 wet
152-160	2A-10	chocolate brown (7.5 YR 4/2) clay with streaks and cracks containing reddish fine (5 YR 7/6) sand
160-168	2A-11	brown (10 YR 4/3) clay with whitish evaporite crystals and coatings on fractures; only slightly moist, some horizontal partings
168-178	2A-12	reddish brown (5 YR 5/3) clay broken in blocks, mixed with brown clay with evaporite coatings
178-185	2A-13	mixture of brown (10 YR 5/6) clay and fine (61-88 u) sand with small globules of evaporites
185-193	2A-14	fine (88 u) 10 YR 6/4 very loose sand
193-203	2A-15	mixture of fine sand and brown (10 YR 6/4) clay containing organics (dark brown-black) and rusty root holes
203-213	2A-16	35% silty strong brown (7.5 YR 6/8) sand (61-88 u) with clay to make mixture plastic
213-224	2A-17	very fine (61-88 u) sand interbedded with 40%

laminated clay (10 YR 6.5/4), including organics and evaporite crystals

224-235 2A-18 brown clay (10 YR 6/4.5, 6/4 at base) full of roots and rust-stained margins around former root holes

235-241 2A-19 top: ~70% clay similar to above (10 YR 5/4); base: fine (61-80 u) silty sand (10 YR 7/4) at 241 cm, iron oxide stain ranges to 5YR 5/8

241-251 2A-20 7.5 YR 6/6 sand and silt (30-61 u)

251-262 2A-21 very fine (30-61 u) (7.5 YR 6/4) sand, silt and clay, very uniform texture with some mottles

262-272 2A-22 very fine (88 u) loose sand (10 YR 6/4)

272-279 2A-23 fine (88 u) sand with brown (10 YR 5/4) clay laminae (actually 3 clay laminae 0.5 cm thick)

279-290 2A-24 fine (88 u) 10 YR 7/4 clean friable sand

290-305 2A-25 very fine (<88 u) 10 YR 7/4 clean sand with no clay

305-315 no sample very fine uniform sand, almost dry, no clay; may be eolian

315-325 2A-26 same very fine (88 u) sand with a few hard nodules of stratified sand

325-338 no sample fine sand with clay nodules

338-348 2A-27 same fine (177-250 u) sand (10 YR 7/4)

348-361 no sample fine sand over clay laminae of different colors (5 YR 6/6 and 10 YR 5/4)

361-368 2A-28 fine (125-177 u) sand with clayey sand blebs (10 YR 6/4); sand at base (7.5 YR 7/4)

368-381 no sample fine (10 YR 7/4) sand

381-391 2A-29 fine (125-177 u) (10 YR 7/4) sand

391-404 no sample nearly dry fine (10 YR 7/4) sand, slightly coarser than overlying sand

404-417 2A-30 fine sand (7.5 YR 7/4) fine with some coarser grains and some clay

417-427 2A-31 fine sand over brecciated red (5 YR 4/6) chunks of clay in brown (10 YR 5/4) clay

427-432 no sample fine sand with chunks of red clay (5 YR 4/4)

432-442 no sample very fine sand with brown silty clay laminations (silty climbing ripples)

442-452 no sample fine (177-250 u) (10 YR 6/4) sand

452-462 no sample coarser (500-710 u) (10 YR 6/4) sand, coarsest grain ~ 1 mm

462-472 no sample fine (250-350 u) sand, largest grain ~ 2 mm

472-482 no sample fine sand with larger rock fragments up to 2 mm

482-493 no sample fine (350 u) sand with larger clasts (5 mm quartz grain, fragment of a snail)

493-503 2A-32 fine (350-500 u) (10YR 6/4) sand and larger clasts up to 3 mm

503-505 no sample sand (350 u) with pebbles at base of hole; large clast will not fit into auger

Site 3A

Depth (cm)	Sample No.	Description
0-5	3A-1	silt (2-61 u) with organic material
5-28	3A-2	finely interlaminated 10 YR 5/4 sand and 7.5 YR 4/2 clay, 1cm of 10 YR 4/3 clay at base
28-51	3A-3	10 YR 4/4 sand (177-250 u) with (10 YR 3/3) clay clasts, and cross-bedded 10 YR 3/3 clay bleb layer below
51-69	3A-4	cross-laminated very fine (88-125 u) sand to clay; clay-streaked rippled sand
69-94	3A-5	fine (125-177 u) friable 10 YR 5/3 to 6/4 sand to clay; clay-streaked undulatory ripple-laminated sand
94-105	3A-6	10 YR 4/2 to 3/3 clay grades downward into fine (30-61 u) sandy clay and 10 YR 4/4 sand; ~60% clay
105-122	3A-7	laminated medium (~177 u) sand (10 YR 6/4) fining upward; many 10 YR 4/2 clay clasts and carbonates
122-137	3A-8	10 YR 3/3 and 5 YR 4/3 clay with fine sand laminae, grading upward to uniform 10 YR 6/4 sand
137-152	3A-9	layered (10 YR 4/2 to 3/3) clay and thin very fine (10 YR 4/3) sand and silt laminae
152-167	no sample	layered 10 YR 4/2 clay and very fine 10 YR 6/4 sand and silt; base of pit at 157 cm
167-178	3A-10	~30% fine (<62 u) 10 YR 6/4 sand and 4 cm thick, 10 YR 5/3 clay bed; sand layers 4 cm thick cracked into polygons.
178-188	3A-11	fine (125-177 u) continuous 10 YR 5.5/4 sand
188-198	3A-12	very fine (88-125 u) 10 YR 5.5/3 sand with some cement
198-208	3A-13	finely laminated fine (125-177 u) 10 YR 5.5/4 sand
208-218	3A-14	fine (125-177 u) 10 YR 5.5/4 sand
218-226	3A-15	hard fine (125-177 u) 10 YR 7/4 sand with ~30% 10 YR 5/3 silty brown clay
218-226	3A-16	10 YR 4/2 clay cracked with fine sand
226-234	3A-17	dry clayey silt

234-241 3A-18 dark reddish gray (5 YR 4/3) clay, orange roots, calcareous

241-254 3A-19 finely laminated (62-88 u) 10 YR 6/4 sand below red clay; ~20% clay

254-264 3A-20 dry medium (250-350 u) 10 YR 6/4 loose sand

264-274 3A-21 dry loose coarse (350-500 u) 10 YR 6/4 sand

274-284 3A-22 loose dry medium (250-350 u) 10 YR 6/4 sand

284-295 3A-23 loose dry medium (250-350 u) 10 YR 6.5/4 sand

295-305 3A-24 loose dry medium (250-350 u) 10 YR 6.5/4 sand with a chunk of clay

305-315 3A-25 loose dry medium (250-350 u) 10 YR 6.5/4 sand with clay balls

315-338 3A-26 loose dry medium (250-350 u) 10 YR 6.5/4 sand with clay fragments

338-348 3A-27 gravelly (350-500 u) sand with charcoal armored mudballs, > 6 mm gravel

348-361 3A-28 coarse (350-500 u) sand with clay balls and pebbles

361-368 3A-29 poorly sorted (177-250 u) 10 YR 6/4 to 7.5 YR 7/4 sand with clay balls

Site 5

Deptn (cm)	Sample No.	Description
0-5	5-Su	clay
5-13	5-3	very fine (88-125 u) brown (10 YR 5/3) sand
13-25	5-4	brownish (10 YR 5/3) fine (~125 u) sand
25-33	5-5	reddish (10 YR 6/4) very fine (88-125 u) sand
33-61	5-6	loose discontinuous laminae of fine (177-250 u) 10 YR 5/3 sand
61-86	5-7	fine (~177 u) 10 YR 6/3 sand
86-112	5-8	hard compacted fine to medium (177-350 u) laminated 10 YR 5/3 sand; upper part is coarser
112-119	5-9	distinctly finer (~88 u) 10 YR 5/3 fine sand with silt 10 YR 6/3; rusty root molds
119-132	5-10	clay-coated 10 YR 6/3 fine (~177 u) sand
132-140	5-11	silty (125-177 u) sand with minor chunks of plastic black clay
140-150	5-12	hard fine (125-177 u) 10 YR 5/3 sand
150-168	5-13	fine (177 u) 10 YR 6/3 sand and some silty 10 YR 6/3 sand (88-125 u) in ripples; coarsest sand (250-350 u)
168-198	5-14	very fine (88-125 u) 10 YR 5/3 sand; base of pit at 198 cm
198-213	5-15	fine (125-177 u) 10 YR 6/3 sand
213-229	5-16	fine (125-177 u) 7.5 YR 6/4 sand
229-244	5-17	fine (177 u) 7.5 YR 6/4 sand
244-254	5-18	fine (177 u) 10 YR 6/4 sand
254-267	5-19	fine (177 u) 10 YR 6/4 sand, very few grains > 2 mm
267-279	5-20	fine (177-250 u) 10 YR 6/4 sand
279-290	5-21	fine (177 u) 10 YR 6/4 sand
290-300	5-22	medium (250-350 u) 10 YR 6/4, a few grains ~ 2 mm
300-310	5-23	fine (177-250 u) 10 YR 6/3 sand; 10 YR 5/3 clay balls
310-320	5-24	very coarse (1,000 u) poorly sorted 2.5 YR 5/8 sand and gravel with 10 YR 5/4 clay balls

320-325 5-25 gravels (>1,410 u) 10 YR 5/3 with lumps of 10 YR 5/4 clay; possibly distinct clay layer, physically deposited, not illuviated

325-330 5-26 (>1,410 u) 10 YR 5/3 gravels with lumps of 7.5 YR 4/2 to 4/4 clay

330-340 5-27 (>1,410 u) 10 YR 5/3 gravels with 10 YR 5/3 clays; size to 3 cm

340-353 5-28 coarse (710-1,000 u) 10 YR 5/3 poorly sorted wet sands

353-366 5-29 10 YR 5/3 sand, coarse at top, fine (177-250 u) at bottom

366-381 5-30 medium (250 u) well sorted 10 YR 5/3 wet sand

381-394 5-31 medium (~250 u) 10 YR 5/3 sand, wet to point of saturation

394 no sample very wet sand, water table

Site 6

Depth (cm)	Sample No.	Description
0-1.3	6-Su-0	very fine (88-125 u) sand
1.3-10	6-1	thin discontinuous laminae, rippled, 10 YR 6/3 to 5/3 fine (125-177 u) sand
10-36	6-2	thin discontinuous laminae, rippled, 10 YR 6/3 to to 5/3 fine (125-177 u) sand
36-46	6-3	granules at base of coarse (350-500 u) cross-laminated sand
46-64	6-4	two fining upward 7.5-10 cm layers; very fine (88-125 u) sand at base to clay at top
64-86	6-5	wavy climbing-ripple-laminated (< 88 u) sand; 15 % silt-clay
86-109	6-6	discontinuously cross-laminated low angle coarse (350-500 u) 10 YR 6/5 to 5/4 sand; peoble 2.5 cm long at base; some finer layers
109-122	6-7	10 YR 6/4 uniform fine (125-177 u) sand
122-137	6-8	uniform fine (~177 u) sand
137-147	6-9	fine (177-250 u) sand
147-163	6-10	medium (250-350 u) sand
163-173	6-11	medium (250-350 u) sand
173-188	6-12	medium (250-350 u) sand
188-198	6-13	medium (250-350 u) sand
198-213	6-14	medium (350-500 u) sand; some grains up to 4 mm
213-229	6-15	medium (350-500 u) sand; some grains up to 2 mm
229-244	6-16	medium (350-500 u) sand
244-264	6-17	coarse (~500 u) sand with pebples up to 1 cm
264-274	6-18	coarse (~500 u) moister sand with clay blebs 2 mm and shell fragments up 4 mm
274-284	6-19	medium (250-350 u) sand up to 3 mm
284-295	6-20	medium (250-350 u) sand
295-305	6-21	coarse (>1,000 u) sand with gravel up to 1.2 cm
305-318	6-22	coarse (500-710 u) sand; base 2.5-5 cm includes 10 YR 4/3 clay ball
318-330	6-23	10 YR 4/3 clay mottled with rust, mud balls in

(1,000-1,400 u) sand with peboles > 1cm

330-335 6-24 mud balls in gravelly (1,000-1,400 u) sand

335-345 6-25 coarse (1,000-1,400 u) sand with clay, pebbles to 1 cm

345-356 6-26 coarse (>1,000 u) sand with clay chucks and pebbles > 2 cm

356-366 6-27 greater amount of (710 to >1,000 u) sand, fewer clay chunks, pebbles to 0.5 cm; clay is wet

366-373 6-28 coarse (>1,000 u) sand and clay, pebbles to 3.5 cm

Site 7A

Depth (cm)	Sample No.	Description
0-10	7A-su	10 YR 5/2 discontinuous sandy clay crust and 2.5 YR 4/2 loose sandy (62-500 u) cover
10-18	7A-1	10 YR 5/3 ripple cross-laminated sand, 10 YR 4/2 fine sand and silt with clay layer at base; discontinous clay layer at top as above
18-26	7A-2	10 YR 5/2 very slightly ripple-laminated subangular to subrounded, fine (62-250 u) sand
26-31	7A-3	10 YR 3/3 clay with fine discontinuous sand zones; rounded pellet structure common in clay zones with possible worm castings
31-38	7A-4	10 YR-2.5 Y 4/4 very fine (<125 u) sandy clay
38-54	7A-5	10 YR 4/3 very fine silty sand; tubular voids with worm castings and rounded clay pellets
54-57	7A-6	10 YR 3/2 laminated clay with scattered tubular pores filled with worm castings
57-60	no sample	very fine 10 YR 4/3 laminated sand
60-70	7A-7	10 YR 3/2 laminated undulatory clay; upper part of thick clay layer
70-79	7A-8	lower part of thick clay layer; 10 YR 3/2 laminated undulatory clay with discontinuous thin 10 YR 4/3 sand laminae
79-85	7A-9	2.5 YR 4/2m very fine laminated sandy clay loam
85-88	7A-9	2.5 YR 4/2m very fine laminated sandy clay loam with a 2.5 YR 4/2 clay streak at 85 cm
88-91	7A-10	10 YR 3/2 laminated undulatory clay
91-97	7A-11	10 YR 4/2 and 2.5 Y 4/2 very fine (<88 u) sandy clay loam with wavy laminations
97-102	7A-12	3-4 cm of 10 YR 3/2 and 2.5 YR 3/2 laminated clay with a layer of 10 YR 4/2 sandy clay loam below
102-107	7A-13	10 YR 3/2 clay with very thin sandy partings and undulatory laminations
107-113	7A-14	10 YR 4/2 laminated very fine sandy loam to very fine sandy clay loam
113-115	7A-15	10 YR 3/2 laminated clay; thins to south
115-125	7A-16	10 YR 5/3-4/3 laminated very fine sand with

sandy loam to sandy clay loam interbeds

125-128	7A-17	5 mm of 10 YR 3/2 clay over 10 YR 5/3 very fine sand; base of pit
128-133	7A-18	fine (<125 u) sand
133-150	7A-19	very fine (<88 u) sand
150-172	7A-20	very fine (<125 u) sand

Depth (cm)	Sample No.	Description
0-1.3	7-Su-0	granular platy clay
0-2.5	7-1	granular platy 10 YR 5/3 clay 0-2 cm thick that breaks in blocks
2.5-18	7-2	sandy clay with horizontal platy breakage along bedding (laminae) and mudcracked, 10 YR 6/3 sand is less than 125 u
18-30.5	7-3	brown (10YR 3/2) damp flakes of clay which break into lighter-colored (10YR 6/4) blocks at 30 cm
30.5-41	7-4	silty (62-88 u) 10 YR 6/4 clay in discrete blocks, non-stratified
41-51	7-5	10 YR 4/2 clay with 10YR 6/4 laminated sand (88 u) partings, bottom is undulatory
51-58	7-6	5 cm of sand over 2.5 cm of hard fine (61 u), laminated 10 YR 6/3 sand with wavy crossbeds
58-74	7-7	low-angle discontinuously cross-laminated fine (177 u) 10 YR 6/3 sand
74-89	7-8	low-angle discontinuously cross-laminated fine (177 u) 10 YR 6/4 sand
89-104	7-9	low-angle discontinuously cross-laminated fine (125 u) 10 YR 6/4 sand
104-114	7-10	fine (125 u) 10 YR 6/3 sand; floor of pit at 107 cm
114-127	7-11	fine (88 u) 10 YR 6/3 sand
127-137	7-12	fine (88-125 u) 10 YR 6/3 sand
137-152	7-13	fine (125 u) 10 YR 6/3 sand
152-168	7-14	fine (125-177 u) 10 YR 6/3 damp sand
168-183	7-15	fine (177-250 u) 10 YR 6/3 sand with laminated clay layer
183-198	7-16	fine (125-177 u) 10 YR 6/3 sand with hard sand chunks and 10 YR 5/3 clay layer
198-213	7-17	fine (125-177 u) 10 YR 6/3 sand with chunks
213-229	7-18	transition to coarser (250-350 u) 10 YR 6/3 sand, grains to 1 mm
229-244	7-19	coarse (500 u) 10 YR 6/3 sand, minor pebbles to 9 mm
243-269	7-20	coarse (350-500 u) (10 YR 6/3) sand, gravel to

Site 9

Depth (cm)	Sample no.	Description
0-2.5	9-su	when dry: structureless loam with lots of roots; when moist: 10 YR 5/6 loam with fine sand
2.5-15	9-1	when dry: structureless loam with lots of roots; when moist: 10 YR 5/6 loam with fine sand
15-25	9-2	when dry: ripple-laminated sand (10 YR 4/3m); when moist: texture is a clay loam
25-36	9-3	when dry: 10 YR 4/3 massive and sandy clay; when moist: sandy loam and 40% clay loam
36-43	9-4	sequence of doublets of 10 YR 5/4 clay over sandy clay
43-48	9-4	10 YR 3/3 clay over sandy clay; clay layers from 2.5-5 cm thick, sand layers grade from loamy sand to clay
48-55	9-5	10 YR 3/3 clay over sandy clay; clay layers from 2.5-5 cm thick, sand layers grade from loamy sand to clay
55-60	9-5	10 YR 3/3 clay over sandy clay; clay layers from 2.5-5 cm thick, sand layers grade from loamy sand to clay
60-69	9-5	10 YR 3/3 clay over sandy clay; clay layers from 2.5-5 cm thick, sand layers grade from loamy sand to clay
69-81	9-6	moist massive plastic 10 YR 4/4 strong clay
81-89	9-7	10 YR 5/4 laminated loamy fine sand
89-91	9-7	10 YR 4/3 clayey sand with evaporites
91-99	9-7	sand (177 u; subrounded)
99-112	9-8	coarse 10 YR 4/3 sandy clay, rare pebbles to 1.2 cm including coal
112-122	9-9	pebble gravel with sandy clay matrix; gravel includes flat pieces of sandstone and mudstone
122-137	9-9	bottom of pit, moist clean sand (10 YR 4/4) with pebbles
137-152	9-10	coarse (1,000-1,400 u) sand with 5-mm pebbles
152-168	9-11	coarse (710-1,000 u) 10 YR 6/4 sand with clay balls and pebbles to 5 cm

168-183 9-12 gravel with coatings of 10 YR 4/3 clay; mostly gravel

183-198 9-13 10 YR 5/2 clay with small amounts of gravel (4 cm clasts)

198-213 9-14 10 YR 5/2 gravel with small amounts of clay; 5-cm clasts

213-234 9-15 10 YR 5/2 gravel in contact with clay and (500-710 u) sand

234-243 9-16 10 YR 5/2-5/1 (blotchy to 5/4) clay-rich layer (overall sandy clay loam) with some pebbles to 1 cm with sand and sandy clay

243-254 9-17 mostly cohesive sand (500-710 u) and 2.5 Y 5/2 cohesive sandy loam

Site SJ1

Depth (cm)	Sample No.	Description
3-10	SJ1-1	10 YR 6/3 to 5 YR 5/4 mottled clay
10-14	SJ1-2	reddish brown (5 YR 4/3) clay on top of pale brown (10 YR 7/4) fine (177-250 u) sand
14-26	SJ1-3	reddish (7.5 YR 5/4) clay in the form of plates and granules with (10 YR 7/4) laminated sand (177-250 u)
26-32	SJ1-3	ripple-laminated 10 YR 7/4 sand (710-1000 u maximum, 350-500 u predominately)
32-38	SJ1-4	fining-upward sequence from basal sand to sandy clay loam to silty clay; includes red-brown plates of clay
38-44	SJ1-4	10 YR 7/4 sand (350-500 u; sub-angular, sub-rounded) bagged separately; 2.5 cm basalt pebble
44-45	SJ1-5	red brown (2.5 YR 4/4) clay between sand; well sorted medium (250-350 u) 10 YR 7/4 sand below; (sand taken seperately as SJ1-5 sand)
48-49	SJ1-6	clay less than 1 cm thick; 2 different-colored laminae pinch out to south
49-65	SJ1-7	laminated fine to medium (250-500 u) 10 YR 7/4 subrounded sand
65-69	SJ1-8	two distinct clay layers (10 YR 4/2 and 4/3) separated by 3-4 mm of medium (500 u) sand which is continuous around trench but which thins to west to become sandy clay; 5 YR 4/6 for reddish streaks in clay
68-77	SJ1-9	laminated fine to medium (250-500 u) 10 YR 6/4 sand
77-80	SJ1-10	10 YR 4/3 to 5/4 sandy clay, evaporites in clay; moist laminated sand (350 u) with clay at base
80-89	SJ1-11	fine-medium (80-125 u; up to 350 u) laminated sand; laminae are coarse, up to 1 mm thick
88-91	SJ1-12	10 YR 4/4 and 7.5 YR 4/6 clay-rich layer which thickens to 4 cm in some places
91-98	SJ1-13	7.5 YR 5/4 and 10 YR 7/4 laminated, moderately dry sand with 10 YR 4/3 clay between 93-94 cm
98-100	SJ1-14	gravelly sandy 7.5 YR 4/4 clay layer locally on gravel, poorly sorted, subrounded clasts,

base of pit

100-105 no sample gravel to 6 cm in diameter

105-120 SJ1-15 massive fine (350-500 u) 10 YR 6/4 sand with a clay layer at 110-112 cm up to 2 cm thick

120-130 SJ1-16 upper part is cross-bedded 10 YR 4/4 sand (250 u) and clay, water saturated

130-140 SJ1-17 10 YR 4/3 sand (>250 u) with clay layers

140-150 SJ1-18 10 YR 4/3 to 7.5 YR 4/4 mottled sandy, clayey gravel 5 cm, Mn stain, mollusk fragments, red sand at water table, water table at 150 cm, not basal zone of valley fill

Site SJ-5

Depth (cm)	Sample no.	Description
0-2	none	surface crust of sand and clay
2-10	SJ5-1	upper clay (10 YR 4/2 m); platy clay less than 1 cm thick (10 YR 3/3 m)
10-13	none	well sorted (177-250 u) structureless sand (10 YR 6/4 m)
13-14	SJ5-2	clay (10 YR 3/2 m) less than 1 cm thick
14-18	none	poorly sorted (avg. 250 u; with grains to 1 mm) laminated sand (10 YR 4/3 m)
18-20	SJ5-3	two thin clay layers with intermediate sand layer from 1 to 3 cm thick; like clay and sand above
20-70	SJ5-4	sand with cross-laminated zones, and scattered clay balls up to small cobble size; one peoble of basalt noted; sand (avg 177-250 u; grains up to 1 mm) 10 YR 5/3 moist; discontinuous lenses of sand and coarse sand with granules from 40-50 cm below surface
70-85	SJ5-5	sand with fine pebble gravel, granule gravel and clay balls up to large cobble size; base of pit
85-110	none	brown clay (7.5 YR 3/2) with 7.5 YR 4/6 mottles and gray-white evaporite (sulfate?) crystals; soil-like "black alkali"; mottles of evaporite increase downward; some charcoal; other colors include 7.5 YR 4/4, 4/6
110-130	none	similar to clay above
130-145	none	very fine sand in vertical cracks in gleyed clay (5 Y 5/1)
145-160	none	clay of 2.5 Y and N 5/ colors; becoming moist
160-185	none	thin layers of water-saturated gray sand in clay layers; dominant colors are 7.5 YR browns with gray mottles. no more evaporite crystals
185-200	none	7.5 YR colors with gray mottles in clay

Site PAG-1

Depth (cm)	Sample No.	Description
0-3	PAG1-SU	surface clay platelets
3-15	PAG1-1	moist blocky clay; 10 YR 4/2.5
15-30	PAG1-2	moist brown (10 YR 4/2.5) clay
30-40	PAG1-3	moist brown (10 YR 4/2.5) clay
40-50	PAG1-4	moist brown (10 YR 4/2.5) clay
50-60	PAG1-5	moist brown (10 YR 5/3 to 5/4) silty clay
60-70	PAG1-6	moist brown (10 YR 5/4) clay
70-80	PAG1-7	moist brown (10 YR 5/4) clay
80-90	PAG1-8	moist brown (10 YR 5/4) clay
90-100	PAG1-9	very fine sand at 90 cm; 10 YR 5/4
100-110	PAG1-10	interbedded fine sand and clayey sand; sand layers are saturated with water; water table at 100 cm.
110-120	PAG1-11	similar fine sand and clay interbeds clay at 120 cm
120-130	PAG1-12	clay with interbeds of saturated sand
130-150	PAG1-13	clayey sand interbedded with sandy clay
150-165	PAG1-14	soupy sandy clay with organics (muck)
165-175	PAG1-15	soupy sand with cohesive clay at base
175-200	PAG1-16	cohesive brown (10 YR 4/2) clay layer
200-220	PAG1-17	brown (10 YR 4/3) clay base of hole due to collapsing sides

2.5 cm and 10 YR 4/2 mudball

269-284 7-21 fine (177-250 u) sand, 10 YR 4/2 mudball in one hole, 1 pebble 7 mm

284-305 7-22 coarse (1,000 u) 10 YR 6/3 sand with clay ball base; other hole has 10 YR 4/2 to 5/3 clay with gypsum, evaporites, 7 mm pebbles

305-320 7-23 coarse (>1,000 u) 10 YR 5/4 sand with pebbles to 2 cm and 10 YR 4/3 clay ball

320-335 7-24 medium (250-350 u) 10 YR 5/3 sand with some 10 YR 4/3) clay with evaporites and coarse pebbles at base; clay layer at 330 cm is 5 cm thick

335-351 7-25 hard brown 10 YR 4/2 clay with some 10 YR 4/3 sand and pebbles, possibly from cracks

351-366 7-26 ~99.5% clay with root hairs and evaporites

366-376 7-27 clay, as above with fine (177-250 u) 10 YR 6/3 sand at bottom

376-386 7-28 coarser (250-350 u) rusty sand with occasional pebbles, some clay from above; colors include 10 YR 6/8 and 10 YR 6/3

386-396 7-29 rusty (10 YR 5/4) medium (250-350 u) sand

396-427 7-30 rusty (10 YR 5/4) medium (350-500 u) sand with pebbles, (10 YR 4/3) mudballs, and (10 YR 6/6) clay

Appendix B

Selected X-Ray Diffraction Data (< 2μ fractions)

	Composition (%)				Relative Abundance (%)			
Sample	Clays	Qtz.	Calc.	Alb.	Ill.	Mont.	Kaol.	Chlor.
1-2	59	25	8	8	16	24	49	12
1-6	82	9	5	4	6	9	80	4
1-16	64	18	10	9	9	8	77	6
1-20	80	14	3	<8	14	18	52	16
2-1	67	19	11	5	19	28	47	6
2-20	60	18	8	14	10	12	67	11
2-27	59	18	13	11	7	3	82	7
2-30	69	14	9	8	14	9	46	31
3-1					18	15	54	12
3-2					23	9	60	8
3-8	74	11	8	8	6	11	64	19
3-23	53	36	5	5	13	12	63	12
3-27	75	15	6	6	12	14	68	6
4-1	80	11	2-3	6	9	16	66	9
4-3	24	37	20	21	11	18	53	18
4-12	74	16	5	9	16	18	47	19
4-14	72	10	12	4	14	16	49	20

Appendix C.

Radionuclide Activities for Individual Samples - pCi/g Dry Weight.

Rio Puerco Site 1a:

Sample	Cs-137	Pb-210	Ra-226	Th-234	Pb-214	Bi-214	Ac-228	Pb-212
su	.1360	1.375	2.264	1.010	1.295	.9680	1.344	1.295
3	.0000	2.278	2.205	1.276	1.248	1.216	1.515	1.295
4	.0412	.9770	1.913	.7822	.9250	.9347	.9716	.9164
6	.0475	1.835	3.302	1.605	1.489	1.410	1.534	1.694
7	.1097	1.956	2.888	1.520	1.440	1.309	1.321	1.451
8	.0694	1.340	2.023	1.072	1.300	1.199	1.409	1.365
10	.0390	1.352	1.716	1.078	.9840	.9904	1.150	.9131
11	.0590	1.357	2.355	.9438	1.294	1.158	1.368	1.349
12	.0000	1.275	2.457	1.087	.7241	.8893	.9760	.8836
14	.0193	1.039	2.811	1.476	1.045	1.015	1.293	1.299
15	.0390	1.039	2.811	1.476	1.045	1.015	1.293	1.299
17	.0104	.9152	1.195	.5472	.6262	.6844	.6944	.6088
18	.0000	.8615	1.876	.6924	.9100	.8684	.8757	.9808

Rio Puerco Site 2

su	.2480	2.147	3.165	1.537	1.258	1.277	1.837	1.817
1	.1766	1.634	2.893	1.341	1.271	1.274	1.729	1.749
2	.3030	1.792	3.130	1.445	1.403	1.425	1.834	1.812
3	.1280	1.528	3.090	1.256	1.329	1.326	1.583	1.597
4	.2300	1.716	2.874	1.331	1.457	1.484	1.689	1.722
6	.1546	1.597	3.047	1.432	1.438	1.320	1.424	1.679
7	.4425	1.415	2.623	1.223	1.191	1.172	1.673	1.646
8	.6120	1.924	2.981	1.221	1.566	1.506	1.934	1.792
9	.5919	1.998	3.877	1.943	1.763	1.749	1.883	1.822
10	.1952	1.326	2.570	1.050	1.268	1.314	1.567	1.587
12	.2430	1.600	2.760	1.320	1.229	1.288	1.480	1.570
13	.1520	1.295	2.420	1.193	1.200	1.216	1.465	1.461
14	.0621	1.133	1.989	.9539	.9163	.8382	.9223	1.078
15	.0370	.7594	1.161	.5590	.5368	.5719	.6570	.5870
16	.0920	1.374	2.350	1.017	1.037	1.020	1.107	1.267
17	.6760	1.231	2.535	1.118	1.129	1.196	1.396	1.396
18	.0937	1.398	2.482	1.286	1.344	1.381	1.600	1.555
19	.0856	1.280	2.553	1.058	1.251	1.227	1.431	1.448
20	.0000	1.373	2.918	1.393	1.399	1.421	1.520	1.663
21	.0891	1.562	2.737	1.396	1.241	1.193	1.590	1.406
22	.0000	1.197	2.878	1.459	1.034	1.024	.9797	1.050
23	.0613	1.260	2.130	0.925	1.042	1.080	1.240	1.230
24	.0220	1.105	1.911	.1432	1.012	1.017	1.099	1.106
25	.0000	1.042	2.256	.6099	.9881	.9493	1.050	1.134
26	.0000	1.078	1.861	.8484	.9257	.8839	1.039	.9477
27	.0000	1.075	1.934	1.102	.9015	.9030	.8156	1.050
28	.0000	1.045	1.813	.0913	.8856	.9150	1.021	.9519
29	.0000	1.035	1.708	.8096	.8870	.8648	.8698	.8706

Rio Puerco Site 3a

1	.2740	2.417	3.045	1.229	1.146	1.182	1.624	1.684
2	.0890	1.224	2.584	1.041	1.118	1.122	1.526	1.420
3	.0418	1.215	2.179	1.116	.9734	1.007	1.290	1.196
4	.1254	1.011	2.242	.9719	1.001	1.010	1.270	1.116
5	.0444	1.058	1.825	.8110	.9365	.9615	.9618	1.045
6	.1689	1.615	3.262	1.382	1.455	1.278	1.672	1.889
7	.0250	.9630	2.223	.9656	1.079	1.085	1.192	1.195
8	.1273	1.649	2.762	1.311	1.386	1.361	1.687	1.622
9	.1234	1.576	2.670	1.521	1.292	1.345	1.774	1.735
10	.0715	1.079	2.144	1.168	.9373	.9633	1.649	1.153
11	.0000	1.132	2.079	1.472	.8906	.9117	1.170	.9876
12	.0170	1.110	2.040	.9220	.9570	1.008	.0381	1.047
13	.0249	1.062	1.811	.755	.9158	.9063	1.014	.9855
14	.0364	1.019	1.994	.8135	.9570	.9142	1.039	1.025
15	.0810	1.454	2.716	1.224	1.113	1.154	1.613	1.532
16	.0185	1.569	2.518	1.147	1.248	1.259	1.553	1.550
17	.0341	1.291	2.390	.9831	1.105	1.480	1.743	1.805
19	.0559	1.828	2.921	1.446	1.533	1.480	1.743	1.805
20	.0000	.8852	1.368	.5596	.7373	.0000	.6938	.7770
21	.0000	.6720	.6678	.5181	.5651	.6070	.6321	.5639
22	.0000	.6103	1.113	.7854	.5251	.5492	.7089	.5696
23	.0000	.7722	1.176	.4440	.5788	.6035	.7026	.5789
24	.0000	.6870	1.054	.4929	.4957	.5343	.5879	.5523
25	.0077	.8440	1.272	.6831	.6064	.6185	.6471	.6425
26	.0000	.9217	1.876	1.189	.9818	1.003	1.537	1.089
27	.0000	.8736	1.533	.5984	.6748	.7198	.9282	.7151
28	.0145	1.007	2.003	.9410	.9563	1.049	1.537	1.017
vf	.0000	.8600	1.545	.7386	.6630	.7063	.9493	.8564

Rio Puerco Site 5

su	0.207	2.041	2.872	1.209	1.299	1.256	1.475	1.450
3	.1180	1.208	2.280	1.148	.9886	1.058	1.162	1.148
4	.0000	.6800	1.474	.8211	.7852	.6834	.8793	.7752
5	.0879	1.692	3.757	1.773	1.555	1.482	2.316	1.655
6	.0299	.7110	1.252	.5798	.6723	.6632	.6996	.6952
7	.0148	.9140	1.472	.7520	.7130	.7800	.8276	.7712
8	.0000	.2209	1.201	.7601	.6191	.6463	.7358	.6961
9	.0603	1.077	1.886	.9402	.9567	.9658	1.117	.9879
10	.0000	.9929	2.239	.6017	.8636	.9940	1.000	.8340
11	.0608	1.110	2.886	1.194	1.278	1.261	2.219	1.464
12	.0451	1.129	2.647	.6090	.7698	.8021	1.113	.7021
13	.0393	.8652	1.722	.7868	.5886	.7449	.8168	.6869
14	.0000	.5369	1.859	.9880	.6752	.6330	.9625	.7670
15	.0198	.8796	1.542	.6028	.7768	.7802	.8492	.7868
16	.0000	.3274	1.090	.3585	.5662	.5653	.6653	.5921
18	.0000	.9217	1.449	.7874	.6087	.8200	.7026	.7143
19	.0106	.7868	1.296	.5714	.6389	.6597	.7498	.6824
20	.0285	.8812	2.648	.9621	.9581	1.010	1.528	1.035
21	.0000	.6789	1.131	.4889	.6294	.5892	.7734	.6346
22	.0000	.7039	.7933	.6305	.5821	.7457	.5243	.5704
23	.0000	.9822	1.693	1.142	1.033	1.001	1.429	.9860
30	.0000	1.382	2.450	.7567	.9567	.9954	1.380	.9912

Rio Puerco Site 6

su0	.0101	.9513	2.103	.1582	.9863	1.001	1.114	1.090
su1	.0541	1.199	2.037	.9490	.7525	.8547	1.020	.9331
su2	.1484	1.385	1.933	1.052	.8518	.8399	1.288	1.308
su3	.0783	1.377	2.263	1.155	.9677	.9804	1.085	1.265
su4	.0986	.7252	1.689	.5589	.8452	.8503	1.232	.9682
su5	.6791	.7872	1.124	.5437	.6494	.6792	.7179	.6499
su7	.0384	.7872	1.232	.4612	.5690	.6332	.7176	.6277
su10	.0740	.8992	1.729	.6850	.7808	.7936	1.007	.8982
su11	.0289	.8820	1.357	.7228	.7357	.7705	.8010	.7839
1	.0000	1.578	1.961	1.183	1.180	1.041	1.378	1.143
2	.0000	1.551	1.885	.8841	1.070	1.063	.7697	1.027
4	.0919	1.244	3.131	.8458	1.210	1.209	1.200	1.403
6	.0000	.8066	1.601	1.015	.7817	.8278	1.057	.8930
7	.0000	.6332	2.219	.6463	.9184	.9484	1.006	.9650
8	.0020	.5893	1.240	.6939	.5366	.7050	.6653	.5078
9	.0000	.5625	1.132	.3446	.6013	.4991	.6631	.5904
12	.0000	.6721	1.384	.9543	.8221	.9108	1.009	.9659
14	.0000	.6118	.8022	.5721	.5275	.5295	.8007	.6597
22	.0000	.4098	1.071	.9691	.6275	.6095	.7248	.4718
23	.0000	.8055	1.643	.6210	.6809	.6439	.7281	.5449
24	.0000	.6183	1.440	.5624	.572	.6105	.7731	.5499
28	.0000	.9794	1.220	.6272	.6424	.8032	.6976	.5687
36	.0000	.8246	1.599	.7543	.7769	.7780	.8599	.8632

Rio Puerco Site 7

su0	.1973	2.015	2.613	1.302	1.190	1.172	1.699	1.646
su1	.1645	1.639	2.488	1.126	1.262	1.201	1.251	1.433
su2	.2021	2.033	2.033	1.609	1.363	1.255	1.887	1.834
su3	.1490	1.956	2.963	1.449	1.313	1.221	1.787	1.777
su4	.2043	1.646	2.109	1.202	.9344	.9243	1.417	1.335
1	.2020	1.767	2.893	1.353	1.377	1.377	1.792	1.706
2	.1400	1.169	2.625	1.576	1.091	1.147	1.379	1.276
3	.3540	1.537	2.598	1.304	1.160	1.199	1.645	1.565
4	.3140	1.515	2.817	1.293	1.310	1.299	1.717	1.641
5	.0000	1.150	2.556	1.138	1.219	1.243	1.583	1.444
6	.0000	1.164	2.106	1.144	1.075	1.107	1.270	1.265
7	.0023	.7512	1.302	.6261	.7422	.7646	.6260	.7660
8	.0000	.9260	1.441	.6851	.8164	.8484	.9457	.8200
9	.0217	1.139	2.071	.9173	1.042	1.061	1.132	1.094
10	.0000	.9874	1.835	.8190	.9720	.9809	1.050	1.018
11	.0000	1.059	2.004	.9195	1.054	1.037	1.099	.0485
12	.0000	.9164	1.531	.6799	.7128	.7429	.9010	.9060
13	.0000	.9813	1.817	.7978	.8736	.8943	.9256	.9119
14	.0000	1.004	1.888	.7702	.9013	.9456	.9674	.9045
15	.0000	.6928	1.253	.6087	.7191	.6968	.7763	.7433
16	.0000	.8628	1.432	.7120	.7167	.6947	.7750	.7579
17	.0110	.9232	1.575	.7133	.8269	.8565	.9104	.8617
19	.0000	.5621	1.211	.5395	.6122	.6132	.6665	.5815
20	.0000	.5872	1.265	.5637	.6396	.6407	.6963	.6075
30	.0000	.7949	1.076	.7737	.5534	.5701	.6243	.5092
33	.0000	.8956	1.631	.5978	.7982	.7896	.8837	.8836

Rio Puerco Site 7a

2	.0812	1.230	2.307	.9615	.9881	1.038	1.181	1.122
3	.1273	1.386	2.268	1.014	1.024	1.049	1.261	1.298
4	.0609	1.302	2.573	1.073	1.102	1.177	1.514	1.339
5	.0557	1.217	2.587	1.118	1.174	1.122	1.413	1.357
6	.2979	1.700	2.854	1.589	1.407	1.369	1.757	1.684
7	.5150	1.384	2.469	1.240	1.223	1.254	1.631	1.649
8	.2736	1.265	2.453	1.083	1.041	1.014	1.456	1.472
9	.0082	1.066	2.158	1.055	1.048	1.055	1.175	1.207
10	.0000	1.347	2.595	1.251	1.291	1.294	1.777	1.620
11	.0000	1.168	2.249	.9859	1.060	1.090	1.241	1.201
12	.0000	1.631	3.085	1.875	1.404	1.421	1.916	1.876
13	.0470	1.615	2.954	1.321	1.338	1.325	1.757	1.693
14	.0000	1.476	2.331	1.068	1.162	1.135	1.316	1.206
15	.0000	1.248	2.552	1.058	1.247	1.250	1.510	1.445

Rio Puerco Site 9

1	.1314	1.146	1.927	.9515	.8390	.8212	1.791	1.028
2	.0301	1.146	2.122	1.035	1.070	1.065	1.230	1.242
4	.0301	1.146	2.122	1.036	1.070	1.065	1.230	1.242
5	.2303	1.174	2.375	1.027	1.225	1.283	1.359	1.355
6	.2305	1.190	2.433	1.131	1.237	1.220	1.536	1.543
7	.0310	.9685	2.016	.7828	.9078	.9448	1.097	1.056
8	.0611	.9294	1.967	.8872	.9492	1.013	1.080	1.043
9	.0000	.7479	1.444	.5288	.7072	.7632	.7078	.6676
10	.0000	.7963	.5882	.5820	.7744	.7807	.6757	.6359
12	.0000	.9582	2.204	.8615	.9699	.9749	1.071	1.076
13	.0092	1.248	2.045	.9569	1.058	.9741	1.420	.7875
14	.0000	.8171	1.834	.6473	.9552	.9019	1.165	1.133
16	.0000	.9533	1.822	.0743	.8568	.8304	1.126	1.157
vf	.0000	.9159	1.657	.7393	.7573	.7703	.8683	.8748

Arroyo Chico Site 10

su1	.0889	1.265	2.147	1.034	.9806	.9365	1.256	1.179
su2	.0253	.7888	.7888	1.288	.6274	.7233	.7023	.7944

Arroyo Chico Site 11

1	.0712	1.164	1.904	1.018	.9724	.9118	1.090	1.052

Rio San Jose Site 1

su1	.1699	2.240	3.736	1.783	1.878	1.877	1.799	1.766
su2	.1944	2.122	3.484	1.597	1.693	1.679	1.686	1.734
su3	.1827	2.144	3.693	1.622	1.727	1.719	1.745	1.794
0	.1827	2.144	3.693	1.622	1.727	1.719	1.745	1.794
1	.2498	2.055	3.015	1.370	1.385	1.400	1.803	1.752
2	.1628	1.733	2.396	1.146	1.094	1.049	1.339	1.296
4	.1300	1.048	1.870	.7933	.8207	.8398	2.085	.8587
6	.1019	.6808	1.239	.5741	.5502	.5767	.5407	.5264
8	.1836	.9531	1.804	.7512	.8195	.8313	.8857	.8068
10	.1538	.9531	1.804	.7512	.8195	.8313	.8857	.8068
12	.2067	1.019	1.663	.8339	.8710	.8521	.9298	.8526
13	.1283	.8620	1.392	.6162	.7630	.8195	.7558	.7029
16	.1987	.8648	1.460	.0000	.7440	.7533	.8373	.7313
17	.0630	1.042	1.888	.9626	1.012	1.005	1.034	.9790
18	.0201	.5497	1.055	.4628	.5118	.5395	.4658	.4390

Rio San Jose Site 3

3	.0102	.9319	1.695	.8752	.8310	.8214	.9439	.9889
4	.0000	1.435	2.883	1.348	1.360	1.376	1.722	1.705
5	.0000	1.416	2.963	1.398	1.444	1.451	1.706	1.608

Rio San Jose Site 4

su1	.3427	2.008	1.996	.8352	.8691	.9132	1.281	1.178

Rio San Jose Site 5

1	.5488	3.291	4.835	2.034	2.517	2.505	1.447	1.387
2	.2068	1.107	1.602	.6493	.7548	.6911	.5861	.5111
3	.1814	.9467	1.313	.5680	.6531	.6327	.6882	.6185
6	.0000	1.183	2.543	.9886	1.260	1.275	1.328	1.293

Rio San Jose Site 6

old	.0000	1.339	2.562	.9240	1.204	1.215	1.531	1.486
su1	.0329	1.077	1.624	.9117	.7627	.8080	.8861	.8488

Paguate Resevoir Site 1

su	.1952	5.391	11.46	4.450	5.376	5.294	2.017	2.079
1	.3820	11.93	22.55	7.864	12.72	12.50	2.044	2.101
2	.4429	15.62	26.85	9.350	13.61	14.36	1.962	2.105
3	.7340	3.472	8.050	4.205	3.539	3.494	1.989	2.164
5	.0238	1.952	4.885	2.522	1.910	1.828	1.851	1.798
6	.0315	1.820	3.917	2.064	1.803	1.784	1.850	1.784
7	.0530	1.757	1.746	3.696	1.769	1.770	1.573	1.567
8	.0253	1.459	3.298	1.456	1.556	1.499	1.624	1.681
9	.1458	.9790	1.941	.8060	.9940	.9890	.8909	.8300
10	.0000	1.184	2.309	1.001	1.115	1.109	1.145	1.064
11	.0000	1.338	2.590	1.369	1.308	1.387	1.335	1.378
12	.2133	3.023	6.642	3.000	3.209	3.083	1.883	1.881
13	.0159	1.491	2.926	1.550	1.476	1.466	1.509	1.500
14	.0151	1.169	2.203	0.777	1.044	0.978	0.974	0.942
15	.0000	1.154	2.330	1.211	1.135	1.161	1.143	1.136
16	.0000	1.559	2.767	1.382	1.454	1.440	1.685	1.880
17	.0000	1.445	2.738	1.260	1.404	1.400	1.806	1.824

Appendix D.

Normalized Cs-137 Activities of Samples from Sites 1-7.

Cs-137 Activity at Site 1A

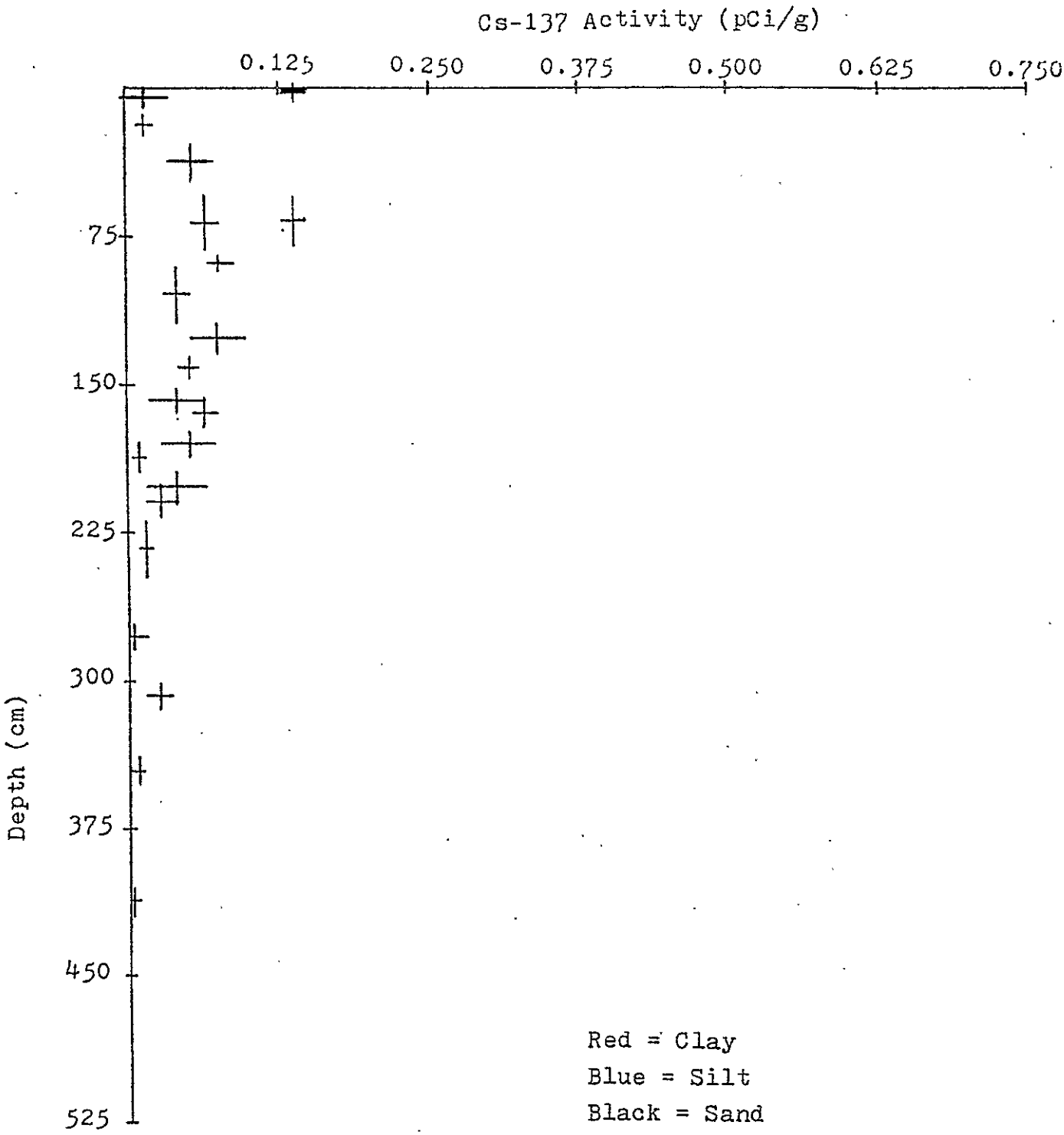

Normalized Cs-137 Activity at Site 1A

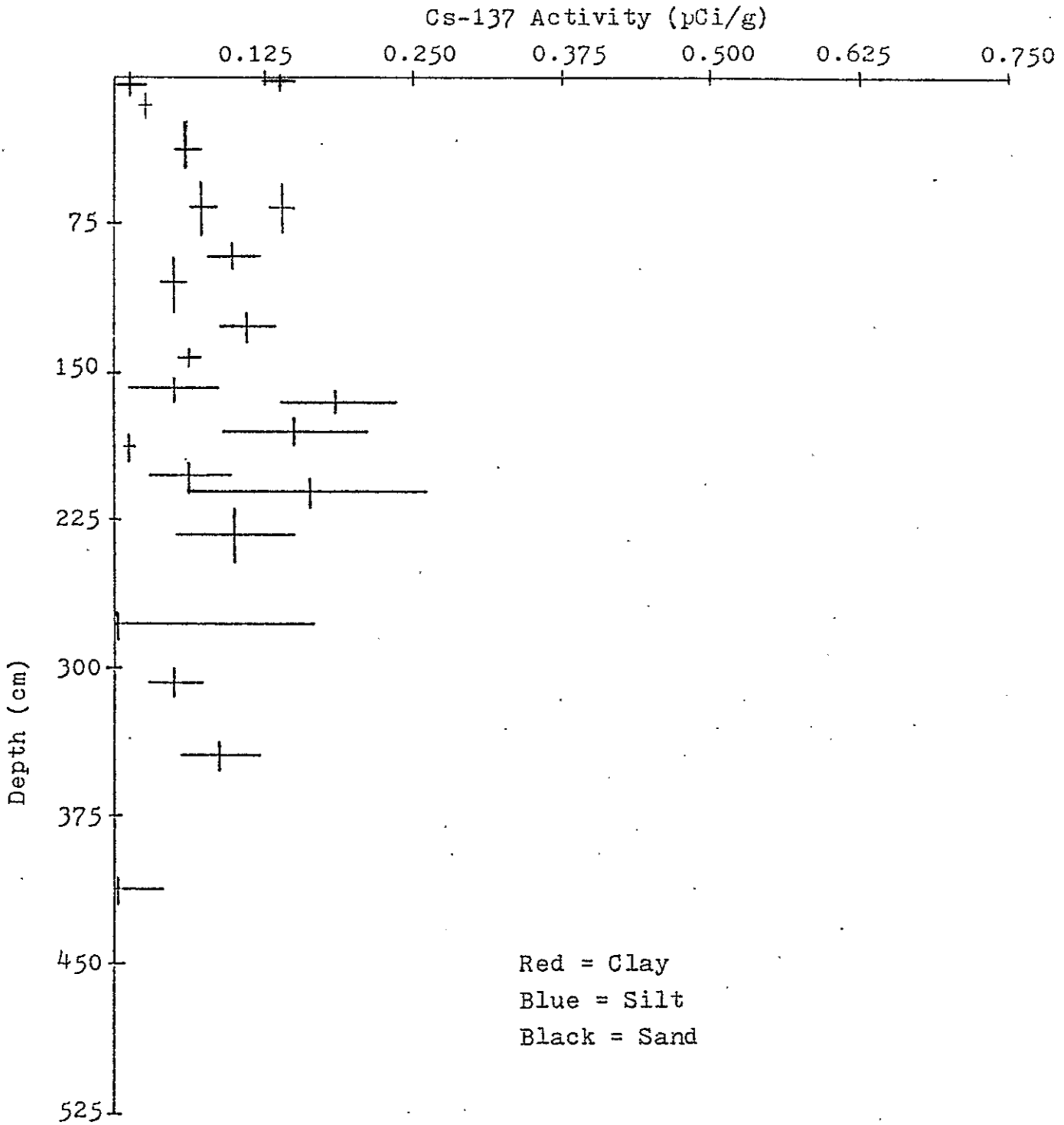

Normalized Cs-137 Activity at Site 2A

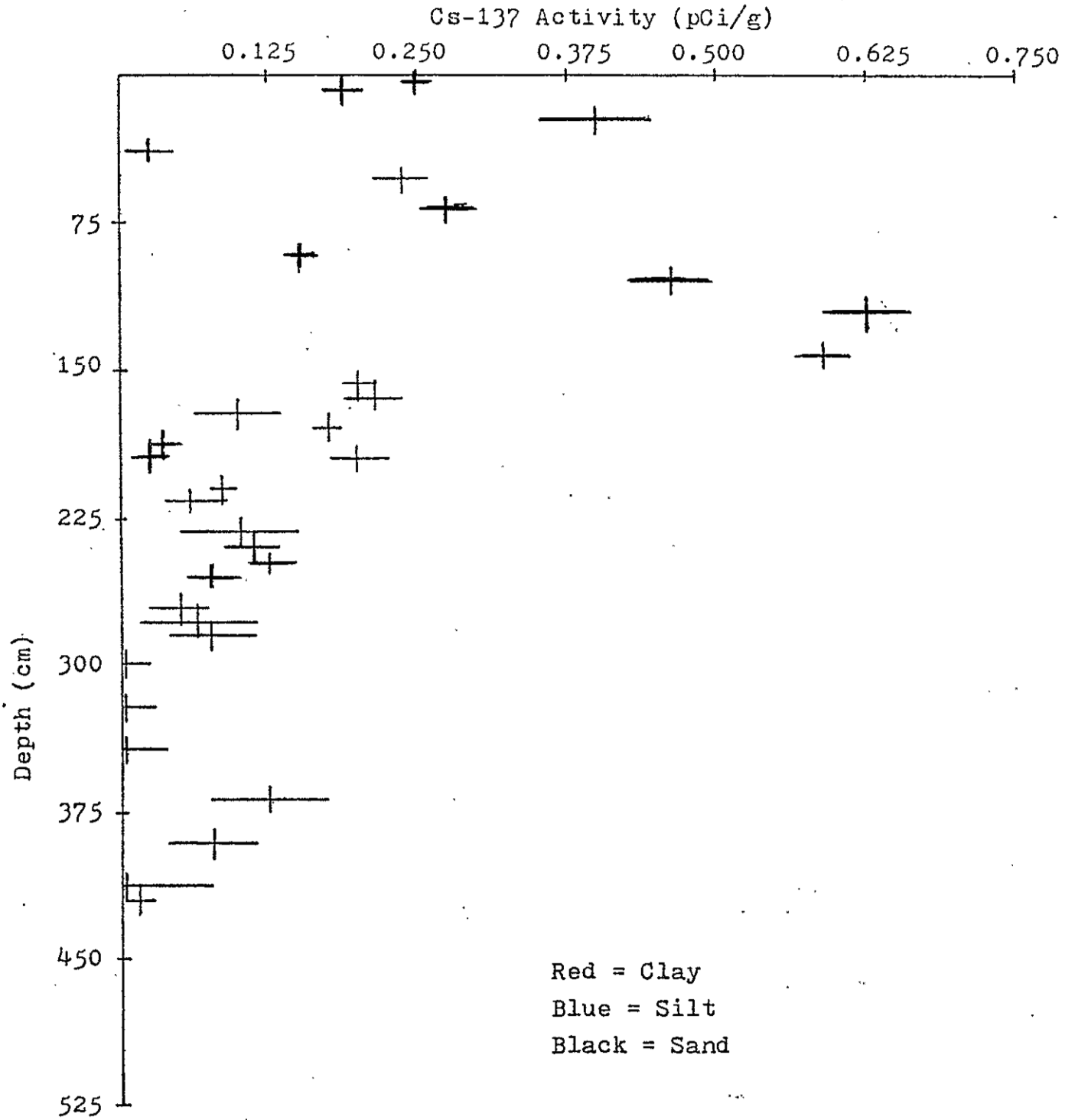

Normalized Cs-137 Activity at Site 3A

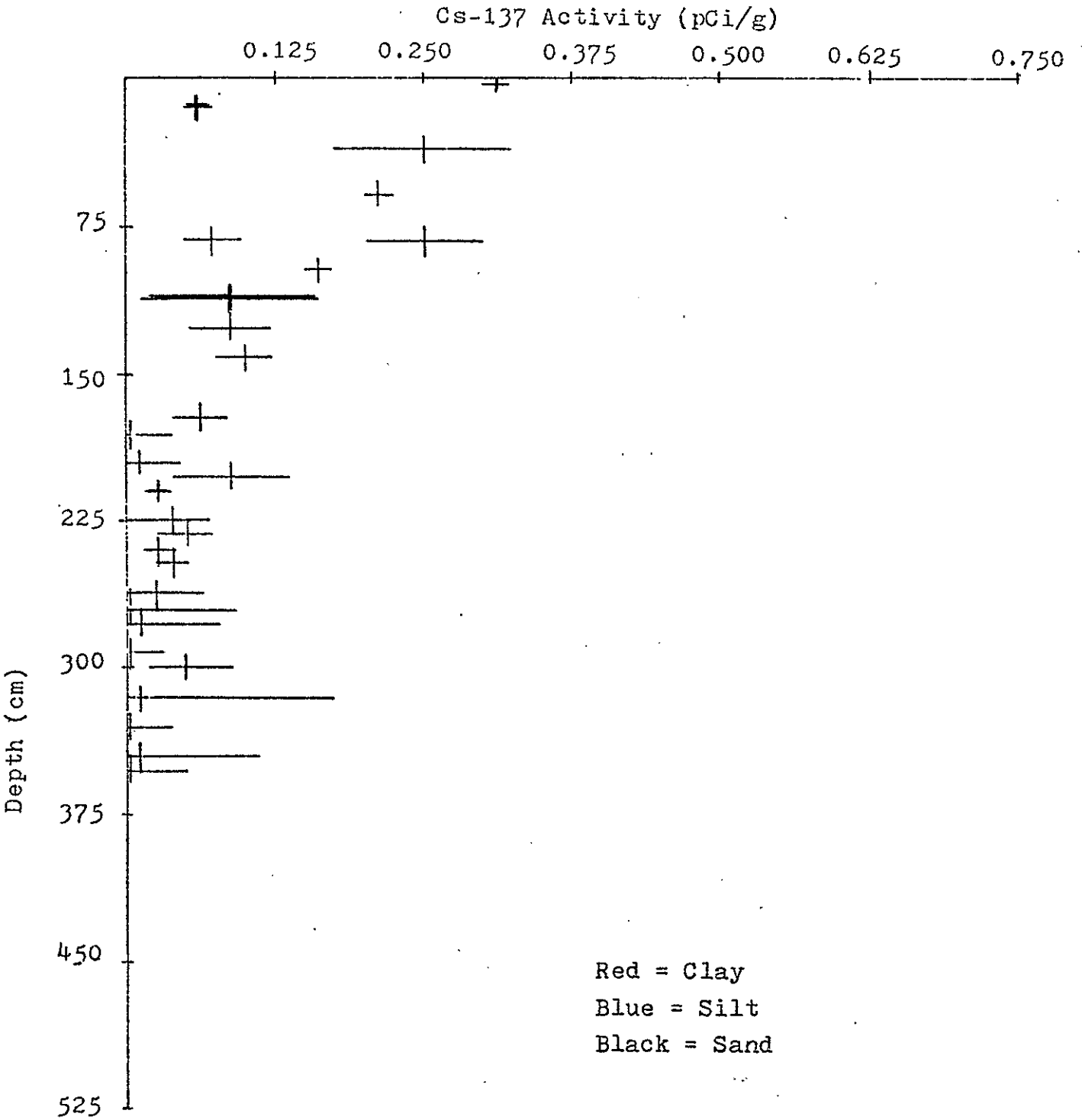

Normalized Cs-137 Activity at Site 5

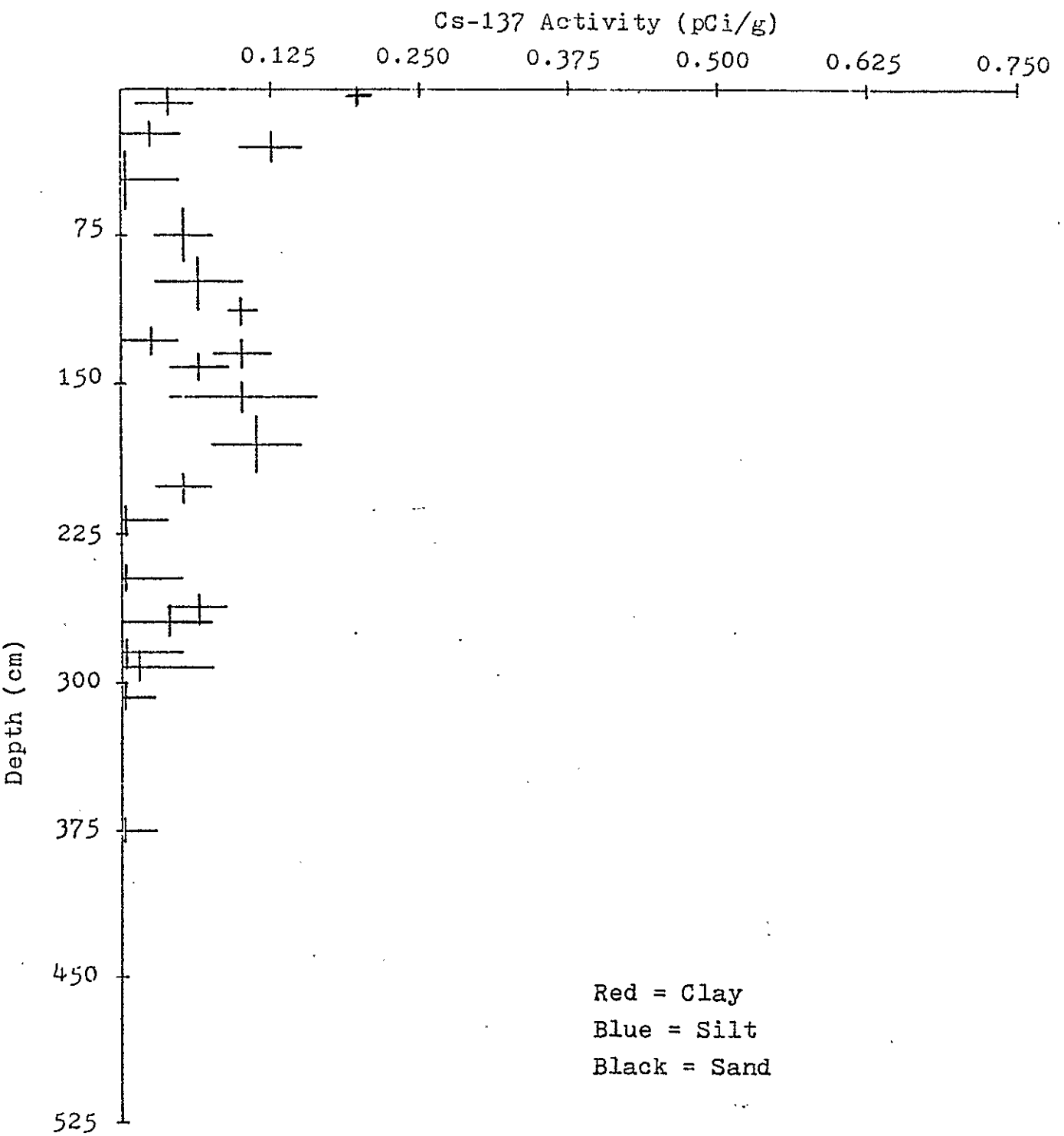

Normalized Cs-137 Activity at Site 6

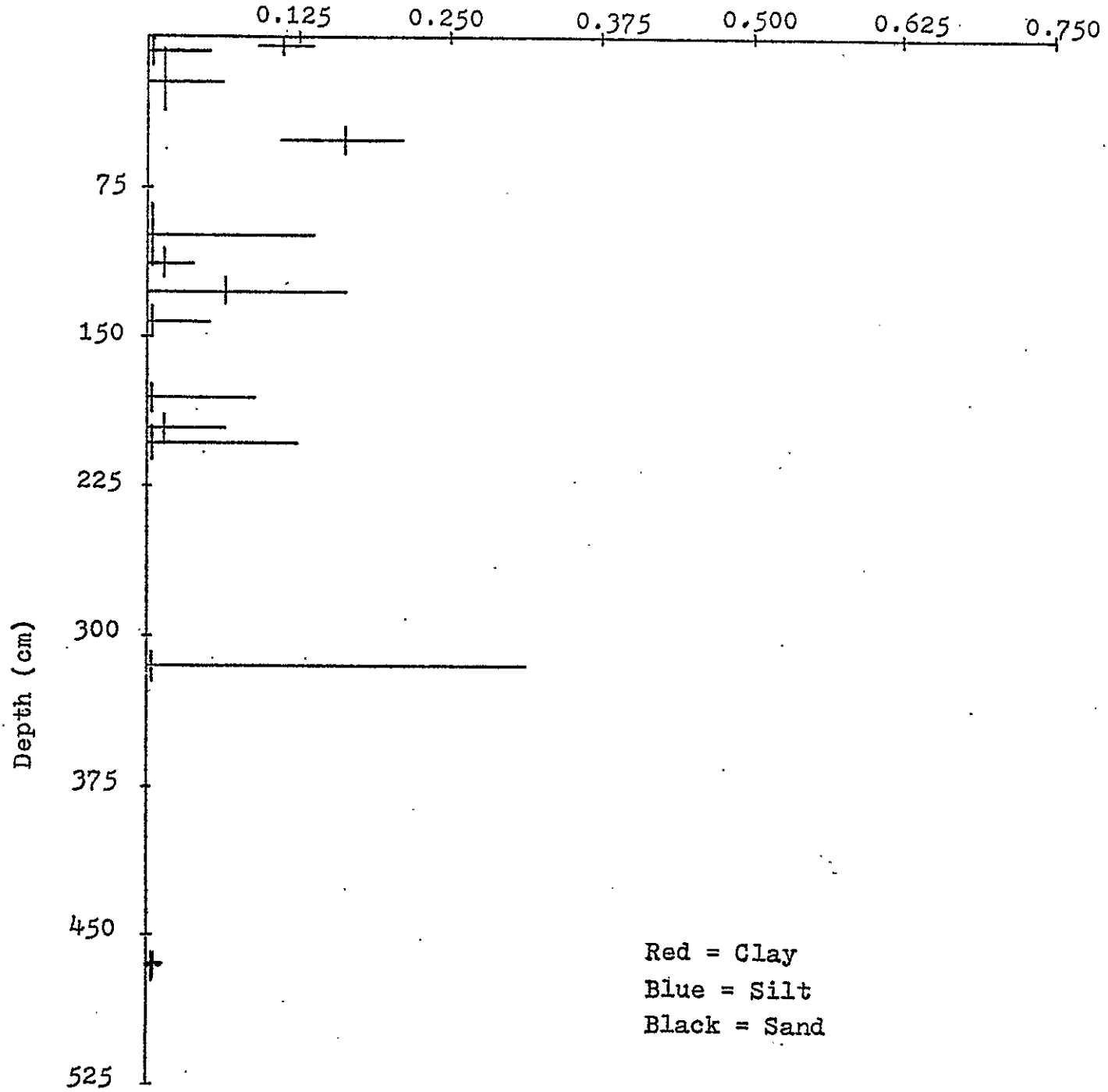

Normalized Cs-137 Activity at Site 7

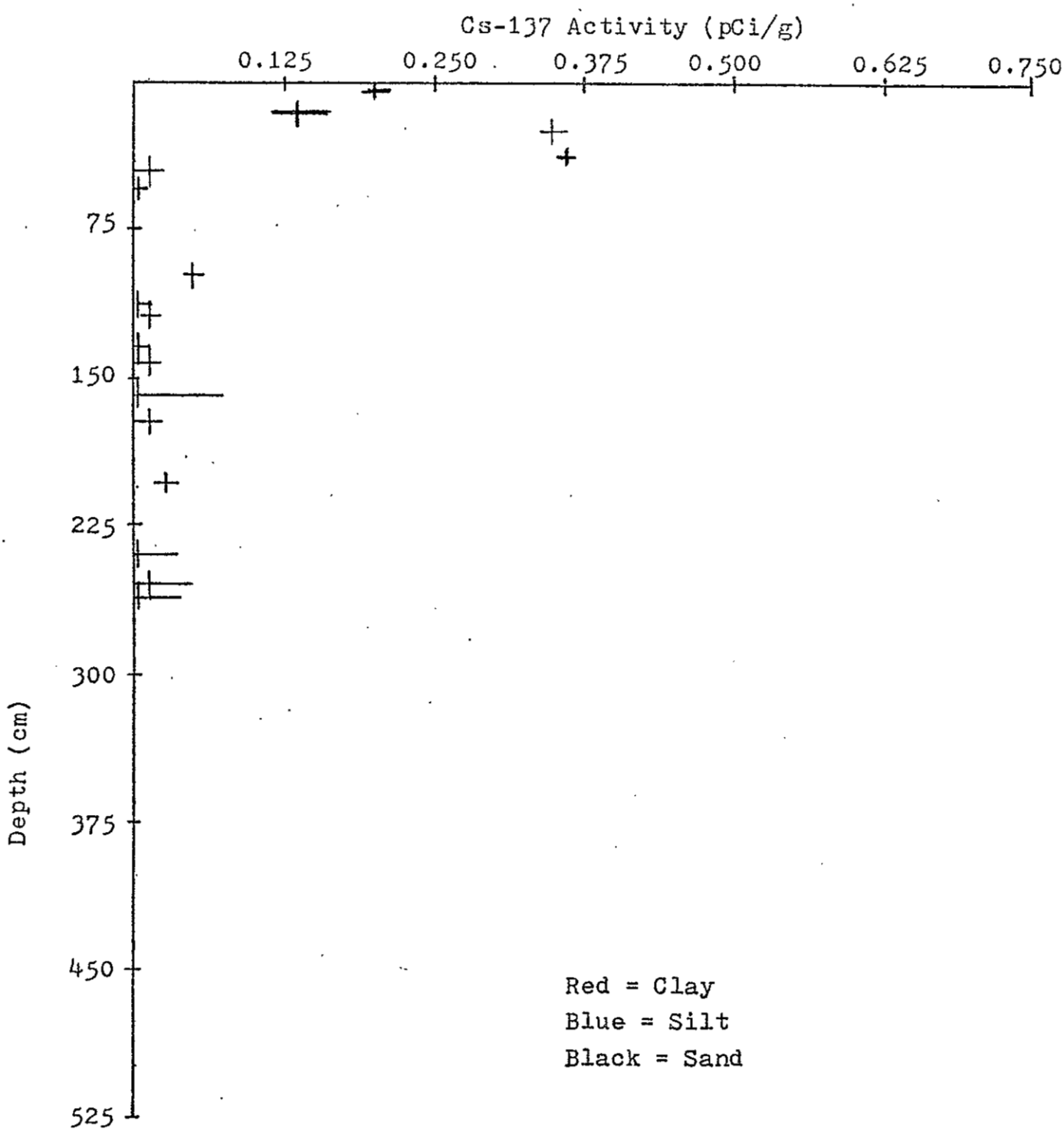

Appendix E.

Histograms of Radionuclide Distribution in Core Samples (grouped according to Radionuclide).

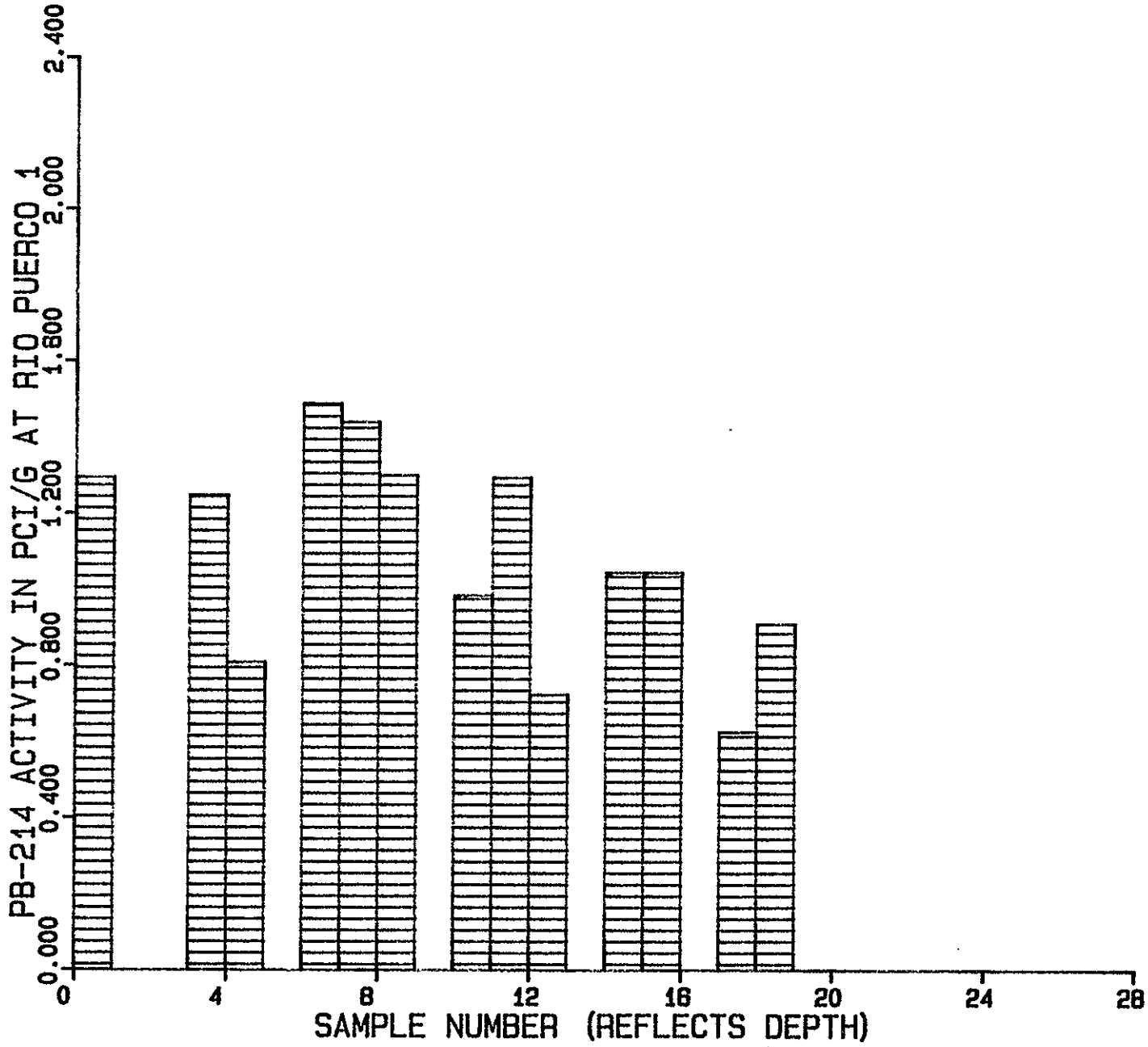
PB-214 ACTIVITY IN PCI/G AT RIO PUERCO 1
0.000
0.400
0.800
1.200
1.800
2.000
2.400
0
4
8
12
16
20
24
28
SAMPLE NUMBER (REFLECTS DEPTH)

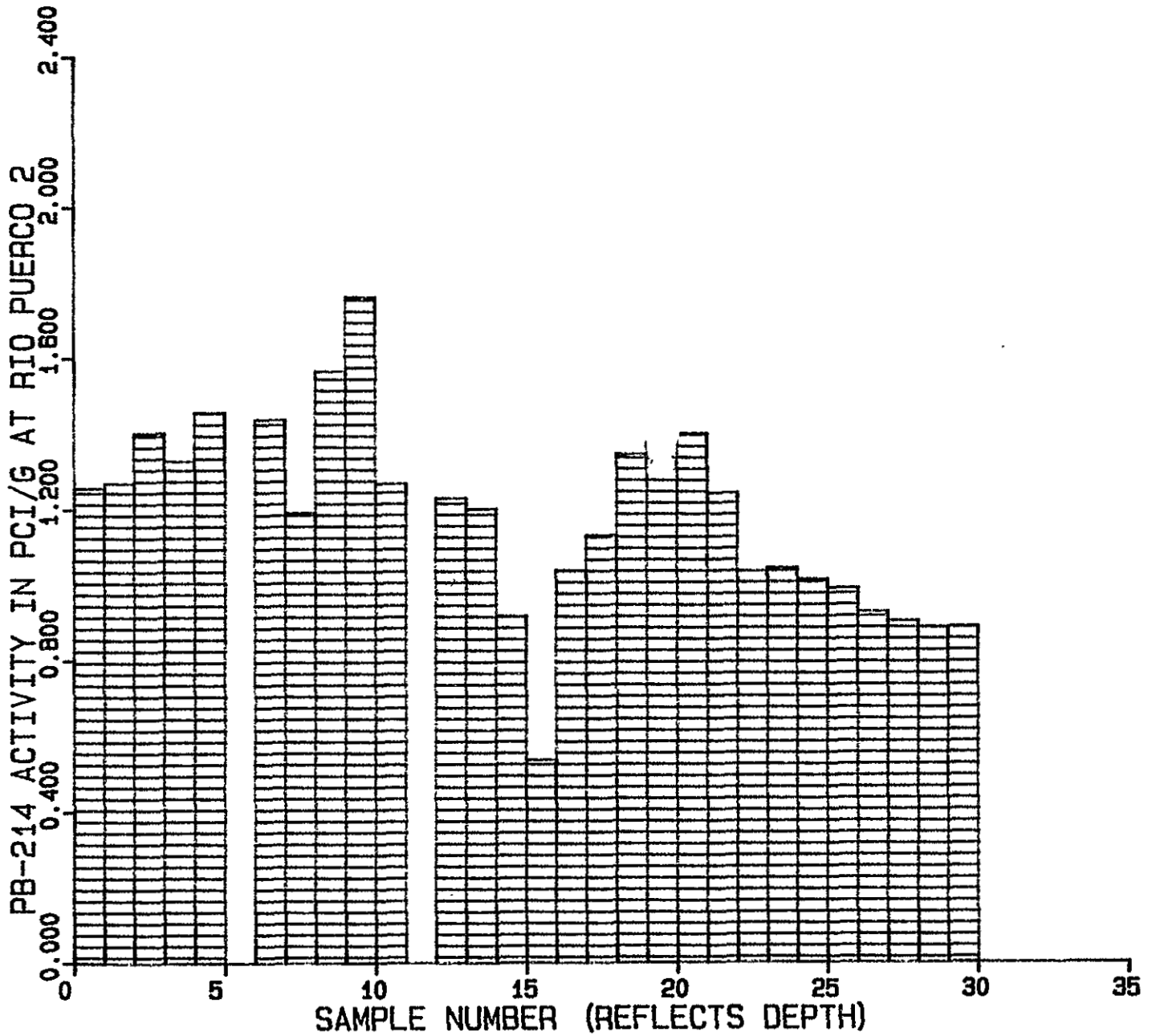
PB-214 ACTIVITY IN PCI/G AT RIO PUERCO 2
0.000
0.400
0.800
1.200
1.600
2.000
2.400
0
5
10
15
20
25
30
35
SAMPLE NUMBER (REFLECTS DEPTH)

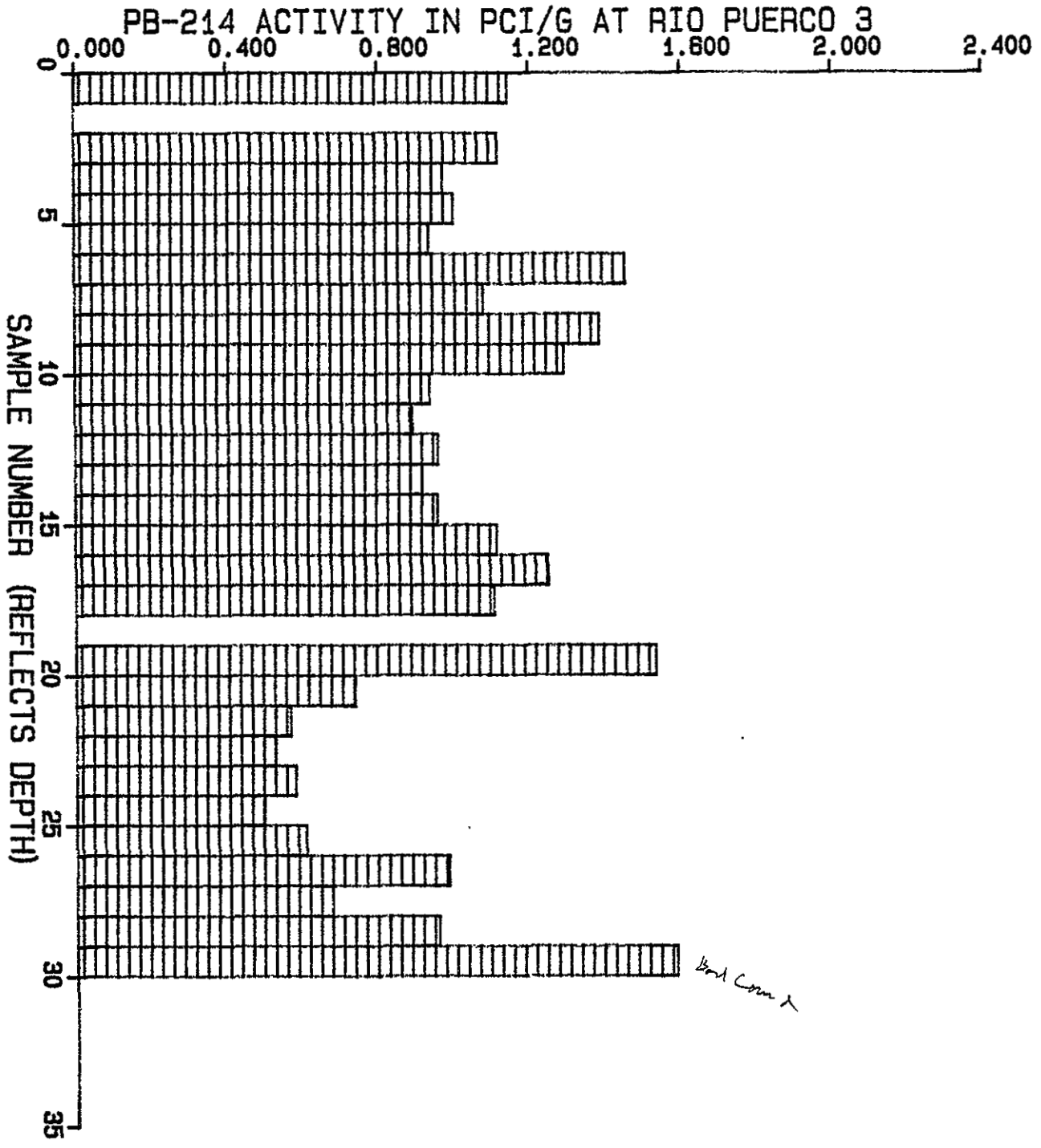
PB-214 ACTIVITY IN PCI/G AT RIO PUERCO 3
0.000
0.400
0.800
1.200
1.600
2.000
2.400
0
5
10
15
20
25
30
35
SAMPLE NUMBER (REFLECTS DEPTH)

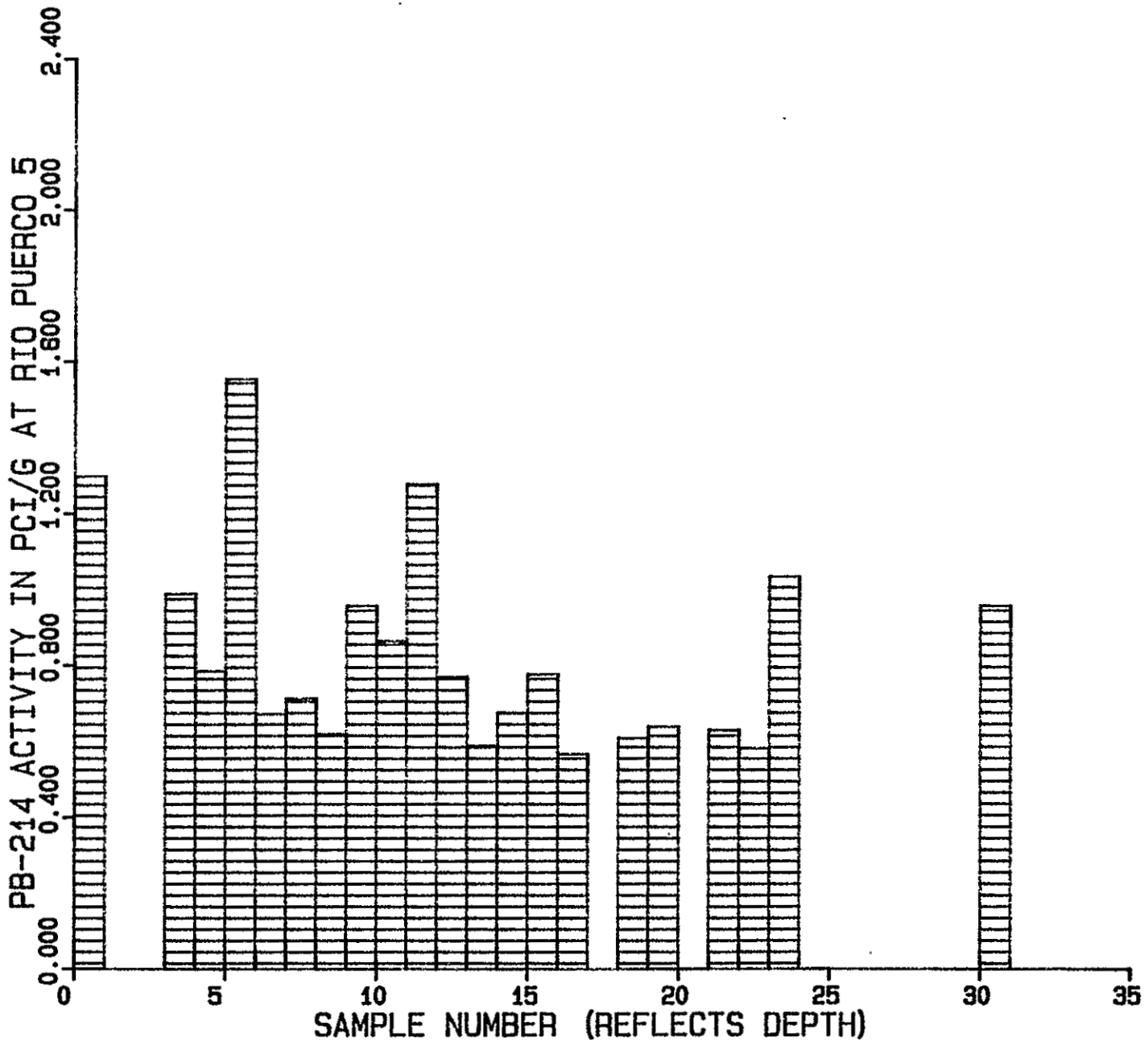
PB-214 ACTIVITY IN PCI/G AT RIO PUERCO 5
0.000
0.400
0.800
1.200
1.800
2.000
2.400
0
5
10
15
20
25
30
35
SAMPLE NUMBER (REFLECTS DEPTH)

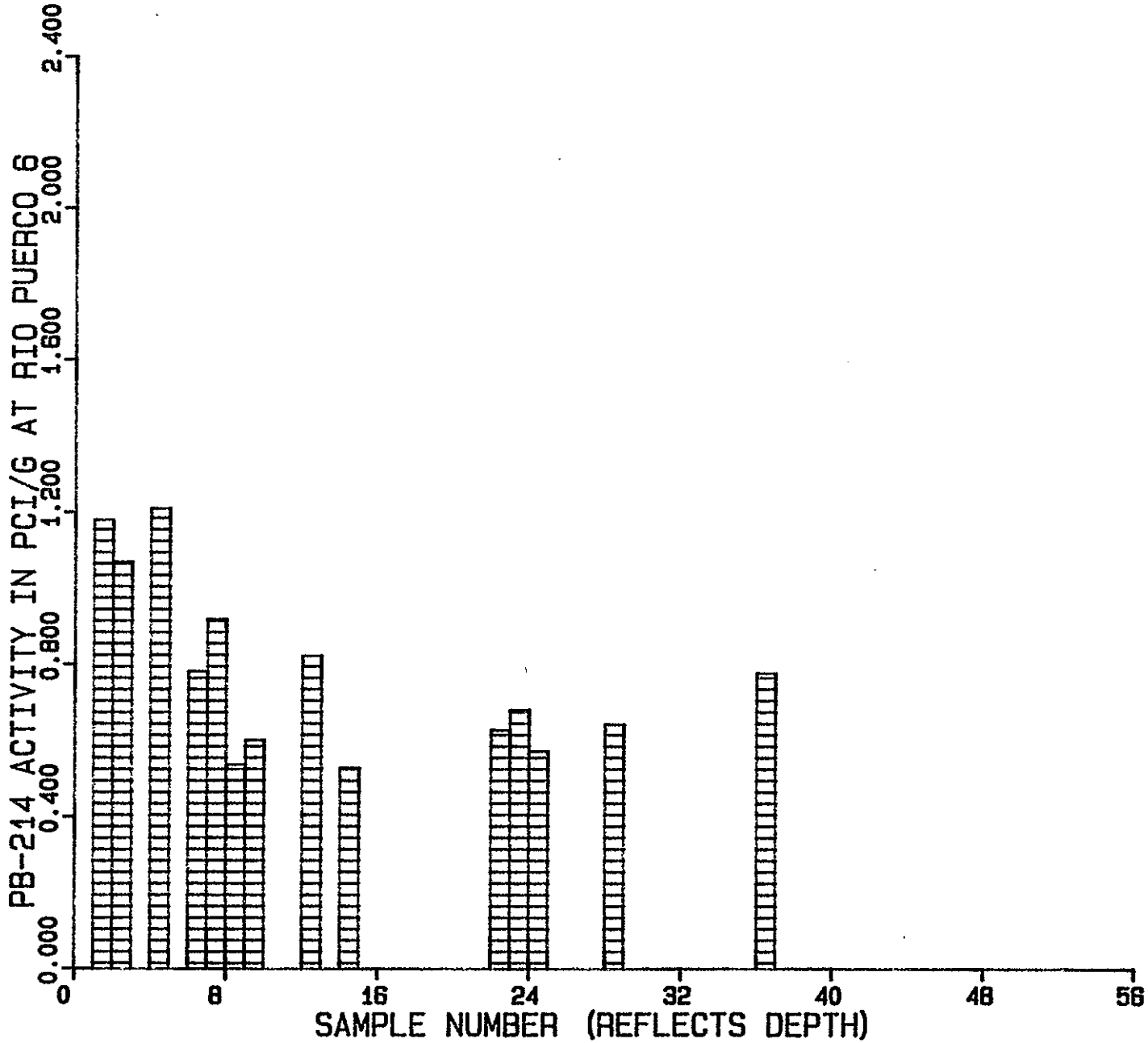
PB-214 ACTIVITY IN PCI/G AT RIO PUERCO 6
0.000
0.400
0.800
1.200
1.600
2.000
2.400
0
8
16
24
32
40
48
56
SAMPLE NUMBER (REFLECTS DEPTH)

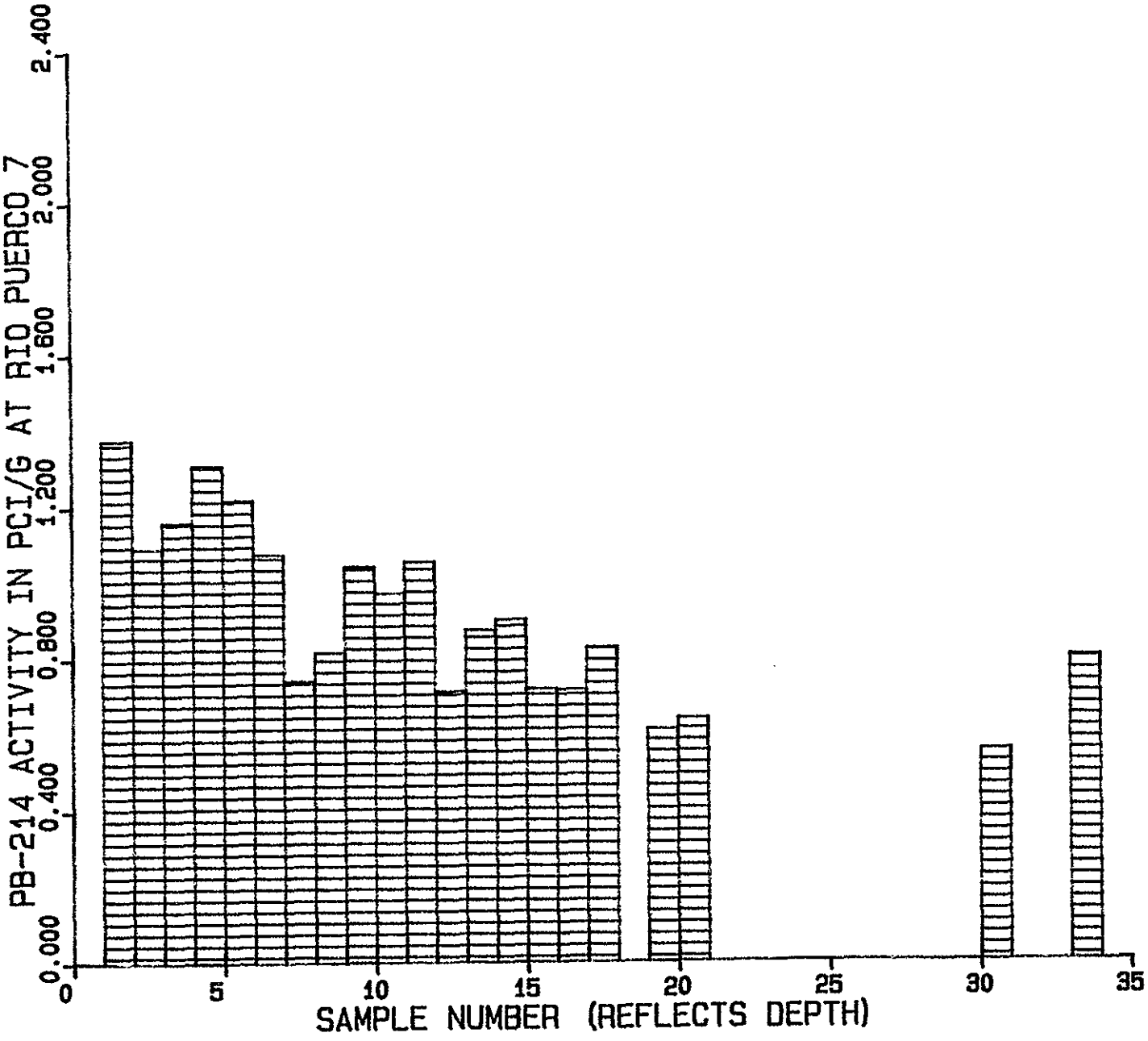
PB-214 ACTIVITY IN PCI/G AT RIO PUERCO 7
0.000
0.400
0.800
1.200
1.600
2.000
2.400
0
5
10
15
20
25
30
35
SAMPLE NUMBER (REFLECTS DEPTH)

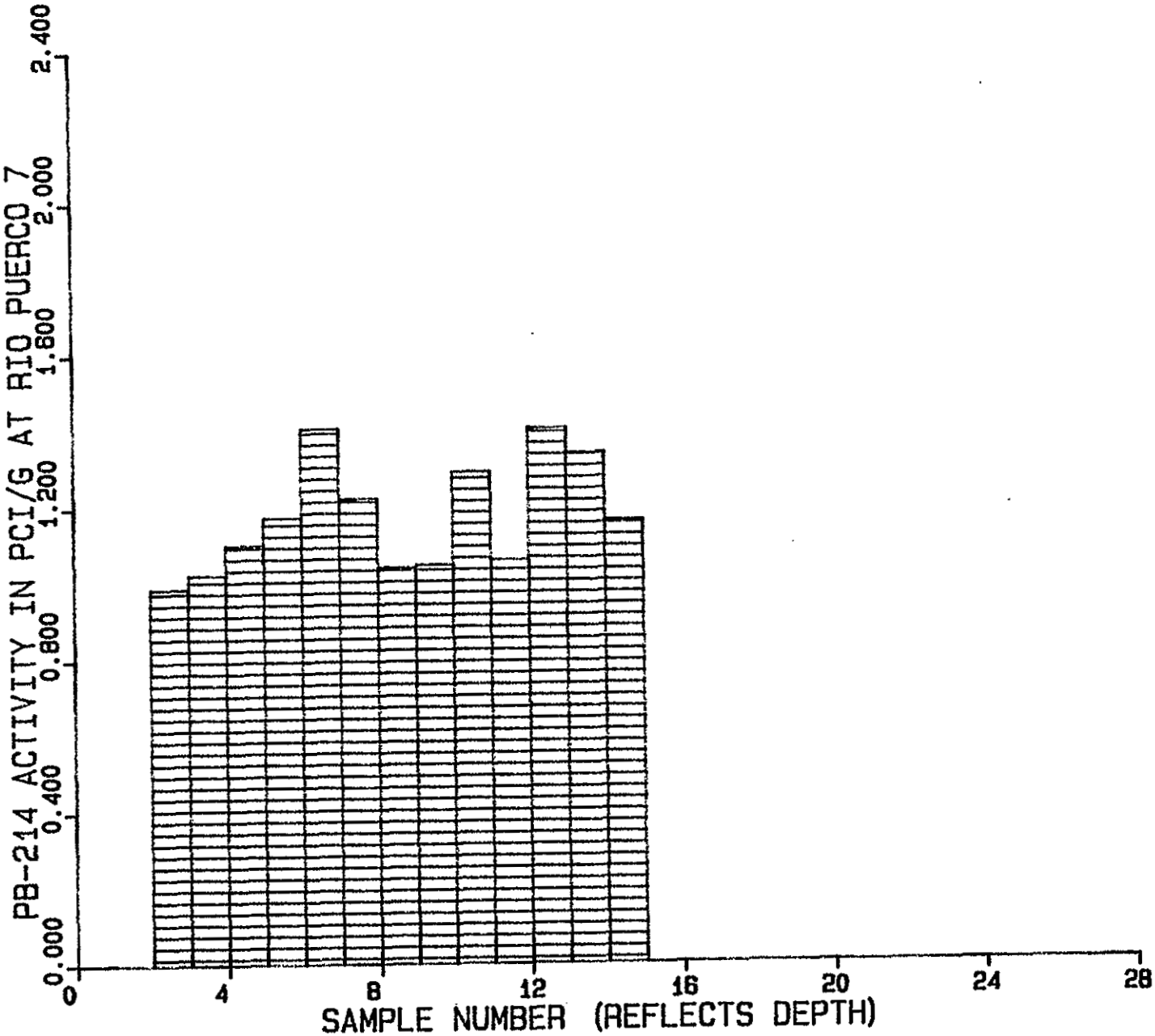
PB-214 ACTIVITY IN PCI/G AT RIO PUERCO 7
0.000
0.400
0.800
1.200
1.800
2.000
2.400
0
4
8
12
16
20
24
28
SAMPLE NUMBER (REFLECTS DEPTH)

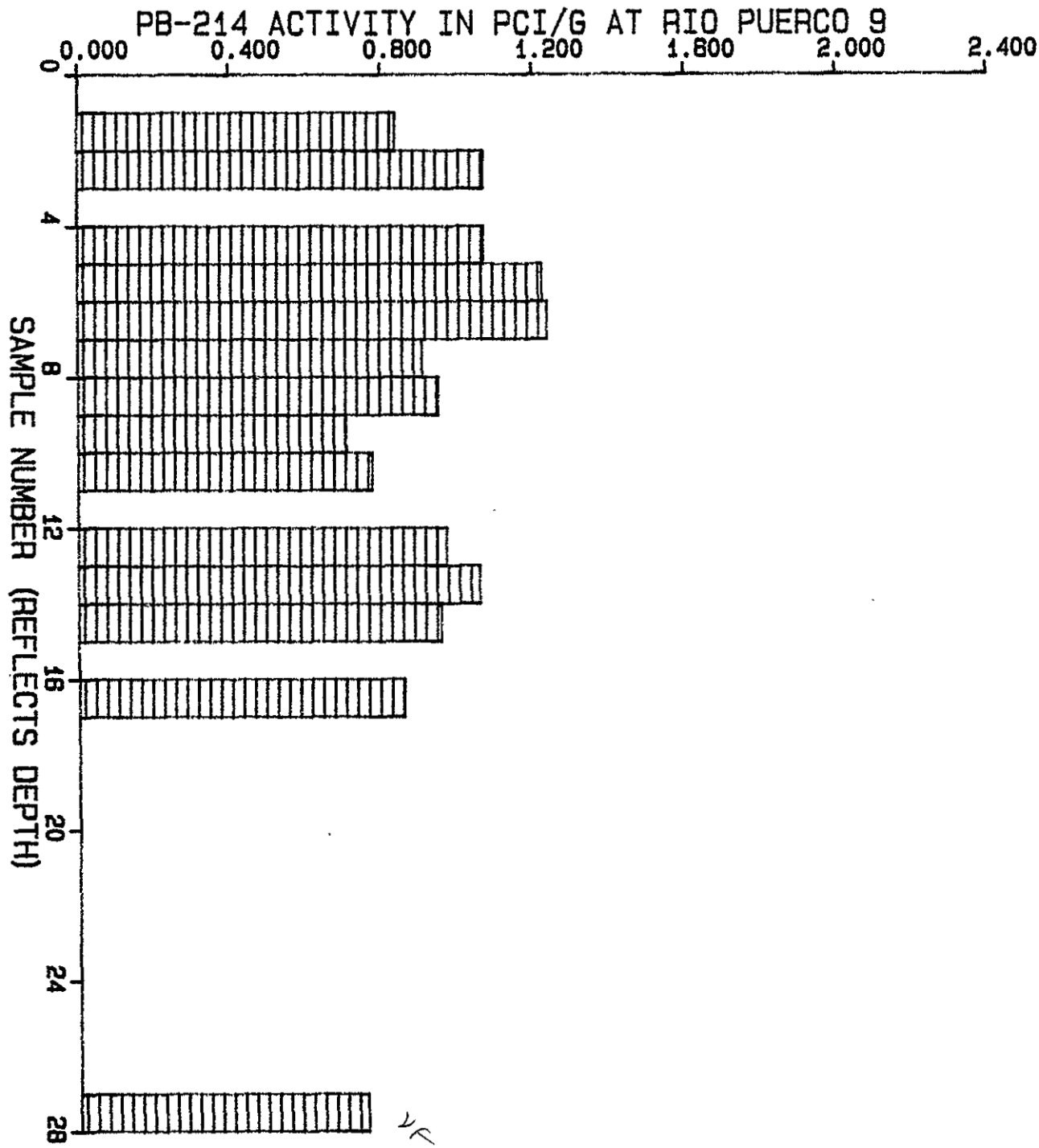
PB-214 ACTIVITY IN PCI/G AT RIO PUERCO 9
0.000
0.400
0.800
1.200
1.600
2.000
2.400
0
4
8
12
16
20
24
28
SAMPLE NUMBER (REFLECTS DEPTH)

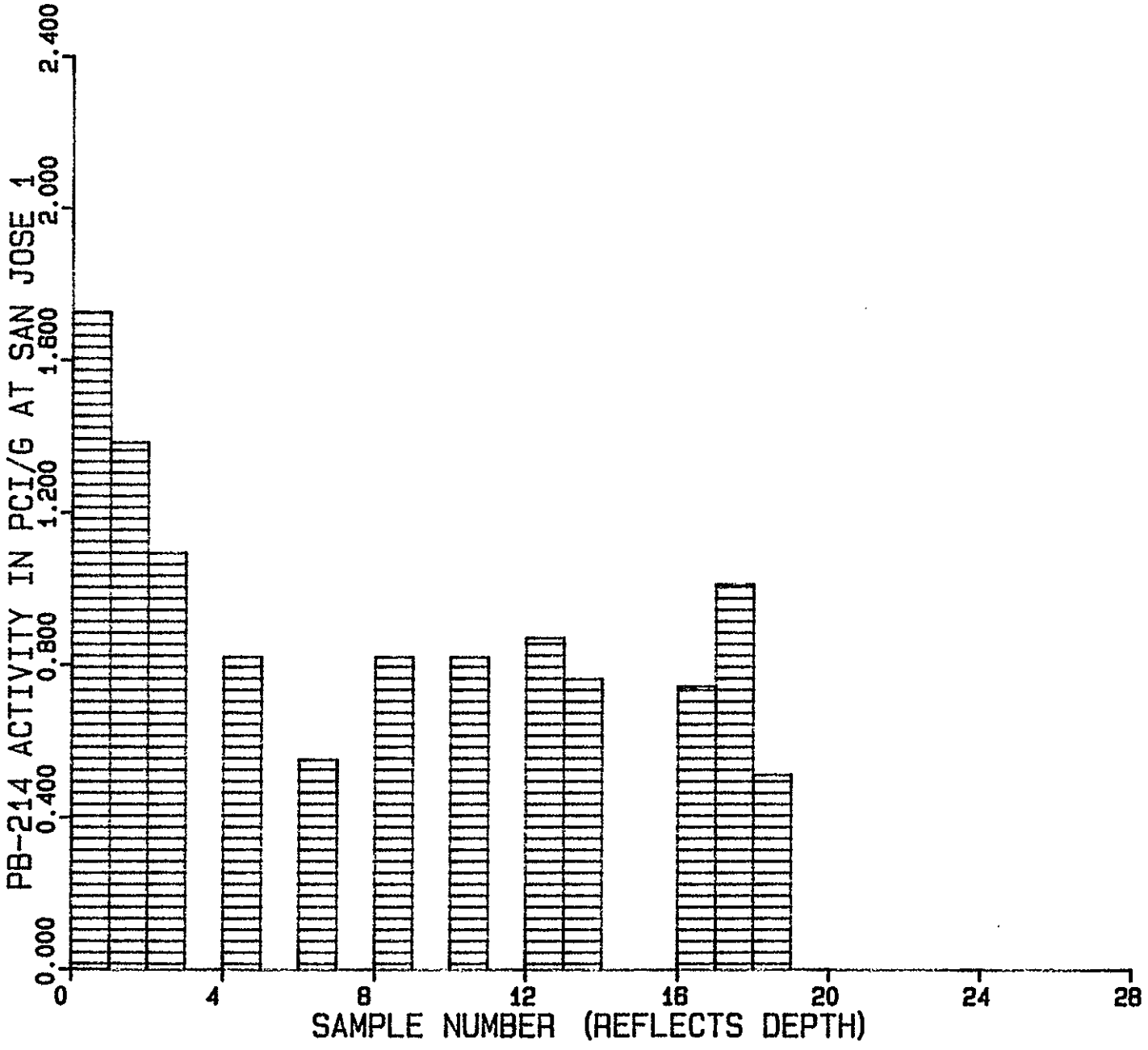
PB-214 ACTIVITY IN PCI/G AT SAN JOSE 1
0.000
0.400
0.800
1.200
1.600
2.000
2.400
0
4
8
12
16
20
24
28
SAMPLE NUMBER (REFLECTS DEPTH)

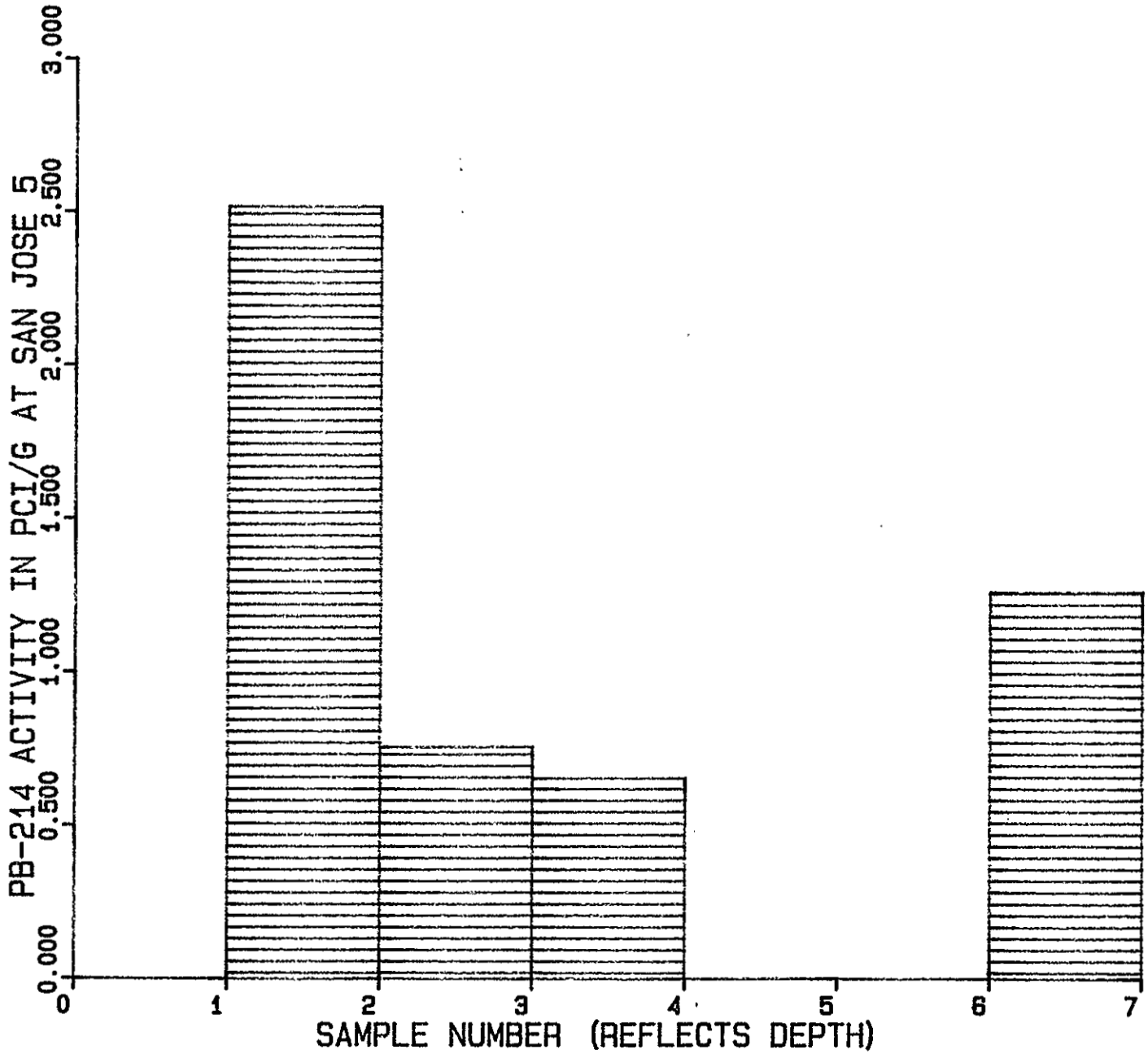
PB-214 ACTIVITY IN PCI/G AT SAN JOSE 5
0.000
0.500
1.000
1.500
2.000
2.500
3.000
0
1
2
3
4
5
6
7
SAMPLE NUMBER (REFLECTS DEPTH)

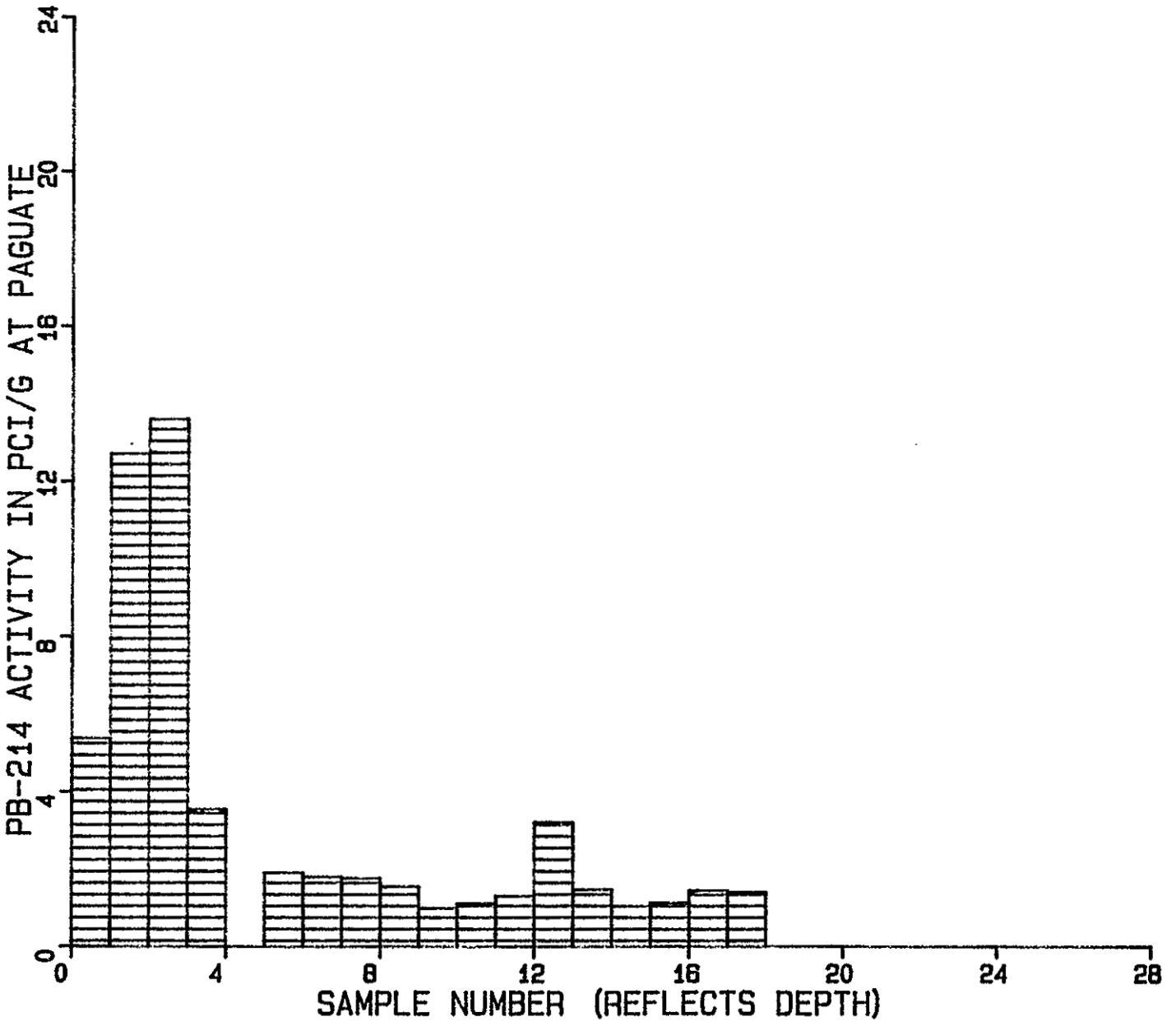
PB-214 ACTIVITY IN PCI/G AT PAGUATE
0
4
8
12
16
20
24
0
4
8
12
16
20
24
28
SAMPLE NUMBER (REFLECTS DEPTH)

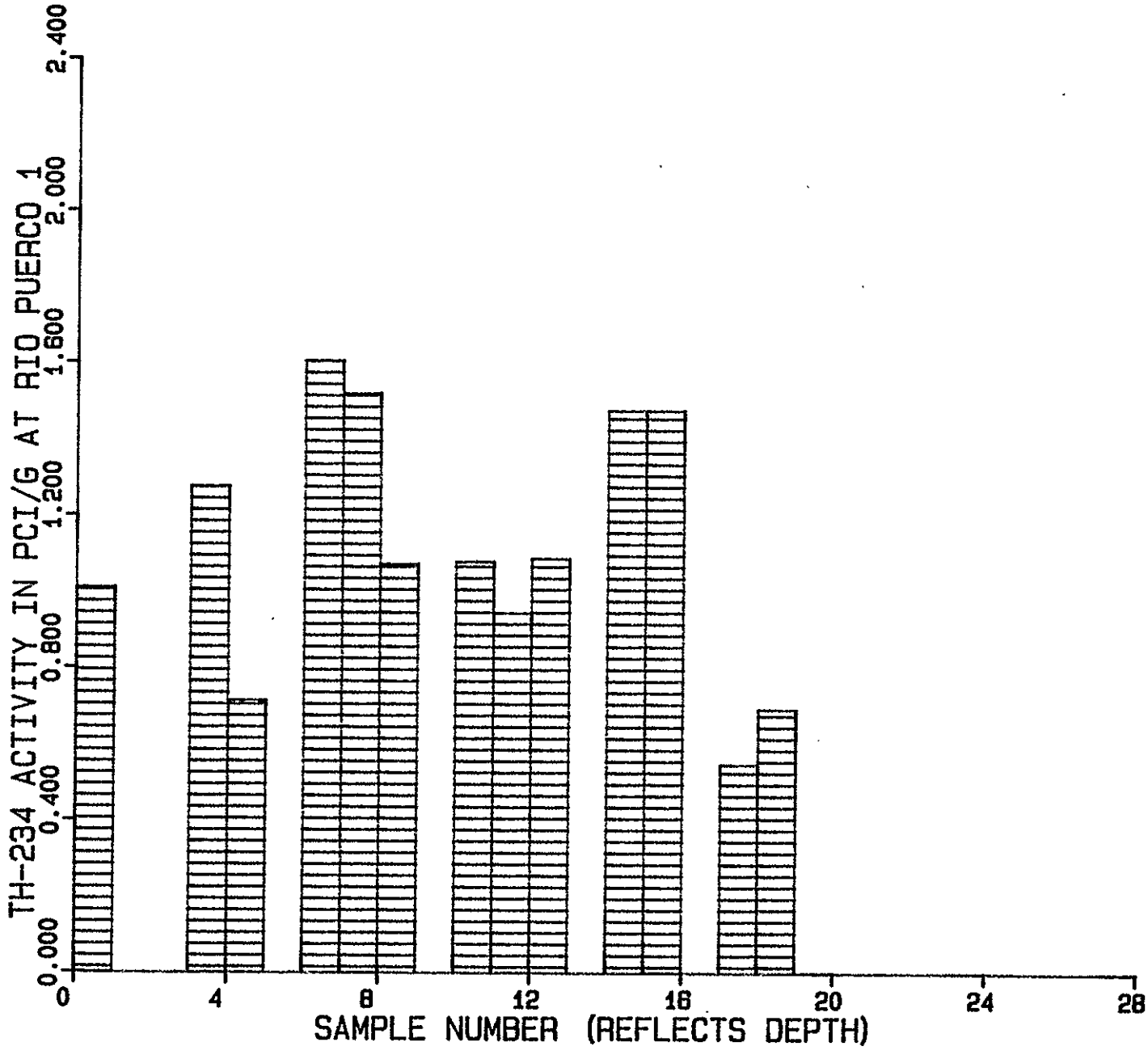
TH-234 ACTIVITY IN PCI/G AT RIO PUERCO 1
0.000
0.400
0.800
1.200
1.600
2.000
2.400
0
4
8
12
16
20
24
28
SAMPLE NUMBER (REFLECTS DEPTH)

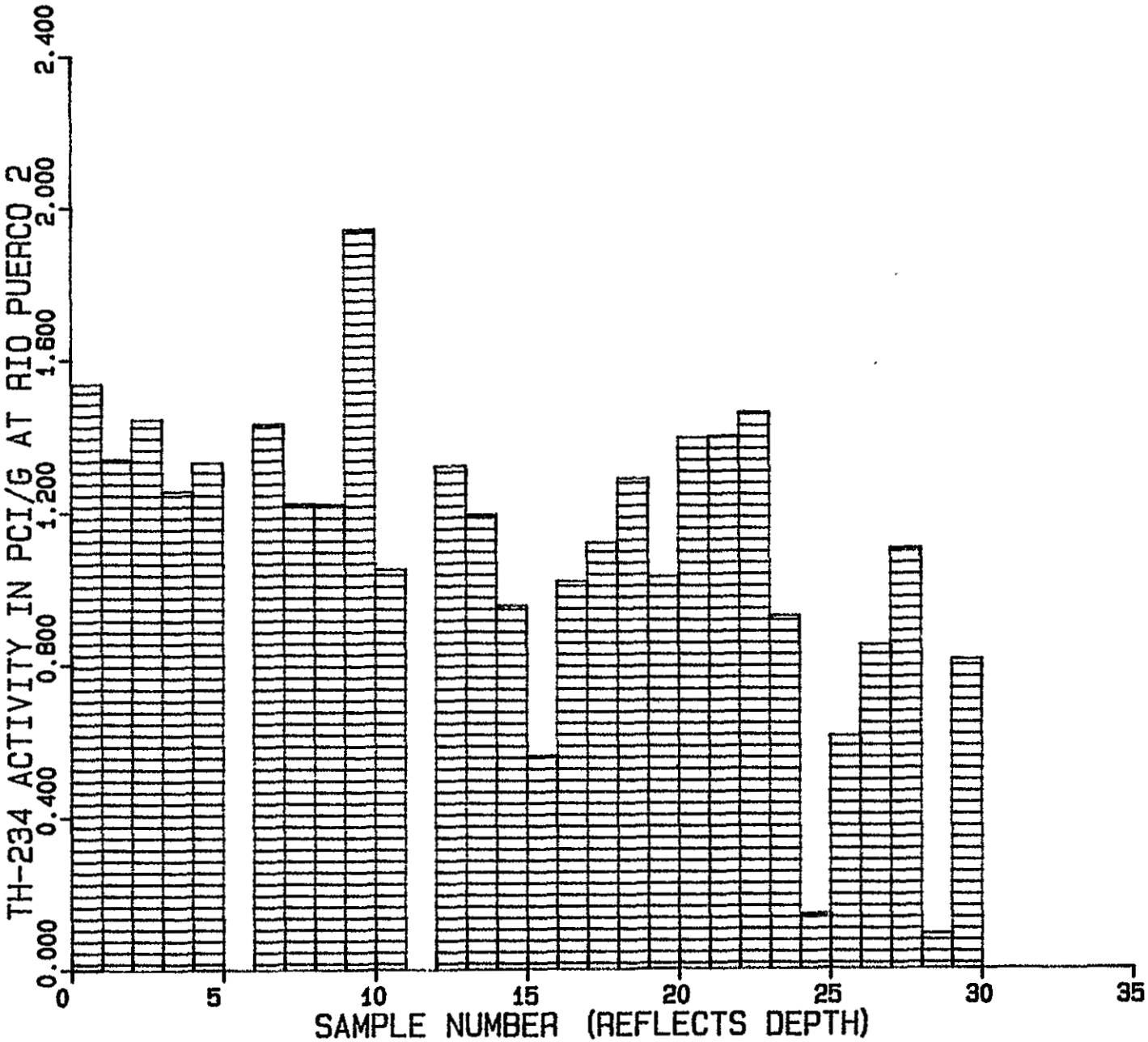
TH-234 ACTIVITY IN PCI/G AT RIO PUERCO 2
0.000
0.400
0.800
1.200
1.600
2.000
2.400
0
5
10
15
20
25
30
35
SAMPLE NUMBER (REFLECTS DEPTH)

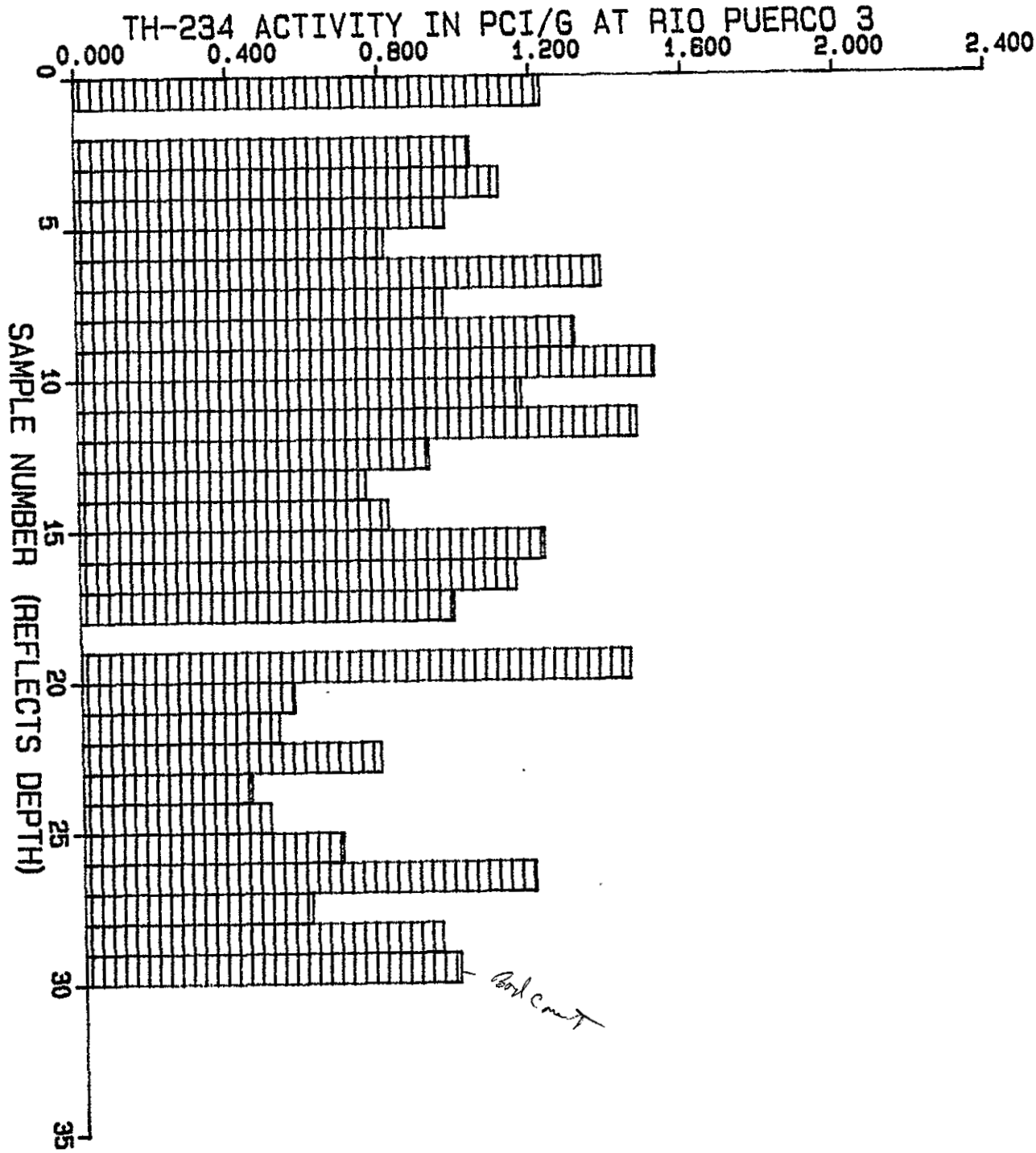
TH-234 ACTIVITY IN PCI/G AT RIO PUERCO 3
0.000
0.400
0.800
1.200
1.600
2.000
2.400
0
5
10
15
20
25
30
35
SAMPLE NUMBER (REFLECTS DEPTH)
Background

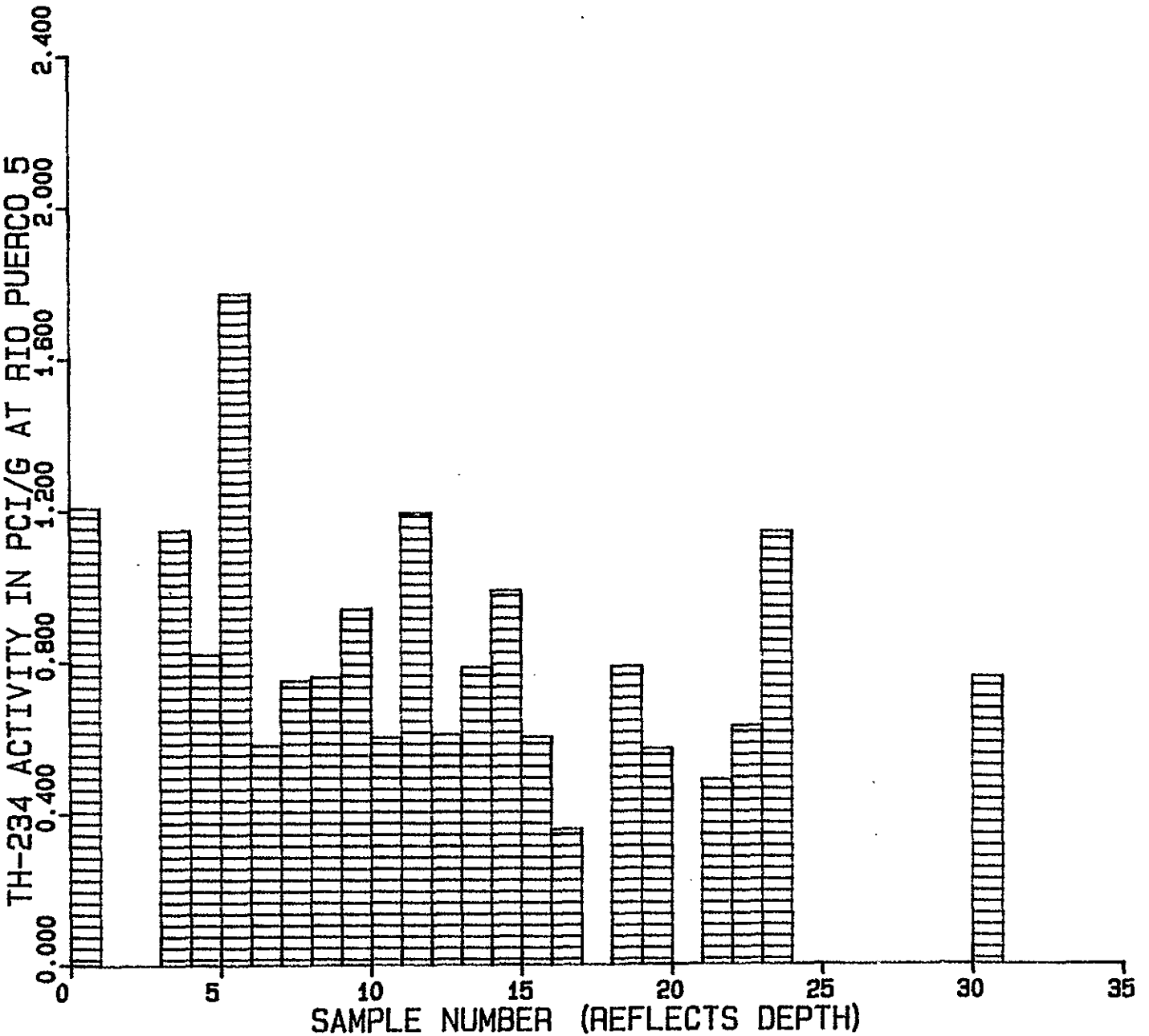
TH-234 ACTIVITY IN PCI/G AT RIO PUERCO 5
0.000
0.400
0.800
1.200
1.600
2.000
2.400
0
5
10
15
20
25
30
35
SAMPLE NUMBER (REFLECTS DEPTH)

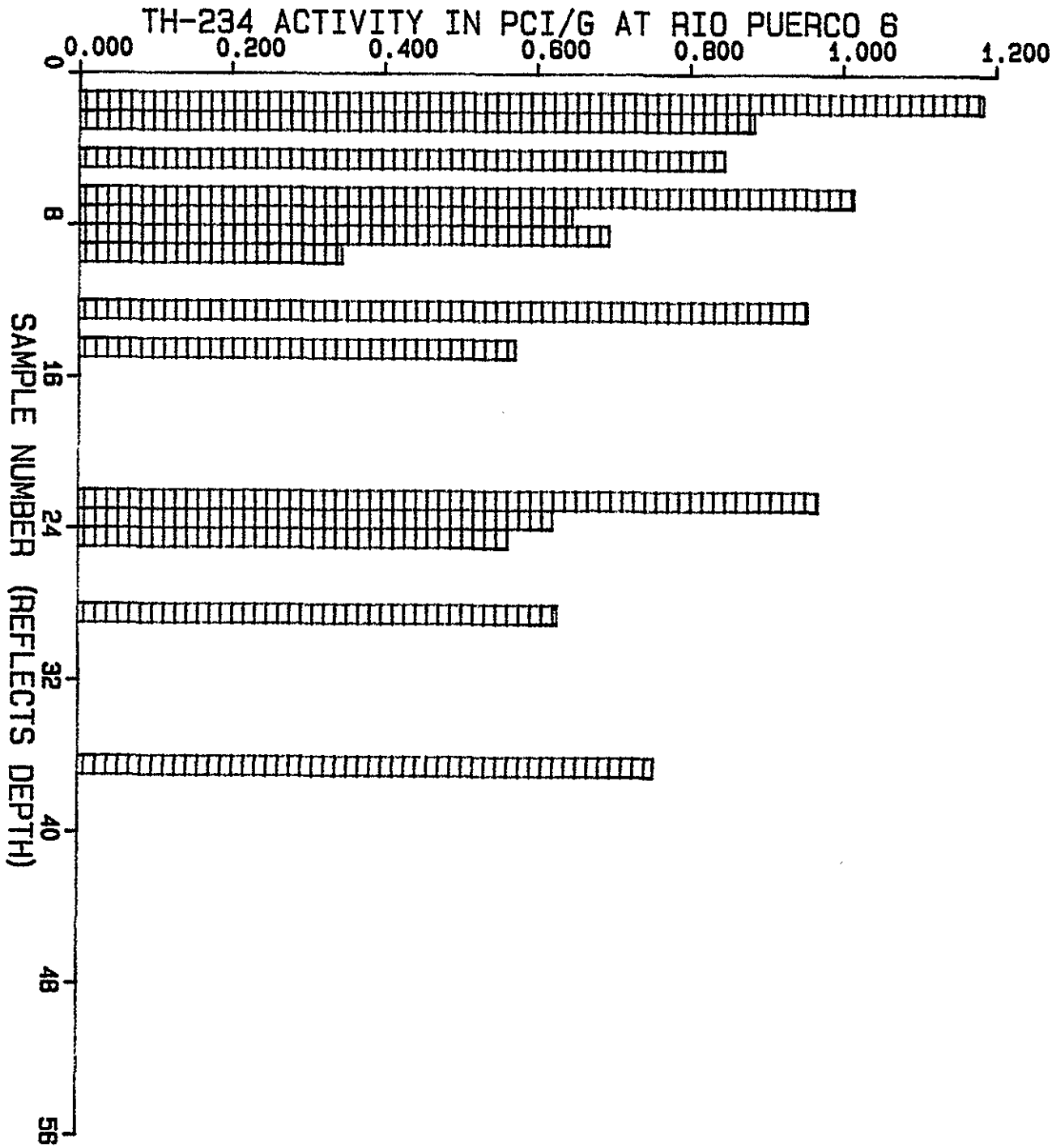
TH-234 ACTIVITY IN PCI/G AT RIO PUERCO 6
0.000
0.200
0.400
0.600
0.800
1.000
1.200
0
8
16
24
32
40
48
56
SAMPLE NUMBER (REFLECTS DEPTH)

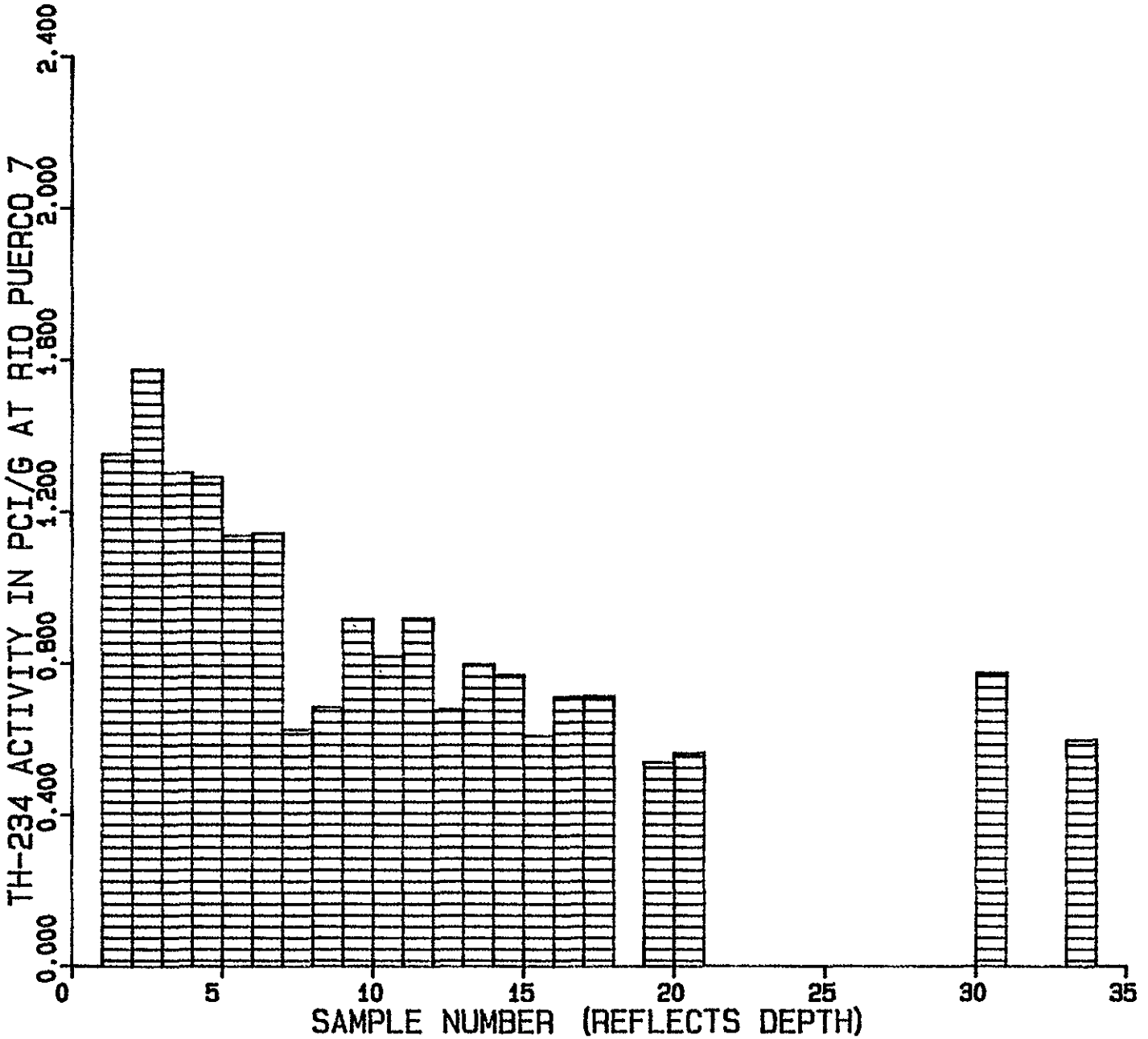
TH-234 ACTIVITY IN PCI/G AT RIO PUERCO 7
0.000
0.400
0.800
1.200
1.600
2.000
2.400
0
5
10
15
20
25
30
35
SAMPLE NUMBER (REFLECTS DEPTH)

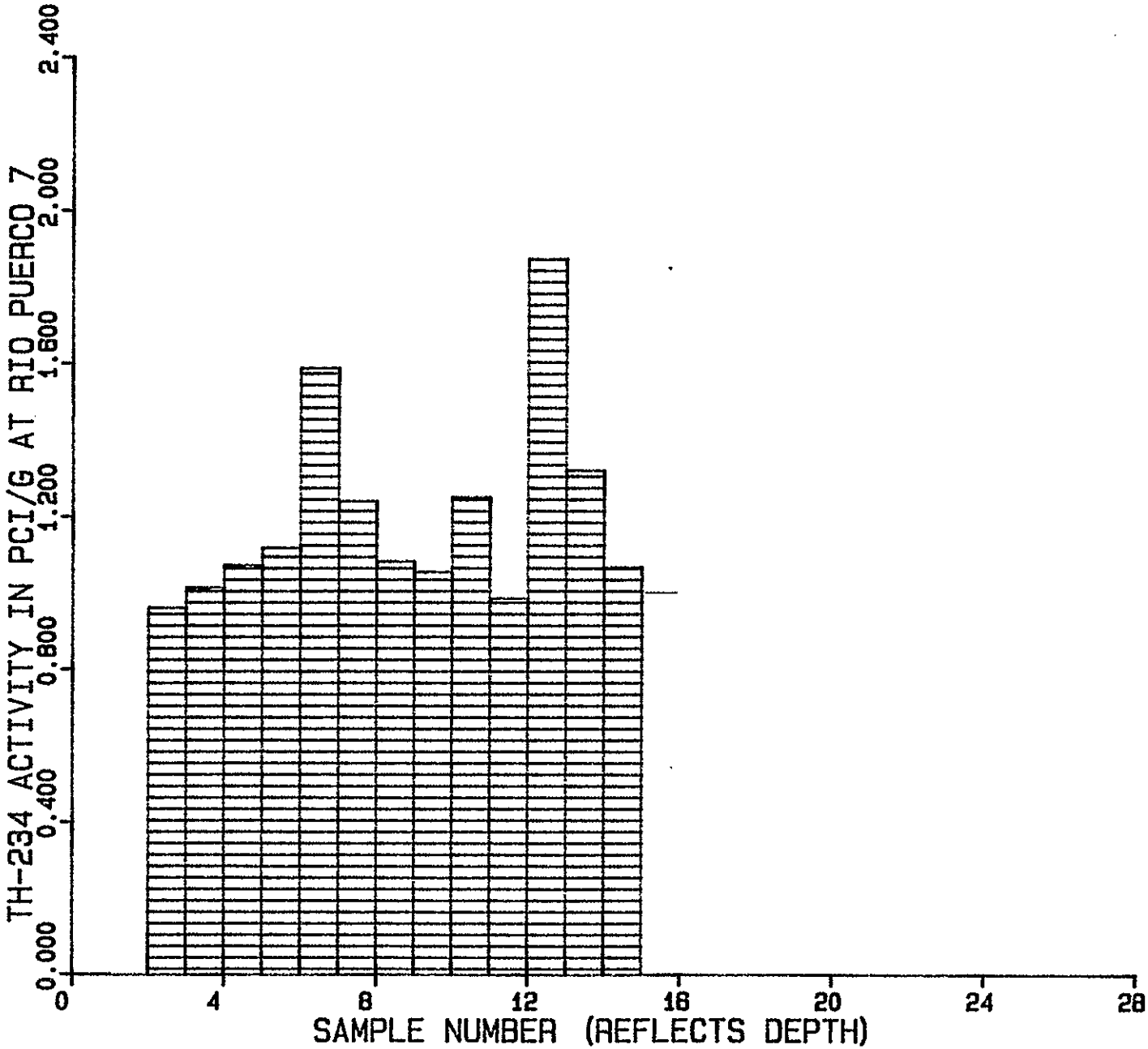
TH-234 ACTIVITY IN PCI/G AT RIO PUERCO 7
0.000
0.400
0.800
1.200
1.600
2.000
2.400
0
4
8
12
16
20
24
28
SAMPLE NUMBER (REFLECTS DEPTH)

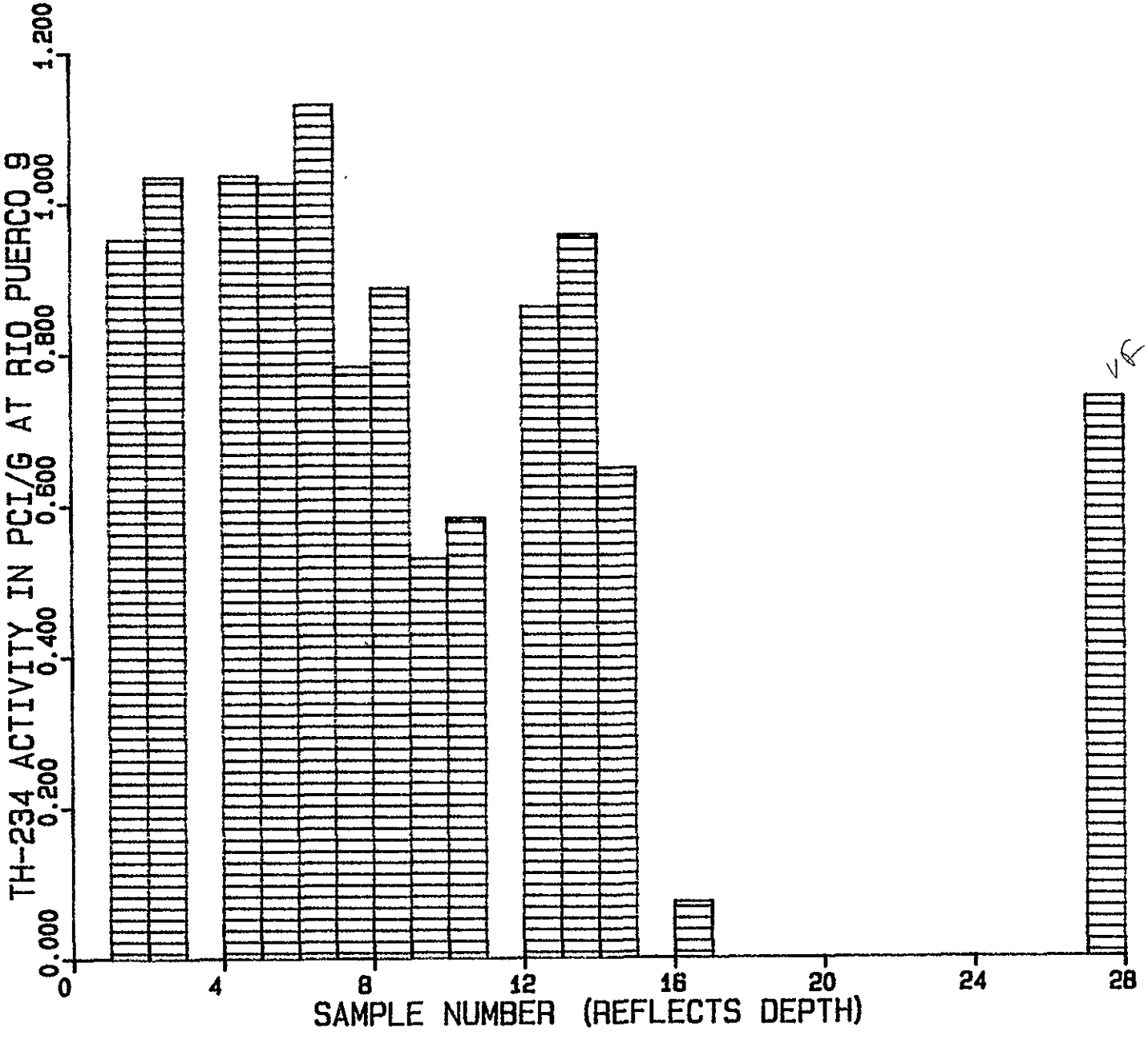
TH-234 ACTIVITY IN PCI/G AT RIO PUERCO 9
0.000
0.200
0.400
0.600
0.800
1.000
1.200
0
4
8
12
16
20
24
28
SAMPLE NUMBER (REFLECTS DEPTH)

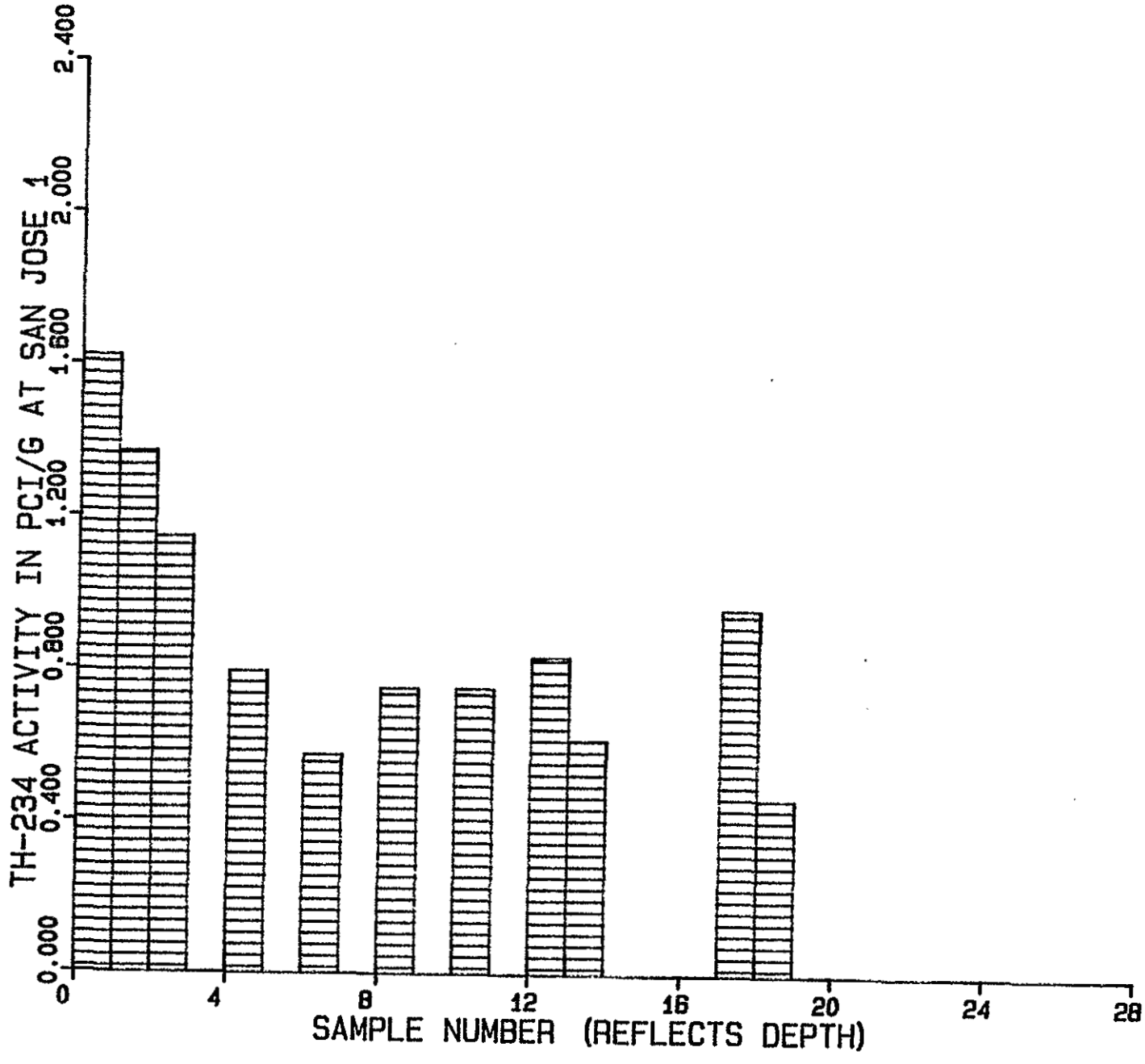
TH-234 ACTIVITY IN PCI/G AT SAN JOSE 1
0.000
0.400
0.800
1.200
1.600
2.000
2.400
0
4
8
12
16
20
24
28
SAMPLE NUMBER (REFLECTS DEPTH)

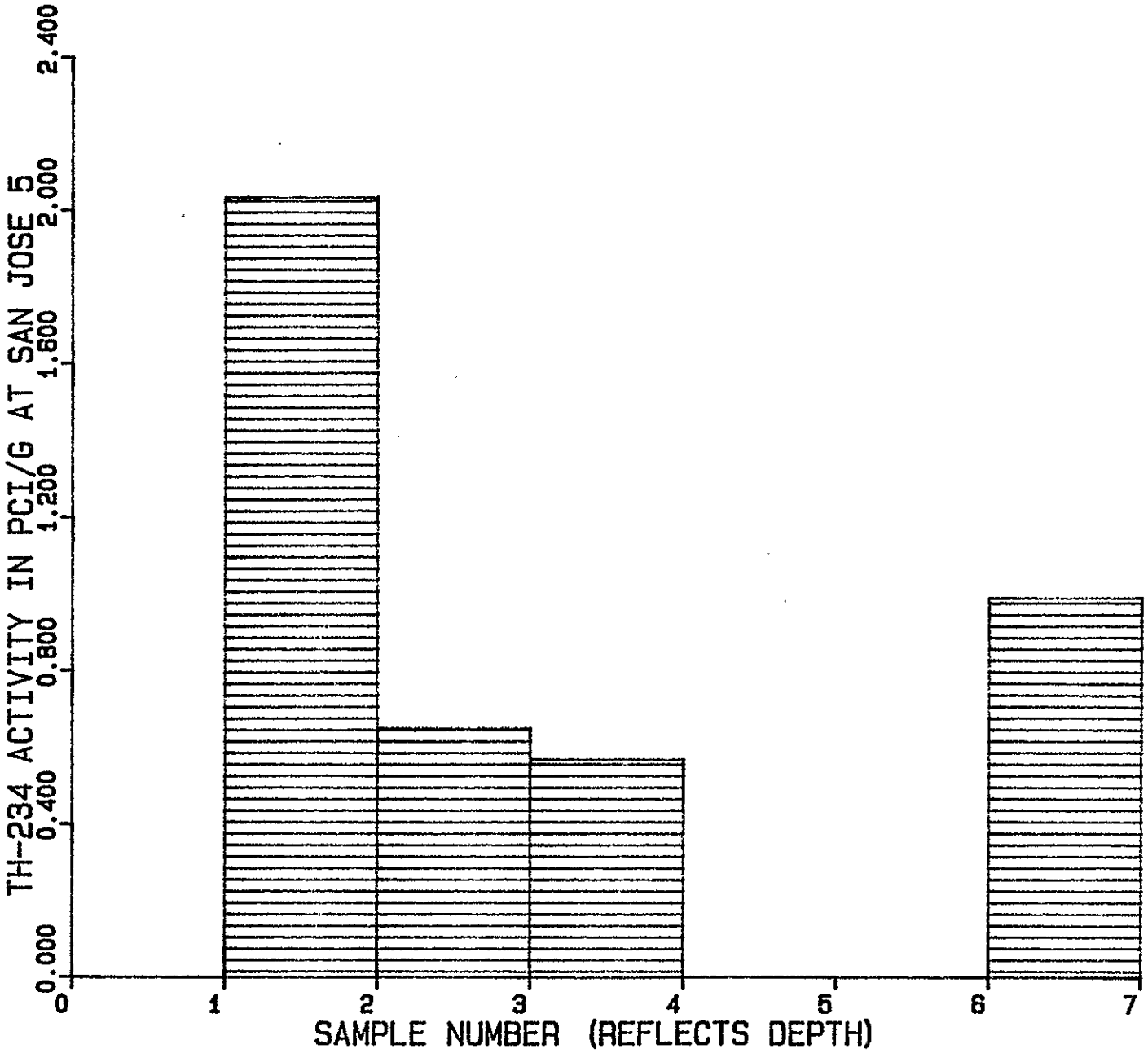
TH-234 ACTIVITY IN PCI/G AT SAN JOSE 5
0.000
0.400
0.800
1.200
1.600
2.000
2.400
0
1
2
3
4
5
6
7
SAMPLE NUMBER (REFLECTS DEPTH)

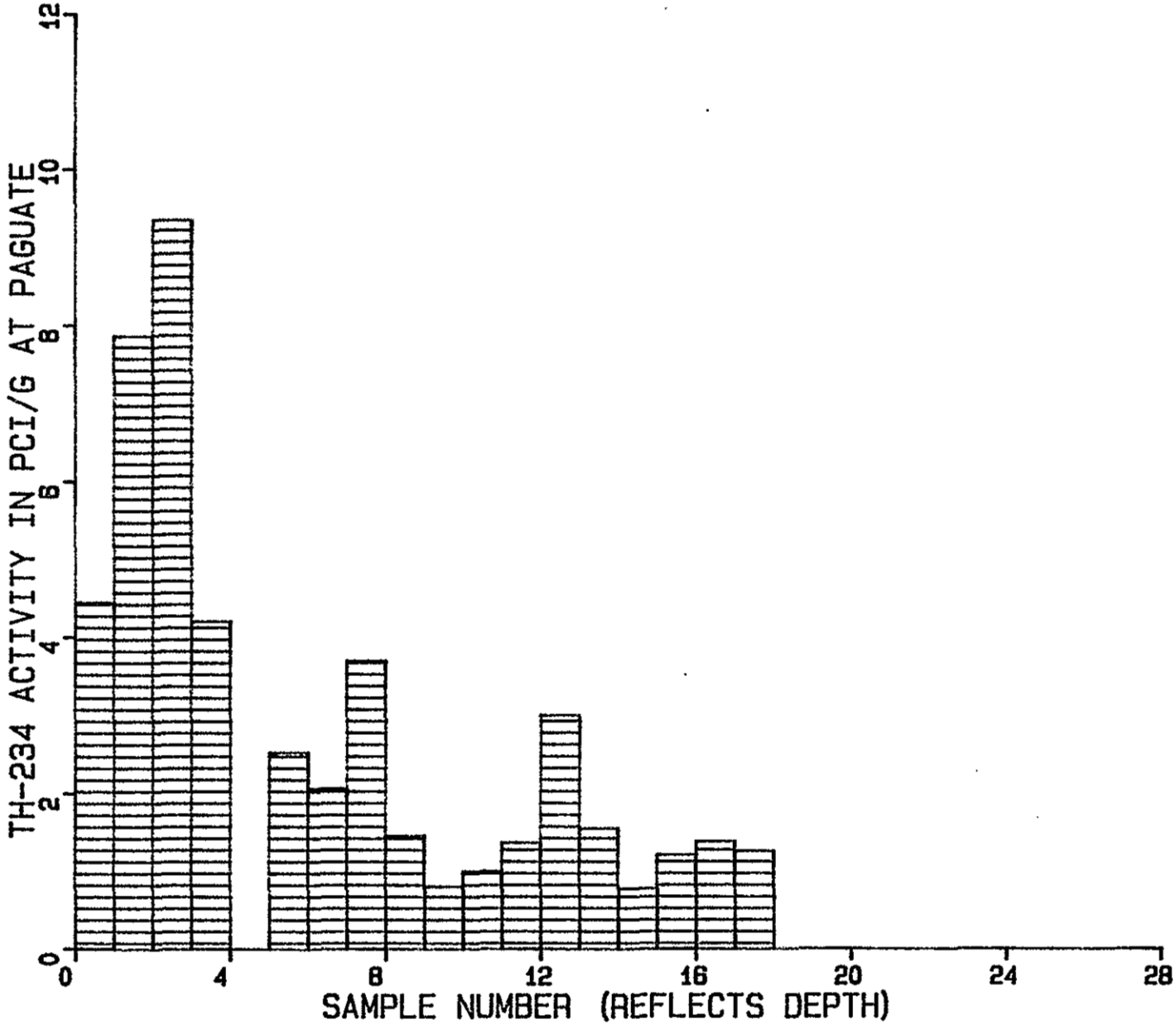
TH-234 ACTIVITY IN PCI/G AT PAGUATE
0
2
4
6
8
10
12
0
4
8
12
16
20
24
28
SAMPLE NUMBER (REFLECTS DEPTH)

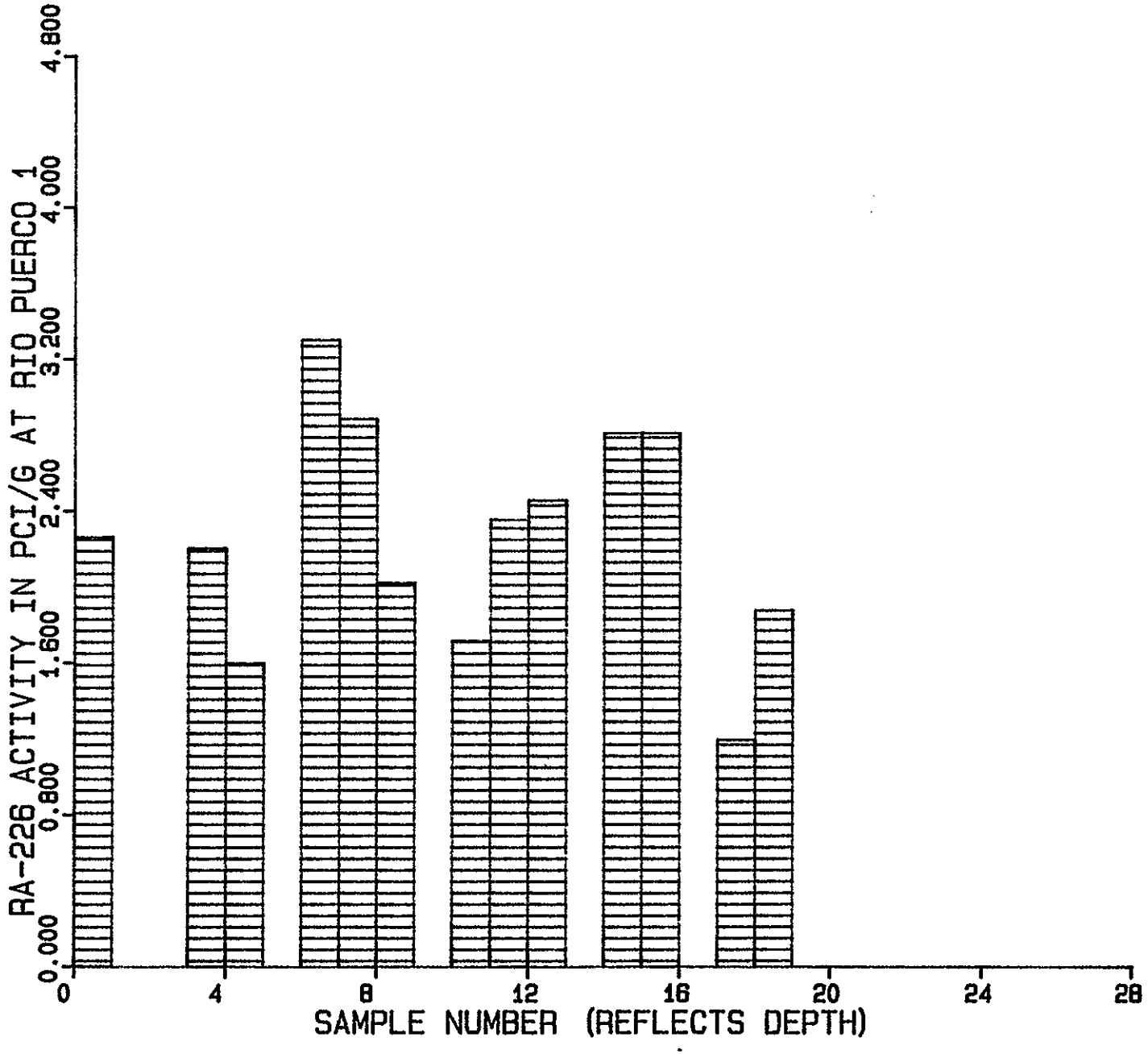
RA-226 ACTIVITY IN PCI/G AT RIO PUERCO 1
0.000
0.800
1.600
2.400
3.200
4.000
4.800
0
4
8
12
16
20
24
28
SAMPLE NUMBER (REFLECTS DEPTH)

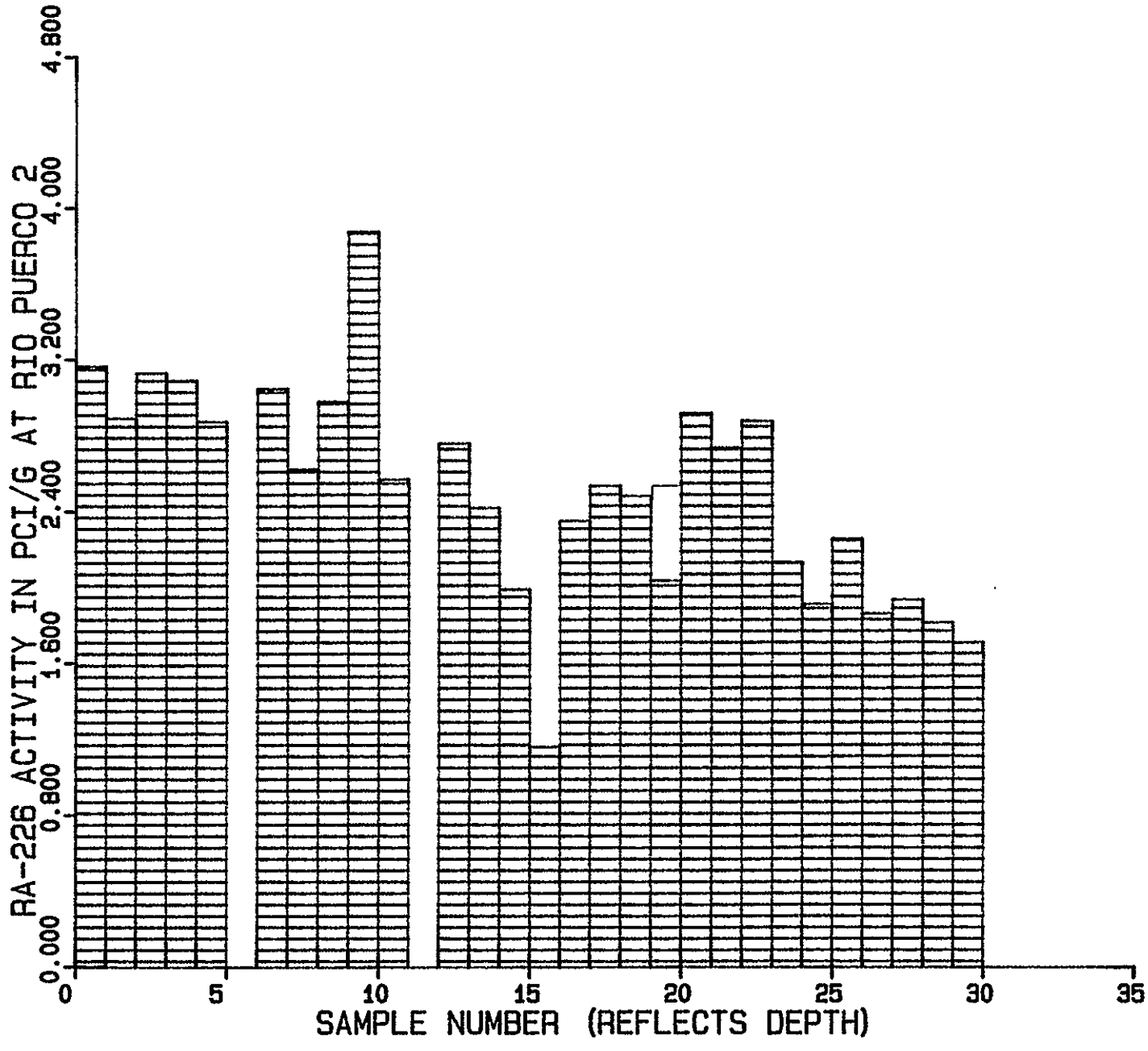
RA-226 ACTIVITY IN PCI/G AT RIO PUERCO 2
0.000
0.800
1.600
2.400
3.200
4.000
4.800
0
5
10
15
20
25
30
35
SAMPLE NUMBER (REFLECTS DEPTH)

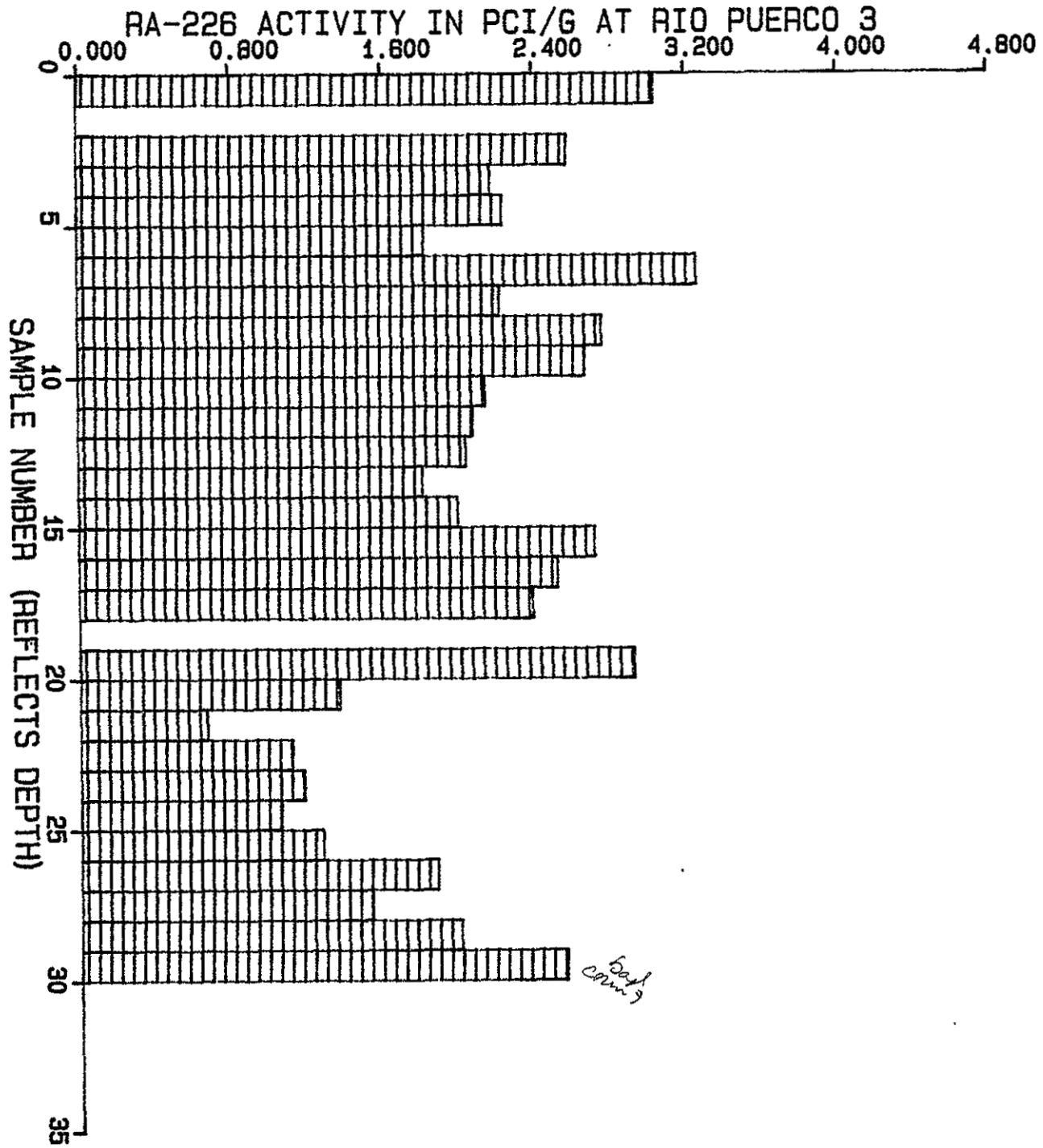
RA-226 ACTIVITY IN PCI/G AT RIO PUERCO 3
0.000
0.800
1.600
2.400
3.200
4.000
4.800
0
5
10
15
20
25
30
35
SAMPLE NUMBER (REFLECTS DEPTH)

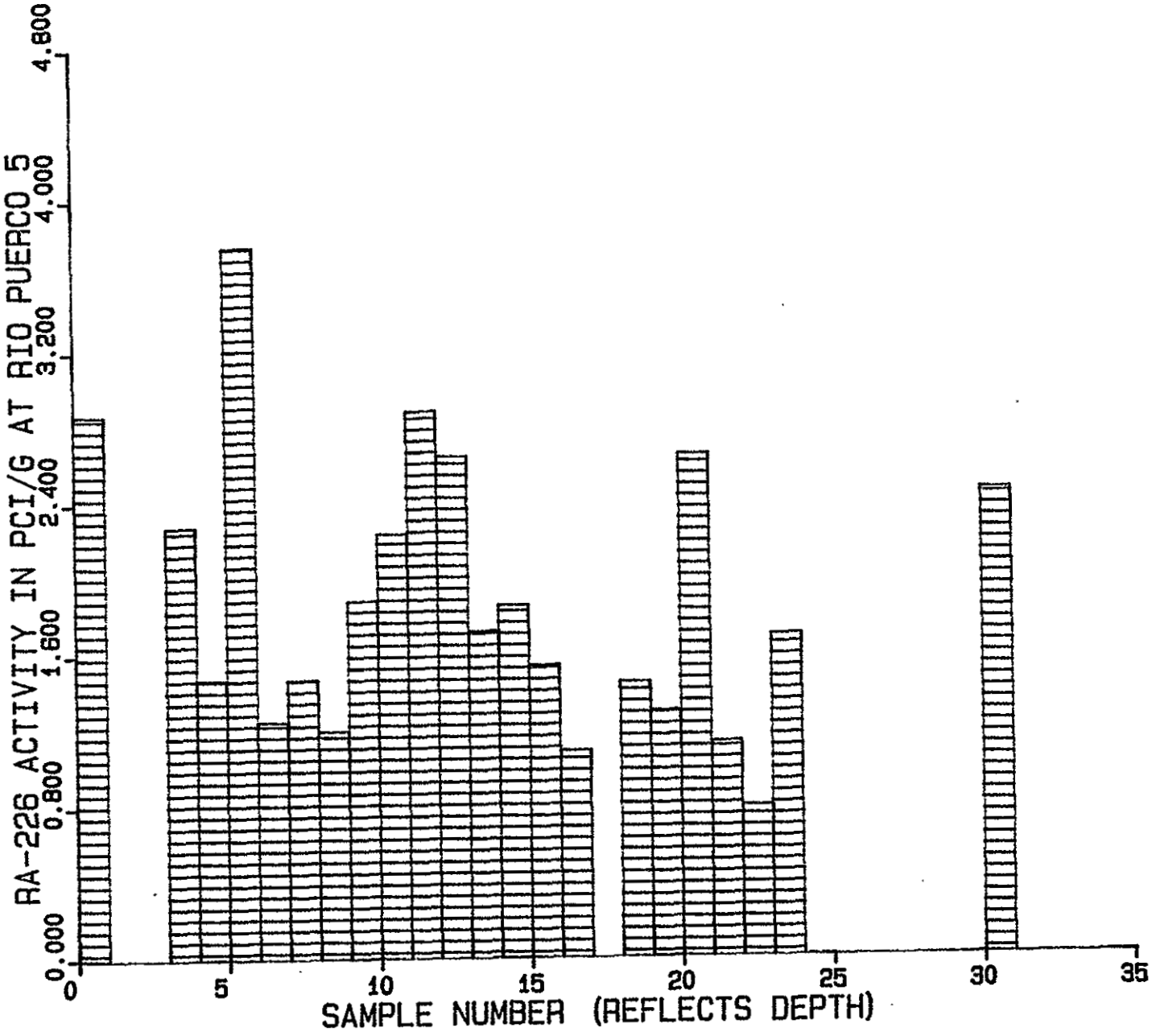
RA-226 ACTIVITY IN PCI/G AT RIO PUERCO 5
0.000
0.800
1.600
2.400
3.200
4.000
4.800
0
5
10
15
20
25
30
35
SAMPLE NUMBER (REFLECTS DEPTH)

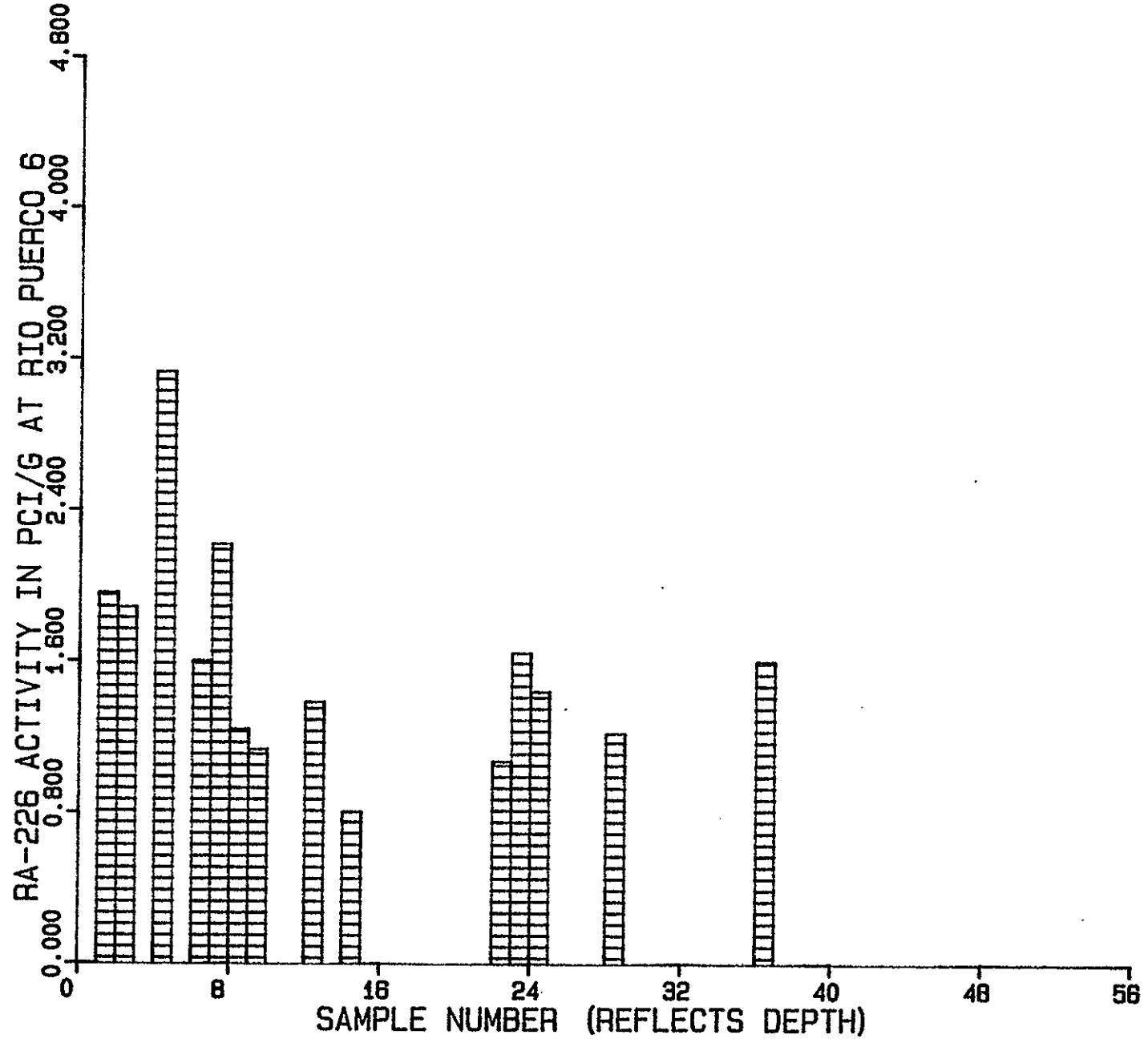
RA-226 ACTIVITY IN PCI/G AT RIO PUERCO 6
0.000
0.800
1.600
2.400
3.200
4.000
4.800
0
8
16
24
32
40
48
56
SAMPLE NUMBER (REFLECTS DEPTH)

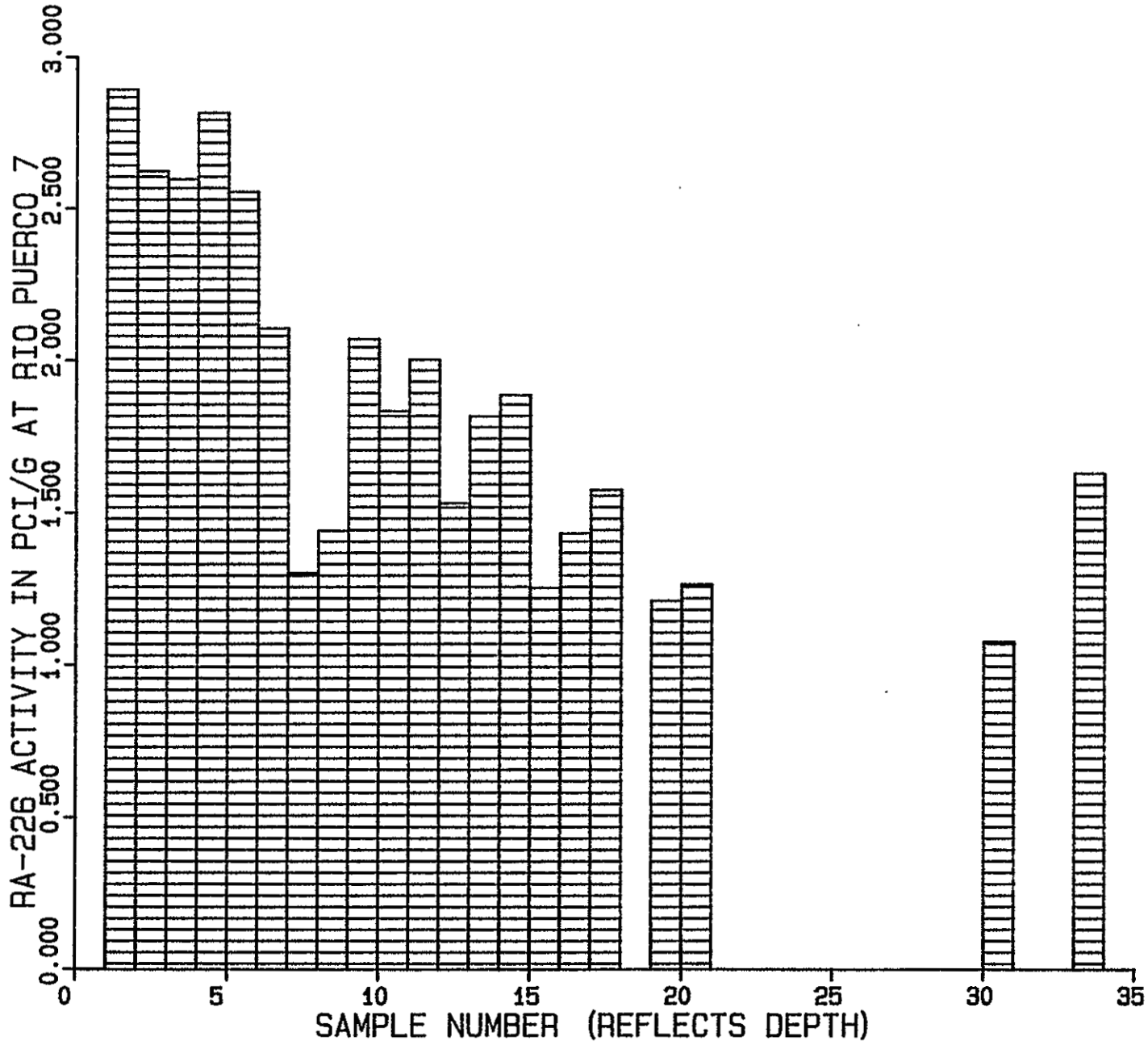
RA-226 ACTIVITY IN PCI/G AT RIO PUERCO 7
0.000
0.500
1.000
1.500
2.000
2.500
3.000
0
5
10
15
20
25
30
35
SAMPLE NUMBER (REFLECTS DEPTH)

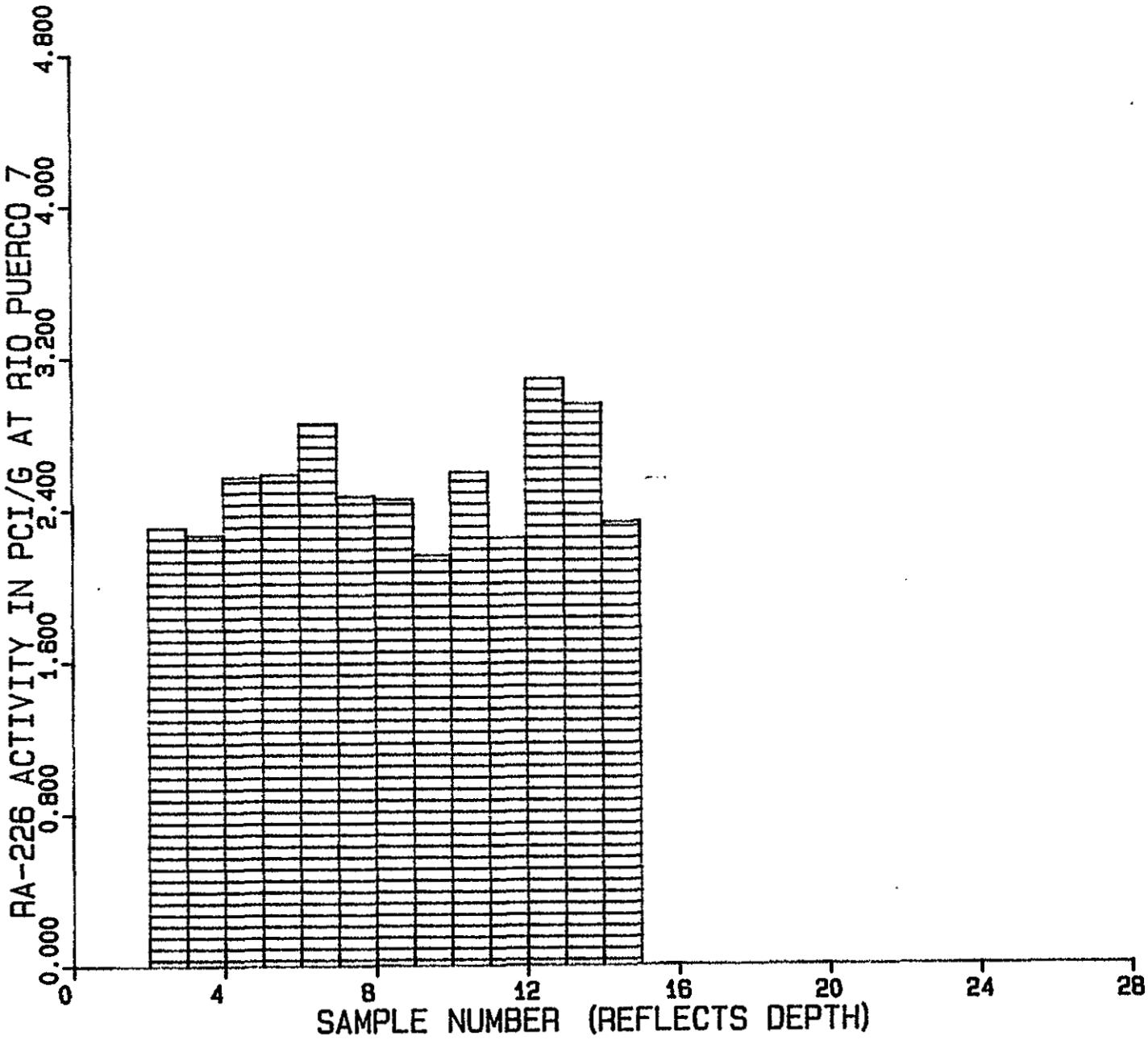
RA-226 ACTIVITY IN PCI/G AT RIO PUERCO 7
0.000
0.800
1.600
2.400
3.200
4.000
4.800
0
4
8
12
16
20
24
28
SAMPLE NUMBER (REFLECTS DEPTH)

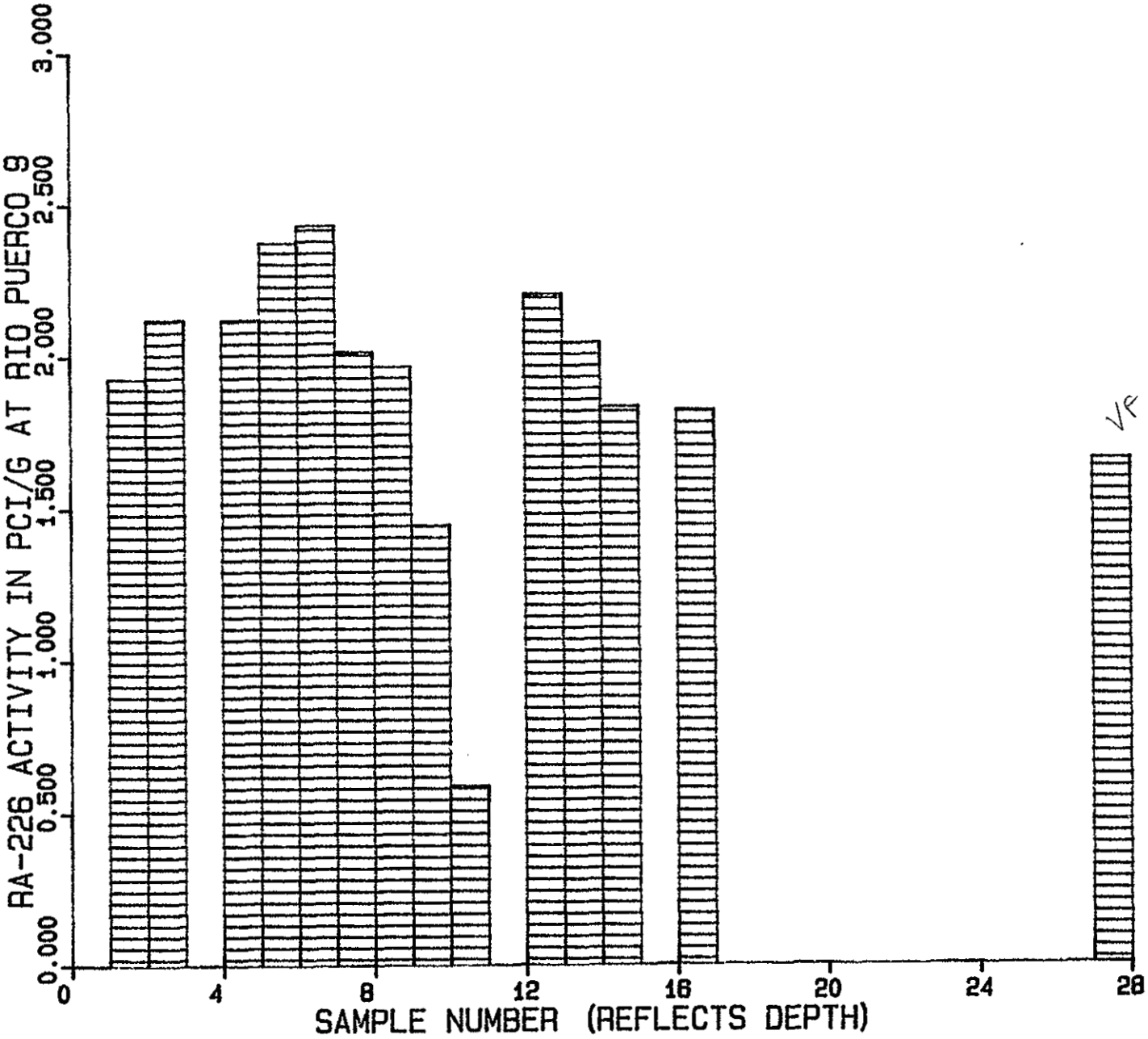
RA-226 ACTIVITY IN PCI/G AT RIO PUERCO 9
0.000
0.500
1.000
1.500
2.000
2.500
3.000
0
4
8
12
16
20
24
28
SAMPLE NUMBER (REFLECTS DEPTH)
VF

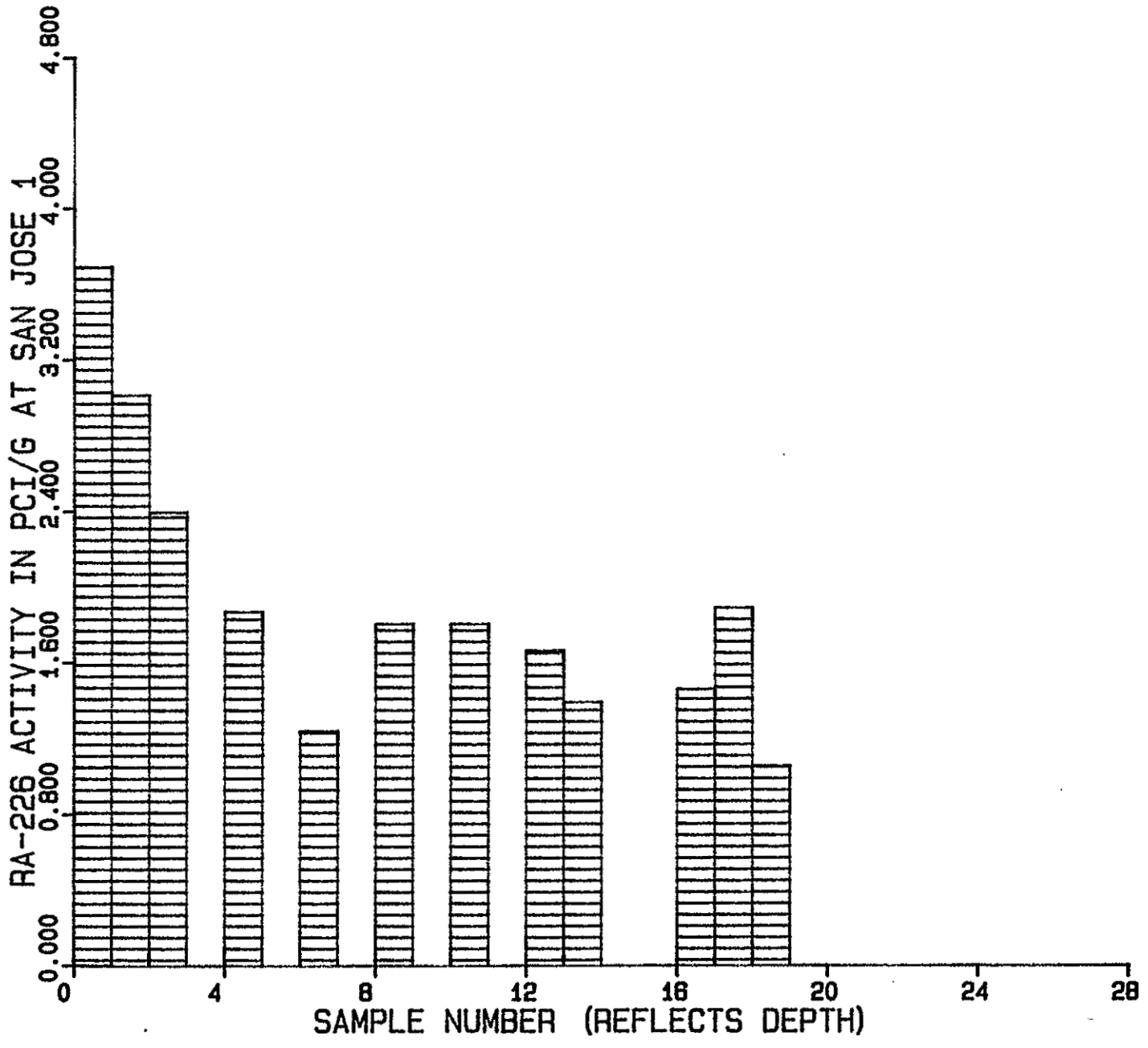
RA-226 ACTIVITY IN PCI/G AT SAN JOSE 1
0.000
0.800
1.600
2.400
3.200
4.000
4.800
0
4
8
12
16
20
24
28
SAMPLE NUMBER (REFLECTS DEPTH)

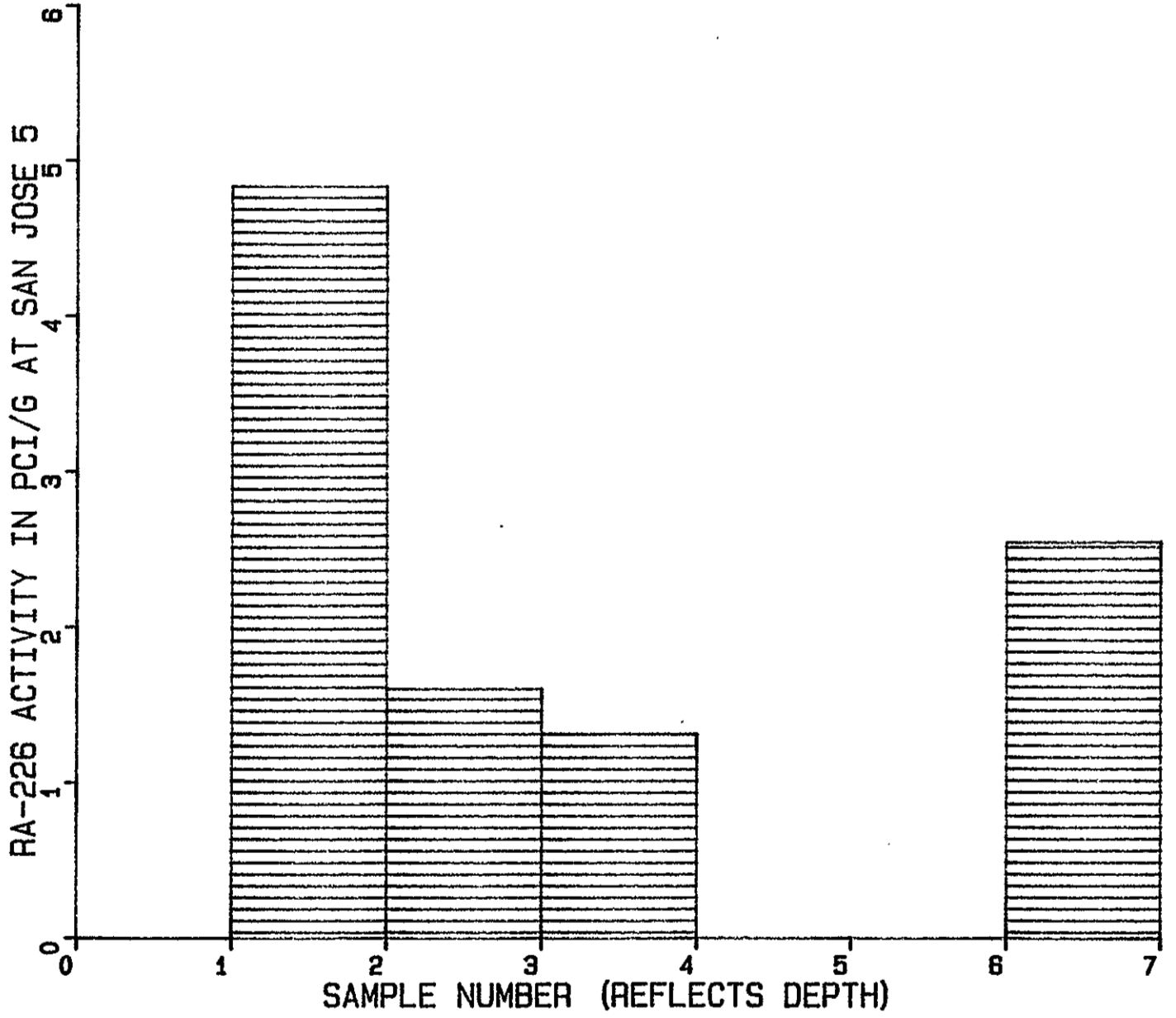
RA-226 ACTIVITY IN PCI/G AT SAN JOSE 5
0
1
2
3
4
5
6
0
1
2
3
4
5
6
7
SAMPLE NUMBER (REFLECTS DEPTH)

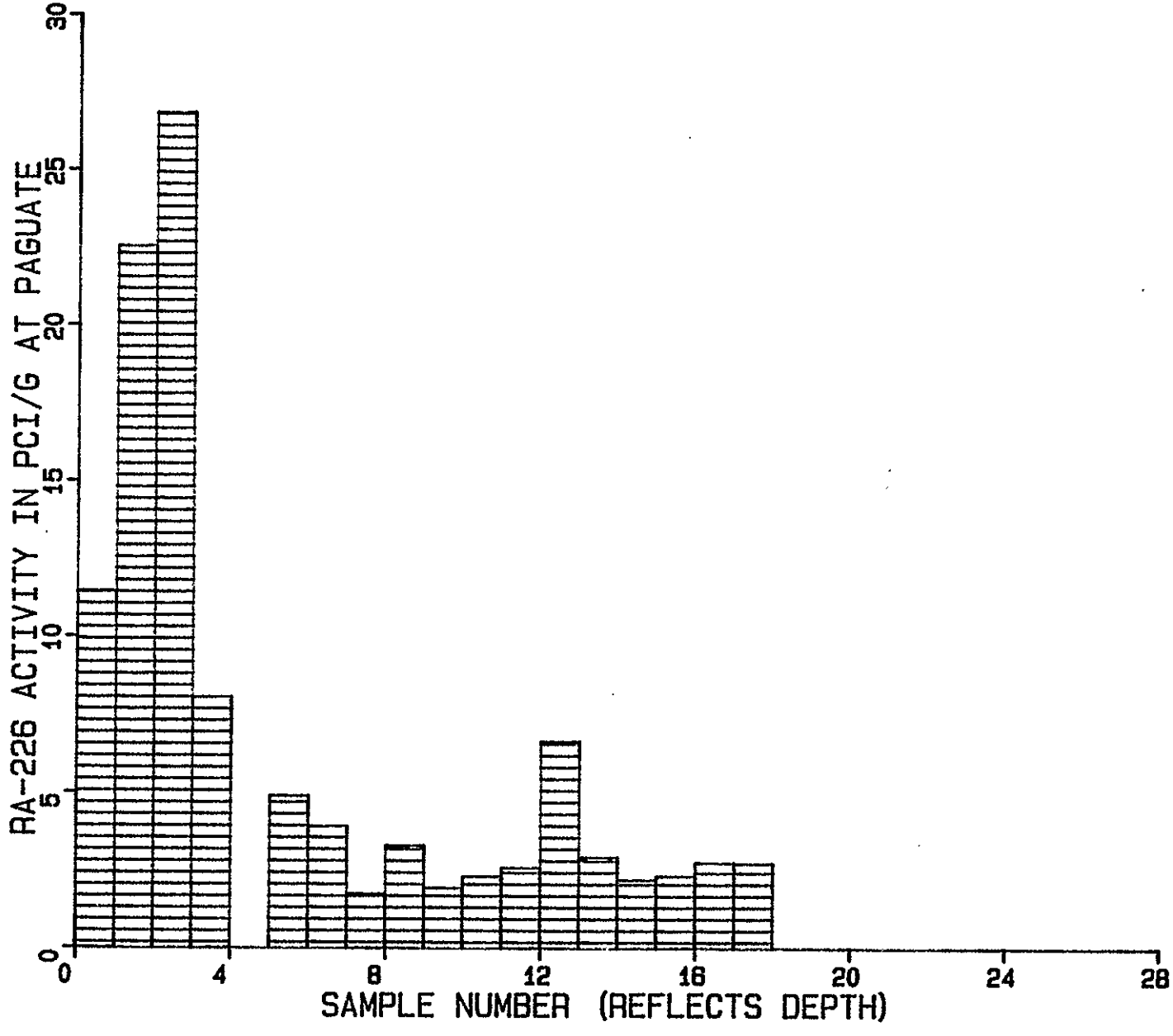
RA-226 ACTIVITY IN PCI/G AT PAGUATE
0
5
10
15
20
25
30
0
4
8
12
16
20
24
28
SAMPLE NUMBER (REFLECTS DEPTH)

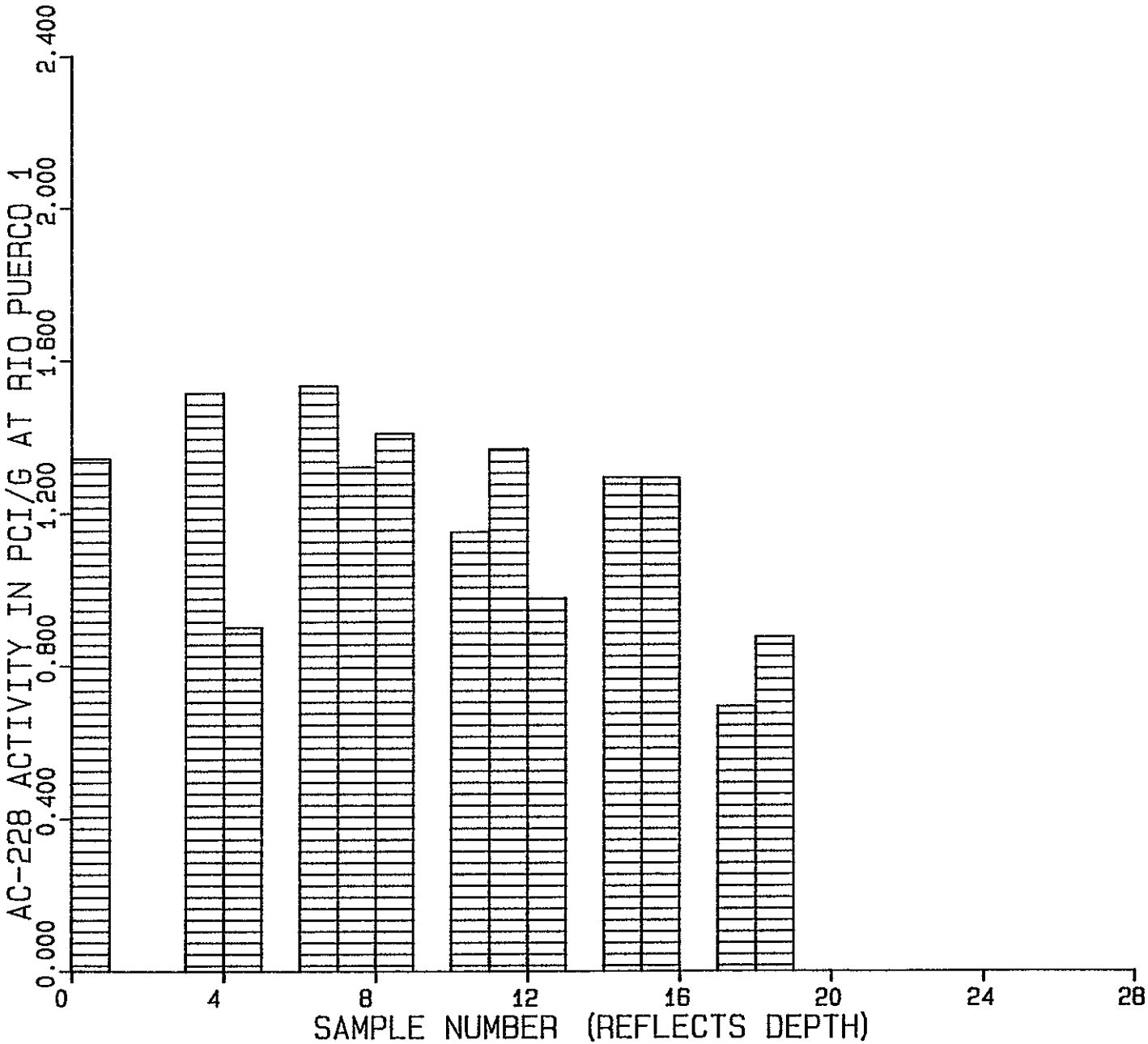
AC-228 ACTIVITY IN PCI/G AT RIO PUERCO 1
0.000
0.400
0.800
1.200
1.600
2.000
2.400
0
4
8
12
16
20
24
28
SAMPLE NUMBER (REFLECTS DEPTH)

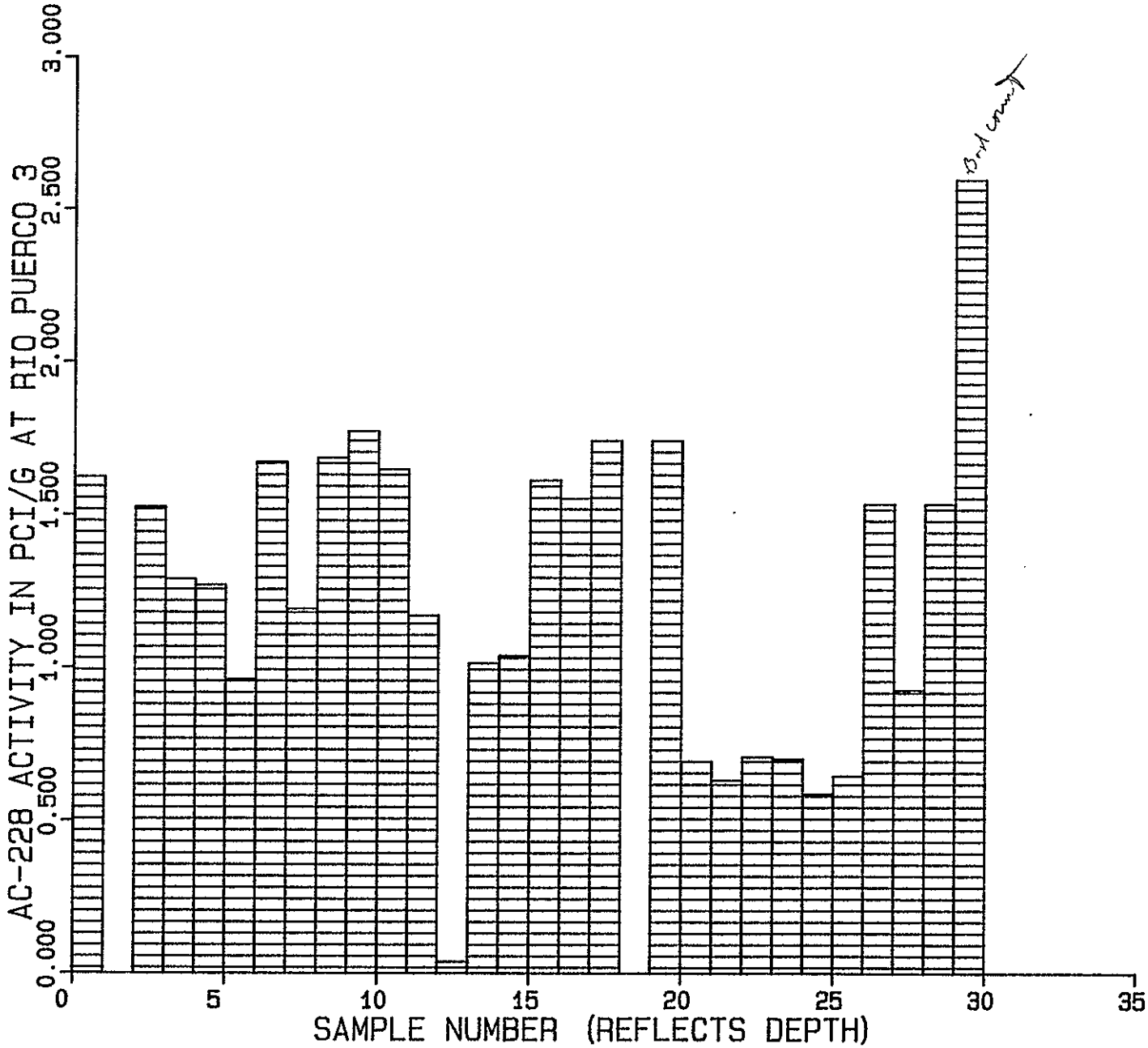
AC-228 ACTIVITY IN PCI/G AT RIO PUERCO 3
0.000
0.500
1.000
1.500
2.000
2.500
3.000
0
5
10
15
20
25
30
35
SAMPLE NUMBER (REFLECTS DEPTH)

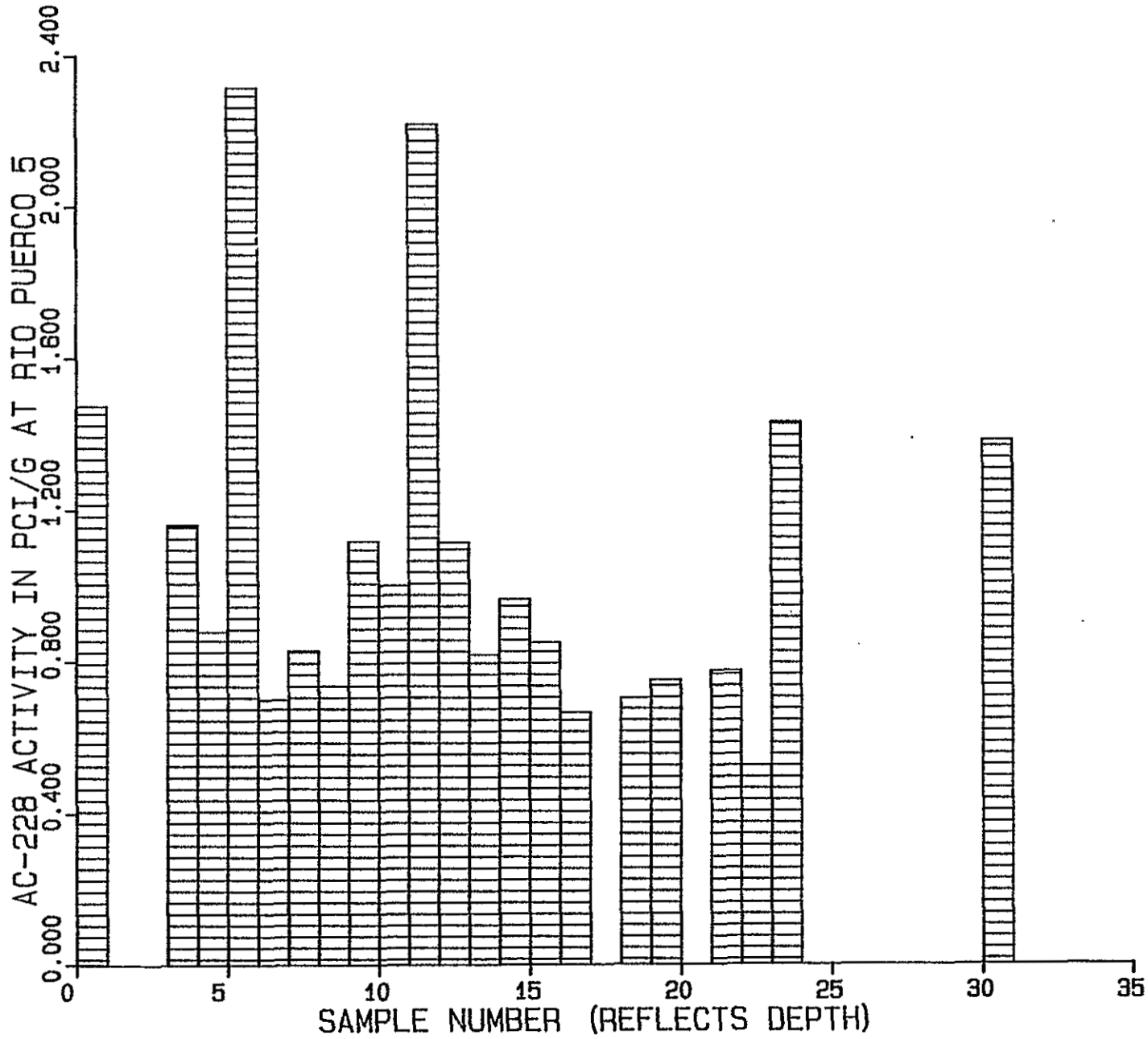
AC-228 ACTIVITY IN PCI/G AT RIO PUERCO 5
0.000
0.400
0.800
1.200
1.600
2.000
2.400
0
5
10
15
20
25
30
35
SAMPLE NUMBER (REFLECTS DEPTH)

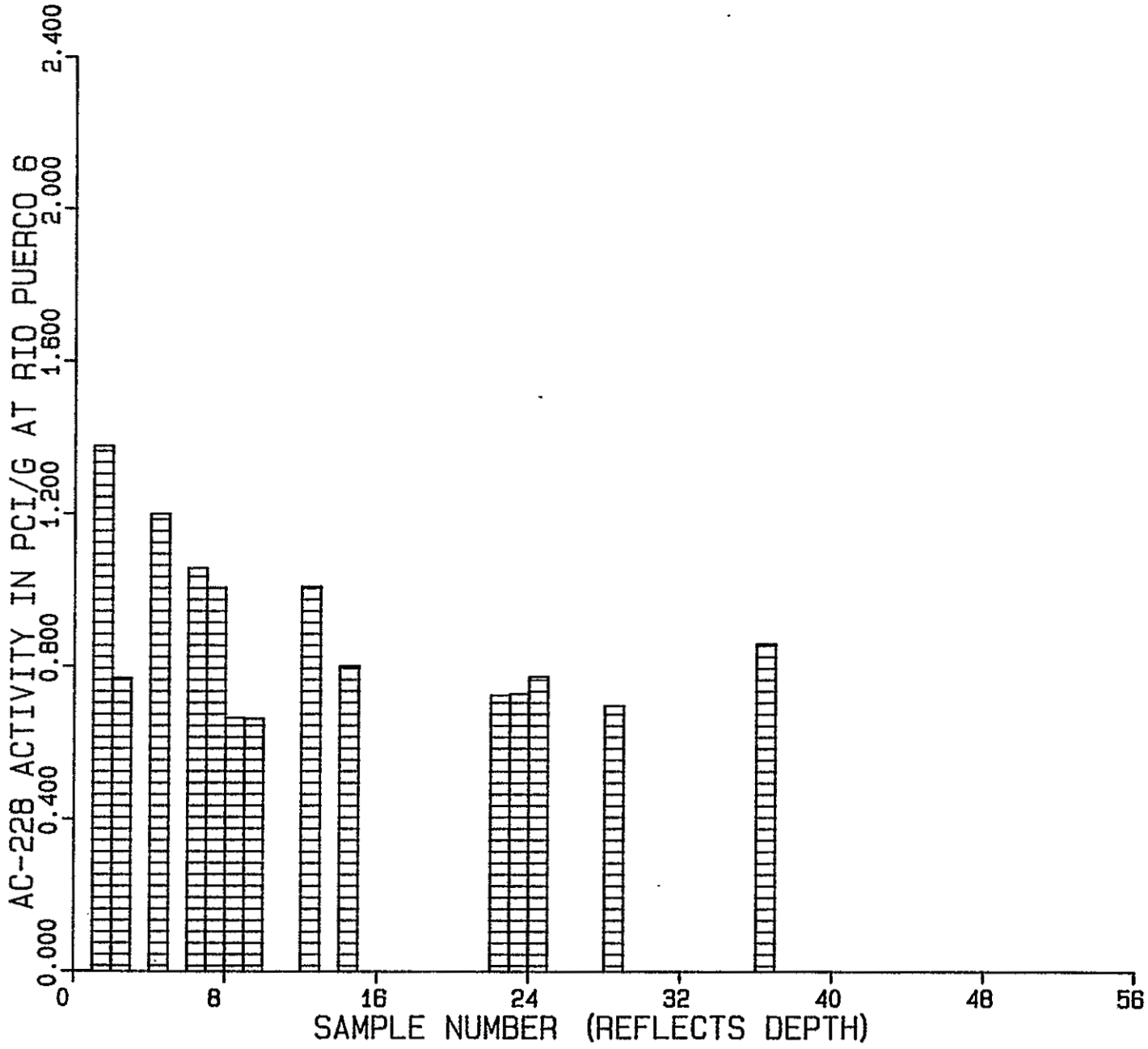
AC-228 ACTIVITY IN PCI/G AT RIO PUERCO 6
0.000
0.400
0.800
1.200
1.600
2.000
2.400
0
8
16
24
32
40
48
56
SAMPLE NUMBER (REFLECTS DEPTH)

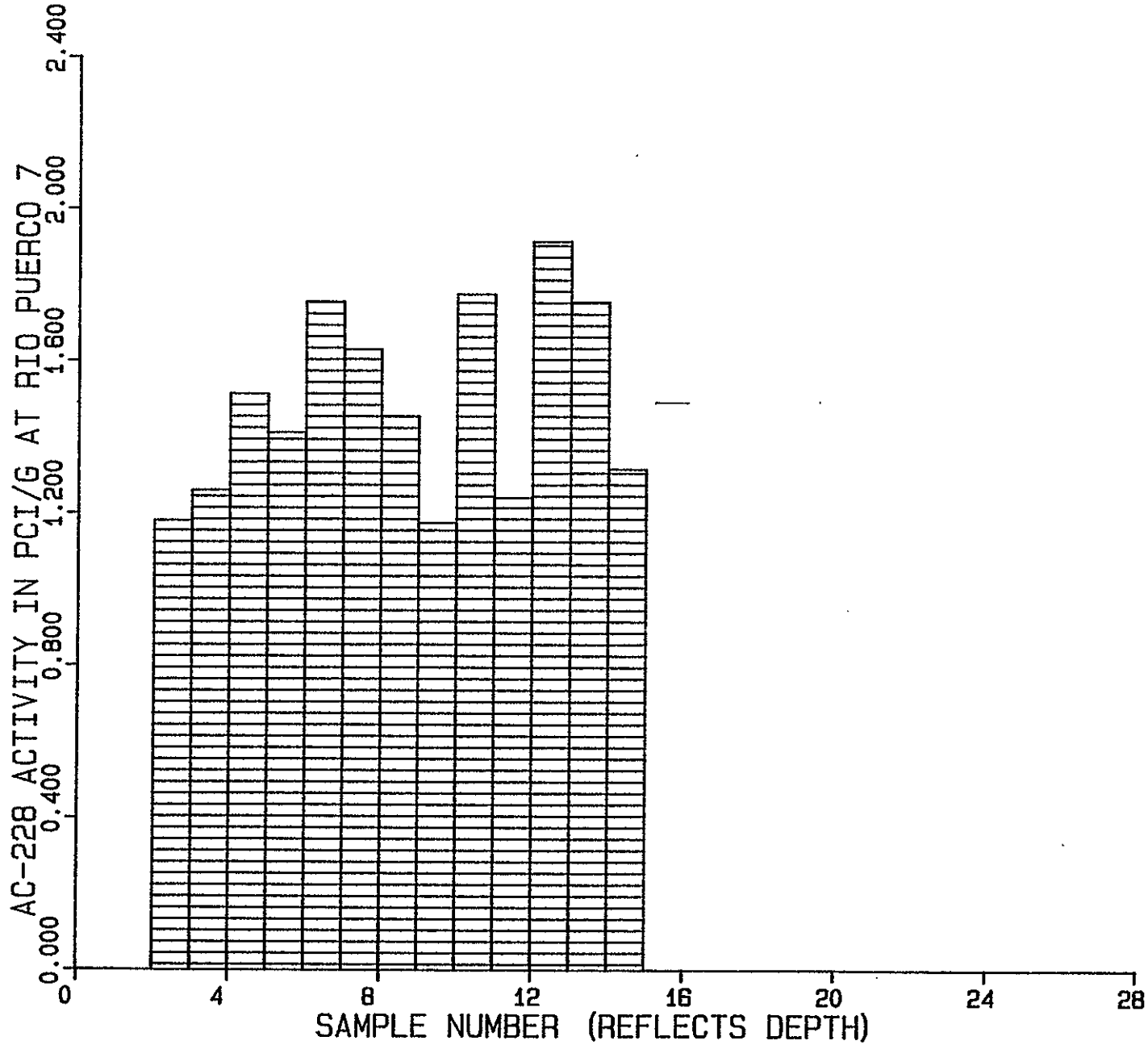
AC-228 ACTIVITY IN PCI/G AT RIO PUERCO 7
0.000
0.400
0.800
1.200
1.600
2.000
2.400
0
4
8
12
16
20
24
28
SAMPLE NUMBER (REFLECTS DEPTH)

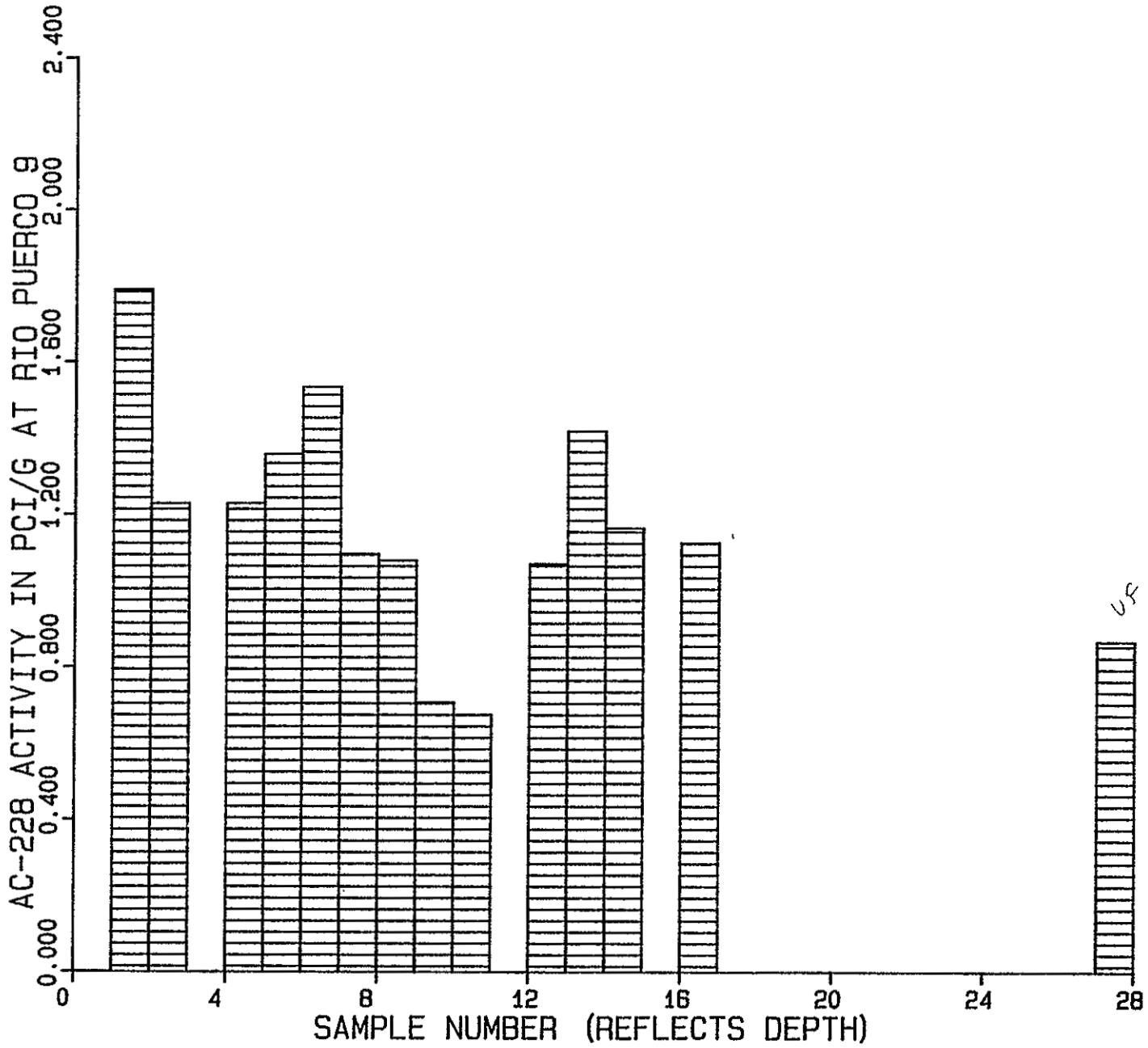
AC-228 ACTIVITY IN PCI/G AT RIO PUERCO 9
0.000
0.400
0.800
1.200
1.600
2.000
2.400
0
4
8
12
16
20
24
28
SAMPLE NUMBER (REFLECTS DEPTH)
UF

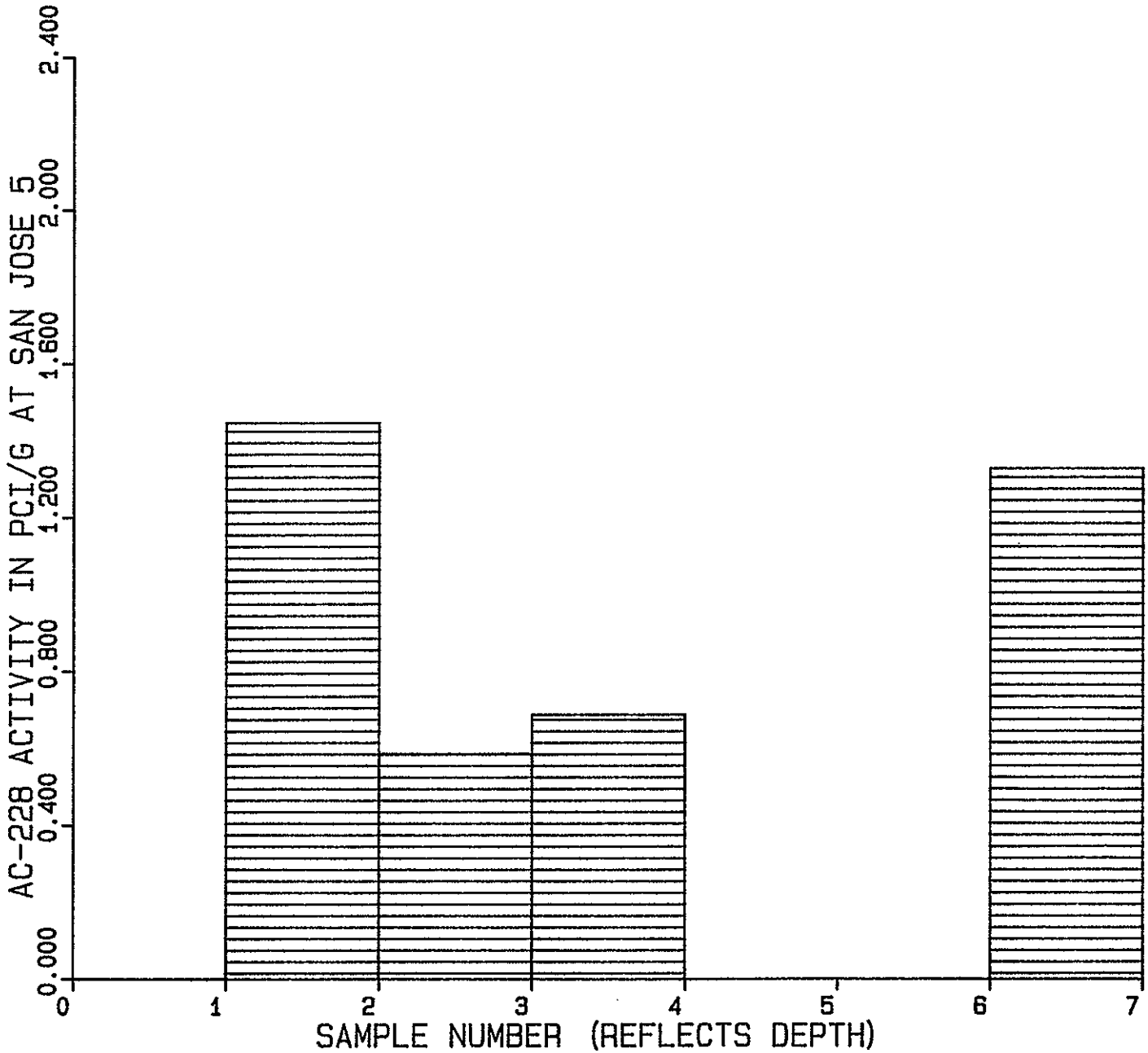
AC-228 ACTIVITY IN PCI/G AT SAN JOSE 5
0.000
0.400
0.800
1.200
1.600
2.000
2.400
0
1
2
3
4
5
6
7
SAMPLE NUMBER (REFLECTS DEPTH)

Appendix F.

Trace Metal Concentrations for Individual Samples. ppm Dry Weight.

Rio Puerco Oxbow Sites

site	deptn	as	cd	cr	cu	hg	mo	pb	se	v	u
2	1	8.0	.13	73.	31.	.21	.08	27.	.24	78.	478.
2	2	8.9	.14	52.	24.	.09	2.0	33.	.23	32.	203.
2	3	8.0	.16			.24	.46		.60	115.	600.
2	4	8.5	.18	48.	30.		1.5	11.	.55	255.	196.
2	5	41.	.47	40.	35.		2.8	26.	.33	105.	135.
2	6	11.	.16	51.	30.		1.0	15.	.58	178.	154.
2	7	11.	.14	50.	26.		1.4	15.	.52	229.	224.
2	8	13.	.39	66.	35.	.10	6.6	19.	.45	104.	297.
2	9	22.	.22			.17	.38	37.	.40	115.	520.
2	10	7.3	.18			.13	.50	20.	.34	90.	490.
2	11	11.				.42	.55	23.	.37	120.	610.
2	12	9.6	.21			.11	.52	16.	.36	125.	440.
2	13	13.	.19			.04	.37	29.	.39	120.	260.
2	14	12.				.16	.50	14.	.33	125.	260.
2	15	7.9	.15	76.	34.	.11	3.0	23.	.46	118.	407.
2	16	6.2	.29	60.	32.	.14	1.2		.22	100.	
2	18	6.3	.36	46.	30.	.11	2.2	32.	.28		410.
2	19	5.6	.45	45.	140.	.29	1.3	25.	.21		300.
2	20	9.3	.44	80.	43.	.32	11.	14.	.37	104.	363.
2	21					.02					
2	22	8.2	.47	60.	37.	.16	2.7		.10	110.	
2	23	15.	.31	60.	35.	.02	4.9	4.2	.20	110.	
2	25	9.7	.21	68.	33.	.07	8.6	22.	.44	105.	564.
2	26		.91	41.	130.		1.5	35.	.22	110.	375.
2	27		.08	45.	50.		2.8	90.	.50	135.	
2	29	7.2	.31	63.	62.	.21	6.4	20.	.25	89.	278.
2	30	9.3	1.2	64.	34.	.06	7.6	23.	.22	89.	329.
2	31	8.3	.31	63.	78.	.25	10.	34.	.35	100.	366.
3	1	7.4	.30	68.	147.	.28	8.7	15.	.47	100.	366.
3	2	8.1	.50	69.	104.	.32	5.4	54.	.35	104.	504.
3	3	6.8	.27	45.	39.		1.3	16.	.95	229.	130.
3	4	5.8	.18	47.	56.		2.1	16.	.41	87.	142.
3	5	17.	.26	52.	70.	.29	2.3	19.	.30	88.	
3	6	5.3	.15	40.	101.		.91	28.	.38	250.	142.
3	7	12.	.33	48.	79.		.93	45.	.35	115.	257.
3	8	17.		73.	62.	.15	7.3	62.	.33	119.	284.
3	9	12.	.27	46.	50.		2.0	31.	.36	50.	117.
3	11	12.	.45	60.	81.	.14	2.8		.13	100.	
3	12	7.1		55.	80.	.14	1.9		.16	90.	
3	13	50.	.35	50.	58.	.30	4.9		.14	90.	
3	14	8.4	.33	61.	62.	.16	4.3	35.	.53	99.	341.
3	16					.34					
3	18	7.0	.43	61.	92.	.15	2.1	24.	.27	120.	170.
3	20					.19					
3	23	5.3	.32	48.	50.	.15	1.8	14.	2.0	75.	434.
3	24		.59	34.	60.	.34	1.1	116.	.27	90.	
3	25			33.	48.					125.	200.
3	28	13.	.30	53.	98.	.22	3.7	17.	.67	84.	427.

7	1	8.6	.23	55.	3.7	.19	.45	15.	.43	120.	743.
7	2	23.	.31	44.	44.	.23	.38	17.	.48	120.	559.
7	3	6.5	.30	60.	37.		4.6		.13	100.	
7	4	9.4	.30	52.	60.	.23	.38	24.	.61	120.	377.
7	5	13.	.26	49.	55.		1.7	33.	.29	116.	141.
7	6	8.4	.27	42.	41.		.45	16.	.66	75.	506.
7	9	11.	.28	45.	53.		.70	16.	.56	90.	771.
7	11	8.0	.35	45.	28.		9.6		.17	80.	
7	13	11.	.08	38.	39.	.15	.17	15.	.34	135.	510.
7	15	13.	.34	41.	57.	.20	.20	19.	.39	90.	205.
7	20	13.	.24	48.	69.	.18	8.9	105.	.34	100.	
7	22	7.3	.27	63.	74.		3.4	10.	.13	125.	
7	25	16.	.10	60.	31.	.19	2.8		.08	127.	257.
7a	1	8.9	.34	50.	30.	.33	4.3		.12	100.	290.
7a	2	4.2	.25	50.	26.	1.2	2.9		.13	95.	250.
7a	3	7.2	.51	55.	29.	.37	2.5		.16	103.	260.
7a	4	3.4	.32	50.	27.	.34	2.4		.12	100.	240.
7a	5	8.2	.30	50.	28.	.31	4.5		.09	110.	220.
7a	6	7.0	.25	55.	35.	.44	1.7		.14	125.	280.
7a	7	4.9	.60	60.	31.	.59	.87		.18	120.	450.
7a	13		.58	36.	25.		1.2	111.	.32	140.	
7a	14		.62	30.	21.		1.2	34.	.32	80.	
7a	16		.62	25.	18.		1.2	23.	.09	80.	
7a	19		.34	28.	19.		1.8	46.	.16	85.	
7a	20		.26	29.	17.		2.8	22.	.07	80.	
9	su1	9.4	.32	38.	95.	.22	1.5	65.	.22	100.	280.
9	su2	45.	.46	63.	59.	.20	1.8	39.	.35	75.	600.
9	3		.20	33.	29.	.28	4.4	52.	.12	100.	450.
9	4	6.5	.27	41.	73.	.22	.75	26.	.32	115.	235.
9	5	6.5	.36		60.	.17	.31	29.	.28	105.	282.
9	12		.32	42.	23.		1.1	38.	.16	140.	
9	13			35.	26.					135.	
9	14	6.1	.47	37.	30.		1.8	23.	.13	125.	
9	16	20.	.34	37.	30.		2.6	20.	.28	135.	275.
11	1	4.4	.33	42.	99.	.22	1.3	40.	.39	70.	450.

San Jose Oxbow Sites

1	1	2.8	.30	68.	22.	.28	3.8			100.	370.
1	2	6.9	.24	50.	24.	.42	5.9		.16	100.	350.
1	3	38.	.70	60.	23.		1.4		.15	115.	570.
1	4	9.8	.27	33.	16.	1.3	1.1		.53	90.	
1	5	13.	.33	50.	22.	.14	1.8		.23	80.	
1	6	6.1	.26	55.	24.	4.3	2.7		.19	108.	380.
1	7	5.3	.42	63.	22.		2.0			75.	450.
1	8	12.	.32	55.	16.		1.2		.20	65.	400.
1	9	11.	.26	50.	21.		2.9		.21	98.	290.
1	10	10.	.32	55.	15.		2.2		.11	90.	570.
1	11	6.1	.48	63.	18.		5.1		.11	122.	630.
1	12	4.6	.31	46.	19.	.61	1.9		.18	78.	310.
1	13	10.		60.	18.		2.1		.18	65.	360.
1	15	6.3	.38	50.	22.	4.0	3.2		.10	88.	310.
1	16	9.3	.39	50.	13.	.63	5.83		.08	85.	260.
1	17	6.1	.36	45.	18.		3.4		.16	70.	330.
1	18	12.	.36	34.	17.		1.8		.17	85.	
1	su1	11.	.16	36.	17.	.65	1.3		.16	95.	
1	su2	27.	.34	39.	18.	.22	1.0		.20	95.	
1	su3	15.	.31	40.	17.		2.2		.18	120.	

3	1	7.8	.34	27.	19.	.17	.07		.08	105.	
3	2	4.1	.37	26.	22.	.07	.20		.10	50.	
3	3	1.5	.25	29.	20.	.08	.58		.07	120.	
5	4			30.	25.					100.	400.
6	old			38.	20.					130.	125.

Paguate Resevoir Site

1	1	4.6	.31	43.	20.	.06	2.4	16.	2.0	175.	550.
1	3	7.2	1.2	39.	18.	.24	1.5	27.	1.1	130.	550.
1	4	8.2	.34	38.	21.	.09	.25	32.	.68	120.	375.
1	5			35.	18.					100.	250.
1	6			41.	20.					120.	250.
1	7			32.	16.					110.	200.
1	8			40.	14.					110.	675.
1	9			38.	17.					130.	250.
1	10			37.	18.					110.	225.
1	12			37.	17.					120.	350.
1	13			30.	16.					90.	250.
1	14	6.7	.89	28.	13.	.72	.97	18.	.42	65.	350.
1	15	5.8	1.1	38.	20.	.62	2.6	27.	.66	100.	475.
1	16	4.8	.76	30.	25.	.80	.88	54.	.41	100.	375.
1	17	12.	.55	35.	19.	.09	4.3	20.	.42	100.	450.

Appendix G.

Neutron Activation Analysis of Clays

Neutron Activation Analysis of Clays

Site	Depth	ppm Cr	ppm Ba	ppm Cs	% Fe
1	1	71	330	3.6	11
1	2	60	390	4.3	13
1	6	32	400	4.3	13
1	10	52	280	3.9	13
1	13	70	370	4.3	14
1	16	60	440	5.0	12
1	20	57	440	4.8	14
1	20	66	500	5.2	13
2	1	56	295	4.0	12
2	2	59	400	4.4	11
2	8	56	290	3.8	10
2	15	23	450	4.0	13
2	19	69	420	4.2	10
2	25	60	372	4.5	11
2	26	89	430	5.2	12
2	30	68	420	4.4	12
2	31	70	360	3.9	13
2	32	29	718	6.9	13
3	1(80+)	16	410	.28	1.8
3	1(80-230)	20	460	.72	2.5
3	1(230-)	32	600	3.0	6.9
3	1(clay)	36	532	4.2	10
3	2	38	582	4.8	11
3	5	67	330	3.8	12
3	8	34	341	3.6	9.6
3	8	50	503	3.8	7.2
3	14	45	340	3.3	10
3	23	49	436	3.8	9.4
3	23	36	430	2.8	8.7
3	24	36	440	4.1	11
3	26	34	440	3.6	11
3	26	66	716	4.5	7.2
3	28	87	617	6.1	11
3	33	34	300	3.2	7.5
4	3	50	440	3.6	9.2
4	12	70	390	4.1	11
4	14	49	370	3.9	10
5	0	40	648	3.9	8.0
5	3	72	493	4.6	9.5
5	5	77	546	5.3	10
5	7	71	390	4.0	10
5	9	16.7	388	5.1	10
5	11	58	520	4.1	11
5	15	53	390	3.6	11
5	23	15	395	4.6	10
5	31	36	470	4.1	11